A Diffuse Reflectance Infrared Study of Butane on EuroPt-1.

Philip D. Holmes

A thesis submitted for the degree of Doctor of Philosophy.

The University of Edinburgh.

1992

I certify that this thesis has been composed by me and, unless otherwise stated, the work presented was performed by me in the Chemistry Department of the University of Edinburgh. Some of the arguments presented in Chapter 3 have been published as Holmes, P.D., M^{c}Dougall, G.S., Wilcock, I.C. and Waugh, K.C., *Catalysis Today*, **9** (1991) 15.

Philip Holmes

Abstract

The chemistry of butane has been studied over two well characterised catalysts, EuroPt-1 and EuroPt-1 doped with potassium hydroxide to 1% weight in potassium.

The exchange of butane with deuterium produced a U shaped distribution of deuterated products, with maxima at the singly exchanged and fully exchanged butanes over both catalysts. The rate of exchange over the 1% potassium doped catalyst was nearly two orders of magnitude lower than over EuroPt-1.

The application of Diffuse Reflectance Infrared Fourier Transform Spectroscopy (DRIFTS) to strongly infrared absorbing catalytic systems was discussed, with the inherent advantages and disadvantages of the technique. It was concluded that it was a useful method for studying the region of the infrared spectrum associated with carbon-hydrogen stretching vibrations, but the strong absorbance of the catalysts' silica support made study of the carbon-hydrogen deformation region difficult for both EuroPt-1 catalysts.

The adsorption of butane on EuroPt-1 and 1% potassium doped EuroPt-1 in a flow system was studied using DRIFTS at 298 K and 378 K. The chemistry was similar over the two catalysts, but all infrared intensities were significantly lower over the 1% potassium doped catalyst. In comparison with equivalent single crystal studies, the main species present at 298 K was assigned to a di-σ or di-σ/π adsorbed butane. Heating preadsorbed butane to 378 K, or adsorbing butane at 378 K produced an infrared spectrum assigned to butylidyne. Further heating evolved hydrocarbon as methane. The reaction of the adsorbed species with pulses of hydrogen was also studied.

Acknowledgments

Firstly, I would like to thank my supervisor, Gordon M^{c}Dougall for the help and advice over the years. The funding for this work was a demonstratorship conjured as from nowhere by Professor Donovan, and the James Watt Bursary, for which I am grateful to him, the Department, the University and to Gordon for choosing me.

I would also like to thank Roni Brown, the man who knows how every bit of apparatus works, where every piece of kit is hidden and the answer to most of the questions I have asked him. I am particularly indebted to him for tolerating my phobia of lecture bottles.

The support staff of the department are always important to research, and I owe much to Stuart Mains and John Ashfield (who machined the environmental chamber) of the mechanical workshop, John Broom and Robert Wilson the glassblowers, and the staff of the electronic workshop.

No job can be complete without workmates, and my time as a demonstrator was made easier by people like the late Liz Bell, Harry MacKenzie and Angus Brown, with whom I spent many of the early years. My friends in the research group I also thank, those who showed me the way, Mushtaq, Hilary, Ian, Gordon, Brian and Andy, and those I am leaving behind, Anne, Keith, Jim, Alister, Peter and Graeme, with their Ayes, woofs, donkeys, ye knaws and bings.

Other members of staff who have helped over the years are Frank Leach, who somehow ended up also being a supervisor, though was equally approachable and helpful before being elevated to that rank, Sandy Blake who put up with me pestering him about the computers, and Bob Gould, who had the right answer to the right question at a psychologically important moment.

Contents

1 Introduction. 1

1.1 Catalysis 1

1.2 Platinum in catalysis 4

1.3 Catalyst Forms 5

1.3.1 Supported Catalysts 6

1.3.2 Preparation 7

1.3.3 Catalyst Promotion. 7

1.4 Catalysis research 8

1.4.1 EuroPt-1. 9

1.4.2 Deuterium Exchange. 9

1.4.3 Surface Science. 10

1.5 Vibrational Spectroscopy. 10

1.5.1 Surface Probes. 11

1.5.2 Vibrational Spectroscopy of Supported Catalysts. 12

1.5.3 Vibrational Spectroscopy in Surface Science 14

1.5.4 Selection Rules. 17

1.5.5 Mixing it : Using Surface Science as a Model for Supported Catalysis. 21

1.6 Alkali Metals in Surface Science. 22

1.7 Thesis Aims. 23

2 Deuterium Exchange 24

2.1 Introduction 24

2.2 Experimental 25
2.2.1 The Vacuum System 25
2.2.2 Mass Spectrometry 28
2.2.3 Gas Chromatography 28
2.2.4 Experimental Procedure 29
2.2.5 Data Analysis 30
2.3 Discussion 32
2.3.1 EuroPt-1 at 331 K 32
2.3.2 EuroPt-1 at 378 K 45
2.3.3 Potassium doped EuroPt-1 at 378 K. 53

3 Diffuse Reflectance Infrared Fourier Transform Spectroscopy 61
3.1 Introduction 61
3.2 Diffuse Reflectance Spectroscopy 62
3.3 Kubelka-Munk Theory. 63
3.3.1 Exact Scattering Theories. 63
3.3.2 Phenomenological Scattering Theory. 65
3.4 Application of the Kubelka-Munk Theory. 67
3.4.1 White Standards 67
3.4.2 Diffuse Reflectance Spectroscopy in the Infrared. 69
3.5 Experimental 70
3.5.1 The Fourier Transform Spectrometer. 70
3.5.2 The Single Beam Profile 72
3.5.3 Data Storage and Manipulation 75
3.5.4 Diffuse Reflectance Optics 77
3.5.5 Environmental Chamber 78
3.5.6 The Gas Handling System 80
3.5.7 Procedure 83
3.6 A Critical Evaluation of DRIFTS and Comparison with Transmission. 84

3.7 The Practical Application of DRIFTS. 91
3.8 Conclusion. 94

4 DRIFTS of butane over EuroPt-1. 95
4.1 Introduction 95
4.2 Results. 109
4.2.1 Gas phase reference spectrum. 109
4.2.2 Butane adsorption on Sorbosil AQ U30. 109
4.2.3 Butane adsorption on outgassed EuroPt-1 at 298 K. 115
4.2.4 Butane adsorption on a hydrogen rich EuroPt-1 surface at 298 K. 127
4.2.5 Hydrogenation of butane adsorbed on EuroPt-1 at 298 K. 130
4.2.6 Temperature programmed desorption of butane on EuroPt-1. 137
4.2.7 Butane adsorption on Sorbosil AQ U30 at 378 K. 140
4.2.8 Butane adsorption on EuroPt-1 at 378 K. 140
4.2.9 Hydrogenation of butane adsorbed on EuroPt-1 at 378 K. 145
4.3 Discussion 148
4.3.1 Butane adsorption and reaction on EuroPt-1 at 298 K. . . 148
4.3.2 Temperature programming of butane adsorbed on EuroPt-1. 154
4.3.3 Butane adsorption and reaction on EuroPt-1 at 378 K. . . 156
4.3.4 Comparison of DRIFTS with deuterium exchange. 158

5 DRIFTS of butane over potassium doped EuroPt-1. 161
5.1 Introduction. 161
5.2 Results. 163
5.2.1 Butane adsorption on 1% potassium doped Sorbosil AQ U30. 163
5.2.2 Butane adsorption on 1% potassium doped EuroPt-1 at 298 K. 163
5.2.3 Temperature programmed desorption of butane from 1% potassium doped EuroPt-1. 166

5.2.4 Butane adsorption on 1% potassium doped Sorbosil AQ U30 at 378 K. 170
5.2.5 Butane adsorption on 1% potassium doped EuroPt-1 at 378 K172
5.2.6 Hydrogenation of the surface species formed from butane on 1% potassium doped EuroPt-1 at 378 K. 172
5.3 Discussion 176

A EuroPt-1 **195**
A.1 Characterisation 195
A.2 Hydrogenolysis of *n*-butane. 197

B Courses and conferences attended **199**

C Published Paper **200**

List of Figures

1.1 Energy for reactions 1.1, 1.2, and 1.3. 2
1.2 The 'volcano plot'. 4
1.3 Image dipoles in a metal surface. 19
1.4 Field lines round a metal particle under the classical model. . . . 20

2.1 Glass vacuum line for deuterium exchange reactions. 27
2.2 The operation of the Carle valve. 29
2.3 Exchange over EuroPt-1 at 331 K to 10.8% reaction 34
2.4 Product distribution by isotope for Figure 2.3 35
2.5 Initial product distribution for Figure 2.3 36
2.6 Exchange over EuroPt-1 at 331 K to 50% reaction 38
2.7 Product distribution for Figure 2.6 40
2.8 Kinetic plots for exchange over EuroPt-1 at 331 K. 42
2.9 The Horiuti-Polanyi associative mechanism for alkene exchange. . 43
2.10 A reaction scheme for butane adsorption. 44
2.11 Exchange over EuroPt-1 at 378 K to 13% reaction. 46
2.12 Product distribution by isotope for Figure 2.11 47
2.13 Initial product distribution for Figure 2.11 48
2.14 Exchange over EuroPt-1 at 378 K for 45% reaction. 49
2.15 Product distribution by isotope for Figure 2.14 51
2.16 Kinetic plots for exchange over EuroPt-1 at 378 K. 52
2.17 Exchange over 1% potassium doped EuroPt-1 at 378 K to 5% reaction. 54

2.18 Product distribution by isotope for Figure 2.17 56
2.19 Initial product distribution for Figure 2.17 57
2.20 Kinetic plots for exchange over 1% potassium doped EuroPt-1 at 378 K. 58

3.1 Light path for transmission. 63
3.2 Light path for diffuse reflection. 63
3.3 Angular distribution of the scattering intensity after single scattering (A) and twofold scattering (B) on dielectric spheres. 65
3.4 Scheme for deriving the Kubelka-Munk equation. 66
3.5 Comparison of the exact and Kubelka-Munk solutions to the radiative transfer equation 68
3.6 Interferogram recorded on the FTS-40. 74
3.7 Single beam spectrum at 4 cm^{-1} resolution. 74
3.8 Mirror unit of the Spectratech 'Collector' accessory. 78
3.9 Environmental chamber and sample block. 79
3.10 Trolley mounted vacuum line for DRIFTS experiments. 81
3.11 A. DRIFTS single beam spectrum of EuroPt-1. B. Transmission single beam spectrum of EuroPt-1. 85
3.12 Variation of light absorption in heterogeneous systems. 87
3.13 Influence of regular reflection on $F(R_\infty)$ of absorbing powders. . . 90
3.14 $F(R_\infty)$ and absorbance, E, as functions of R_∞ and T respectively. 93

4.1 1,2 di-σ ethene surface complex 96
4.2 Ethylidene surface complex 97
4.3 Ethylidyne surface complex 98
4.4 Vinyl surface complex 98
4.5 Di-σ adsorbed but-2-ene retaining a cis configuration. 102
4.6 Di-σ adsorbed but-2-ene retaining a trans configuration. 102
4.7 Di-σ adsorbed but-2-yne 103

4.8 Di-σ/π adsorbed but-2-yne 103
4.9 Butylidyne in the *trans* conformation. 104
4.10 Butylidyne in the *gauche* conformation. 105
4.11 Gas phase infrared spectrum of butane 110
4.12 Butane a sorption on Sorbosil: C–H stretch region 112
4.13 Butane adsorption on Sorbosil: changes in the C–H stretch spectrum with time. 113
4.14 Variation of absorbance with time for selected frequencies of Figure 4.13. 114
4.15 Figures 4.11 and 4.12 arbitrarily scaled for ease of comparison. . . 116
4.16 Butane a sorption on EuroPt-1: full spectral range 117
4.17 Butane a sorption on EuroPt-1: C–H stretch region 120
4.18 Butane a sorption on EuroPt-1: changes in the C–H stretch spectrum with time. 121
4.19 Variation of absorbance with time for selected frequencies of Figure 4.18 (inset at expanded y scale). 122
4.20 Surface species formed by butane adsorption on EuroPt-1. 125
4.21 Propylidyne surface complex. 126
4.22 Butane adsorption on a hydrogen rich EuroPt-1 surface. 128
4.23 Variation of absorbance with time for selected frequencies of Figure 4.22 (inset at expanded y scale). 129
4.24 Surface species formed by butane adsorption on a hydrogen rich EuroPt-1 surface. 131
4.25 Butane adsorption on EuroPt-1: changes in the C–H stretch spectrum with addition of hydrogen 133
4.26 Absorbance subtraction spectra to show changes in Figure 4.25 . . 134
4.27 Butane adsorption on EuroPt-1 at 298 K: mature spectrum after hydrogenation. 136
4.28 Changes in the butane spectrum over EuroPt-1 with temperature. 138

4.29 Variation of absorbance with temperature for selected frequencies of Figure 4.28 139
4.30 Variation of absorbance with time for butane adsorption on Sorbosil at 378 K. 141
4.31 Variation of absorbance with time for butane adsorption on EuroPt-1 at 378 K (inset at expanded y scale). 143
4.32 Surfaces species formed by butane adsorption on EuroPt-1 at 378 K.144
4.33 Butane adsorption on EuroPt-1 at 378 K: changes in the C–H stretch spectrum with addition of hydrogen. 146
4.34 Absorbance subtraction spectra to show changes in Figure 4.33 . . 147
4.35 Butane adsorption on EuroPt-1 at 378 K: mature spectrum after hydrogenation. 149
4.36 Mono-adsorbed butane 150
4.37 Suggested reaction scheme for butane on EuroPt-1 at room temperature. 153
4.38 Suggested reaction scheme for butane on EuroPt-1 during temperature programmed desorption. 157
4.39 Suggested reaction scheme for butane on EuroPt-1 at 378 K. . . . 158

5.1 Variation of absorbance with time for the C–H stretch region over 1% potassium doped Sorbosil. 164
5.2 Variation of absorbance with time for the C–H stretch region over 1% potassium doped EuroPt-1 (inset at expanded y scale). 165
5.3 Surface species formed by butane adsorption on 1% potassium doped EuroPt-1. 167
5.4 Changes in the butane spectrum over 1% potassium doped EuroPt-1 with temperature. 168
5.5 Variation of absorbance with temperature for selected frequencies of Figure 5.4 169

5.6 Variation of absorbance with time for butane adsorption on 1% potassium doped Sorbosil at 378 K. 171
5.7 Variation of absorbance with time for the C–H stretch region over 1% potassium doped EuroPt-1 at 378 K (inset at expanded y scale).173
5.8 Surface species formed by butane adsorption on 1% potassium doped EuroPt-1 at 378 K. 174
5.9 Butane adsorption on 1% potassium doped EuroPt-1 at 378 K: changes in the C–H stretch spectrum with addition of hydrogen. . 175

List of Tables

2.1 Exchange data for as received EuroPt-1 at 331 K. 33

2.2 Exchange data for as received EuroPt-1 at 378 K 50

2.3 Exchange data for 1% potassium doped EuroPt-1 at 378 K. . . . 53

2.4 Metal particle characteristics of EuroPt-1. 59

4.1 Literature vibrational data for but-1-ene on Pt(111). 104

4.2 Literature vibrational data for but-2-ene on Pt(111). 105

A.1 Characterisation results 198

A.2 Hydrogenolysis results 198

Chapter 1

Introduction.

1.1 Catalysis

A catalyst may be defined as a substance that increases the rate at which equilibrium is reached in a chemical reaction, without itself being changed. This serviceable definition was first promulgated by J.J. Berzelius [1] in a review of work by Edmund [2] and Humphrey [3] Davy and J.W. Döbereiner [4]. Following the translation of Rideal and Taylor [5]:

> By means of this action they produce, in these (other) bodies, decompositions of their elements and different recombinations of these same elements to which they themselves remain indifferent. This new force, which was hitherto unknown, is common to organic and inorganic nature ... I will ...call this force the catalytic force, and I will call catalysis the decomposition of bodies by this force ...

Catalysis today is frequently divided into two camps, homogeneous, where the reagents and catalyst are in the same physical state (gas/gas, liquid/liquid or rarely solid/solid) and heterogeneous, where the physical states differ. The latter term is on occasion used with the specific implication of gas/solid systems [6]. These were the first described in catalytic terms, today accounting for many of the world's major industrial processes, and will be the subject of this thesis.

In a general chemical reaction, say

$$AB_{(g)} + C_{(g)} \rightleftharpoons AC_{(g)} + B_{(g)} \tag{1.1}$$

there is an activation energy, E_a, associated with the formation of some intermediate transition state, $A \cdots B \cdots C$, Figure 1.1. This state, and hence the reaction products, can be reached if there is sufficient thermal energy in the system to supply E_a to a statistically significant number of reagent molecules. In the presence

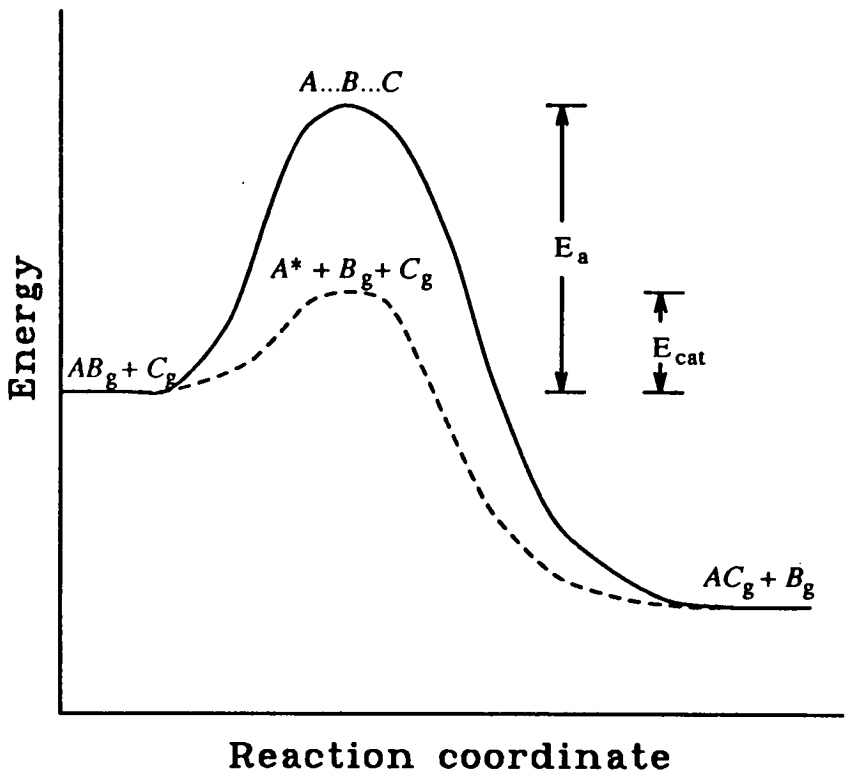

Figure 1.1: Energy for reactions 1.1, 1.2, and 1.3.

of active catalyst sites, *, an alternative route may be provided, such as

$$AB_{(g)} + * \rightleftharpoons A* + B_{(g)} \tag{1.2}$$

$$C_{(g)} + A* \rightleftharpoons AC* \rightleftharpoons AC_{(g)} + * \tag{1.3}$$

where dissociation takes place on the surface prior to formation of products. From the free energy diagram, it is clear that the activation energy for both forward and reverse reactions is reduced. The thermodynamic equilibrium, with its proportion of products and reagents, is therefore not changed, but the ease of reaching it is. If the catalyst acts on only one of several alternative reactions, the equilibrium may be established preferentially for a particular set of desired products. Such selectivity is demonstrated *eg.* in formic acid decomposition, where carbon dioxide and hydrogen are produced over metal catalysts, and carbon monoxide and water are produced over oxides [7]. Another feature of this scheme, as implied by the opening statement above, is the re-formation of the original active site, leaving it

available for further reaction. In this system, there are several possible limiting steps:

1. Diffusion of reagents to the active site of the catalyst
2. Adsorption of reagents at the active site.
3. Surface reaction giving desired products.
4. Desorption of the products into the gas phase.
5. Diffusion of the products away from the surface.

In practice, many reaction systems are specifically designed to eliminate points 1. and 5.

A simple observation which can be made using this scheme is the importance of adsorption and desorption on the catalyst surface. If the initial adsorption step, 2., is too weak, or the reagent has a low sticking probability, the opportunity for step 3., surface reaction, is reduced. If on the other hand, the catalyst displays strong enough affinity for the products, these will never be desorbed, and further reaction will be inhibited. This characteristic is well illustrated in the decomposition of formic acid over metals. Taking the reaction temperature required to give a certain turnover as a measure of activity, a classic volcano shaped plot, Figure 1.2 is produced by plotting activity against the heat of formation of metal formate [8]. With the heat of formate formation as a measure of the stability of the surface species (shown to be involved in the reaction $HCOOH \rightarrow H_2 + CO_2$), it is clear that over gold, with weak adsorption of HCOOH, the decomposition is less likely to occur. Over iron, the stability of the formate is prohibitive to ready decomposition, hence the fall in the curve. The most active metals from Figure 1.2, are the heavier (noble) group VIII metals, ruthenium (Ru), rhodium (Rh), palladium (Pd), iridium (Ir) and platinum (Pt).

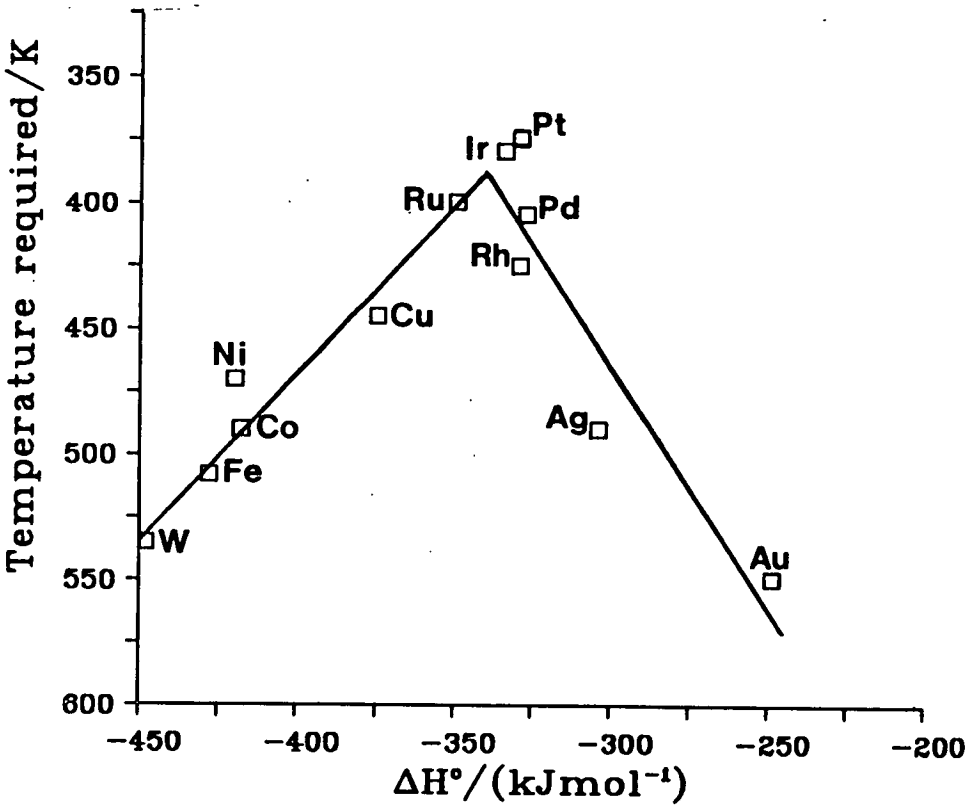

Figure 1.2: The 'volcano plot' adapted from [8]

1.2 Platinum in catalysis

The catalytic action of the group VIII metal platinum figured in the early work of H. Davy [3] (during research for his safety lamp). He discovered that when a hot platinum wire was exposed to oxygen/coal gas mixtures, the heat of the reaction induced was sufficient to make the wire incandescent. In 1820, E. Davy [2] created a finely divided form of platinum which could oxidise alcohol, again with a bright glow – a reaction still used today in a cigarette lighter [9].

Since these early days, all the group VIII metals have been used as catalysts in a wide variety of applications. One major use for iron catalysts is in ammonia synthesis, where the rate determining step is chemisorption of nitrogen [10]. As mentioned above, the adsorbate stability is a major factor in catalyst choice, metals to the right of iron in the periodic table only adsorbing nitrogen weakly, and those to the left having a greater tendency to form nitrides. Nickel features as a steam reforming catalyst. Platinum and palladium, although generally

less reactive than the first series group VIII transition elements, do not fit the 'noble' description as well as the other platinum metals [11]. They are used in petroleum reforming due to their abilities in hydrocarbon adsorption, facilitating hydrogenation/dehydrogenation reactions, and as oxidation catalysts.

The biggest use of platinum catalysts is in vehicle emission control. With many European countries following the lead of Japan and the USA in introducing limits for CO, NO_x and unburnt hydrocarbon species in automobile exhausts, this market is likely to continue expanding. The convertor used is a trifunctional ruthenium/ platinum/ ceria catalyst supported on monolithic cordierite ($2MgO.2Al_2O_3.5SiO_2$) [12]. The platinum is an oxidising catalyst for carbon monoxide. The importance of this as a use for platinum is underlined by the drop in the metal's market value following a spurious announcement in 1989 by the Ford Motor Company that an alternative catalyst had been found [13].

1.3 Catalyst Forms

The physical form of a catalyst must obviously be considered in conjunction with the function it is being asked to perform, and the environment to which it will be subjected. As the catalytic function is determined by adsorption at the metal surface, a first criterion must be an increase in surface area per unit metal. Humphrey Davy's first experiments with platinum wires [3] were quickly improved on when his cousin Edmund produced a powdered form, which was active at room temperature.

The most finely divided form of pure platinum is known as platinum black. This is formed by precipitation of platinum oxide or hydroxide from a basic solution of a platinum salt (*eg.* from H_2PtCl_6 at 275 K in HCHO in the presence of NaOH [14]) followed by reduction, often with hydrogen. An alternative method is from vapourised metals produced by a plasma hydrogen gas – molten metal reaction under an arc melting condition [15]. Both techniques produce platinum with a very small particle size, 15 nm or less for precipitation [14, 16], 40 nm

for vapourised metals [16] . This can produce metal surface areas of the order 20 m^2g^{-1} and 3 m^2g^{-1} respectively.

Despite this large surface area, metal blacks are not often used as catalysts for gas/solid reactions [17]. The most obvious problem is in physically retaining such small particles in a gas stream reactor. Perhaps less obvious, but no less a problem, is sintering [18] . At the temperatures and pressures required for many industrial processes, the metal particles tend to agglomerate, (even well below the melting point) reducing surface area and hence activity. This is due to the small particle size, and can be equated to ice metamorphosis in snow [19, 20]. Smaller particles, with larger curvature of the surface, have a higher vapour pressure over them than crystallites with more gentle surface curvature, following the Kelvin equation. Small metal crystals have been shown to have some liquid like properties, and reduced melting points, typically one-half of normal for a cluster of 55 atoms [21], again aiding particle build-up.

Vapour phase transport will be assisted by formation of more volatile complexes during reaction. Species such as PtH_2 and $Pt(CH_3)_2$ have been suggested [7], though this idea is most widely accepted for metal oxides in oxidising environments [22].

1.3.1 Supported Catalysts

The twin problems of mechanical and thermal properties of a catalyst are both salved (if not solved) by supporting the metal on an inert, refractory, high surface area material such as silica, alumina or carbon. The high surface area of these supports allow them to accommodate highly dispersed metals while providing a physical barrier to agglomeration. The bulk properties allow industrial catalysts to be pelleted, extruded and ground to give lumps of desired dimensions (often in the range 1 to 10mm) with diffusional limits taken into consideration. In supported catalysts, noble metals are usually present in the order of 1 per cent by weight or less.

1.3.2 Preparation

Supported catalysts are made by two main methods, impregnation and co-precipitation. In impregnation, the support is soaked in a solution of an appropriate metal salt, then dried. The salt is then reduced to the metal by heating in hydrogen, possibly after a calcination stage to form the metal oxide. In co-precipitation, a solution is made up of both the metal salt and a precursor for the support, which are precipitated out together by adjusting the pH of the solution.

1.3.3 Catalyst Promotion.

When a catalyst has been created, it is often found that the rate of attainment of equilibrium can be further speeded by the addition of a promoter. Promoters may or may not be active in the reaction themselves, but by definition the improvements in activity (or selectivity) must be greater than the sum of the individual activities of the catalyst and promoter.

Promoters have been found for many catalytic systems and can act in many different ways, but are usually divided into two categories, structural and chemical. The catalyst which has perhaps been studied for the longest is that for ammonia synthesis. This is a doubly promoted iron based catalyst. Alumina is added as a structural promoter. When the initial iron oxide Fe_3O_4 is reduced, Al^{3+} ions replace Fe^{3+} in the spinel magnetite structure, and porosity is developed. The alumina, which is not reduced under the conditions used, forms a coating of small crystallites on the surface of the iron crystals. Gas adsorption studies show [17] that 2% weight of alumina can cover at least one third of the total surface. It thus minimises sintering during reduction as well as during the ammonia synthesis, giving catalysts with 15 m^2g^{-1} surface area, compared with about 0.5 m^2g^{-1} for unpromoted iron under the same conditions. The chemical promoter added is potassium oxide, K_2O. The understanding of its action is not complete, but it is thought to keep the iron surface free of blocking groups such as NH, NH_2, or NH_3 [23], especially important at the high pressures used in the

synthesis.

Promoted or mixed catalysts account for many of the heterogeneous systems used industrially. In a surprising number of these the promoter, acting to improve selectivity, activity or lifetime, is an alkali metal compound. A list of over thirty different alkali promoted reactions was given by Mross [24].

1.4 Catalysis research

An area of such great industrial importance is clearly one which warrants intensive research. Improvements in catalysis give energy savings in faster, or lower temperature reactions, reduced purification problems with increased selectivity and alternative synthesis routes avoiding expensive raw materials. Much research, particularly early work, has been of the approach typified by Haber, Bosch and Mittasch in their search for an ammonia synthesis catalyst. They tried many thousands of catalyst combinations in more than two dozen laboratory scale reactors capable of working at a hundred atmospheres [25]. This gives a wealth of information about the effectiveness of the catalysts, but understanding of the physical processes involved is to some degree limited by the extrapolation required from the reactants and products back to the catalytic intermediates.

One problem with catalytic research is reproducibility. With the complex nature of its preparation, there are many variables which can have an effect on the finished catalyst. As well as the profound changes which traces of poisons and promoters can produce, physical factors such as reduction temperatures can alter metal particle size and hence activity. Even within one laboratory it can be difficult to ascribe observed changes to the intended experimental variable, rather than some fluctuation in contaminants or the preparation scheme. This means comparison of results with the literature must be done very carefully, to avoid such unintended variations.

One approach which reduces the number of variables is to use a standard catalyst. In 1975, the European Research Group on Catalysis was founded under

Professor E.G. Derouane with funding from the Council of Europe. To promote direct comparability between European laboratories, a series of standard catalysts was created in large batches, and distributed among the separate research groups.

1.4.1 EuroPt-1.

One of the European Research group catalysts, EuroPt-1, has been extensively characterised, with a high degree of accord among the research group members, despite different techniques being used on different designs of apparatus throughout Europe [26, 27, 28].

EuroPt-1 is a 6.3% weight platinum silica catalyst prepared by Johnson Matthey Chemicals plc by ion exchange of $Pt(NH_3)_4Cl_2$ and $Pt(NH_3)_4(OH)_2$ with the silica gel Sorbosil grade AQ U30. It was washed, dried in air at 378 K, and reduced under flowing hydrogen for half an hour at 673 K. In the as received form, it is partly oxidised. It has a total surface area of 185 ± 5 m^2g^{-1}, with a 60% metal dispersion. The particle size distribution ranges from 0.9 to 3.5 nm, with 75% less than or equal to 2.0 nm in diameter [26, 29]. In comparison with practical platinum catalysts, EuroPt-1 has a high metal loading (*cf.* 1% weight for vehicle emission control [12]). This has advantages for experimental techniques such as infrared spectroscopy. The particle size distribution is also narrower than real catalysts.

The aim of the European Research Group on Catalysis was for the Euro series of catalysts to become research standards. This has to some extent succeeded, with a steady trickle of papers using EuroPt-1 for spectroscopic and catalytic studies [30, 31]

1.4.2 Deuterium Exchange.

The traditional approach of Mittasch *et al.* outlined above gives useful rate and product information. One method for gaining more information on reaction

intermediates for hydrocarbon reaction is using deuterium exchange. When an exchange catalyst is exposed to a hydrocarbon/deuterium mixture, the deuterated products formed by the initial exchanges are determined by the nature of the adsorbed intermediate. When backed up by gas chromatography to examine for isomerisation and hydrogenolysis, mass spectrometric analysis of the products reveals the degree of deuteration. Although a mature technique [32, 33], it is still producing useful pointers towards reaction intermediates and mechanisms [34].

1.4.3 Surface Science.

The modern trend in research has been to work more towards the mechanism of the surface reaction and the chemistry of the catalyst/adsorbate interface, with the hope of making catalyst choice and development more deterministic. Heterogeneous catalysts are multiphase, multicomponent systems where it can be difficult to relate cause and effect. In an effort to simplify the situation, much research has been invested in the study of specially prepared surfaces with fewer variables, in a form accessible to a wider variety of analytical methods.

Single crystals of any catalytically important metal can be grown, cut and polished to present a face of known orientation (normally denoted by the Miller indices of the plane [35]). When placed in an ultra-high vacuum (UHV) system, pumped by oil diffusion, turbomolecular, ion or cryogenic pumps, the single crystal can be examined by electron, atomic and electromagnetic spectroscopies, many not applicable at atmospheric pressures. Lists of these spectroscopies and their acronyms have been collected in general texts [36, 37].

A fundamental disadvantage of this field is that in simplifying the system, it has been distanced from the catalysts that are being modelled.

1.5 Vibrational Spectroscopy.

In the investigation of the nature of adsorbates, many of the important tools come under the umbrella of vibrational spectroscopy. In any chemical system,

where two species are joined together by a bond of force constant, k, there will be a vibration along the bond at some frequency, ν. Quantum mechanics tells us that the bond may vibrate with an energy, $(n + 1/2)\nu$, with n any non-negative integer [38]. The frequency is a function of the force constant (bond strength) and reduced mass of the system. By exciting the molecular vibrator with a photon or particle as a probe and monitoring changes in the probe, or in some secondary process, we can discover the frequency of the vibration, as it moves between quantum states (values of n). This frequency is characteristic of that bond energy, and thus acts as a label for that species.

In heterogeneous catalysis, our primary objective is an understanding of the mechanism of reaction, derived from knowledge of the adsorbed state. If vibrational spectroscopy can be applied to that adsorbate, we may be able to identify the surface species, and hence pinpoint the actual reaction path.

1.5.1 Surface Probes.

Within the range of molecular vibrational energies, there are two main variables in the spectroscopic techniques, the probing method, and the detection of the induced changes. The probes may be quanta of electromagnetic radiation, or particle beams of energy chosen to give de Broglie wavelengths comparable to that of the vibration being monitored. The commonly used probes are as follows:

1. Helium atoms. Due to the nature of the helium atom, it interacts very strongly with the sample, and penetrates no further than the surface layer. It interacts best with vibrational modes involving a large change in momentum. Although adsorbates might be visible with helium atom scattering, it is most commonly used to investigate surface phonon modes [39] involving the generally heavier substrate atoms. Collimated atomic beams can only be used under high vacuum.

2. Neutrons. Neutrons are inherently less interacting than atoms or charged particles. For a 1cm thick sample exposed to a neutron beam, most of the

neutrons will pass straight through. Some will be scattered inelastically with an energy change equal to the scatterer's vibrational frequency. The scattering cross-section in Inelastic Neutron Scattering (INS) is a strong function of the scattering isotope nucleus, and is by far highest for hydrogen [40]. When looking at a hydrogen containing adsorbate on a carbon supported platinum or nickel catalyst, the three elements of which each have a small scattering cross section, the technique becomes highly surface specific. It is less useful for silica and alumina supported catalysts.

3. Electrons. A beam of electrons incident on a planar surface may be reflected specularly by various scattering mechanisms. Although most will be elastically scattered, a number will experience energy losses which correspond to surface vibrational modes.

4. Photons. Electromagnetic wave packets are the longest established probe for vibrational spectroscopy. The wavelength range corresponding to molecular vibrations is the infrared, but higher frequencies may be used for scattering (in a manner similar to the three probes mentioned above) in Raman spectroscopy. Light is generally surface selective, especially for adsorbates on non-transparent substrates such as metals.

Once the probe has interacted with the adsorbate, it is detected by whatever means is appropriate, and the resulting spectrum analysed.

1.5.2 Vibrational Spectroscopy of Supported Catalysts.

Infrared Spectroscopy

Transmission infrared spectra of catalysis supports and adsorbed species have been recorded since the late 1940s [41], though the first work on supported metal catalysts was carried out some years later by Eischens and co-workers [42]. This technique, described as "one of the most noteworthy achievements of surface

chemistry" [43] proved both powerful and popular, sufficient to fuel a major review in 1958 [44].

The first problem in transmission infrared spectroscopy is the introduction of the sample into the beam path of a spectrometer. In some of the early work this was achieved by placing the powdered catalyst on top of a horizontal infrared transparent window, and passing the light through vertically [44]. With the supporting window as part of a glass cell, the catalyst could be prepared and dosed with gases *in situ*. This arrangement is somewhat awkward with the design of modern spectrometers, and most current research uses catalyst pressed into self supporting discs [45]. The choice of sample must also be made carefully. The support particle size must be low to prevent scattering losses [46], and metal particle size must not be too large or absorption by the infrared impermeable metal will become large. Another method of sample presentation is evaporation of the metal directly onto monolithic support material such as silica or alumina [47], though again this might be regarded as somewhat *passé*.

Diffuse reflectance spectroscopy does not generally require the same degree of sample preparation as transmission infrared. The powdered sample is illuminated either diffusely or by a collimated beam, and only the scattered light (the loss mechanism in transmission spectroscopy) measured. This is of much lower intensity than the levels measured in transmission, and has in the past been used mainly in the ultra violet and visible regions of the spectrum to investigate coloured compounds [48]. Recent improvements in Fourier transform spectrometers and redesign of the optics specifically for infrared work [49] have led to a resurgence under the acronym DRIFT(S) {Diffuse Reflectance Infrared Fourier Transform (Spectroscopy)}. The main advantages of DRIFTS are ease of sample preparation and increased relative signal at high wavenumbers for particulate samples. As the chosen technique for this thesis, DRIFTS will be discussed further in Chapter 3.

Raman Spectroscopy.

Raman spectroscopy is based on a scattering rather than resonant absorption process, and hence has very low signal levels, typically 10^{-6} of the input energy [50]. This leads to problems of sample heating for supported metal catalysts, from absorption of the powerful laser light used as the probe, giving desorption of adsorbates and degradation of the sample, or alternatively, very long collection times.

Raman spectroscopy has the advantage that good transmission of the probe light is not required, so even under strong absorption, a scattered signal may be obtained. Catalyst support materials tend to be weak Raman scatterers, so the recorded spectrum does not have the blackouts and support peaks typical of infrared spectra. The information produced tends to be complementary to that of infrared, due to the selection rules of the interaction. Despite this, the publishing rate for Raman studies is as much as an order of magnitude lower than that for infrared studies [51].

The surface enhanced Raman effect, with signal increases of six orders of magnitude, seems confined to particular systems, involving only highly conducting metal surfaces such as silver and gold [52].

1.5.3 Vibrational Spectroscopy in Surface Science

Electron Energy Loss Spectroscopy

Far and away the most generally used vibrational technique used in surface science is Electron Energy Loss Spectroscopy (EELS) [53]. Electrons have been used as a structural probe for many years, since the famous Davisson and Germer discovery of electron diffraction by single crystals [54] and its application to surface and overlayer analysis as low energy electron diffraction (LEED) [55, 56]. The first vibrational spectra, of hydrogen on tungsten, were published in 1967 [57], and the field was quickly opened up by Ibach and co-workers [58]. Although early work concentrated on surface phonons, Ibach *et al.* soon moved on to more catalytically

interesting systems, such as ethyne on Pt(111) [59].

Since then, a wealth of information has been obtained on adsorbate/single crystal systems. The advantages of EELS for this work include the large spectral range and high sensitivity. The accessible frequency range stretches from the tail of the elastic peak (from which modes of a few hundred wavenumbers may be resolved) to above three thousand wavenumbers. It is also a very sensitive technique capable of detecting fractions of a monolayer of even weak chromophores.

Of the disadvantages, perhaps the most serious is the need for high vacuum to make the measurements. Studies at real catalytic pressures (typically atmospheric and higher) are limited to exposure followed by evacuation, which begs the question of the immutability of the adsorbates under the pressure change. The uncertainty in what exactly is being measured is also apparent in some submonolayer studies, where coverage is varied by heating to a certain temperature, then cooling back down to a low measuring temperature. In such experiments, the adsorbate is often assumed to be 'frozen' in the high temperature form, an assumption on which doubt has been cast in the literature [60]. Another weakness of EELS is the low resolution. The absolute limit is determined by the energy spread of the incident electron beam, though spectra are usually run with a trade-off between resolution and sensitivity to give around 40 cm^{-1} resolution.

Reflection Infrared.

A technique which avoids some of the drawbacks of EELS is variously known as Reflection Absorption InfraRed Spectroscopy (RAIRS), Reflection Absorption Spectroscopy (RAS) and Infrared Reflection Absorption Spectroscopy (IRAS). The first experiments of this type were performed using multiple reflections of the infrared radiation from mirrors of catalytically interesting metal films on glass [61, 62]. Following theoretical analysis by Greenler [63, 64], it became clear that a single reflection gave near optimum signal, and with the advantages of simpler experimental design and the availability of single crystals, this has become the

norm.

The sample area in RAIRS is limited by the physical size of the single crystal. Typical surface areas are about $1cm^2$, which give approximately 10^{15} adsorption sites. Although this is the same as for the EELS set up, the interaction probability, even at the optimal near grazing incidence, is lower for photons than electrons. This lower sensitivity limited much of the early RAIRS work to adsorption of CO, a strong chromophore. With improvements in experimental design, advances in detector technology and replacement of dispersive spectrometers with more sensitive Fourier transform instruments, this has become less of a problem, and hydrocarbon adsorbates are now regularly studied [65, 66, 67].

The two main advantages of RAIRS are its resolution and tolerance of atmospheric gas phase pressures above the sample. Although resolution always has a trade-off with sensitivity, better than 1 cm^{-1} may be achieved in realistic situations [65, 66], though around 5 cm^{-1} is often adequate. Gas phase spectra may be eliminated by subtraction of a reference spectrum, or by polarisation of the infrared beam [68]. In RAIRS, only the p component of the infrared beam can interact with the adsorbate, whereas the gas phase interacts with both p and s radiation [69]. Polarisation modulation can thus cancel out the gas phase leaving only the features of interest.

Other spectroscopies which are used include helium atom scattering from single crystals, and photoacoustic spectroscopy, inelastic neutron scattering and inelastic electron tunneling spectroscopy from supported catalysts and other model systems. Each has its particular pros and cons, but all are less well developed or routinely available than those mentioned above, and will have little bearing on this thesis.

1.5.4 Selection Rules.

When a probe is incident on an adsorbate, it may or may not interact with it. The probability of interaction is governed by physical rules, derived from electromagnetic and quantum mechanical principles.

Free Molecules.

Any free molecule containing N atoms has 3N degrees of freedom (combinations of the N atoms moving in three directions). Of these, three will correspond to translations of the molecule as a whole, three to molecular rotations (two for linear molecules), the remaining 3N–6 (or 5) due to molecular vibrations.

When an infrared photon is incident on a free molecule, it is equivalent to an incoming electromagnetic wave of appropriate frequency. The photon can only be absorbed by setting up a corresponding electromagnetic fluctuation in the molecule. This will occur when there is an electric dipole with a component in the direction of a molecular vibration which matches the frequency of the photon.

Alternatively, a higher energy photon can be scattered by dipole moments induced in the molecule due to the electron polarisability. This Rayleigh scattering becomes Raman scattering when the electron polarisability is modulated by a molecular vibration, and an energy quantum lost or gained by the photon [70].

Thus for a vibrational mode to be infrared active, it must have a dipole change associated with it, and to be Raman active, it must give rise to a change in the polarisability ellipsoid. For a molecule with an inversion centre, these two requirements are mutually exclusive, making infrared modes Raman inactive, and *vice versa.*

Surface Adsorbed Molecules.

When the free molecule is adsorbed on a surface, it is no longer free to translate and rotate as before, and so regains the six (or five) degrees of freedom associated

with these motions as vibrations. These are known as frustrated translations and rotations. The next complication is that the surface has its own set of normal modes. With three modes per surface atom, there are too many to be regarded individually. They are considered together as a continuum of phonons (vibrational quanta), which may be measured by helium atom scattering or other techniques [39]. Thankfully for the catalytic chemist, because these modes involve very heavy metal atoms, the frequencies are much lower than those of adsorbates involving light elements such as carbon, oxygen, nitrogen and hydrogen. This frequency gap prevents significant mixing of the adsorbate and substrate modes, and adsorbate vibrations may be identified by comparison with the spectrum of the free molecule. Changes from the free space behaviour give information on the bonding, configuration and environment of the adsorbate in the form of frequency shifts [71] and line widths [72].

The metal substrate alters not only the physical form of the adsorbate, but also the probe/molecule interaction. When a conductor is placed in an electromagnetic field (such as that produced by an incident photon or electron), by Maxwell's equations, the tangential electric field must be continuous across the boundary between the metal and its surroundings. However, inside a perfect conductor, there are no electric fields, as any induced field will be cancelled by the freely moving electrons. The tangential field at the surface is thus zero as well, and so the electric field is purely perpendicular. If there is no tangential field, adsorbed molecules with dipoles parallel to the surface see no effect of the incident photon, and cannot interact with it. Thus only vibrational modes with dipoles perpendicular to the surface are allowed in RAIRS and dipole scattering EELS.

An alternative picture for this is the image dipole model. When a dipole exists above a metal surface, it induces an image dipole in the bulk metal (Figure 1.3). From the point of view of the approaching photon or electron, this cancels out any horizontal dipoles, and enhances vertical ones, so interaction can only occur

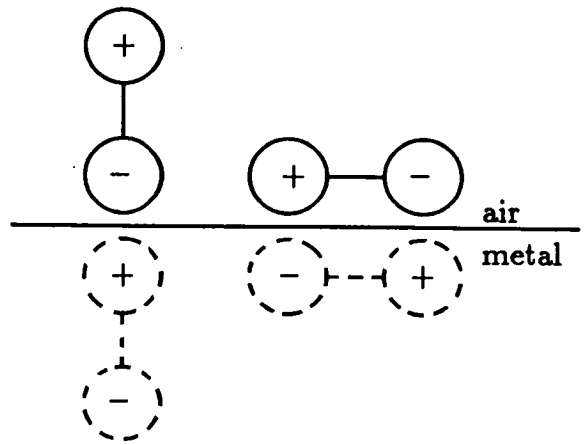

Figure 1.3: Image dipoles in a metal surface.

for vertical dipoles. This is simply a different way of describing the previous paragraph, and both models are only good for infrared frequencies. At higher frequencies, most metals are not sufficiently good conductors to respond to the imposed fields.

This effect, known as the Metal Surface Selection Rule (MSSR) has been shown to hold over 25nm above copper single crystals in RAIRS spectra [73]. The MSSR will also hold for large spherical particles - the plane surface is after all the surface of an infinitely large sphere. However, if the metallic sphere is made progressively smaller, it will eventually become a single atom, which cannot give the MSSR effect. There must therefore be some intermediate size where the MSSR tends to break down. This situation has been analysed by Greenler *et al.* [74]. They defined the surface ratio, SR as

$$SR = \overline{E_t^2}/\overline{E_r^2} \tag{1.4}$$

where E_t and E_r are the electric field components tangential and radial to a metal sphere. As the infrared absorption intensity is proportional to the square of the field, SR gives a measure of how well the MSSR holds. For the ideal conducting infinite sphere, when the MSSR holds perfectly, SR will be zero. If the imposed field is not affected by the metal sphere at all, then SR will be two.

Greenler solved Maxwell's equations for a sinusoidal wave incident on a sphere

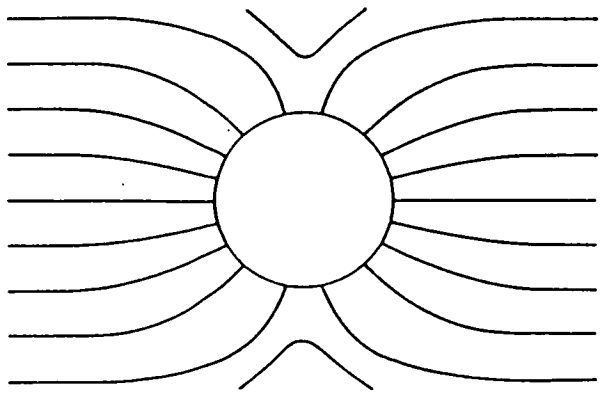

Figure 1.4: Field lines round a metal particle under the classical model.

using scattering theory formalism, which gave Mie type scattering [75]. Applying the finite radius condition and other assumptions allows the electric field to be calculated from a static potential, E_t and E_r extracted, and their squares averaged over the metal surface to give SR as a function of $\tilde{n}$, the complex refractive index of the metal, r_0 the particle radius, and d, the distance from the surface for which SR was being evaluated. By choosing copper as an example, SR was calculated for various r_0 and d. This led to the slightly surprising result that at $d = 0$, SR was close to zero for any sphere, even with very small values of r_0. At higher d values, SR increased sharply for small r_0. The applied electric field was therefore perpendicular to the metal sphere at its surface, with the curvature from the parallel dependent on r_0. The field lines thus are constant relative to the sphere, and Figure 1.4 may be scaled for any particle radius.

The above was a purely classical derivation for a sharp spherical boundary. This description is clearly not valid for particles in a catalyst such as EuroPt-1 with its approximately 50 atom clusters [30]. Greenler also considered quantum effects using various models from the literature [76]. Following these calculations, he concluded that the MSSR would hold for particles larger than about 2nm. This value has been widely quoted in subsequent infrared studies [77], but from tables in Greenler's paper [74], it is clear that this is a conservative value. The most pessimistic calculations of the four methods he used (one classical, three quantum) suggests that for even 1.0 nm particles, at 0.2 nm above the surface,

$SR = 0.2$. Thus provided an adsorbate is not too large, the MSSR will hold to good approximation even for catalysts such as EuroPt-1 with its 1·8 nm average particle size.

As stated above, the MSSR holds for RAIRS, infrared of supported metals (unless the particles are *very* small), and EELS when the electrons are dipole scattered. There is, however, a second scattering mechanism in EELS known as impact scattering. This is a shorter range multipolar interaction which has more efficient momentum exchange with the electron and hence increases the angular distribution. Impact scattering may thus best be seen away from the specular angle where it is swamped by dipole scattering. The selection rules are also less restrictive, with only vibrations antisymmetric to the plane of incidence forbidden, and then only if the plane of incidence is a plane of symmetry of the scattering system [78]. The more intimate nature of the impact scattering interaction also leads to a higher probability of scattering at overtone frequencies [79].

1.5.5 Mixing it : Using Surface Science as a Model for Supported Catalysis.

As is clear from some of the references cited in Section 1.5.3 above, scientists have been collecting infrared spectra of adsorbates on supported metal catalysts for decades. The number of studies in enormous, as is the range of systems which have been investigated, and the enquiring mind starts to wonder how much can be gained from similar work now. The big differences today have come about due to advances in instrumentation, a better understanding of the physical basis of infrared spectroscopy (see Section 1.5.4), and a wealth of information from surface science.

Early work, such as that of Morrow and Sheppard [80, 81] produced spectra which were too complicated to be fully understood. The only comparisons they had at the time were spectra of the gas and liquid phase hydrocarbons, and supported metal work by other workers, *eg.* [44, 82]. Several of their assignments of infrared bands to surface species have since been shown to be wrong. Part

of the reason for this is because they eliminated species from consideration due to missing bands, whereas we now know that the missing bands were forbidden by the MSSR. The wealth of information from EELS and RAIRS, especially in conjunction with other surface science techniques such as Low Energy Electron Diffraction (LEED) and Angle Resolved Ultraviolet Photoelectron Spectroscopy (ARUPS), has produced assignments for adsorbates on single crystal surfaces. When only a restricted range of surface sites are available, fewer types of surface species are formed and the spectra are generally simpler [72]. This has produced triumphs such as the identification of ethylidyne as the main species produced on ethene adsorption on Pt(111) [83]. One of the final pieces of that jigsaw was the comparison with an organometallic model compound containing an ethylidyne ligand [84]. Model compounds thus are another useful tool in the assignment armoury.

With high resolution RAIRS spectra being produced for hydrocarbons on metal single crystals [85], the opening now exists for reappraisal of infrared spectra on supported metals, especially given the recent improvements in spectrometer technology.

1.6 Alkali Metals in Surface Science.

Alkali metals were first introduced into surface science before the second world war by Langmuir *et al.* [86] who hoped that potassium's low work function would improve the electron emission of cathodes in electrical valves. Although this particular application has been superceded by semiconductor devices, research in alkali metal adsorption on metals has not died down. Part of the reason for this is no doubt similar to that for the wealth of carbon monoxide adsorption work. It is very easy to work with, and it produces experimentally measurable changes to metal single crystal surfaces. Alkali metal sources are easily available (from SAES Getters [87]) which deposit high purity films down to fractions of a monolayer. Such films have been extensively studied by vibrational and electronic

spectroscopy in coadsorption with carbon monoxide and other adsorbates.

This research is often justified with reference to the promotion effects noted in heterogeneous catalysis of additives containing alkali metals, generally as the cation, as described in Section 1.3.3 above and in reference [24]. The most important metals mentioned in this review by Mross are iron, for the ammonia synthesis catalyst, and nickel, used for the Fischer-Tropsch reaction. These metals have therefore been one area of concentration for the surface scientists, with studies such as those of Ertl *et al.* on coadsorption of hydrogen, nitrogen and potassium on iron single crystals [88]. As is so often the case in surface science though, the majority of the work for both iron and nickel has been alkali metal coadsorption with carbon monoxide [89].

Platinum single crystals have also proved popular as substrates for alkali metal coadsorption studies. This is in part due to interest from electrochemists, as model systems for ion/water interaction such as that of Sass [90]. The systems examined, as well as extensive CO/K studies [91], include potassium coadsorption with ethene [92], benzene [93], and other π-electron donating adsorbates [94].

1.7 Thesis Aims.

The platinum single crystal studies of potassium coadsorption with hydrocarbon adsorbates suggest that study of supported platinum catalysts with alkali doping should prove of some interest. Such catalysts were made and characterised by Mushtaq Ahmad in this university [95], based on the standard research catalyst EuroPt-1. The aim of this thesis was to examine hydrocarbon adsorbates on these catalysts by diffuse reflectance spectroscopy, identifying surface intermediates through comparison with single crystal surface studies of similar systems. Further information on the adsorbates was gained using deuterium exchange.

Chapter 2

Deuterium Exchange

2.1 Introduction

The heavy isotope of hydrogen has been a tool in catalytic investigations since it became available for use in 1933 [96]. Early experiments detected the extent of hydrogen replacement with deuterium in catalytic reactions by different techniques. Farkas and Farkas [97] monitored the change of conductivity of deuterated water, Horiuti and Polanyi [98] measured its density by micropyknometer, and Taylor and Morikawa [99] compared the intensity of gas phase infrared spectra with those of prepared isotopic mixtures, but the subject really took off with the introduction of the mass spectrometer.

The three first mentioned techniques give an average number of deuteriums incorporated per molecule, D_{av}. The mass spectrometer, however, gives the isotopic distribution, D_i, the percentage of the hydrocarbon containing i hydrogens replaced by deuterium, provided the parent molecule is monitored. Even in molecules like 2,2-dimethylpentane, which are difficult to ionise without fragmentation, the distribution may be found using a major fragment such as $C_4H_9^+$.

The mass spectrometer does not give information on exactly which hydrogens within the molecule are exchanged. The use of arguments of molecular symmetry (*eg.* in the case of the D_5 peak in cyclopentane exchange [100]), the analysis of different fragment ions under harsher ionising conditions [101], infrared spectroscopy [102], and microwave spectroscopy [103] have all been used for this with varying success. Perhaps the best technique though has been nuclear magnetic resonance (nmr) spectroscopy. Earlier studies monitored decrease of proton nmr signal against a standard during exchange, but more recently, with instrumental improvements, the deuteron signal can be measured directly [104].

A major surprise for the early experimenters was that despite a much lower carbon–carbon than carbon–hydrogen bond energy (typically 347 $kJmol^{-1}$ compared with 414 $kJmol^{-1}$ [105]), deuterium/hydrogen exchange for hydrocarbons started at temperatures approximately 60 K lower than hydrogenolysis [99]. The ready exchange into alkanes clearly could not follow the Horiuti-Polanyi associative mechanism suggested for alkene exchange. Various dissociative absorption mechanisms have been suggested, and many subsequent studies have pursued the experimental theme to discover information on the chemisorbed intermediates in hydrocarbon reactions.

It was hoped that deuterium exchange studies of butane over EuroPt-1 would produce information on the number, and possibly the types, of hydrogens lost from the molecule during chemisorption on the metal crystallites. Butane exchange with a Pt/SiO_2 catalyst has been studied in this university [106], but the catalyst had a very dfferent dispersion from EuroPt-1. The effect of potassium doping on the exchange activity of EuroPt-1 was also studied.

2.2 Experimental

2.2.1 The Vacuum System

These experiments were carried out on a Pyrex glass vacuum line with gas handling facilities, as shown in Figure 2.1. All taps were Springhams high vacuum ground glass stopcocks lubricated with Apiezon L high vacuum grease. The circulating loop and catalyst reaction vessel (H to J) and the gas handling side of the line (A to E) were pumped independently using electrically heated three stage mercury diffusion pumps, each backed by an Edwards ED50 rotary pump. Mercury contamination of the line was reduced by liquid nitrogen cooled cold traps. The vacuum level was monitored using a McLeod gauge at all relevant stages of the experiment, and was typically of the order 10^{-2} Nm^{-2}.

Deuterium [163] was introduced into the line from a regulated lecture bottle via a ground glass joint (A) to a reservoir (B). This was purified by passage

through a palladium thimble (heated to dull red heat) and a liquid nitrogen cooled cold trap to the previously evacuated volume (C). Butane [163] was admitted from a regulated lecture bottle through a ground glass joint (D) to reservoir (E). Before use any contamination by air was removed by repeated freeze/degas/thaw cycles using the cold trap in the recirculating loop. Pressures of reagent gases were measured using the mercury manometer. Hydrogen for reduction of the catalysts was introduced via joint (D) from a regulated gas cylinder (BOC) after passage through a Deoxo unit (Englehard) to remove oxygen and a liquid nitrogen cooled cold trap containing zeolite 4A molecular sieve to remove water. Positive pressures in the line were prevented by the open ended mercury manometer and the hydrogen flow vented to atmosphere via tap (H).

The recirculating loop could be isolated from the gas handling line by multiple port glass taps (F). The reactant mixture was circulated by an all metal reciprocating pump (Metal Bellows Corporation, MB21E). This produced a flow rate in excess of 0.8 $lmin^{-1}$ as measured by a floating head rotameter incorporated in the loop (also used to monitor the hydrogen flow rate during reduction). This ensured that reaction rates were not limited by pumping speed [108]. A glass finger in the loop was used as a cold trap for butane purification (see above) and to freeze down the butane during admission of the deuterium to the loop. The reaction vessel (G) was mounted in the loop by ground glass ball and socket joints, sealed by high temperature Apiezon T vacuum grease and secured by lockable spring clips. The catalyst was held in the sample bulb by plugs of glass wool above and below. A small well in the bulb wall allowed the reaction temperature to be monitored using a type K (Chromel/Almumel) thermocouple and a Comark 3000 digital thermometer. The whole vessel was heated using a purpose built close fitting electrical furnace [108], controlled by a Eurotherm (PID-SCR) proportional temperature controller, also connected to the thermocouple.

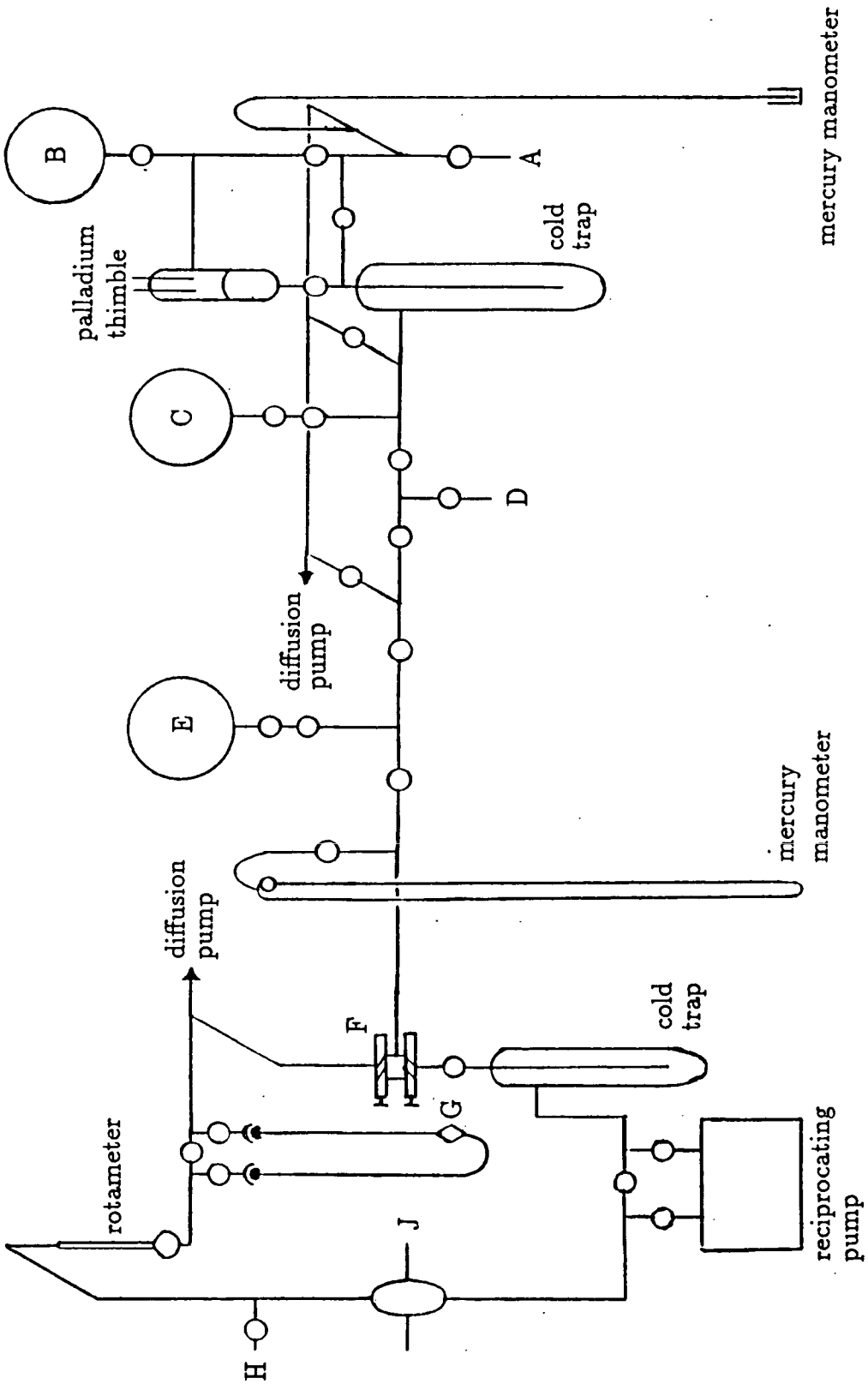

Figure 2.1: Glass vacuum line for deuterium exchange reactions.

2.2.2 Mass Spectrometry

The recirculating loop was connected to a mass spectrometer via a capillary leak (I) which allowed the loss of about 2% $hour^{-1}$ of the reaction mixture, giving a pressure of 10^{-2} Nm^{-2} in the ionising chamber. The Vacuum Generators Ltd Micromass 601 used is a fast scanning 90° magnetic sector instrument. The gas was ionised by electron bombardment from a heated tungsten filament. The electron energy was adjusted to achieve a compromise between adequate sensitivity and minimum fragmentation of the gas molecules.

The mass region covering the parent ion, its adjacent fragments and the deuterated derivatives was scanned by varying the magnetic field strength at constant ion accelerating voltage. The resulting spectra were recorded on a fast response potentiometric chart recorder (Kipp and Zonen, BD40). The typical range of fifteen mass units was scanned over approximately four minutes. During the scan, the amplifier (Vacuum Generators Ltd, Chopper Amplifier CA2) was adjusted to maximise peak heights, which when the peaks were measured manually resulted in a dynamic range (*ie.* the ratio of largest to smallest intensity measured) of the order 10^4.

2.2.3 Gas Chromatography

Samples from the reaction mixture were introduced to the gas chromatograph (Perkin Elmer F33) via (J) of Figure 2.1. As illustrated in Figure 2.2, the sample loop of a six-way gas sampling valve (Carle Instruments Inc.) could be evacuated via a three-way ground glass tap before being filled from (J). Turning the Carle valve introduced the sample to the carrier gas stream, and it was flushed into the g.c. column. The column packing (3% squalane on activated alumina H in 2 m of 1/8″ o.d. stainless steel tubing) and oxygen free nitrogen carrier gas pressure of $3.3x10^5$ Nm^{-2} at an oven temperature of 390 K were chosen to optimise separation of potential reaction products (*ie.* chosen to give different partition ratios between stationary and mobile phases for any reaction products). Detection was by a

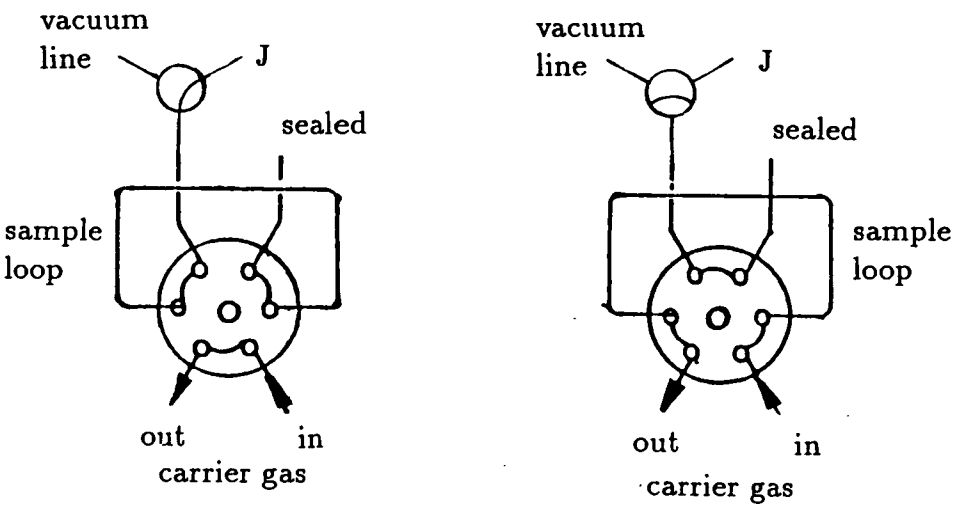

Figure 2.2: The operation of the Carle valve.

flame ionisation detector. The conductivity of the hydrogen flame changed when material in the eluent was burnt, and the resulting signal was sent to a Perkin-Elmer laboratory computing integrator (LCI–100).

2.2.4 Experimental Procedure

A weighed catalyst sample was placed in the reaction vessel, connected to the vacuum line and the sample outgassed until a good vacuum was obtained. A flow of hydrogen was set up in the bypass loop, then diverted over the catalyst. After an hour's reduction at 670 K the sample was again outgassed at the elevated temperature for thirty minutes, then cooled to the experimental temperature.

During this cooling period, the reagent gases were prepared in the recirculating loop. Purified butane was expanded into the cold finger, condensed, and deuterium added, usually in 5- to 10-fold excess, before allowing the butane to heat up to room temperature. Reagent flow was set up round the bypass using the pump, and sample mass spectra taken for future reference. The catalyst was introduced to the gas flow on reaching reaction temperature and the bypass closed. Mass spectra were taken at intervals and gas chromatograms recorded when significant reaction had taken place. The experiments were run for several

hours, or until the extent of reaction reached *circa* 50%.

2.2.5 Data Analysis

The mass spectral data was analysed using a FORTRAN computer program [109] on the university mainframe, a Sequent Symmetry S81, running the Unix operating system (DYNIX(R) V3.1.4). Each mass spectrum was recorded as a series of chart recorder peaks corresponding to a selected range of mass/charge ratios. The peak intensities were measured by hand, scaled according to the amplifier gain used during collection, and collated for data entry. D_i is used to denote the hydrocarbon containing i hydrogens replaced by deuterium, and D_∞ the equilibrium value for the unexchanged hydrocarbon, D_0.

Once entered, the first correction to the data was for naturally occurring isotopes of carbon and hydrogen, which were assumed to be present in the normal ratios. The contribution these would make to higher mass/charge peaks was calculated for the smallest mass peak, and then subtracted from the spectrum. This procedure was then iterated for each of the increasing mass peaks, not surprisingly making the biggest difference to the D_1 peak corresponding to singly deuterated butane.

The other correction was for the contribution of fragmented high mass species to mass/charge peaks of less exchanged moities, necessarily starting at D_{10}, the most exchanged butane. The calculation involved the fragmentation patterns for the fully deuterated and undeuterated butanes, and factors Γ and Π with appropriate statistical weighting for each D_i peak. Following Dowie [110] in analogy with Evans *et al.* [111],

$$\Gamma = \frac{\text{observed probability of losing H from } C_nH_{N-1}D}{\text{statistical probability of losing H from } C_nH_{N-1}D} \qquad (2.1)$$

the enhanced probability of losing a hydrogen from a mixed hydrogen/deuterium hydrocarbon of n carbons and N hydrogen species, and

$$\Pi = \frac{\text{observed probability of losing D from } C_nHD_{N-1}}{\text{statistical probability of losing D from } C_nHD_{N-1}} \qquad (2.2)$$

the reduced probability of losing a deuterium.

The values of Γ and Π used here are those suggested by Dowie [112] for hydrocarbons of unknown isotopic fragmentation patterns.

Assuming that the corrected peak intensities now give a true measure of the isotopic distribution of the butane, they can be subjected to further analysis, following the classic example of Kemball [32]. A useful first step is to define a parameter to describe the mean deuterium content of the butane,

$$\Phi = \sum_{i=1}^{10} iD_i \tag{2.3}$$

where D_i is expressed as a percentage. By this definition, the theoretical maximum value, $\Phi_{max} = 1000$, though this can never be reached in a real exchange reaction, because the deuterium pool will be diluted by hydrogen liberated from the hydrocarbon. A better measure of the maximum, the value for infinite reaction time or equilibrium, Φ_∞, is a function of the reagent pressures of deuterium, a and butane, b used for the exchange:

$$\Phi_\infty = \Phi_{max} \cdot \frac{2a}{2a + 10b} \tag{2.4}$$

In the real experimental situation, this may be further complicated by hydrogen adsorbed on the catalyst, though exchange in excess of Φ_∞ may also be observed [113].

If a rate constant, k_Φ is defined as the initial number of deuterium atoms entering 100 molecules of hydrocarbon in unit time, a first order rate equation may be written as

$$\frac{d\Phi}{dt} = k_\Phi(1 - \frac{\Phi}{\Phi_\infty}), \tag{2.5}$$

which integrates to

$$\log_{10}(\Phi_\infty - \Phi) = -\frac{k_\Phi t}{2.303\Phi_\infty} + \log_{10}(\Phi_\infty - \Phi_o), \tag{2.6}$$

where Φ_o is the initial value of Φ. A graph of $\log_{10}(\Phi_\infty - \Phi)$ against t therefore gives an indication of whether the exchange is a first order process, and from the gradient a value for the first order rate constant, k_Φ.

When the rate of disappearance of the unexchanged butane is represented by k expressed in percentage per unit time, an equivalent first order equation can be set up,

$$\log_{10}(D_0 - D_\infty) = -\frac{kt}{2.303(100 - D_\infty)} + \log_{10}(100 - D_\infty). \qquad (2.7)$$

A graph of $\log_{10}(D_0 - D_\infty)$ against t again gives a straight line for first order reactions, but a more important result of this analysis is the quantity is

$$M = \frac{k_\Phi}{k}, \qquad (2.8)$$

which gives the mean number of hydrogen atoms replaced by deuterium on each visit to the surface during the initial stage of the reaction. Both k_Φ and k are normalised for weight of catalyst used, and therefore have units of number of deuteriums entering 100 molecules per second per gramme of catalyst, and percentage of butane reacting per second per gramme of catalyst respectively, which will be rendered as $s^{-1}g^{-1}$ in the results tables.

2.3 Discussion

The experiment was run on two types of sample, as received EuroPt-1, and 1% potassium doped EuroPt-1. Sample doping was achieved by soaking as received EuroPt-1 in a potassium hydroxide solution and evaporating to dryness in a rotary evaporator, as described in Appendix A. The nominal potassium concentration is its elemental weight as a percentage of the weight of catalyst doped [95].

A good rate of exchange was achieved at *circa* 330 K for the as received catalyst. The doped catalyst was considerably less reactive, and required a temperature of over 370 K to achieve measurable exchange. The reaction was therefore repeated at the same temperature for the as received catalyst.

2.3.1 EuroPt-1 at 331 K

The low temperature exchange of butane with deuterium was run to approaching 50% reaction. First, though, the exchange to 10.8% will be considered. The

As received EuroPt-1 at 331 K				D_2:C_4H_{10} 9.3:1							
$k_\Phi = 0.068\ s^{-1}g^{-1}$				$k = 0.012\ s^{-1}g^{-1}$				M = 5.5			
Product distributions											
	D_0	D_1	D_2	D_3	D_4	D_5	D_6	D_7	D_8	D_9	D_{10}
Initial	–	9.1	7.3	7.7	7.9	8.1	4.1	7.6	6.4	9.9	32.1
15% reaction	89.2	2.1	0.9	0.7	0.8	0.7	0.5	0.7	0.6	1.0	2.8
$\Phi = 62.9$	–	19.4	8.0	6.3	7.1	6.6	5.0	6.4	6.1	9.6	25.6
50% reaction	51.0	8.7	4.1	3.5	3.6	3.5	2.9	3.5	3.9	5.8	9.52
$\Phi = 279.6$	–	18.4	8.6	7.1	7.3	7.1	6.0	7.0	7.7	11.7	19.2

Table 2.1: Exchange data for as received EuroPt-1 at 331 K.

results are shown in Figure 2.3. This shows the percentage converted by isotope against the total butane conversion, *ie.* the variation in D_i with extent of exchange. The first feature to note is that there is measurable exchange into the full range of possible isotopes at the second set of data points, indicating that stepwise exchange is unlikely to be a major contributor to the reaction. The majority species recorded is at D_{10}, with very fast initial exchange, above the scope of the least mean squares line fitted to the data points [115]. The proportion in this species, however, does not retain the same degree of ascendency, and the quadratic fitted to the data has a negative coefficient for the squared term. The second most populated species, D_1, displays an opposing trend over this region. Although it must be realised that due to correction for naturally occurring ^{13}C and ^{2}H, there is more error in this graph than for D_{10}, the least mean squares line curves up quite considerably. The behaviour of the D_9 and D_2 lines mirror the D_{10} and D_1 behaviour, though to a significantly lesser extent.

The behaviour just described is perhaps better illustrated by contrasting Figures 2.4 and 2.5, histograms of product distribution. In Figure 2.4, the distribution was calculated as the gradient of the best fit straight line through the points of Figure 2.3. In Figure 2.5, the linear coefficient of the plotted quadratic was

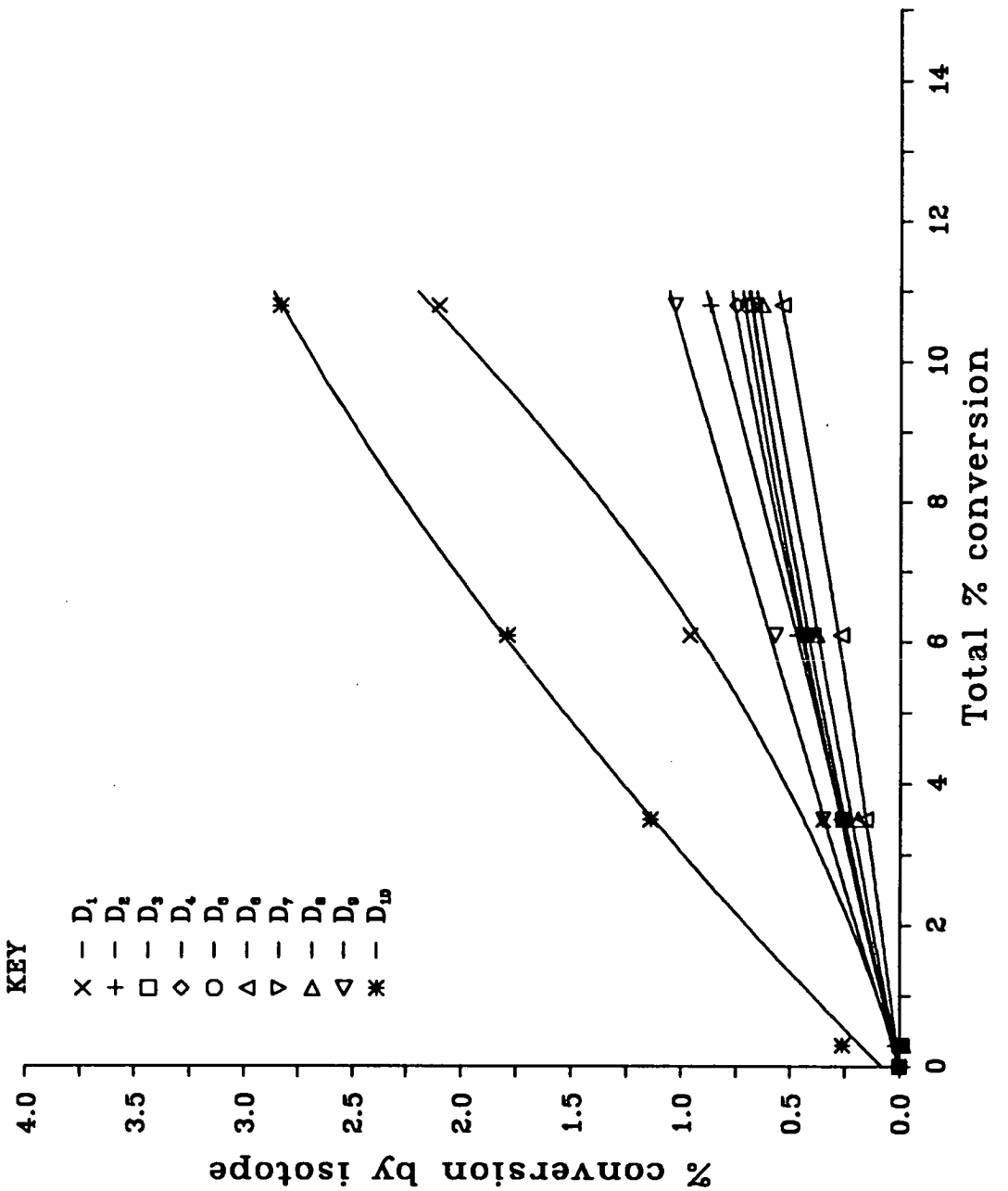

Figure 2.3: Exchange over EuroPt-1 at 331 K to 10.8% reaction

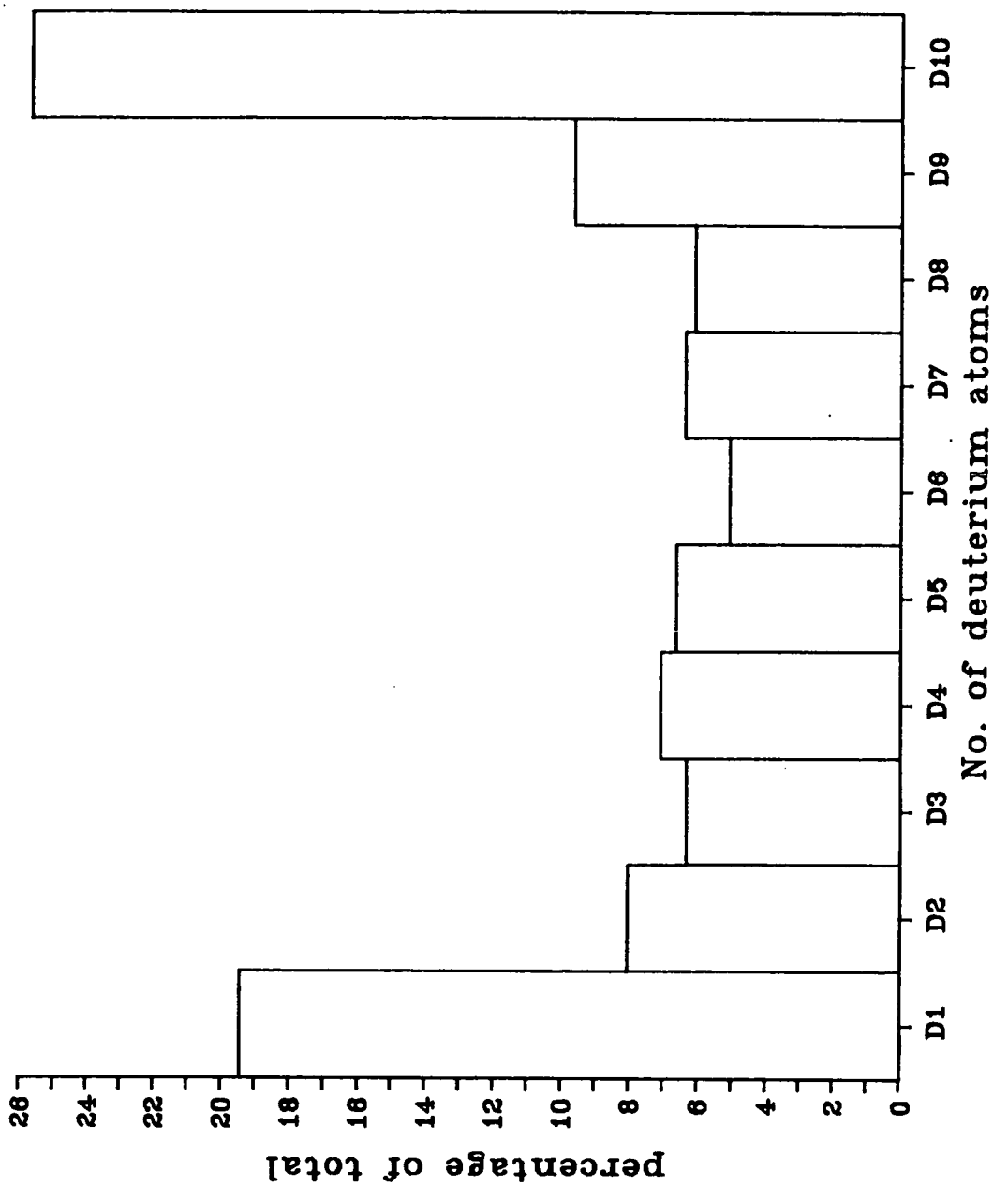

Figure 2.4: Product distribution by isotope for Figure 2.3

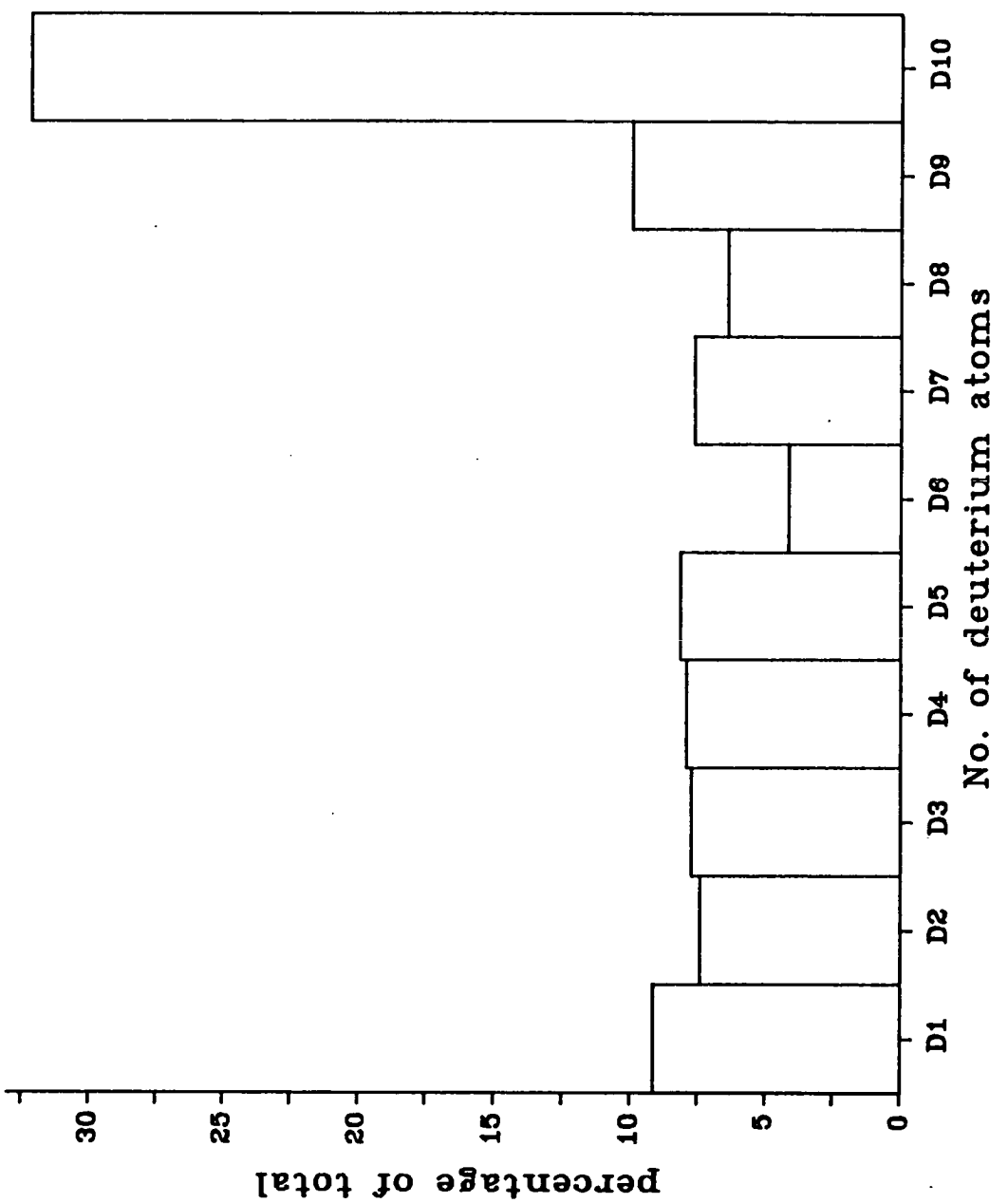

Figure 2.5: Initial product distribution for Figure 2.3

used, *ie.* the tangent to the curves at the zero of Figure 2.3. Figure 2.4 shows a U shaped product distribution, which is in agreement with results over platinum catalysts found by Oliver *et al.* [106] A point of difference in this work is the skew of the U towards the fully deuterated product, compared with Oliver and co-workers, who found greater emphasis on the lower part of the distribution. Figure 2.4 on the other hand bears considerably less resemblance to the Oliver distributions. Far and away the most significant product is D_{10}, with no major contribution discernible from D_1.

Figure 2.6 shows the same exchange reaction taken to nearly 50% conversion, with some trends apparently contradicting Figure 2.3. At this degree of conversion, it is likely that much of the material in the reaction mixture will have reacted more than once. The addition law of probability states that when there are several ways an event can occur, the probability of the event happening is the sum of the probabilities of each of the discrete ways [116]. Thus once one item (molecule) out of a hundred is chosen (reacts), the chances of the same molecule being the next to react is $\frac{1}{99}$. This generalises to the chance of n molecules out of a hundred reacting twice as

$$\text{Probability, } p = \sum_{x=0}^{n} \frac{x}{100 - x}. \tag{2.9}$$

For the effectively infinite number of molecules present in the reaction vessel, the chance that $n\%$ have reacted twice can be similarly calculated from the equivalent integral expression,

$$p = \int_{x=0}^{n} \frac{x}{100 - x} \, \mathrm{d}x \tag{2.10}$$

which from tables of standard integrals [114] reduces to

$$p = 100 \ln 100 - n - 100 \ln(100 - n). \tag{2.11}$$

Thus whereas at 10.8% reaction, only 0.63% of the molecules have reacted twice, at 49.0%, this proportion increases to 18.3%.

Another *caveat* at this degree of conversion is the dilution of the deuterium pool with hydrogen exchanged out of the butane. Assuming that hydroxyls on the

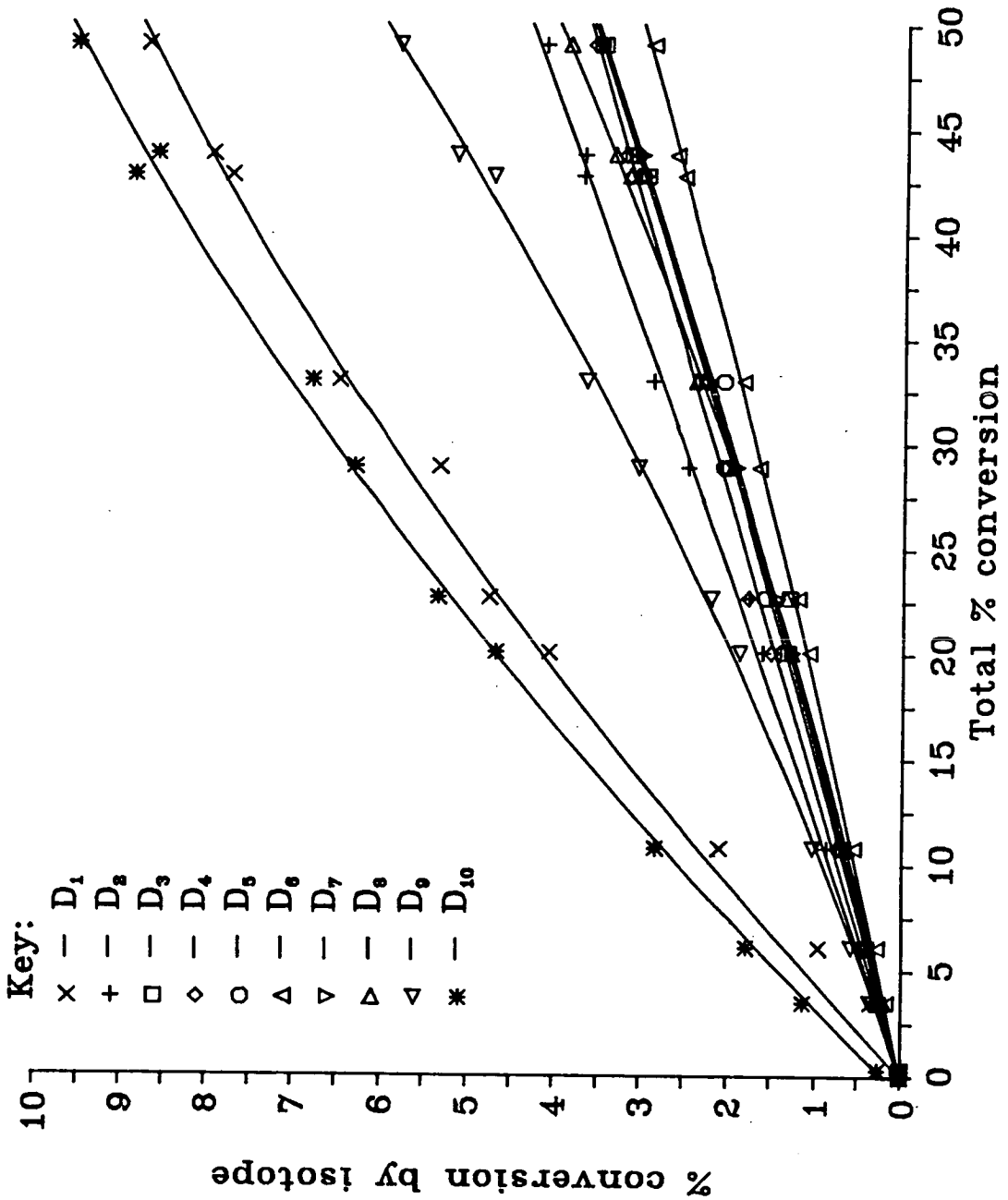

Figure 2.6: Exchange over EuroPt-1 at 331 K to 50% reaction

silica support and any hydrogen left on the metal or spilt over from the reduction do not have a large contribution, the lower limit for exchangeable ^1H may be calculated for the final product distribution. Taking the Φ value from Table 2.1, the percentage of ^1H in the hydrogen pool, f is given by

$$f = \frac{10b.\Phi.10^{-3}}{2a - 10b.\Phi.10^{-3}}.100, \tag{2.12}$$

where a and b are the pressures of deuterium and butane respectively (as on Page 31). For Figure 2.6 f comes out as 15.3%.

The effect these two factors bring to bear on the reaction is shown in the different curvatures of the quadratics fitted to Figure 2.6. The line for D_1, which taken to 10.8% reaction in Figure 2.3 is concave up, is here concave down. The rate is reduced both by the dilution, which means an unreacted butane may be adsorbed and undergo hydrogen/hydrogen exchange rather than hydrogen/deuterium exchange, and by multiple reaction. On a second visit to the surface, as there are two sets of chemically equivalent hydrogens, six in methyl groups and four in methylene groups, statistically there is at best a 1 in 4 chance that a D_1 species will not be further exchanged. This will be only marginally increased by the 15% dilution. Considering also the kinetic isotope effect, which leaves C–D bonds less likely to be broken, the switch from an increasing to decreasing relative rate for D_1 formation during the course of the reaction is well understood.

In a similar vein, the accelerating downward curvature of the D_{10} results may be explained by significant chance of dilution following the exchange of 10 hydrogens with the available pool. This also leads to the increasing rates of D_9 and D_8 production shown on the graph. The product distribution, Figure 2.7, of the straight line gradients derived from Figure 2.6 clearly shows the blurring effect of the dilution under comparison with the distribution at 10.8% reaction. The ratio of highest to lowest column heights is much reduced (see also Table 2.1), and there is a general trend to a higher degree of conversion, which will be due to multiple reaction.

The kinetics of the reaction are shown in Figure 2.8 with plots of $\log_{10}(\Phi_\infty - \Phi)$

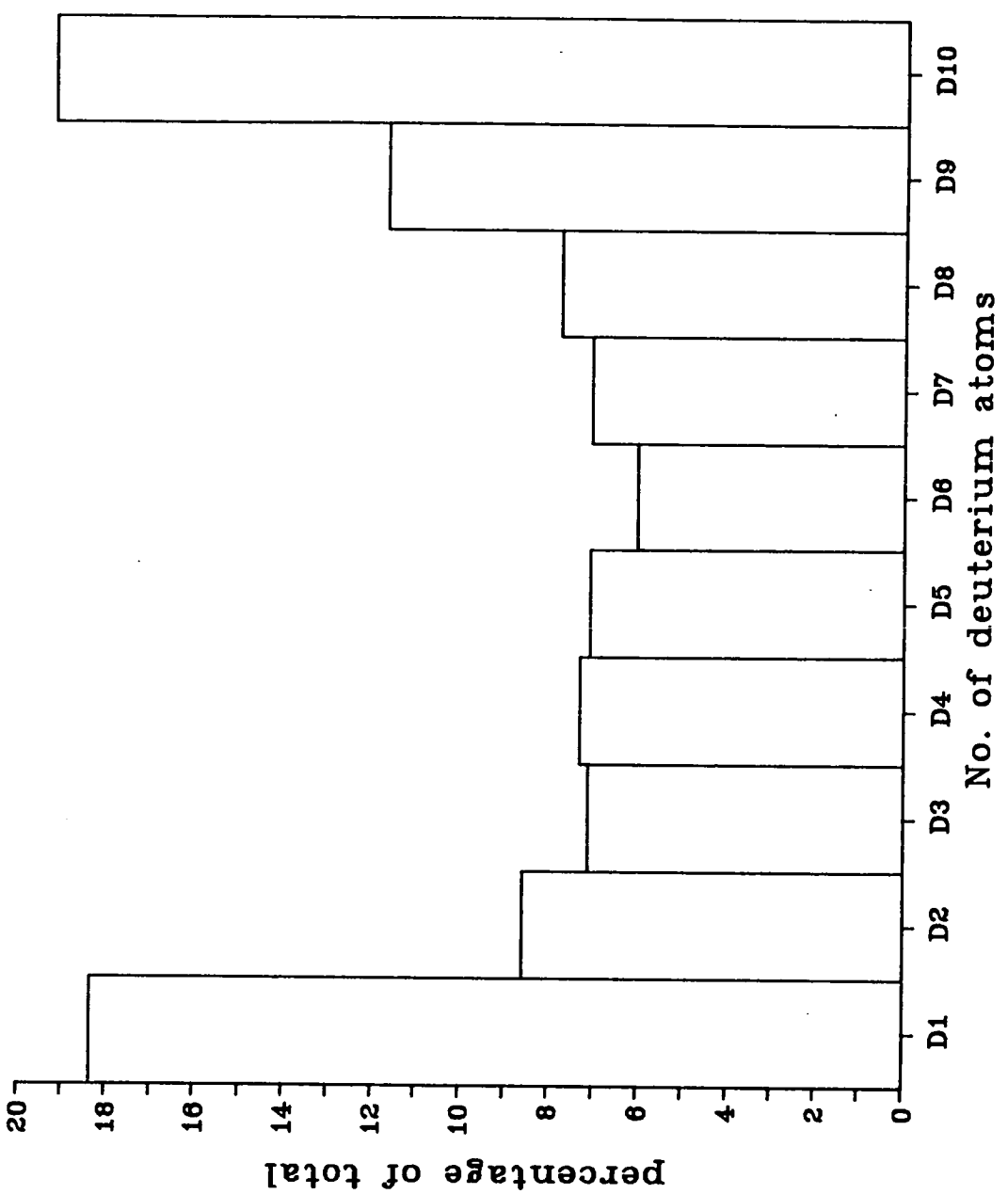

Figure 2.7: Product distribution for Figure 2.6

and $\log_{10}(D_0 - D_\infty)$ against time as described in Section 2.2.5 above. The assumption of first order kinetics implicit in the derivation of Equations 2.6 and 2.7 only holds for the initial five or six data points, the period covered in Figure 2.3. In a similar manner to the initial product distribution from Figure 2.3, the points are fitted with a quadratic function, and the gradient is given by the tangent to this line, as drawn on the graph. Values of k_Φ, k and M are calculated from this gradient, and shown in Table 2.1.

Most of the change of gradient observed in Figure 2.8 will be caused by the dilution effects discussed above. Some of the rate reduction may be due to poisoning of reaction sites, which could be connected with the switch from complete exchange in the initial reaction (Figure 2.4) to single or double exchange which Figures 2.3 and 2.4 show to have increasing importance over the first 10% of reaction. As mentioned in the introduction to this chapter, alkenes may exchange by the associative Horiuti-Polanyi mechanism (Figure 2.9). The alkene is supposed to gain a deuteron adsorbed on the surface, and adsorb itself at the vacated site. Exchange may then propagate through the molecule by what is known as $\alpha\beta$ exchange. A β carbon, or next neighbour to the surface bonded α carbon, looses a hydrogen to the surface in exchange for a carbon metal bond. If the α carbon reverses this step to take up a surface deuterium, the exchange may then propagate through all chemically similar hydrogens. It is well established [117] by experiments on molecules with quaternary carbon atoms such as 2,2-dimethylpropane, that $\alpha\gamma$ exchange does not occur readily. These experiments, along with methane exchange [118] also show that $\alpha\alpha$ exchange has a much higher energy barrier than the $\alpha\beta$ mechanism.

For an alkane to undergo multiple exchange, the associative mechanism is clearly impossible, and the first step in chemisorption must be losing a hydrogen atom. As the surface reactivity for C–H bond scission must be high in order to commence exchange, it is no surprise that the initial trend in reaction is overwhelmingly to completion, with many C–H bond breaking events before

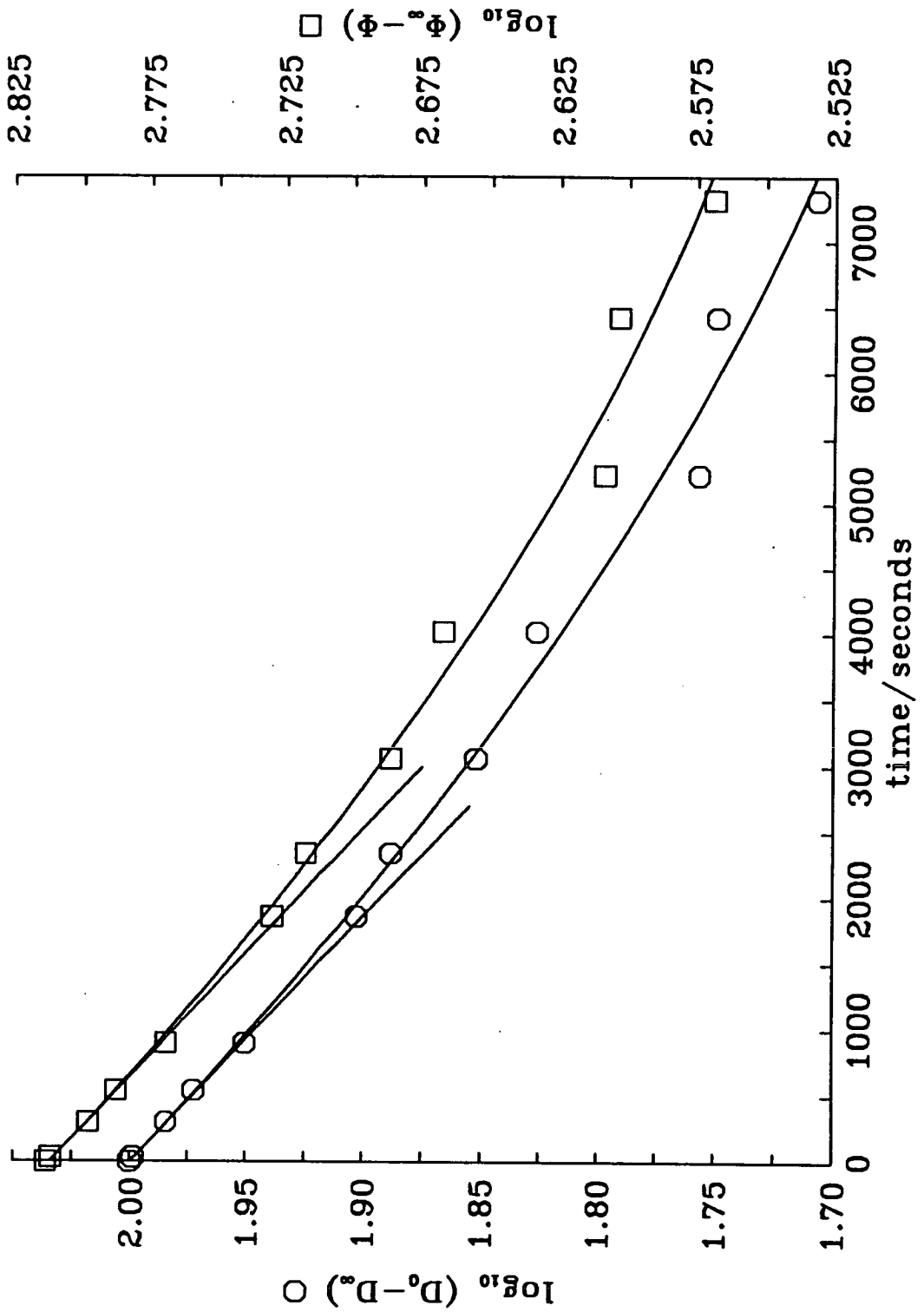

Figure 2.8: Kinetic plots for exchange over EuroPt-1 at 331 K.

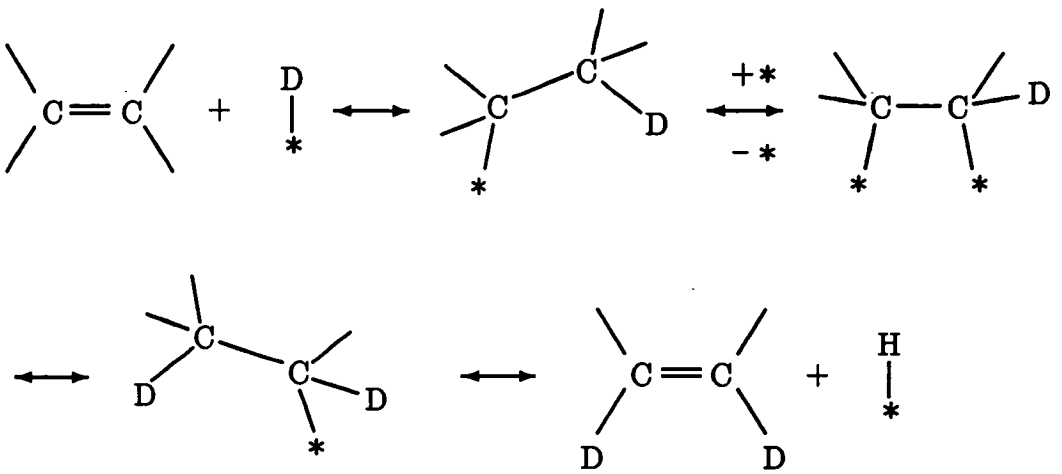

Figure 2.9: The Horiuti-Polanyi associative mechanism for alkene exchange.

desorption back into the gas phase. This $\alpha\beta$ model does not really allow for the butane to loose any more than two hydrogens at once to form surface σ bonds, due to the steric effect of the relative C–C and Pt–Pt bond lengths. Gault, Rooney and Kemball [119] proposed, following experiments on polymethylcyclopentanes, that exchange might occur by a less coordinatively hindered π-allyl species centred on one platinum atom. Such unsaturated species, and indeed more extensively dehydrogenated moities might well be responsible for some poisoning of the reaction by blocking of the reactive sites. The general reaction scheme just outlined is illustrated in Figure 2.10. This would also be the cause of the increasing proportion of D_1 hydrocarbon formed. The simple reversible formation of a surface n-alkyl group with a single carbon–surface bond is clearly less sterically demanding than $\alpha\beta$ or π-allyl adsorption, which require the hydrocarbon to be parallel to the metal surface. As active sites become fewer, single exchange will be encouraged. Overall reaction rate may not be initially affected, as surface residence times are reduced by the blocking of further reaction. As the surface becomes more crowded, after 30 minutes of reaction, this mechanism may contribute to the reduction in reaction rate.

This discussion will be affected by the size of the platinum particles available

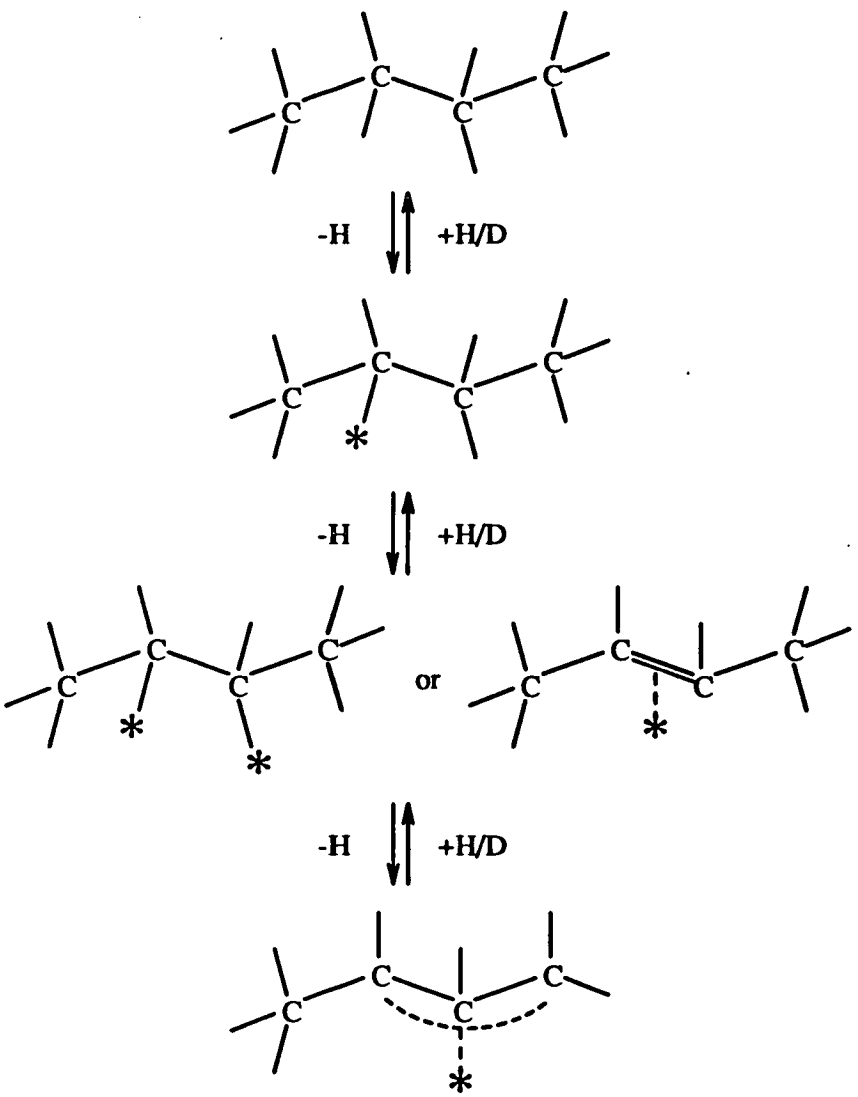

Figure 2.10: A reaction scheme for butane adsorption.

for reaction. In EuroPt-1 the dispersion of 63%, and the metal crystallite size are well known. The metal aggregates have a range of sizes, peaking around 60 atoms [30], of which 63% are assumed, from hydrogen adsorption measurements, to be surface atoms [120]. Even allowing for few of these atoms being arranged in organised planes comparable with single crystal surfaces, there should be numerous sites per crystallite available for $\alpha\beta$ and π adsorption. The proportion of the surface blocked will be higher for smaller particles where one or two molecules $\alpha\beta$ adsorbed may hinder all save simple alkyl adsorption. The Pt/SiO_2 catalyst used by Oliver *et al.* had a quoted dispersion of 98%, which would explain the larger fraction of D_1 species formed in their exchange reaction.

2.3.2 EuroPt-1 at 378 K

The high temperature exchange was run to 45% reaction, but as above, the reaction course will first be considered at a lower extent of reaction. Figure 2.11 is the high temperature analogue of Figure 2.3. Not surprisingly, stepwise reaction is not observed, with all species significantly populated by the second data point. The majority D_{10} species again has a very fast initial rate which for the first data point exceeds the scope of a quadratic fit, and which tails off with increasing conversion. The D_1 species is no longer in such a position of importance, with D_9 formation being much more extensive. D_8 and D_7 are also significant even at this early stage in the reaction.

The product distribution to 13% reaction, and the initial product distribution, Figures 2.12 and 2.13 may be constructively compared with the histograms made in analogous fashion for the 331 K reaction, Figures 2.4 and 2.5. Figure 2.12 can again be described as a skewed U distribution, with added intensity in D_8 and D_9 as well as D_{10}. Not only is the D_1 column much lower, but all species from D_2 to D_6 are also less common. The initial distribution, Figure 2.13, shows most exchange into D_{10}, as for low temperature, but D_9 has a significant contribution.

The full range of reaction monitored is shown in Figure 2.14. As in Figure 2.6,

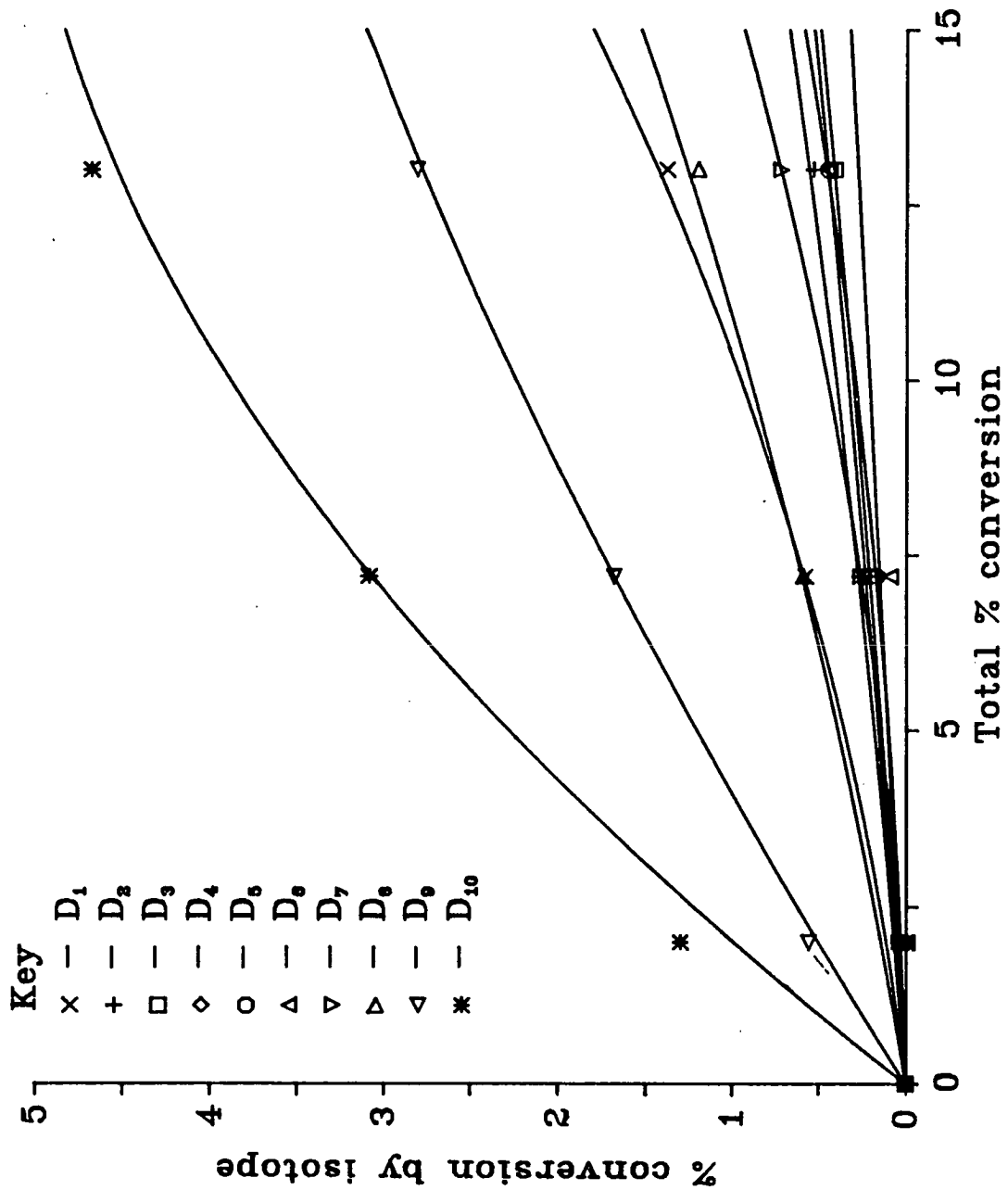

Figure 2.11: Exchange over EuroPt-1 at 378 K to 13% reaction.

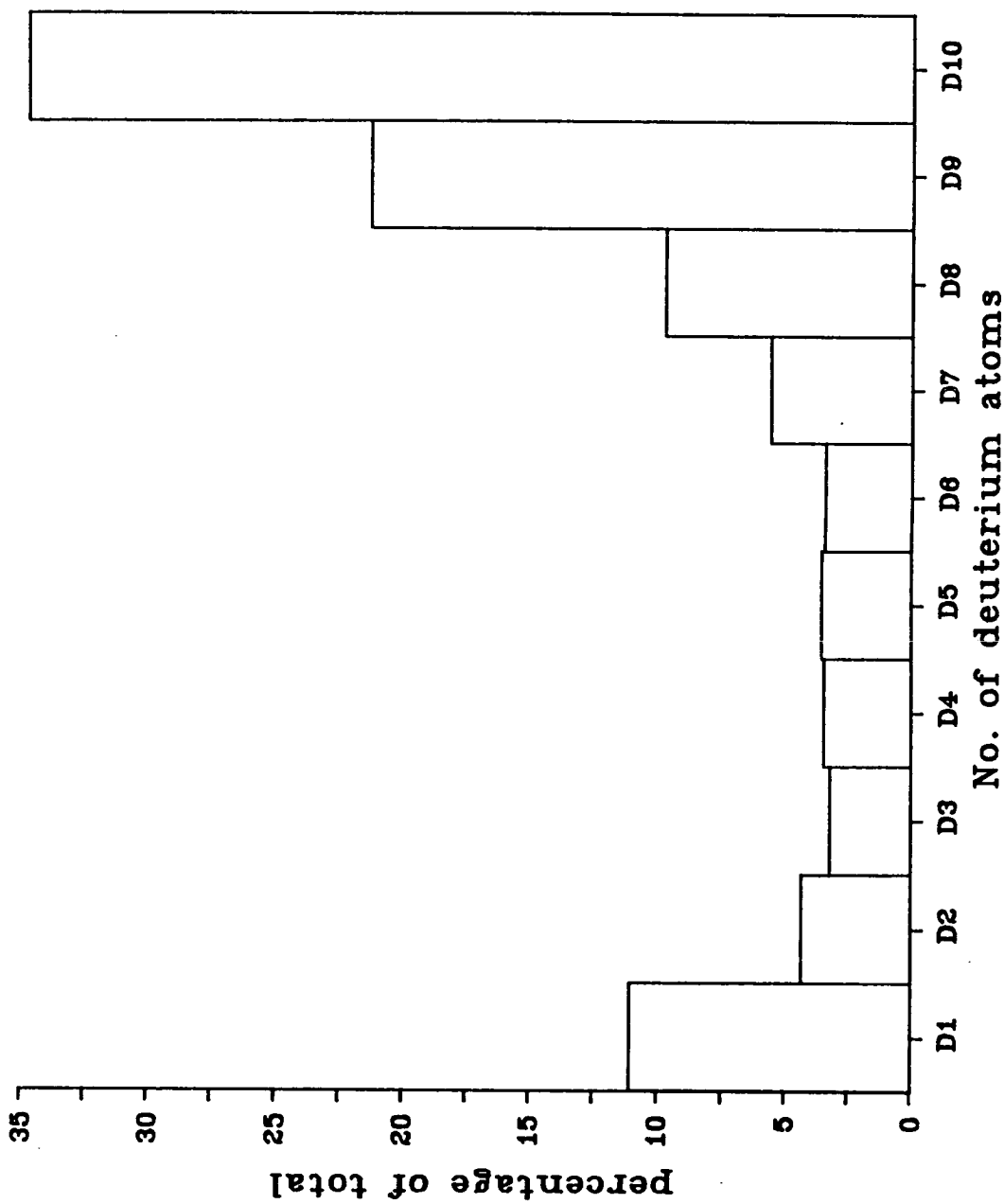

Figure 2.12: Product distribution by isotope for Figure 2.11

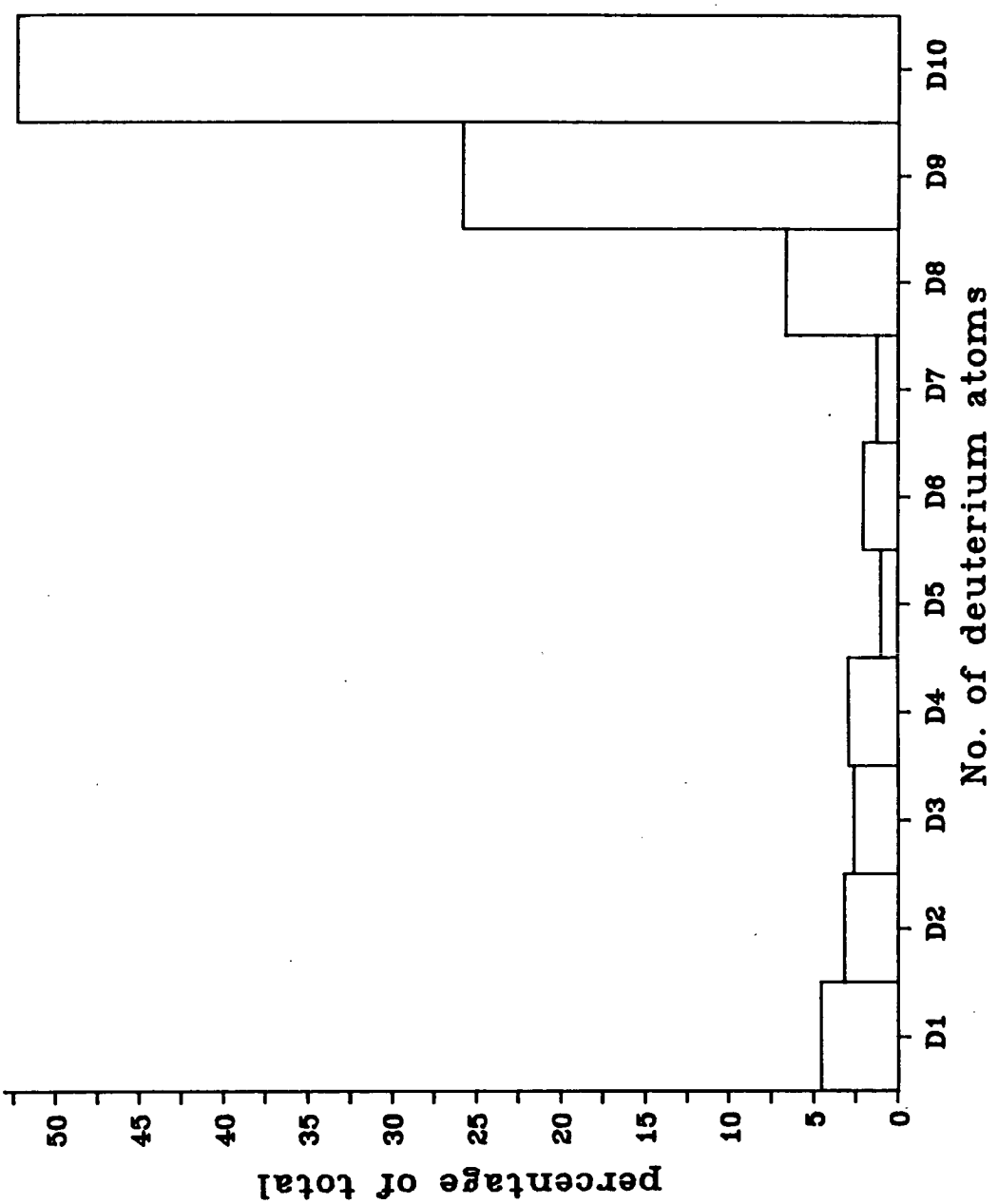

Figure 2.13: Initial product distribution for Figure 2.11

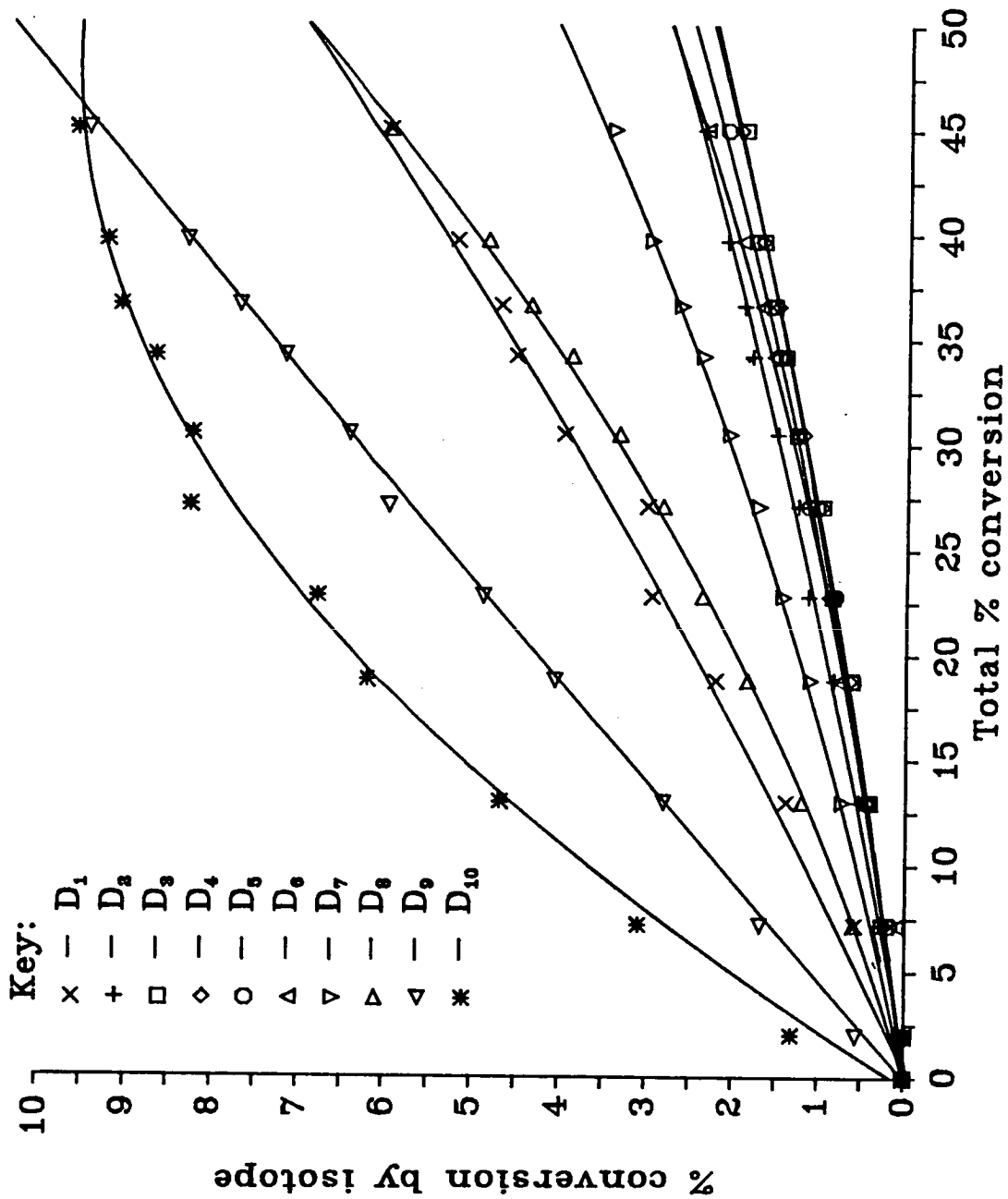

Figure 2.14: Exchange over EuroPt-1 at 378 K for 45% reaction.

As received EuroPt-1 at 378 K					D_2:C_4H_{10} 8.4:1						
$k_\Phi = 0.17\ s^{-1}g^{-1}$					$k = 0.023\ s^{-1}g^{-1}$				M = 7.3		
Product distributions											
	D_0	D_1	D_2	D_3	D_4	D_5	D_6	D_7	D_8	D_9	D_{10}
Initial	-	4.6	3.2	2.6	2.9	1.0	2.0	1.2	6.6	25.7	52.2
13% reaction	87.0	1.4	0.5	0.4	0.4	0.5	0.4	0.7	1.2	2.8	4.7
$\Phi = 96.9$	-	11.1	4.3	3.2	3.5	3.5	3.4	5.6	9.7	21.3	34.7
45% reaction	55.0	6.0	2.4	1.9	2.0	2.1	2.4	3.4	6.0	9.4	9.6
$\Phi = 301.1$	-	13.2	5.3	4.2	4.3	4.9	5.2	7.6	13.3	21.0	21.2

Table 2.2: Exchange data for as received EuroPt-1 at 378 K

the D_1 trend switches at moderate conversion from increasing to decreasing, with a final product level equal to D_8 production. The D_{10} reaction rate falls off markedly, finishing at a similar proportion to D_9, which unlike in the lower temperature experiment, is not increasing. An accelerating trend is, however, noticeable from D_8 to D_5, in contrast to the first experiment where it was barely discernible down to D_6.

Part of the difference is due to a greater dilution of the deuterium pool. A slightly lower deuterium/hydrocarbon ratio was used, and when this and the larger Φ value noted in Table 2.2 are substituted into Equation 2.12, the hydrogen proportion is up to 36.6%, over twice that of the low temperature experiment. This explains the difference in trends just mentioned, as population is transferred from higher to lower degrees of exchange, shown by the product distribution, Figure 2.15.

The plots of $\log_{10}(\Phi_\infty - \Phi)$ and $\log_{10}(D_0 - D_\infty)$ in Figure 2.16 show marked deviation from first order behaviour, though a fair straight line could be drawn through the points corresponding to Figure 2.11, over the first 13% of the reaction. This indicates that most of the rate reduction will be due to the dilution effect though some may also be caused by poisoning. The values for k_Φ and k

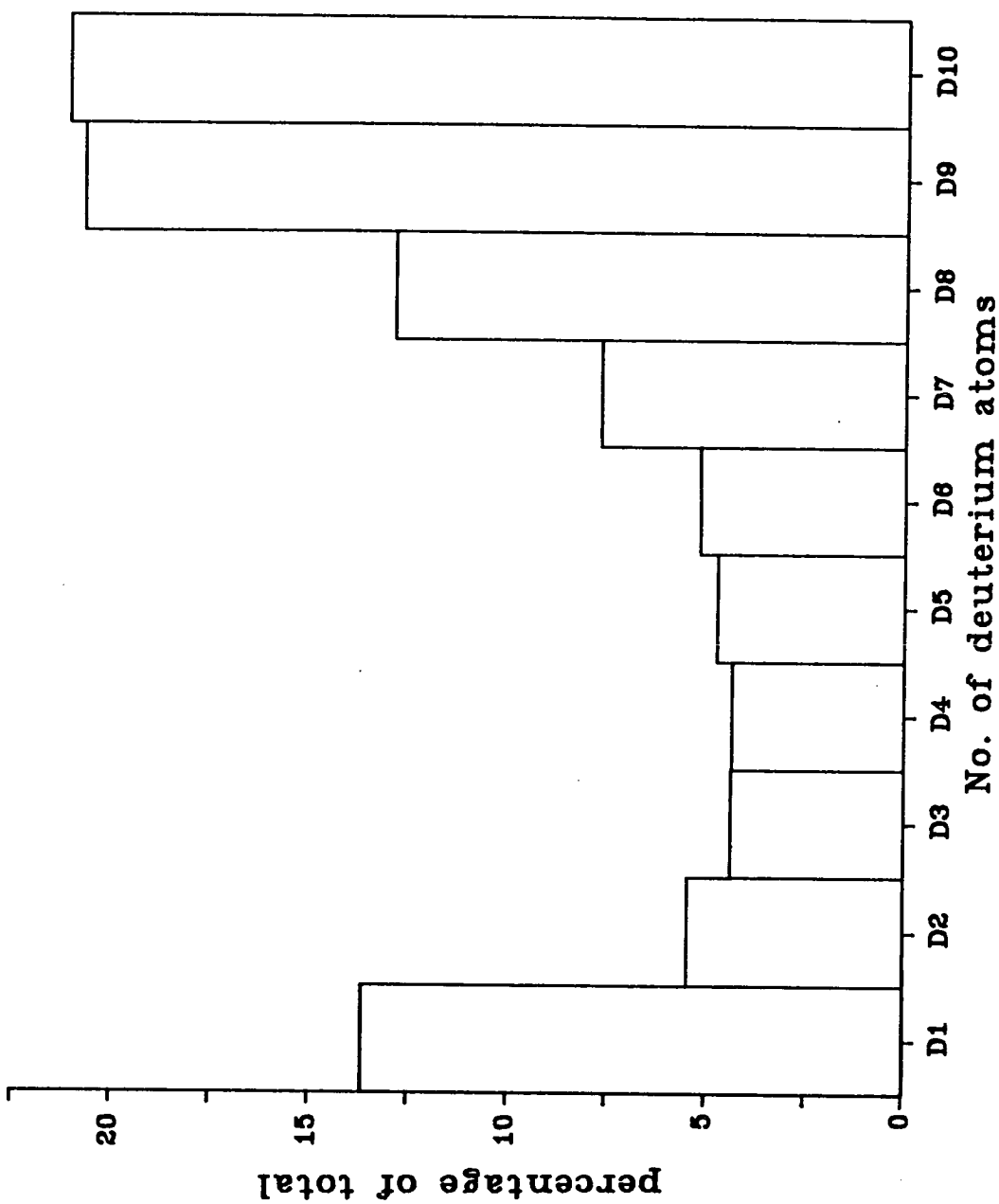

Figure 2.15: Product distribution by isotope for Figure 2.14

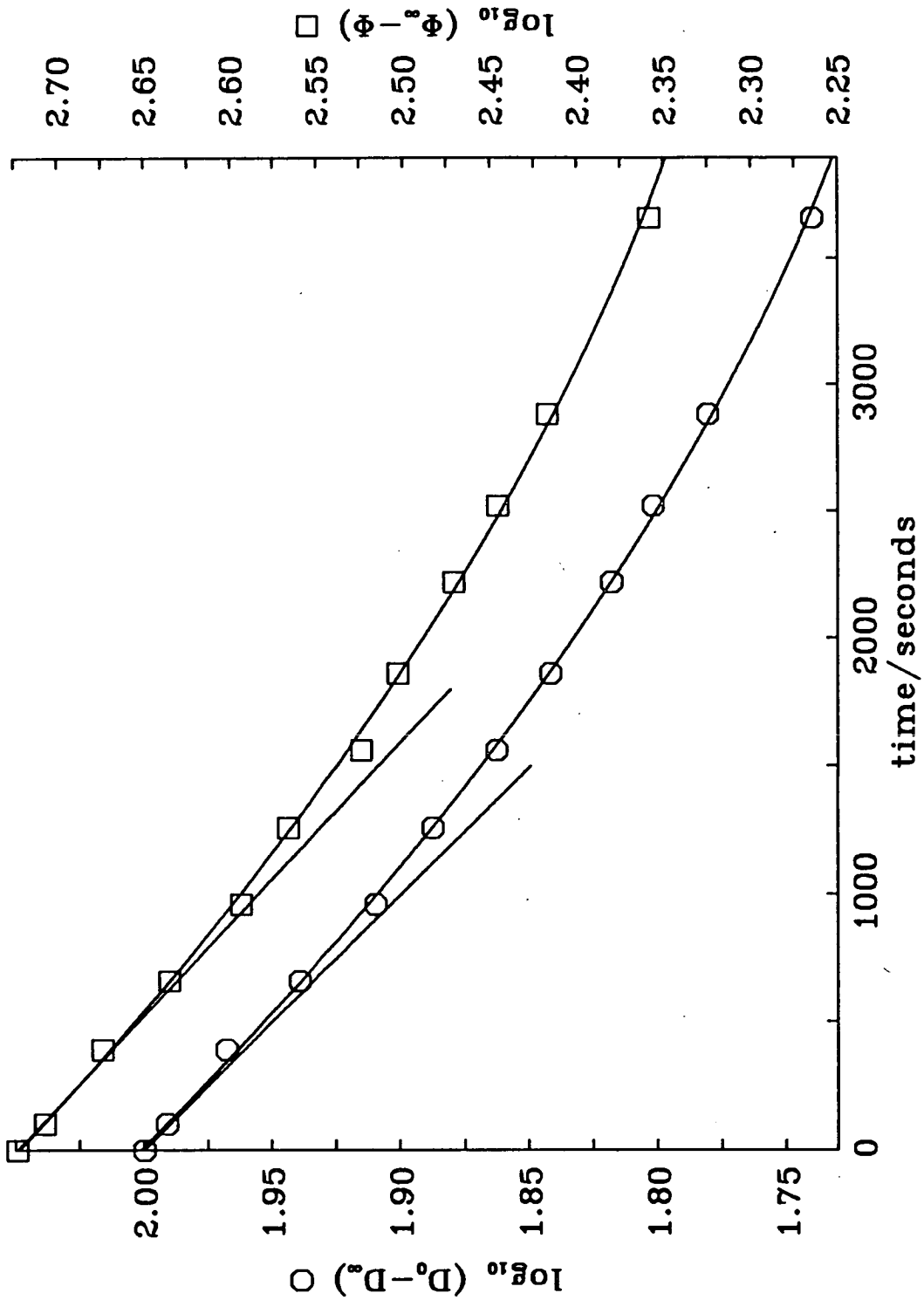

Figure 2.16: Kinetic plots for exchange over EuroPt-1 at 378 K.

1% K doped EuroPt-1 at 378 K					D_2:C_4H_{10} 4.7:1						
$k_\Phi = 0.0039$ $s^{-1}g^{-1}$					$k = 0.00060$ $s^{-1}g^{-1}$				M = 6.5		
Product distributions											
	D_0	D_1	D_2	D_3	D_4	D_5	D_6	D_7	D_8	D_9	D_{10}
Initial	–	15.3	4.0	2.1	1.6	0.6	0.7	5.7	7.9	11.8	50.2
5% reaction	95.2	1.0	0.3	0.2	0.2	0.2	0.1	0.1	0.3	0.5	2.0
$\Phi = 31.6$	–	21.0	6.4	3.8	2.8	3.4	2.0	3.3	7.2	9.9	40.4

Table 2.3: Exchange data for 1% potassium doped EuroPt-1 at 378 K.

in Table 2.2 are considerably higher than for the 331 K reaction, as would be expected. In keeping with the initial product distribution, the calculation of M showed a much higher degree of exchange (7.3 deuteriums per butane, *cf.* 5.5 at 331 K).

2.3.3 Potassium doped EuroPt-1 at 378 K.

As mentioned above, significant reaction was only obtained for the 1% potassium doped EuroPt-1 at elevated temperature. Even then, reaction was slow, and only monitored to 5%. The lower values recorded may have had a higher proportional error attached, but an advantage displayed in the graph of conversion by isotope, Figure 2.17, is that many data points cover a range of exchange represented by only one or two in Figures 2.3 and 2.11. This area produced anomalously high values for production of D_{10} species in both of the previous experiments, but over this catalyst, the D_{10} plot, again the major feature, could be well represented by a simple quadratic fit over all the measured range. The form of the plots was most like Figure 2.3, with D_1 giving the second most populated butane, with an increasing trend, compared with the D_{10} curve which was concave down. D_9 and D_8, next in population, vary in a manner similar to D_{10}, and D_2, D_3 and D_4 mirror D_1, though these curvatures were slight, and only comparable with the scatter of the points.

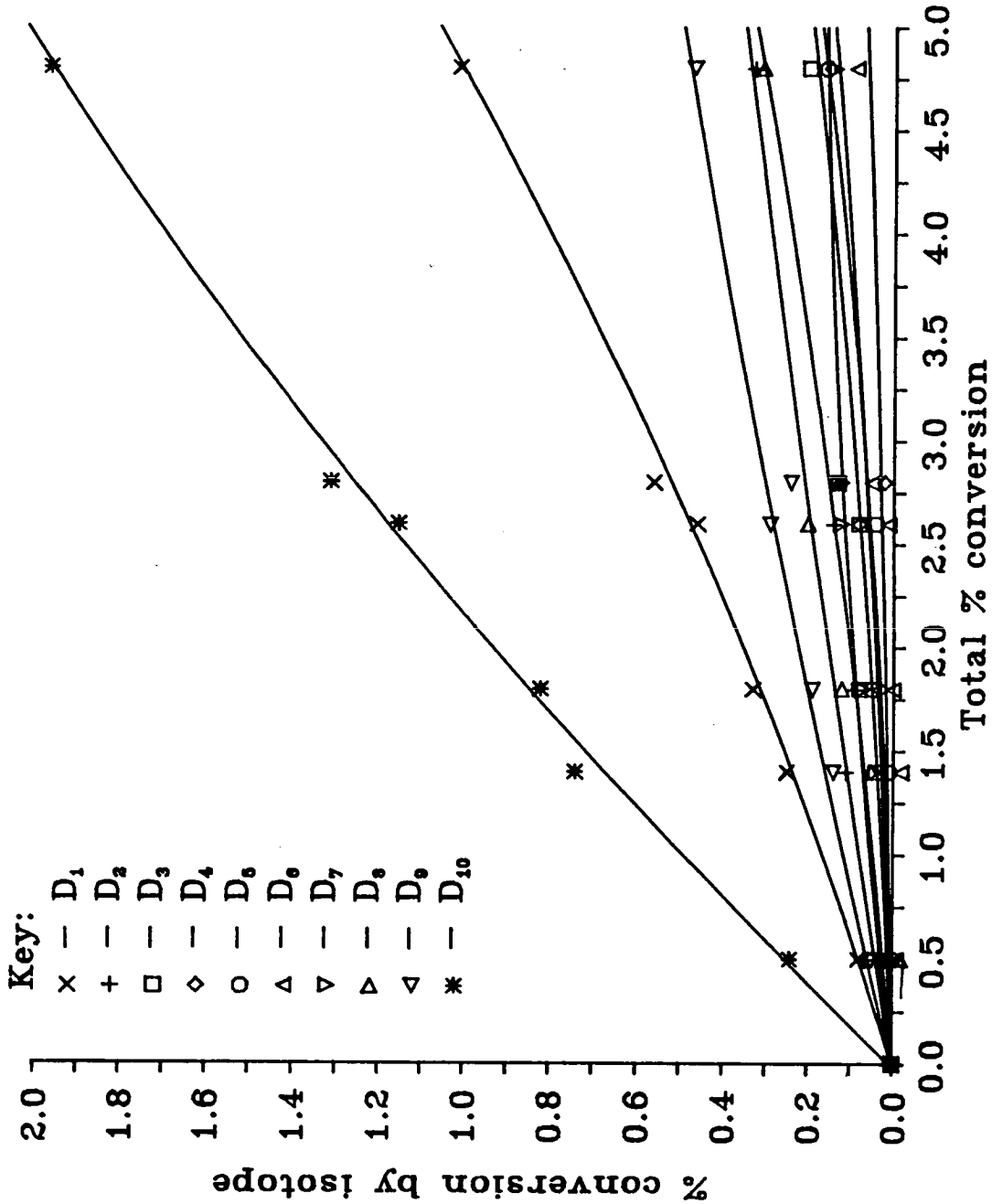

Figure 2.17: Exchange over 1% potassium doped EuroPt-1 at 378 K to 5% reaction.

The product distribution, Figure 2.18 is the now familiar skew U of Figures 2.4 and 2.12. The fraction of products in D_1 and D_{10} forms was significantly higher than in both of the previous distributions, with only D_2, D_8 and D_9 outside the extremes giving more than 5% of the products (Table 2.3). When the tangents to the curves in Figure 2.17 are plotted for the initial product distribution, Figure 2.19, this was further exaggerated. With the shift in emphasis to the more extensively exchanged species, D_7 rises above the 5% mark as D_2 falls below it.

When the results are subjected to the usual kinetic analysis, Figure 2.20, reasonable straight lines are found for plots of both $\log_{10}(\Phi_\infty - \Phi)$ and $\log_{10}(D_0 - D_\infty)$, without the tail off found in reaction over as received EuroPt-1. That a good fit was found, compared with the previous analyses is in part because of the restricted rate of exchange, and hence the removal of dilution of the deuterium supply as a factor in the experiment. There was, however, a significant scatter in the points, and some poisoning may be present in the latter stages. As Kemball [32] explained, that an exchange reaction should appear as first order is mainly due to the equilibrium pool of surface adsorbates. In the reaction system, the equilibrium surface coverage in adsorbed species will only account for a small percentage of the reaction mixture. The equilibrium isotopic mixture, however, is only achieved when approaching 100% of the molecules react. For most of the duration of the exchange reaction, therefore, there will be equilibrium concentrations of the surface species, and only the approach of the hydrogen isotopes distribution to equilibrium will reduce the reaction rate, giving apparent first order behaviour for the initial period.

As already mentioned, the doping of EuroPt-1 with potassium hydroxide has been extensively characterised in this department by Mushtaq Ahmad [95]. It was found in that work that a 1% KOH doped catalyst had an overall surface area reduced from the 185 m^2g^{-1} of the as received material [120], to 132 m^2g^{-1}. The metal dispersion of the catalysts was measured three different ways, by oxygen chemisorption using a Cahn balance, and by hydrogen and carbon monoxide

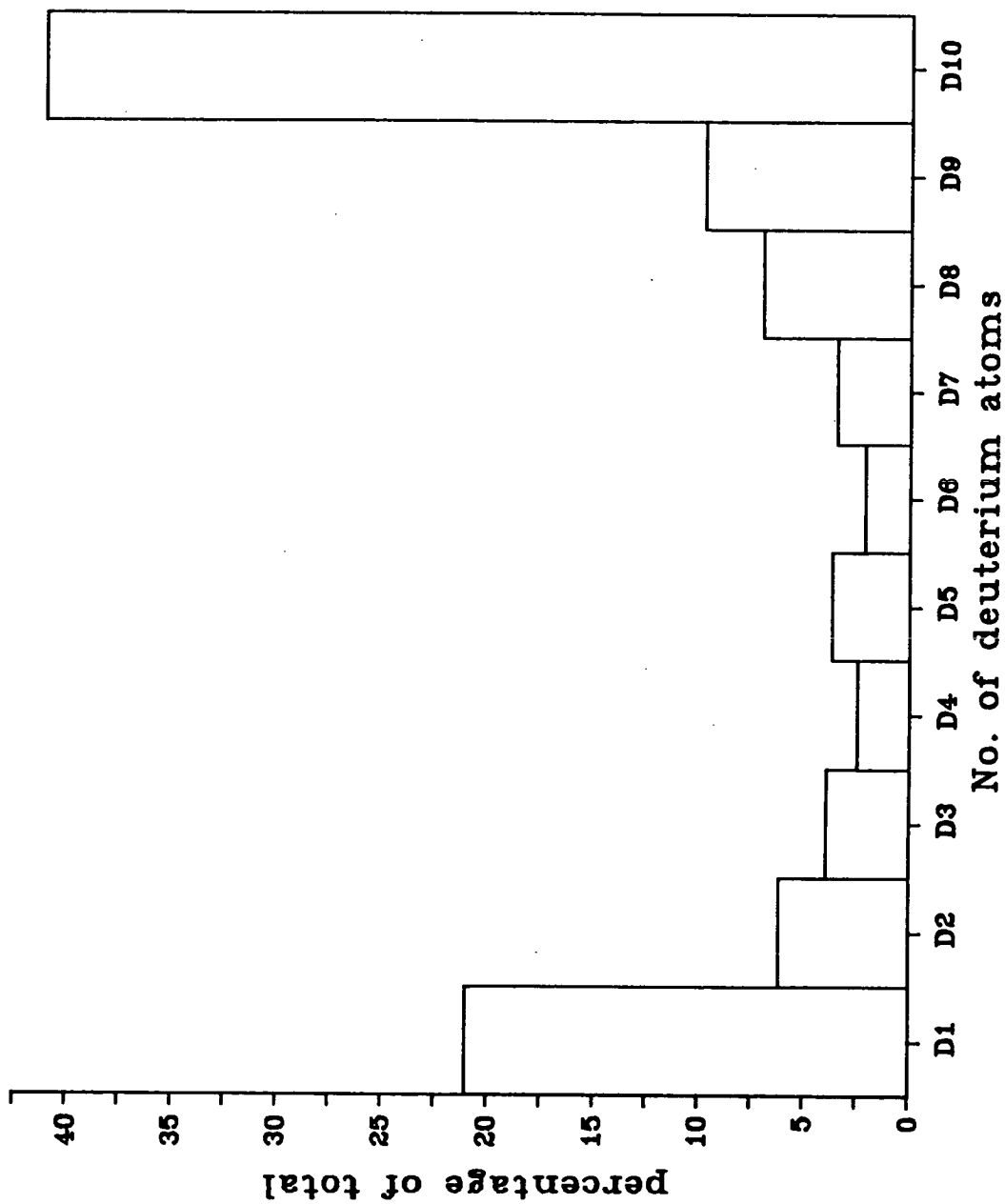

Figure 2.18: Product distribution by isotope for Figure 2.17

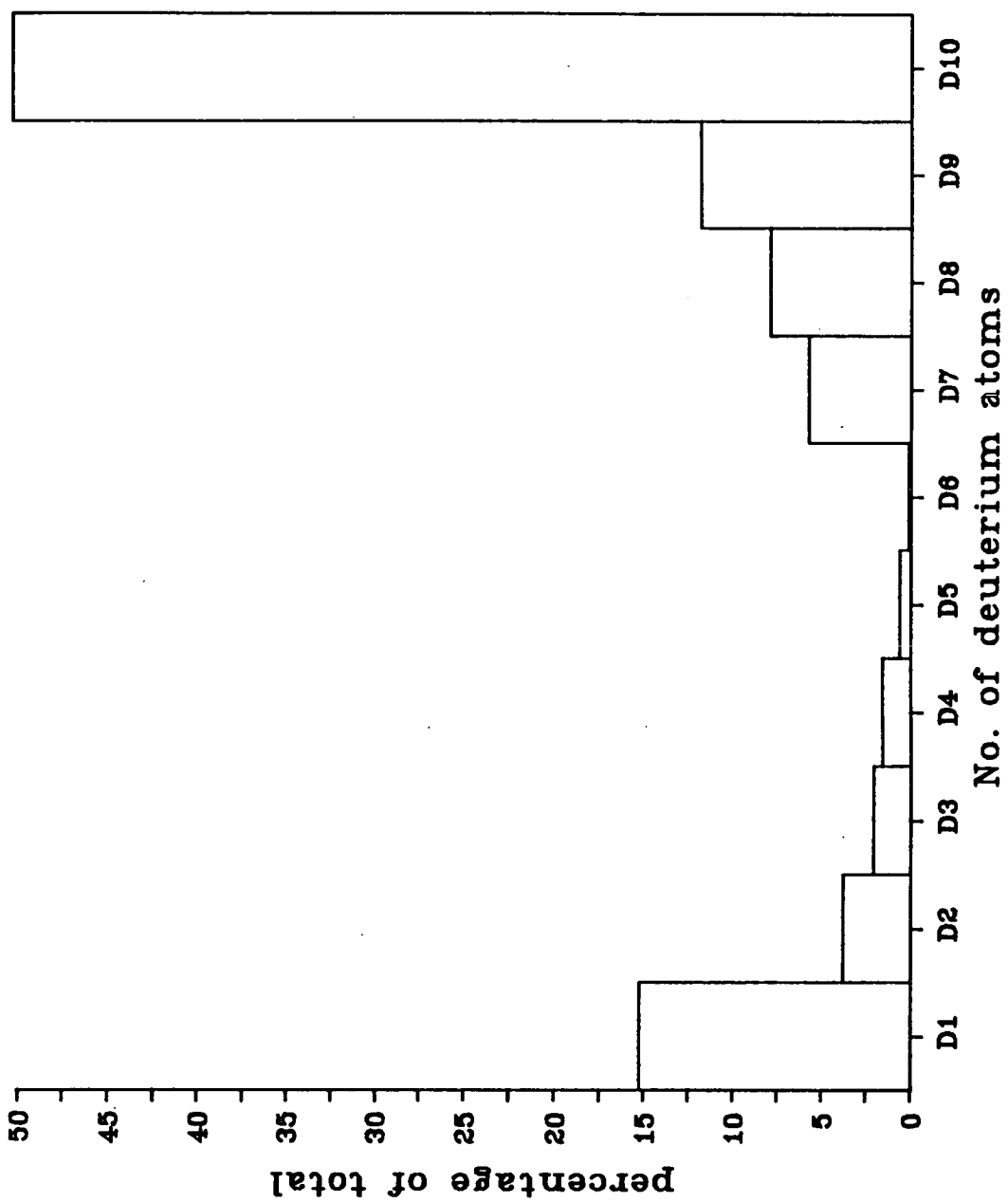

Figure 2.19: Initial product distribution for Figure 2.17

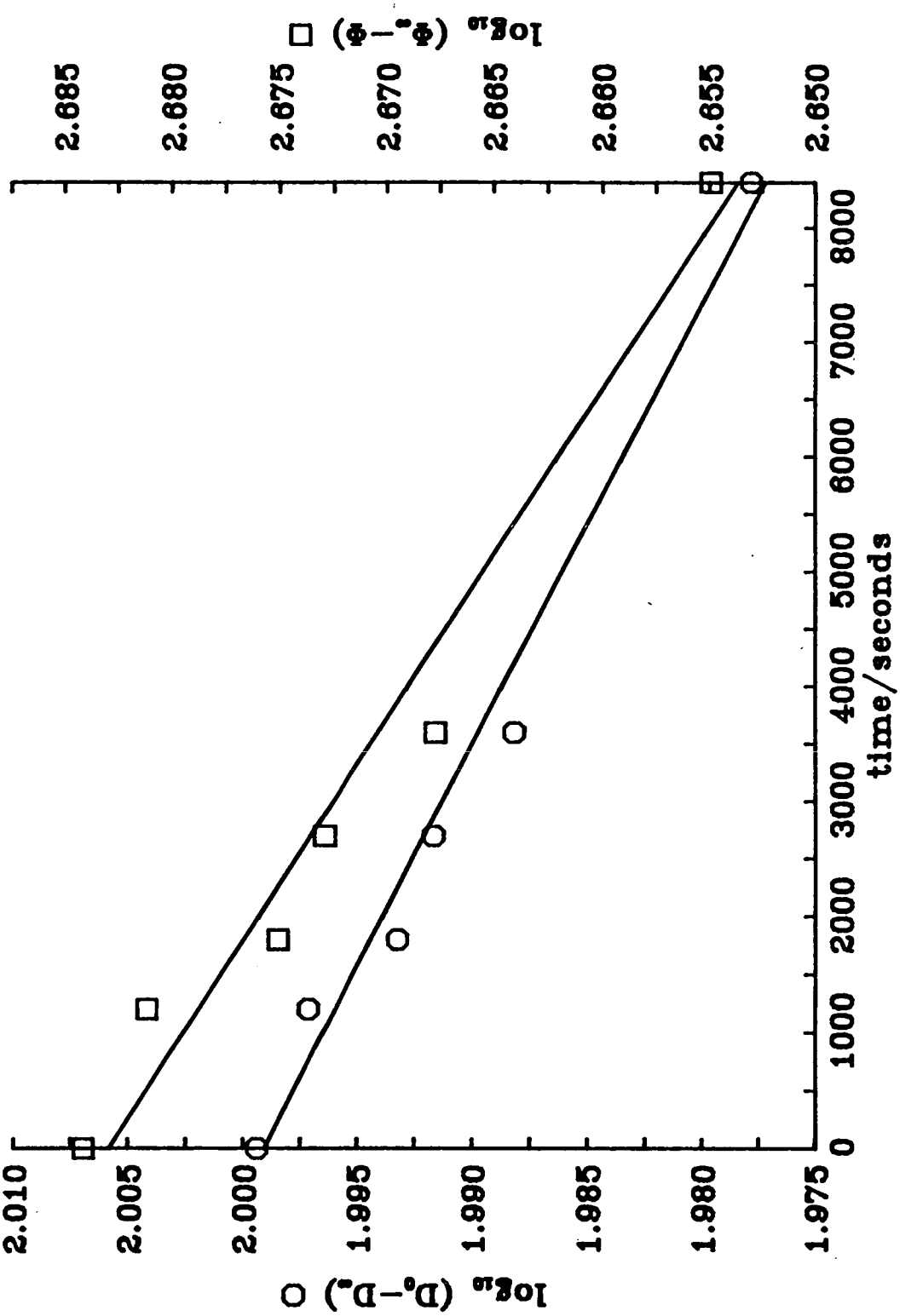

Figure 2.20: Kinetic plots for exchange over 1% potassium doped EuroPt-1 at 378 K.

Probe	O_2		H_2		CO		TEM [123]	
	D*	A†	D	A	D	A	D	A
EuroPt-1	0.53	9.2	0.66	11.5	0.66	11.5	0.60	10.4
1%K EuroPt-1	0.23	4.0	0.36	6.3	0.39	6.8		

*D : Ratio of surface metal atoms to bulk metal atoms.

†A : Metal surface area/ m^2g^{-1}.

Table 2.4: Metal particle characteristics of EuroPt-1.

desorption over a thermal conductivity detector following pulsed chemisorption. If the platinum is assumed to have low order planes exposed, with a surface density of $1.12x10^{15}$ atom cm^{-2} [121], and the usual adsorbate:metal atom stoichiometries, then metal surface areas are as shown in Table 2.4. The lower area found for EuroPt-1 with oxygen chemisorption was in agreement with the original characterisation [122].

Mushtaq also studied the hydrogenolysis reaction over the two catalysts studied here, at the higher temperature of 523 K. No hydrogenolysis was detected by gas chromatography in any of the experiments described in this Chapter.

Simply from the metal surface area reduction in Table 2.4, a reaction rate reduction of approximately 50% might be expected. This bears little or no comparison with the drop of nearly two orders of magnitude found when k_Φ is compared between Tables 2.2 and 2.3, so the potassium doping seems to exerts a chemical as well as a physical effect.

The potassium was added to the catalyst as an aqueous solution of the hydroxide. At the reaction temperature used, the hydroxide, with a heat of formation from the elements of –428 $kJmol^{-1}$ is more stable than any potassium oxide [124], though carbon dioxide and other weak acids can react to form thermally stable salts. During the reduction cycle for the catalyst, however, the temperature would have been sufficient to form K_2O. This would be converted rapidly back to KOH on exposure to any water in the vaccum system. During the exchange reaction,

the potassium will be present either as the oxide or hydroxide, with a tendency to form the latter with time and water contamination. The drastic conditions required for chemical reduction of potassium hydroxide to the metal are way beyond those applied in these experiments. This is further backed up by UHV studies of potassium doped transition metal single crystals and foils, which find KOH to be the residual species after simulated reaction conditions over Fe [125] and Pt [126].

The falling reaction rate for exchange agrees with the decreased activity produced by potassium over both nickel single crystals [127] and supported nickel catalysts [128, 129] for the carbon monoxide hydrogenation reaction. In that reaction, there are several features in common with the 1%K EuroPt-1 system. An important one is the increase of H adatom stability, shown by Mushtaq [95] to have an 85 K higher thermal desorption peak *cf.* as received EuroPt-1. In the reaction over Ni, this has been suggested as decreasing the likelihood of hydrogenation of the carbidic precursor for methane (and higher hydrocarbons). A more strongly bound hydrogen will also decrease the number of active sites available for hydrocarbon bonding, which agrees with the reduced rate of exchange. Over Ni, potassium encourages larger hydrocarbons to be formed than the methane dominant on undoped catalysts, and these are more likely to be unsaturated.

A small difference observed in the reaction over the doped EuroPt-1 to the unadulterated catalyst is in the initial behaviour. In Figures 2.3 and 2.11, D_{10} products were detected before any other isotopic products, and at a level which, compared with the noise level, should have produced other product peaks if the distribution was the same as was observed later in those experiments. This was not observed in Figure 2.17, and may indicate that in the initial reaction with the reduced and outgassed surface, species which are rapidly dehydrogenated, exchanged and desorb over as received EuroPt-1 are more strongly held over the potassium surface, and block sites for further reaction.

Chapter 3

Diffuse Reflectance Infrared Fourier Transform Spectroscopy

3.1 Introduction

Infrared spectroscopy has a long history in catalysis, and is still a widely used analytical tool, as described in Section 1.5.2 above. The traditional transmission technique is not, however, without its problems.

When it comes to making a self supporting disc of catalyst there is a conflict of interest between the need of a thick disc to give the self support, and a thin sample which will transmit enough infrared light through the strongly absorbing metal and oxide support. The pressing of discs thus becomes to an extent a 'black art'. The strong absorption of the metal means that metal particle size, dispersion and loading must be considered. A higher metal loading tends to reduce the transmittance of the disc. More metal sites, however, are needed to increase adsorption of reagent gases, so the dispersion, or ratio of surface metal atoms to bulk metal atoms, is an important factor.

Another significant reduction in transmission is due to light scattering. When an electromagnetic wave encounters a catalyst particle, that part of the wavefront which is incident on the particle will undergo refraction and (possibly multiple) reflection. The part of the wavefront not directly impinging on the granule will be diffracted at the boundary. For a particle large compared with the wavelength, these processes will be distinguishable. When the wavelength of the radiation is comparable with the particle dimensions, the diffraction, refraction and reflection become inseparable, and are referred to simply as scattering. The Beer-Lambert law [130] is used to quantify transmission spectra,

$$log(I/I_o) = -\alpha\, Cl \tag{3.1}$$

with I the recorded light intensity and I_o the original intensity before passing through the sample l thick with a concentration C of absorbers of absorption coefficient α, but takes no account of light scattered by the sample. Light will be scattered from the surface of randomly oriented particles by Fresnel reflection, and also undergo Rayleigh or Mie scattering. This scattering, S

$$S \propto r^3 \nu^a \tag{3.2}$$

is a function of the particle radius r cubed and the frequency of the light source, ν to a power $a \leq 4$ [131] (see Section 3.3.1). Reducing the particle size of the catalyst by grinding reduces r, and therefore the scattering. At higher wavenumbers, however, the scattering losses become considerably larger. An alternative method of reducing scattering is to introduce a filler with a similar refractive index to the catalyst, such as an alkyl halide. This can exacerbate problems of catalyst treatment, and also acts as a serious contaminant of the catalyst.

The pressed disc also has disadvantages for *in situ* studies, due to diffusional problems. If an adsorbate's spectrum demonstrates coverage dependent effects (well known for carbon monoxide [132]), anomalous results may occur due to unexpected local adsorbate concentration variations. Diffusion may also limit the effectiveness of pretreatments such as metal reduction and out gassing.

3.2 Diffuse Reflectance Spectroscopy

Diffuse reflectance spectroscopy avoids several of the disadvantages mentioned above. Although this technique has existed since the middle of the century [133], with a thorough investigation and review by Kortüm *et al.* [48, and references therein] in the 1960s, it has only seen significant usage in surface chemistry in the last dozen years.

When light is incident on a powdered sample, there are several processes it may undergo. In transmission spectroscopy, where the sample is thin, most of the light passes through with only small losses due to scattering, and of course

the desired signal reduction from absorption by the sample (Figure 3.1). How much of the scattered light is detected will depend on the sampling aperture of the detector and its optics. For a thicker sample, the transmitted beam will be reduced, and a higher proportion scattered or absorbed. For a sufficiently

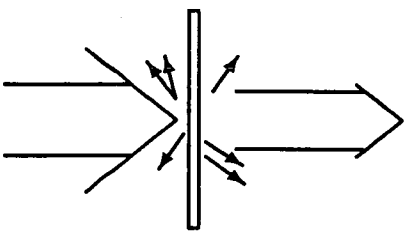

Figure 3.1: Light path for transmission.

thick sample, no radiation will reach the back surface, and instead will either be absorbed or exit via the front surface (Figure 3.2). This diffusely scattered radiation is what is measured in diffuse reflectance spectroscopy.

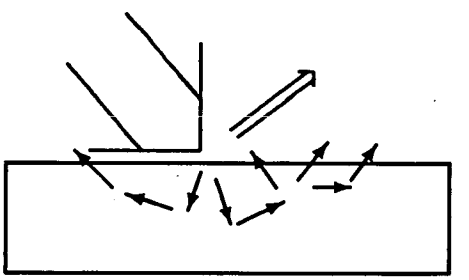

Figure 3.2: Light path for diffuse reflection.

3.3 Kubelka-Munk Theory.

3.3.1 Exact Scattering Theories.

The mechanism for diffuse reflectance spectroscopy is explicitly ignored in the Beer-Lambert law, so a different theoretical basis must clearly be derived to find appropriate equations. One well known scattering theory is that of Rayleigh, who showed that the blue colour of the sky was due to molecular scattering [136]. He assumed that the electric field of an approaching electromagnetic wave excited

forced oscillations of the electrons in a molecule at the photon frequency. When the molecular dimensions are small *cf.* the wavelength of the light, the electrons oscillate in phase and so re-radiate or scatter the light. A catalyst sample with particles of micron or larger size does not, however, meet this assumption.

Mie's scattering theory [75] is derived for scattering of plane electromagnetic waves from dielectric and absorbing spheres of any size. The equations are often given in terms of the variable χ,

$$\chi \equiv 2\pi r/\lambda \tag{3.3}$$

with r the sphere radius and λ the wavelength of the radiation. In the region $\chi < 0.8$, Mie theory reduces to Rayleigh scattering, with a term in λ^{-4}. For larger values of χ, the expressions become more complicated, but the λ dependence decreases, until the scattering becomes independent of χ and hence λ. For macroscopic spheres, where the scattering distribution may be calculated from the laws of geometric optics by considering reflection, diffraction and refraction separately, the results correspond to those from the Mie formalism in the limit $\chi \rightarrow \infty$ [137].

Rayleigh and Mie scattering are both exact solutions for an interaction between an electromagnetic wave and a dielectric sphere. They both, however, allow for only single scattering, whereas any catalyst powder will exhibit multiple scattering. Theissing [138] extended Mie's single scattering theory to multiple scattering from particles sufficiently far apart that there was no interference between scattered light from different particles. One interesting result of this theory is the angular distribution of the scattered light. Under Mie scattering, most of the light is forward rather than back scattered. Under multiple scattering, the distribution very quickly becomes isotropic, with the number of scattering events required for this depending on χ and the complex refractive index of the spheres [139].

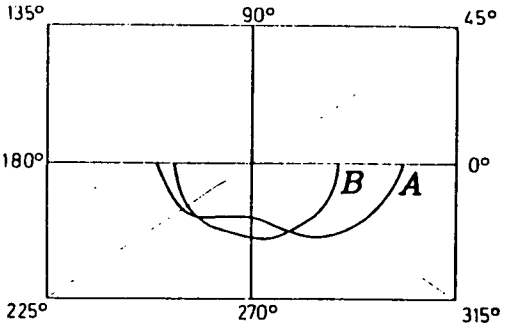

Figure 3.3: Angular distribution of the scattering intensity after single scattering (A) and twofold scattering (B) on dielectric spheres (from [48] page 99).

3.3.2 Phenomenological Scattering Theory.

In a real catalyst powder, the assumption noted above does not hold, *ie.* multiple scattering will occur when support particles are sufficiently close (generally actually touching) that there will be interference among light scattered from neighbouring particles. The qualitative theory developed for this situation by Chandrasekhar [140] involves evaluation of a radiation transfer equation in an arbitrary number of directions. A simpler, phenomenological theory has been developed by several authors using two constants to represent the absorbance and the scattering of the powder, with the radiation divided into two opposing fluxes.

The best known of these theories is that of Kubelka and Munk (KM) [134]. The derivation is basically the same as the earlier one of Schuster [141], though more general, and better known. Several other theories were developed in the same period, but these have been subsequently shown to be special cases of the KM theory [142].

The KM equations are derived for a plane parallel layer of scattering and absorbing material of thickness d, extending in the xy plane to infinity (or at least far enough to render edge effects negligible). It is irradiated by a diffuse incident flux of I in the negative x direction, with a resulting back scatter J in the positive x direction. Considering an element of thickness dx, the incident radiation will be attenuated by $kI2dx$ due to the absorption of coefficient k, and $sI2dx$ by scattering when s is the scattering coefficient per unit length. The

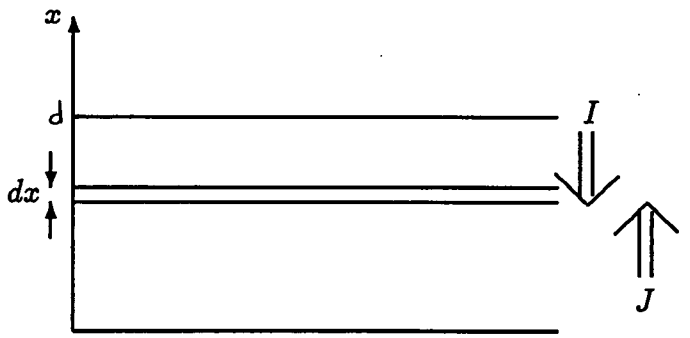

Figure 3.4: Scheme for deriving the Kubelka-Munk equation.

factor of two arises because the incident light is diffuse. The path it takes across dx is longer than dx for oblique angles, and averages over all angles to twice the layer thickness. The incident radiation will also be augmented by the opposite radiation flux J being scattered back into the negative x direction. The change in I over dx is therefore given by,

$$-dI = -kI2dx - sI2dx + sJ2dx. \tag{3.4}$$

By a similar argument, the change in J can be expressed as

$$dJ = -kJ2dx - sJ2dx + sI2dx. \tag{3.5}$$

These two equations can be combined by substituting $K \equiv 2k$, $S \equiv 2s$, and $a \equiv (1 + K/S)$ and changing the variable to $r \equiv J/I$. This produces the single differential equation,

$$\frac{dr}{Sdx} = r^2 - 2ar + 1. \tag{3.6}$$

This can be integrated over d, the layer thickness, by the method of partial fractions, given the boundary conditions of

$$\text{at } x = 0 : (J/I) = R_g = \text{ the reflectance of the background} \tag{3.7}$$

$$\text{at } x = \mathrm{d} : (J/I) = R = \text{ the reflectance of the sample,} \tag{3.8}$$

to give a rather big and complicated solution

$$\ln \frac{(R - a - \sqrt{a^2 - 1})(R_g - a + \sqrt{a^2 - 1})}{(R_g - a - \sqrt{a^2 - 1})(R - a + \sqrt{a^2 - 1})} = 2S\mathrm{d}\sqrt{a^2 - 1}. \tag{3.9}$$

This equation is, however, easily simplified for the case of an infinitely thick layer of catalyst, *ie.* one where no light reaches the back surface, and so d = ∞ and $R_g = 0$. This sets the right hand side of Equation 3.9 to infinity, and hence the denominator in the log term to zero. This may then be solved for the reflectance of the infinite layer,

$$R_\infty = 1 + \frac{K}{S} - \sqrt{\frac{K^2}{S^2} + 2\frac{K}{S}}. \tag{3.10}$$

The diffuse reflectance thus depends only on the ratio of the absorption and scattering coefficients, not their absolute values, and so by rearranging Equation 3.10 the Kubelka-Munk function can be found:

$$F(R_\infty) \equiv \frac{K}{S} = \frac{(1 - R_\infty)^2}{2R_\infty}. \tag{3.11}$$

The expression $F(R_\infty)$ is a function of an experimentally measurable variable, R_∞, the ratio J/I for an infinitely thick diffusely reflecting layer, which gives the ratio of the absorbance and scattering of the powder under investigation. The starting point for this derivation was a simplification of the radiation transfer into the two opposite directions represented by I and J, and an obvious query is how good an approximation this gives to the solution for an arbitrary number of directions. This question was addressed by Hecht [143], who concluded on comparison of the calculated values (Figure 3.5), that the deviation was less than the inaccuracies introduced into both theories by their common assumptions.

3.4 Application of the Kubelka-Munk Theory.

3.4.1 White Standards

An important fact to note about the KM function is that the variable is the ratio of two absolute values, the irradiation of the sample, I, and the flux diffusely reradiated from the sample, J. In order to measure these absolute values, the early work on diffuse reflectance spectroscopy was carried out using integrating spheres or hemispheres, coated internally with some white reflecting standard such as

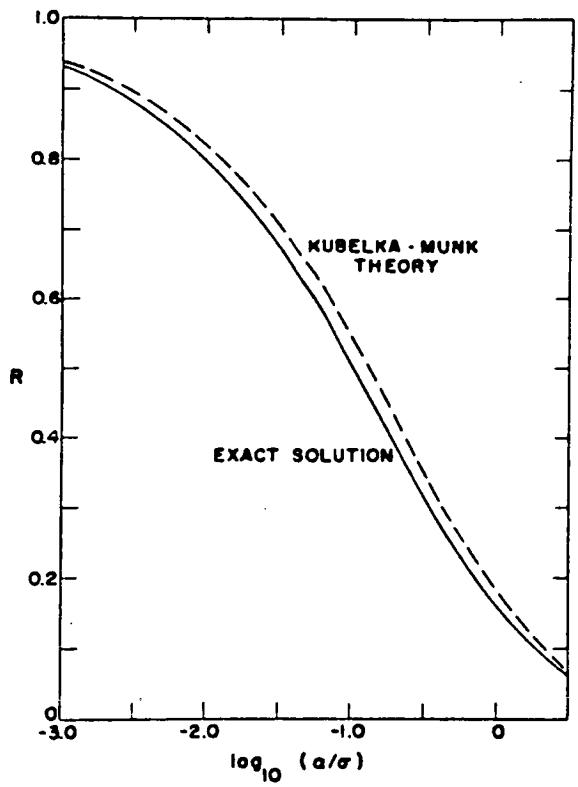

Exact solution to the equation of radiative transfer for diffused incident radiation and isotropic scatter (solid curve), compared with the Kubelka-Munk solution (dashed curve).

Figure 3.5: Comparison of the exact and Kubelka-Munk solutions to the radiative transfer equation (from [143] page 12)

magnesium oxide, with windows for irradiation, sample exposure and measurement. The reflecting sphere gave both isotropic irradiation of the sample, and measurement of light reflected in all directions. In order to use more conventional collection optics within modern commercial spectrometers, measurements are often taken against a standard, such as magnesium oxide or potassium chloride. If the standard can be assumed to have unit reflectance, then the relative reflectance,

$$R'_{\infty,sample} \equiv \frac{J_{sample}}{J_{standard}} = \frac{J_{sample}}{I}\frac{I}{J_{standard}} = \frac{R_{\infty,sample}}{R_{\infty,standard}} = R_{\infty,sample} \qquad (3.12)$$

for $R_{\infty,standard} = 1$. The calculation of $F(R'_\infty)$ will thus give the ratio K/S. At a given wavelength, if the chromophore concentration does not affect the scattering coefficient,

$$F(R'_\infty) = \text{constant}.\alpha C \qquad (3.13)$$

replacing K with $2.303\alpha C$ in analogy with the Beer-Lambert law (Equation 3.1). The KM theory has thus been experimentally verified by several authors [133, 144, and others] by plotting $F(R'_\infty)$ against C where the concentration was varied by diluting a chromophore with a white standard.

3.4.2 Diffuse Reflectance Spectroscopy in the Infrared.

Most of the work on diffuse reflectance spectroscopy by Kortüm and associates was carried out in the ultraviolet and visible regions of the spectrum, with particular emphasis on studying pigments, dyes and paper quality. These areas are particularly suited to diffuse reflectance spectroscopy because of the high absorbance of the materials, and the sensitivity of photocells for detecting the weak diffusely reflected signal. In the infrared region, however, the detectors available do not have the same single photon efficiency. Studies were therefore originally limited to rather low resolution studies of adsorbates such as that of Kortüm [145]. The use of integrating spheres was completely impossible because unlike in the visible, where inorganic solids such as magnesium oxide and barium sulphate have near

complete reflectance ($R_\infty = 0.987$ for MgO for 530 nm radiation [146]), even the best non-absorbing materials such as alkali halides have reflectances of no more than 0.95 [147]. With the necessarily large surface area of the integrating sphere compared with the detector and sample areas, the signal reaching the detector would be a small fraction of that diffusely reflected from the sample.

The solution employed by Kortüm [145] (and subsequently by others with their own variations) was to use ellipsoidal mirrors, a route followed by the manufacturers of several diffuse reflectance accessories available today. Such mirrors can focus a broad source onto a small area of sample, with light incident from a range of angles, as discussed in more detail below. The major breakthrough was, however, when Fourier transform spectrometers became readily available. The enhanced sensitivity of these spectrometers over conventional grating machines is sufficient to remove many of the worries over low signal levels – enough for Willey to market a Total Reflectance Spectrometer [148] with a gold coated integrating sphere. One of the early research groups to develop this field for catalytic studies was that of the FT-IR pioneer, P.R. Griffiths, who published their first paper on the subject in 1978, coining the acronym DRIFT(S), Diffuse Reflectance Infrared Fourier Transform (Spectroscopy) [149].

3.5 Experimental

3.5.1 The Fourier Transform Spectrometer.

The spectrometer used for all the infrared experiments in this thesis was a Digilab FTS-40 produced by the Digilab division of Bio-Rad [150], with data storage and manipulation on a Bio-Rad 3240SPC dedicated workstation.

The FTS-40 optical bench has a Michelson interferometer with a beam splitter made of a thin germanium film supported by potassium bromide plates. To provide a near friction free movement, the moving mirror is run on an air bearing supplied with dry air from a Gast compressor [151]. A HeNe laser beam passes through the interferometer, and is monitored with a light sensitive diode to give

by its interference fringes a precise measure of the mirror motion (retardation). The main laser beam exits to the diode via a hole in the centre of one of the stationary mirrors, with several of the focusing mirrors further down the beam path having centre holes to ensure that a large laser signal does not reach the infrared detector. Stray multiply reflected laser beams still occur, which are useful in locating the infrared beam path during alignment of the optics. The infrared source is a Globar lamp, a blackbody radiator at 1520 K [152] , with a recirculating water cooler to thermally isolate it from the rest of the spectrometer.

A major difference between this and other FTS-40 benches is that it is evacuable. The bench has a solid bulkhead between the main optical components mentioned above and the sample compartment, with a thick KBr window for the infrared beam. The two halves may be pumped independently by rotary vacuum pumps, which may each be valved off from the bench. To prevent contamination of the optics with volatalised pump oil, Edwards Foreline traps were added, filled with zeolite 5A. The sample chamber also has a solenoid valve which can be used to let it up to atmospheric pressure. To accomodate the extra plumbing, the electronic control circuitry normally incorporated within the base of the standard spectrometer model is housed in a separate module. This also protects it from the strong magnetic fields generated by the solenoid. The extra communications cables involved must be carefully shielded to prevent external electrical interference.

The reason for having the evacuation facility is to remove interference from atmospheric chromophores such as water and carbon dioxide. A solution often employed by others is to purge the beam path with dry air, reducing the water to a sufficiently constant low level that any miscancellation errors in ratioed spectra are small compared with the features under investigation. This is not always completely effective *eg.* [153], and unless the carbon dioxide is also scrubbed, this may remain as a major miscancellation feature [154, 155].

The use of a Fourier transform spectrometer gives the well documented

benefits over dispersive instruments of accurate wavelength determination (Connes advantage, necessary for co-addition of interferograms for signal averaging) higher throughput (Jaquinot's advantage due to lack of narrow slits to define resolution) and multiplexing (Fellgett's advantage, as all wavelengths are recorded simultaneously) [156]. The latter two are of course necessary to overcome the inherent weakness of the diffusely reflected signal. Because the data must be stored electronically to allow the Fourier transform to be computed, the required workstation is also available for data manipulation, storage and presentation.

The limiting factor for the signal to noise ratio (SNR) is usually the dynamic range of the analogue to digital converter (ADC). If the noise level is not greater than the least significant bit of the ADC, then during digitisation of the interferogram, the noise level will be rounded up to the digitisation level. Although spectral information is carried in all parts of the interferogram, corresponding to the full range of retardation, the SNR is limited by the centre burst, the zero retardation point where all light from the infrared source interferes constructively, giving the maximum signal (Figure 3.6). When the interferogram is transformed using the Cooley-Tukey fast Fourier transform algorithm [157], it is changed from a function of retardation to one of frequency, and the resultant spectrum is normally known as a single beam spectrum (Figure 3.7).

3.5.2 The Single Beam Profile

The form of the single beam spectrum is a function of several variables:

1. The radiation profile of the Globar source – that of a black body at 1520 K.
2. The absorbance of optical components in the beam path such as the beam splitter and the window between the vacuum compartments. This will unavoidably include organic contamination on their surfaces.
3. Absorbance of atmospheric contaminants, generally negligible under evacuation.

4. The signal remitted by the sample.

5. The sensitivity profile of the detector.

Of this list, it is clear that 4 is the item of interest, and the others are hopefully constants that can be removed by comparison with some reference spectrum. In practice, of course, all four of these factors in the signal vary to some degree, though 3 will be almost constant using the vacuum bench.

Despite a constant power input and water cooling system, the infrared source does exhibit some minor shifts over time. Along with changes in background emission, this may lead to long period variations or wobbles when considering ratioed spectra.

The beam profile will be restricted to within an envelope corresponding to the transmission of KBr, which is of course constant. Although the optical components will have some organic contamination, this should have little temporal variation provided rotary pump vapour is excluded using Foreline traps. The major errors under point 2 are probably due to slight instabilities in the mirror travel, which may cause steady slopes across the spectral range, possibly significant for weak spectra [154].

The evacuation of the optical bench of the spectrometer effectively removes nearly all gases from the beam path. When the sample is enclosed in an environmental chamber (Section 3.5.5 below) for processing and dosing with gases, however, approximately 1.5 cm of the beam path is not evacuated. Gas phase species may therefore be easily seen during dosing, with water vapour being significant during reduction and heating of the catalyst. This water was rarely a problem, though the gaseous hydrocarbons sometimes obscured the spectra of surface species.

The change in the signal due to the sample is of course what infrared spectroscopy is trying to find. As the simple absorbance of the material under study is not necessarily the dominant cause for this change in DRIFTS, this will be discussed in depth below.

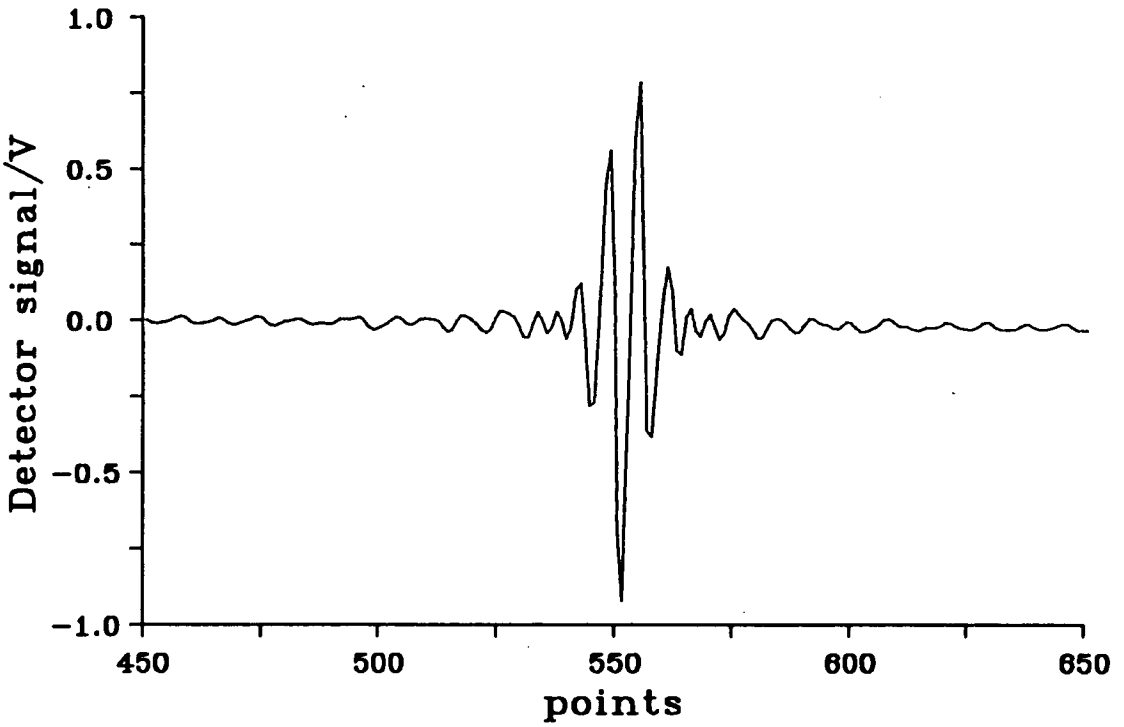

Figure 3.6: Interferogram recorded on the FTS-40.

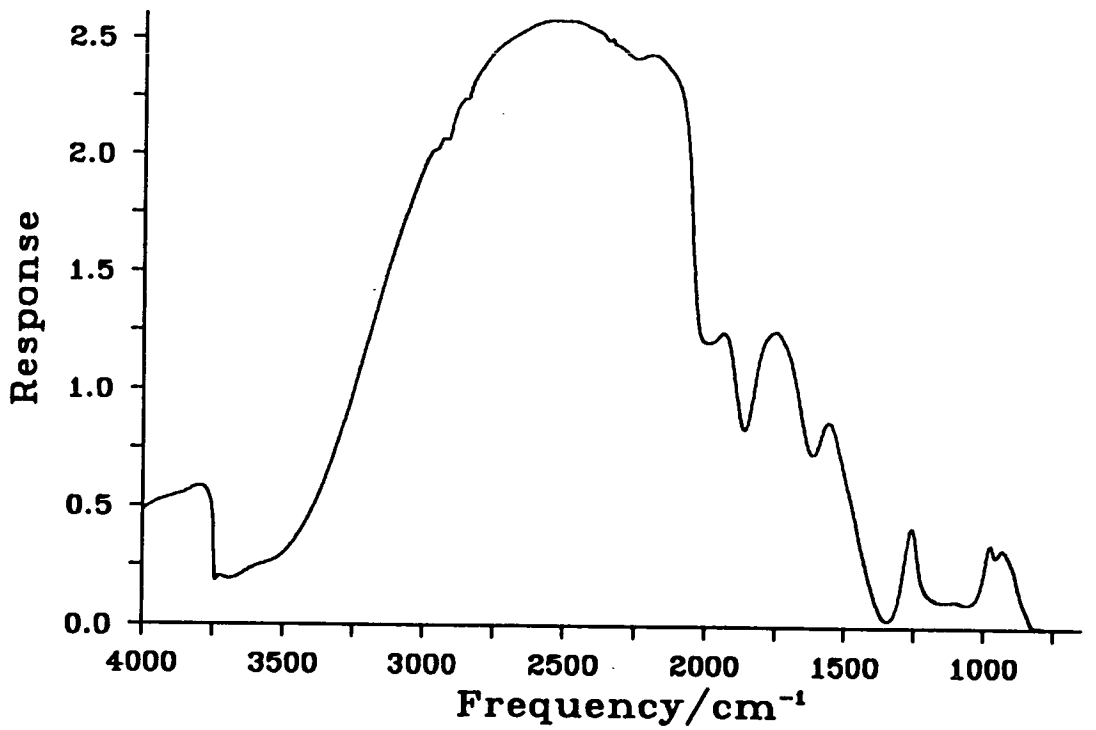

Figure 3.7: Single beam spectrum at 4 cm^{-1} resolution produced by Fourier transformation of Figure 3.6.

Another envelope delimiting the single beam profile is the detector response. The detector used was a liquid nitrogen cooled narrow band mercury cadmium telluride (MCT) detector capable of monitoring the spectral range 4000–700 cm^{-1} at a frequency of 20 kHz. At saturation, the output signal was an interferogram of 20 V peak to peak (maximum value 10 V), which caused the ADC to overflow. The signal level was therefore always reduced where necessary by attenuating the beam with an aperture, or reducing the gain on the detector pre-amp. The liquid nitrogen cooling for the operation of the detector requires the detector to be cased in a vacuum jacket. One of the functions of this, beyond the obvious one of reducing the reheating rate of the copper heat sink, is to keep contaminants away from the detector lens. On exposure to atmosphere, ice condenses onto the lens and reduces the infrared signal. The detector could thus contribute two sources of signal drift, due to a reduction in sensitivity on warming up from liquid nitrogen temperatures, and ice build-up due to softening of the vacuum. Both these were reduced by regular evacuation via an ultra high vacuum rig [158], and the former by frequently refilling the liquid nitrogen reservoir during the course of an experiment.

3.5.3 Data Storage and Manipulation

The detector signal is digitally stored in the 3240SPC after conversion through the ADC. The fast response and good sensitivity of the MCT detector reduce the collection time per scan compared with other available detectors. This allows rapid co-addition of interferograms to reduce the noise level by signal averaging. The noise level in the single beam is of course related to that in the recorded interferograms. When the interferogram produces a spectrum of n points or spectral elements where

$$n = \frac{\tilde{\nu}_{max} - \tilde{\nu}_{min}}{\Delta\tilde{\nu}}, \tag{3.14}$$

the wavelength range divided by the resolution of the single beam, the noise level in the single beam isincreasedfrom that of the interferogram by a factor of $\sqrt{n}$

[154]. When the start of the mirror travel is accurately marked by a flag crossing between a light beam and a photocell, the spectra may be co-added with a precise point to point matching of retardation. This gives an improvement in SNR to a factor $\sqrt{N}$, where N is the number of co-added spectra (limited only by the dynamic range of the 16 bit word computer with double precision arithmetic).

Once the single beam spectra have been calculated the 3240SPC has several software routines for data handling. Two such spectra may be ratioed to produce either absorbance or transmittance spectra, and transmittance spectra converted to Kubelka-Munk units. Several spectra could be displayed concurrently on the monitor for direct comparisons, and subsequently be plotted out on a Graphtec WX4751 Watanabe plotter. The *basecorr* routine allowed a spectrum to be corrected to a baseline defined by the user with up to twenty fixed points joined by straight line segments or a spline fit. This was used, always with a spline fit to remove broad changes in the underlying silica spectrum caused by the state of hydration, temperature effects, or movement of the sample. Spectral peaks were automatically integrated using the *class* script, which also gave values for the maxima within predefined wavelength ranges. Another useful feature was the interactive *SUBTRACT* program, where one spectrum could be subtracted from another. The spectrum to be subtracted could be scaled by an arbitrary scaling factor chosen with a joystick. This was particularly valuable for identifying common features between spectra, removing gas phase contributions by subtraction of references, and averaging spectra. This last task was achieved by setting the scaling factor to –1, therefore adding the spectra, and subtracting half of the resultant spectrum from itself to divide by two. All software used, including the items just mentioned, was either standard on the 3240SPC or obtained from Digilab [150], except for some small routines to control timed data collection, store data on floppy disc and plot multiple spectra written using spectrometer commands detailed in the 3240SPC manual, and shell commands of the IDRIS operating system of Whitesmiths Ltd.

The use of the MCT detector meant spectra could be collected very quickly, at around half a second a scan for 4 cm^{-1} resolution. At this resolution, an adequate SNR could be achieved by co-adding only a small number of scans, which meant that including the storage of the interferogram onto hard disc, spectra could be collected with a repeat time of thirty to forty seconds, depending on the amount of free space on the hard disc. 4 cm^{-1} resolution was used for all spectra in this thesis. There is always a trade off between sensitivity or speed of recording and resolution, but because the infrared bands of molecules adsorbed on supported metal catalysts are typically quite broad, 4 cm^{-1} appeared to by adequate. All frequencies recorded for this thesis are therefore only quoted to the nearest 2 cm^{-1}.

3.5.4 Diffuse Reflectance Optics

The optical system used to collect the diffuse reflectance spectra was an off the shelf unit, the Spectratech 'Collector' [159] designed to fit in the sample compartment of commercial spectrometers such as the FTS-40, with locating pegs and a lock screw (Figure 3.8). It has four planar and two ellipsoidal mirrors, each silvered to give an infrared reflective surface. The planar mirrors could be both rotated and tilted for and aft to adjust the beam path onto the sample.

The unit fitted in the sample compartment so as to position the sample post in the vertical plane where the infrared beam was normally focused. The infrared beam was deflected by the two input mirrors, initially down, then up onto the underside of the first ellipsoidal mirror, which focuses the beam onto the sample. The range of angles from which the light is incident will be a function of the original spread of the beam, and the solid angle subtended by the window of the environmental chamber (see below). This range is important in consideration of the validity of the KM theory. Light reflected or remitted by the sample will be collected by the second ellipsoidal mirror and redirected back to the original beam path of the spectrometer for detection. The ellipsoidal mirrors could be withdrawn along grooves to allow access to the sample, and the back plate of the

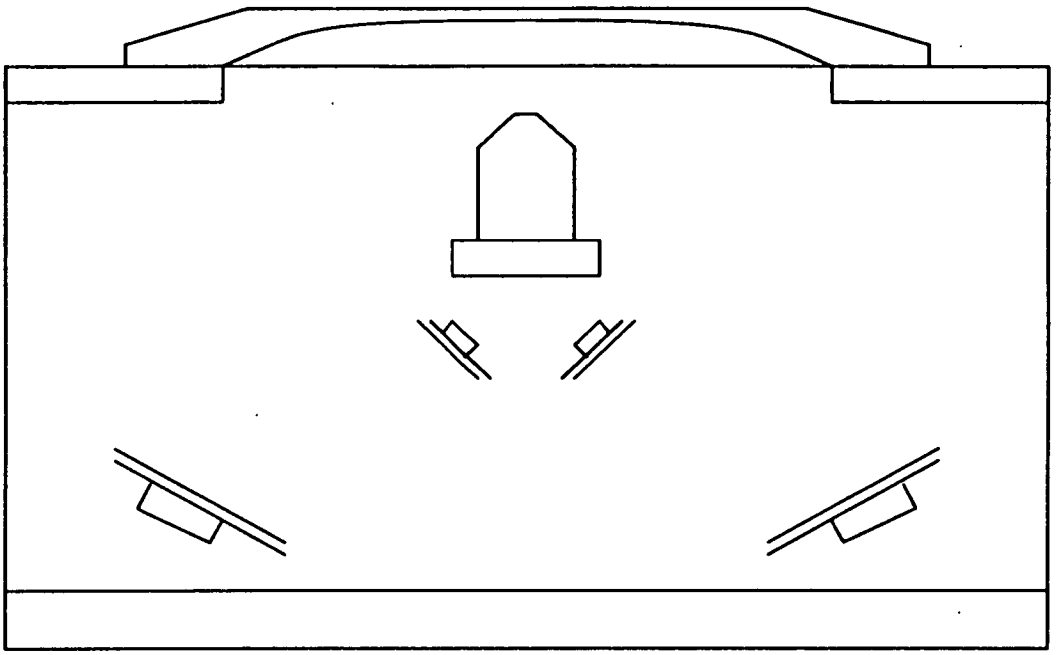

Figure 3.8: Mirror unit of the Spectratech 'Collector' accessory.

accessory had runners for adjustment of the sample height.

3.5.5 Environmental Chamber

The Collector accessory was augmented by a compatible environmental chamber, Figure 3.9 [160], which allowed sample processing under controlled gaseous environments. The sample post incorporated a heater unit with in built thermocouple and three outlets for gas dosing, one at the base of the post, one directly under the sample, and the third from a tube opening level with the sample cup. In the experiments, the first of these was the gas inlet, the second used as a gas outlet, and the third was blanked off. The sample was isolated from the ambient spectrometer atmosphere by a stainless steel cap fitted with two KBr windows, each sealed by a thin Viton o-ring and brass clamping plate. The base was sealed by a larger Viton o-ring which was protected from the temperature extremes of the heater by an internal water cooling system.

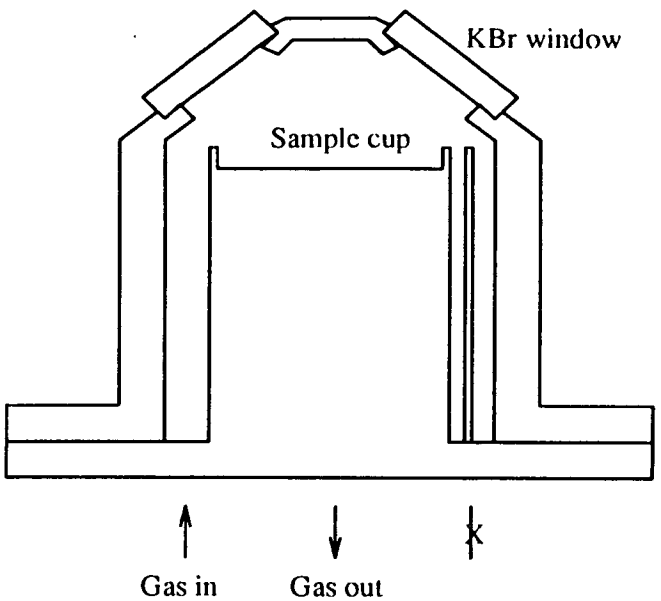

Figure 3.9: Environmental chamber and sample block.

The sample temperature was monitored in one of two ways. Initially, the integral K-type thermocouple was used. This, however, recorded the temperature at the top of the heater, rather than directly at the sample, which could show a considerable discrepancy. A calibration curve was therefore plotted for the heater temperature by gluing a K-type thermocouple through a KBr window in the cap, and monitoring the sample temperature and heater temperature through a blank experiment. A more straightforward method of direct measurement was later adopted. A replacement cap was machined by John Ashfield of the mechanical workshop, incorporating a hollow side arm which extended beyond the ellipsoidal mirrors. Through this a thermocouple was placed directly in the sample. The thermocouple leads were Araldited [161] into a stainless steel tube which was attached to the side arm with a Swagelok [162] coupling for full vacuum and pressure tightness, and complete demountability.

Three gas ports and two connectors for the water heater were attached by

Swagelok couplings at the rear of the baseplate to stainless steel $\frac{1}{16}''$ tubing. In pilot experiments, these tubes and the heater and thermocouple leads were sealed using sticky tape into a polythene sheet covering the sample compartment entrance, and the volume purged with dry air from the compressor. For the experiments described in this thesis, a metal plate was modified to provide a vacuum seal. Seven Swagelok bulkhead connections, two of $\frac{1}{4}''$ and five of $\frac{1}{16}''$ were tapped into this lid, and drilled through to allow piping of appropriate dimensions to pass freely. The heater and thermocouple wires were each Araldited into $\frac{1}{4}''$ o.d. nylon tubing. By using specially straightened $\frac{1}{16}''$ tubing for the gas and water supplies, and PTFE Swagelok ferrules, the lid could be moved up and down relative to the DRIFTS accessory for access and adjustment, then lowered onto an o-ring round the sample compartment port and the whole beam path evacuated.

3.5.6 The Gas Handling System

The sample was treated with gases prepared using a trolley mounted vacuum rig and flow system, as shown schematically in Figure 3.10, refered to through this section. The basis of the flow was cylinder helium (BOC Ltd.) with several extra stages of purification. The first was a glass trap (A) filled with copper turnings (BDH Ltd.) and heated to 620 K for the duration of the experiment, with the intention of reducing carbon monoxide. Although this is not a major contaminant of the helium, it can be a problem when studying supported platinum catalysts in the infrared. As can be seen in a profusion of papers on the subject, the strength of the chromophore makes even a small surface coverage a large spectral feature. Chemical effects can also be seen in coadsorption studies, when the donation of electrons to the surface by carbon monoxide [63, 64] alters bonding strength and hence vibrational frequencies. Adsorbed carbon monoxide would also reduce the availability of binding sites.

The helium stream passes through a Perkin Elmer control box (B) with valve

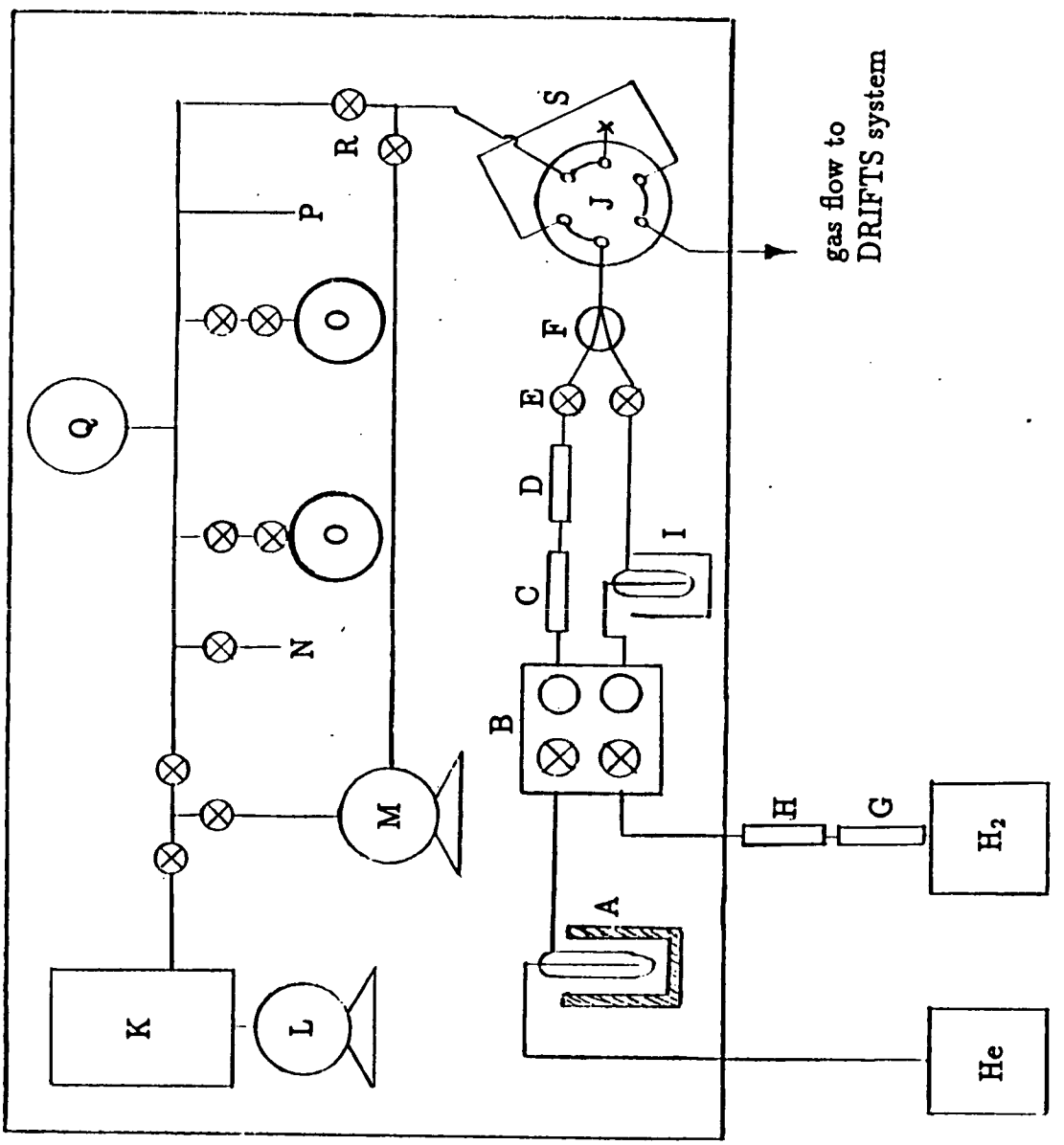

Figure 3.10: Trolley mounted vacuum line for DRIFTS experiments. Key as described in the text, page 80 to page 83

and pressure gauge, followed by an Englehard oxytrap (C) and zeolite sieve trap (D) to remove any water the oxytrap creates. Fine flow control was achieved with a Brooks leak valve (E), before the Perkin Elmer six way valve (F) adapted to switch between helium and the hydrogen supply for reduction.

The hydrogen supply was also purified before use, with a Deoxo oxytrap (G) and sieve trap (H) at the cylinder, and after the Perkin Elmer control box, a zeolite 4A filled cold trap in liquid nitrogen (I). A leak valve allowed fine flow control before the union of the two supply lines.

From that point, the flow system passes through a Carle six way valve (J), used in a similar manner to that described previously (Figure 2.2), into $\frac{1}{16}''$ o.d. stainless steel tubing to the environmental chamber of the DRIFTS apparatus (Section 3.5.5). The thin tubing allowed full flexibility of movement of the cell, with Swagelok fittings for demountability and gas tightness. During many of the experiments described below, a Gow Mack thermal conductivity detector was under trial to monitor dosing gases entering and leaving the environmental chamber, though no results from this will be discussed in this thesis. In order to separate in time the incoming and exit signals, a delay loop of $\frac{1}{4}''$ tubing was used to increase the sweep volume of the input gas stream between the two halves of the detector. The exit stream passed through a simple bubble meter for flow measurement before being vented outside the laboratory.

Dosing gases were prepared in the glass vacuum line pumped by an Edwards EO2 oil diffusion pump (K) backed with an Edwards ED50 type rotary vacuum pump (L). A second rotary pump (M) was available to rough out the line, and to evacuate the sample loop of the Carle valve (*cf.* Figure 2.2). Gases were introduced via a Youngs greaseless tap with a $\frac{1}{4}''$ ground glass port from regulated lecture bottles [163]. They could be stored in detachable glass bulbs (O), and purified with freeze/pump/thaw cycles in the glass finger (P). Pressures were measured on a Leybold-Hereaus spiral gauge (Q). A gas sample was introduced to the flow by first evacuating the sample loop, establishing a known pressure of

gas in the glass line, opening this to the sample loop via a Nupro toggle valve (R), and turning the Carle valve so the sample loop became part of the helium path, and the gas swept onward to the catalyst. The sample loop was then removed from the flow by returning the Carle valve, and evacuated ready for the next pulse.

3.5.7 Procedure

The sample to be studied was crushed in an agate mortar, and placed in the cup of the sample holder. Typically between 45 and 50 mg were required to give a surface level with the edges of the cup. The cap for the environmental chamber was added, with the thermocouple just buried in the catalyst surface, and the gas flow established. The whole sample and mirror assembly was lowered into the spectrometer, and the mirror angles and sample height adjusted to give maximum diffuse signal. Care had to be taken that a specular maximum had not been found, and therefore surface information lost. The lid was then slid down the tubes of the gas, power and thermocouple connections, and the optical bench evacuated. The Swagelok fittings on the lid were not tightened until a moderate vacuum had been reached, to allow relaxation of the spectrometer and optics under the pressure change.

With the sample under vacuum, the hydrogen flow rate was compared with the rate prior to evacuation to check for leaks, and set to 50 $mlmin^{-1}$. The temperature was raised at *circa* 15 $Kmin^{-1}$ to prevent sintering, and the sample reduced for an hour at 570 K. The flow was switched to helium at 10 $mlmin^{-1}$, and the sample outgassed at the slightly higher temperature (590 K) achieved under the slower flow. After half an hour, the catalyst was cooled to the desired temperature for the experiment. A background spectrum was then recorded, of 250 scans at 4 cm^{-1} resolution.

The dosing gas was prepared at the required pressure in the glass line. The data station was set up to collect 32 scan interferograms sequentially. With

each taking about 10 seconds to record, with 20 to 30 seconds required for data storage, depending on the amount of space on the hard disc, a spectrum could be recorded every 30 to 40 seconds. The gas pulse was introduced to the flow, then data collection started. The volume swept out between the Carle valve and the environmental chamber meant gas was detected in the infrared signal by the third or fourth spectrum. After typically thirty spectra had been collected, and most of the surface chemistry had taken place, a spectrum of 128 scans was collected, for a better signal to noise ratio.

Further pulses of gas were monitored in a similar manner. Temperature programmed desorption (TPD) experiments were run by recording 50 scan spectra with a slight time delay in the collection loop, and a heating rate of 12 $Kmin^{-1}$, to give a spectrum every 10 K.

The data was Fourier transformed to single beam spectra, and absorbance spectra calculated using the background collected earlier. For presentation, spectra were baseline corrected where necessary.

3.6 A Critical Evaluation of DRIFTS and Comparison with Transmission.

The very different nature of DRIFTS and transmission spectra is illustrated by Figure 3.11, the single beam spectra of the same sample recorded on the same spectrometer by the two techniques. This section will discuss the physical reasons behind these differences, and the implications on analysis of the spectra. The argument in part follows that set forward by Holmes *et al.* [164].

Without reference to Figure 3.11, a major difference between the SNR in the two techniques is apparent simply by examination of the equations used to produce the spectra, following an argument by Griffiths *et al.* [165]. Considering Equation 3.1, replacing I/I_o by T, the transmittance,

$$\begin{aligned} -\log_{10} T &= \alpha C l \\ T &= 10^{-\alpha C l} = e^{-2.303 \alpha C l} \end{aligned}$$

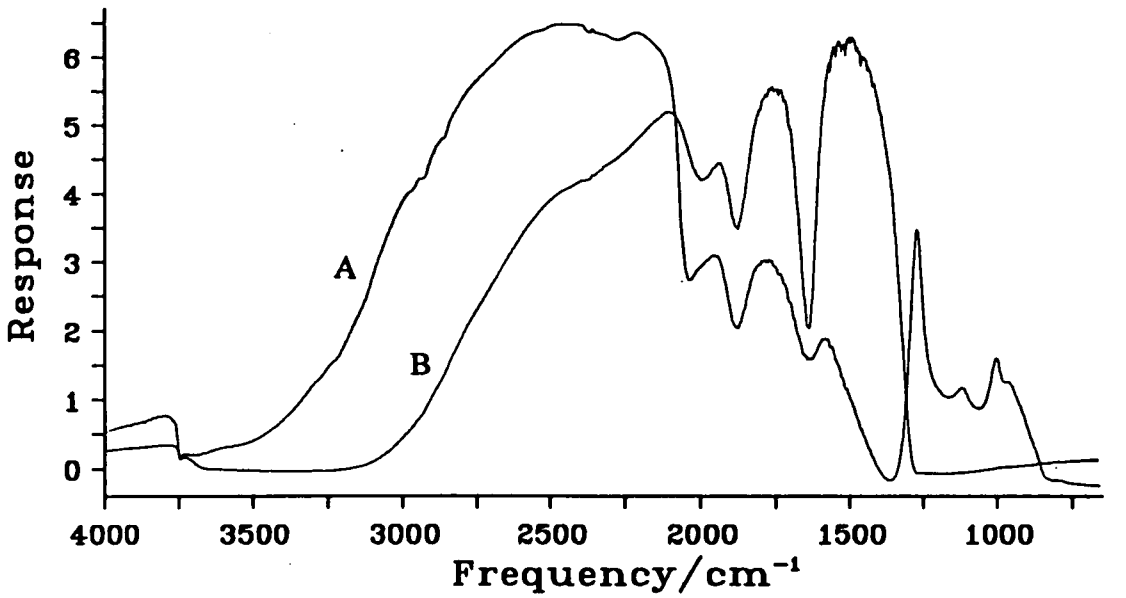

Figure 3.11: A. DRIFTS single beam spectrum of EuroPt-1. B. Transmission single beam spectrum of EuroPt-1.

$$T = 1 - 2.303\alpha Cl + 2.651\alpha^2 C^2 l^2 - (\alpha^3 C^3) + \ldots \qquad (3.15)$$

from the definition of the exponential function. The signal which is due to absorption by the sample is $1 - T$, so for constant noise level (ADC limited) and low absorbance, when squared and higher terms become insignificant, the SNR will be linear in absorption coefficient. When a similar analysis is applied to the diffuse reflectance and the Kubelka-Munk function (Equation 3.11) the absorption signal level is given by

$$(1 - R_\infty) = \sqrt{\frac{4.605\alpha C}{S}} \qquad (3.16)$$

when the absorption coefficient is low and $R_\infty \simeq 1$. In diffuse reflectance spectroscopy the SNR is therefore greater at low absorption coefficient being proportional to $\sqrt{\alpha}$ rather than α. This will play against the technique at higher absorption coefficient though of course the assumptions of the above argument will no longer apply.

The first point to note about Figure 3.11 is that the two spectra have been normalised to the maximum signal level. In absolute value, the DRIFTS spectrum may typically lag the transmission signal by a factor of 10 or 20. This is a result of the efficiencies of the two processes. As described in Section 3.2 above, the

transmission signal is attenuated by absorption and scattering, and is nearly all collected by the detection optics. The DRIFTS signal may be considered as the sum of two parts, firstly the diffuse reflectance, which has undergone at least one scattering incident within the sample of diffraction, refraction and reflection, and which will have an isotropic distribution. The second is the specular or mirror like reflection from planar surfaces of the sample. Although the particle positions will lead to many reflections directed away from the optical axis of the DRIFTS accessory, the levelling of the sample surface skews the position distribution to give more faces level with the top of the sample cup. Specular radiation, which has only undergone a single reflection is thus predominantly directed along the optical axis. When the mirror arrangement of Figure 3.8 and the vignetting effect of environmental chamber windows are taken into consideration, it is clear that only a portion of the true diffusely reflected light will be collected, along with a larger fraction of the specular reflection. (This is a situation avoided by some other diffuse reflection accessories, such as that used by the Ohio group [149]. It also contributes to the increased intensities recorded with the ellipsoidal mirror arrangement.) When edge losses due to the finite width and depth of the sample are also considered, the lower signal is well understood.

The next point of interest in Figure 3.11 is the relative single beam profiles. Despite being of the same sample in the same spectrometer, the spectra are very different. With the DRIFTS accessory only introducing extra silvered mirrors and KBr windows over the transmission experiment, the difference must be due to the different processes involved.

Over the frequency range from 4000 cm^{-1} to 2200 cm^{-1}, the proportional signal in DRIFTS is much greater than that of transmission. Around 3000 cm^{-1} is the region where DRIFTS has the greatest advantage, due to the high equivalent path length through the sample. In non infrared absorbing regions such as this, the sampling depths are of the order 2.5 mm [166, 167]. As the sample cup is 2 mm deep, the radiation will pass through as much as 4 mm thickness of sample in its

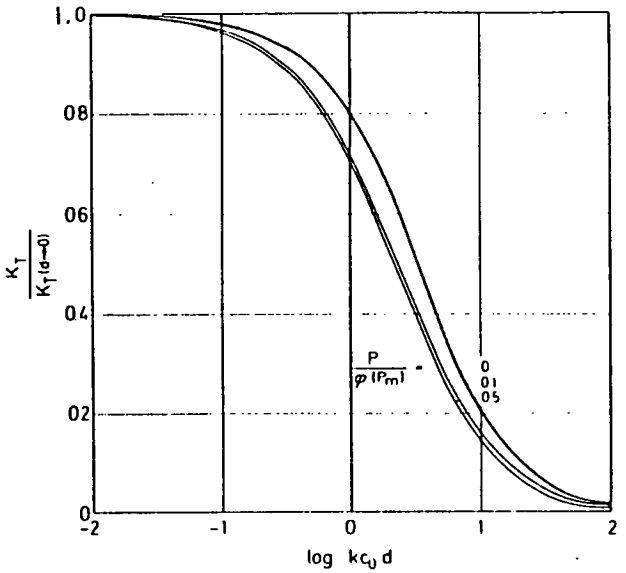

Figure 3.12: Variation of light absorption in heterogeneous systems (from [169])

two way journey. The path length for isotropic radiation, however, is greater than that for directed radiation because it is travelling at all angles from the vertical to horizontal. Averaged over all angles, this gives a further factor of 2. This path length is therefore large compared with the transmission samples, typically a small fraction of a millimeter.

The high wavenumber region is also where transmission spectra start to suffer scattering losses. Following the arguments of Sections 3.1 and 3.3.1 above, for the catalyst particle size used (1 to 40 μm determined by optical microscopy), the scattering will increase for higher wavenumbers, and less information will reach the detector, leading to decreased SNR compared with the fingerprint region [168].

At frequencies above 2200 cm^{-1}, the beam profile starts to be influenced more by the sample than above. The intense absorption due to overtone and combination bands of the lattice modes of EuroPt-1's silica support is more pronounced in Figure 3.11 A than B. This can again be attributed to the greater path length experienced in DRIFTS. Another feature to be noted between 2200 and 1500 cm^{-1} is the comparative flatness of the spectrum A. This flatness is in part explained by the shape of the graph in Figure 3.12 [169]. This shows the behaviour of equations

derived by Felder [170] (though unfortunately the function plotted approaches the problem from a different direction to the priorities of this discussion). Plotted along the x axis is the logarithm of the product of the true absorption coefficient, the concentration and particle diameter for a system of monodisperse particles. If the concentration and particle diameter are set as constants (which they are through the frequency range of one DRIFT spectrum) this therefore becomes a measure of the absorption coefficient. The y axis gives the ratio of the observed absorption coefficient as a fraction of the absorption coefficient for infinitely small particles (and the parameter of the three curves is the packing density, which is not relevant to this discussion). The prediction of the graph is therefore that when absorbance is low, the measured absorption coefficient will be close to ideal. As the absorbance increases, however, measured absorbances will be less than expected for the equivalent infinitely dispersed system. The implication of this is that at strong absorbance bands, the measured absorbance will not increase in line with the actual absorbance. This is also implied by the Kubelka-Munk theory discussed above.

The region below 1500 cm^{-1} exhibits perhaps the largest contrast between the spectra in Figure 3.11. The transmission spectrum falls to complete blackout below 1260 cm^{-1}. The DRIFTS spectrum also touches down for a blackout in this region, and it is initially surprising that this occurs at 100 wavenumbers higher than in transmission. This difference is due to the Christiansen effect [171], and is a feature caused by the rapid variation of the refractive index with frequency around strong absorption features, known as anomalous dispersion. This variation starts for silica at the onset of the Si – O absorption band at 1450 cm^{-1} with a rapid reduction from the steady value of *circa* 1.5 through zero to negative values, before rising and falling again to *circa* 1.5 by 600 cm^{-1} with a derivative form [172]. At 1300 cm^{-1}, $n = 1$ and the sample no longer presents a significant refractive index change from the surrounding medium, so no scattering can occur. Specular reflectance will also be low at this point, as the decrease in real refractive

index occurs before the main increase in absorption, and so near zero signal levels are reached.

At wavenumbers below the initial blackout, whereas the transmission spectrum has no further intensity, the DRIFTS spectrum shows considerable signal levels, particularly at 1268 cm^{-1} and to a lesser extent at 990 cm^{-1}. This effect was discussed by Vincent and Hunt [173] and is due to specular reflection. When a material has a strong absorbance region, there is an increase in specular reflection as given by Fresnel's theory of reflectance, bearing in mind the contribution of absorbance to the complex refractive index. With moderate absorbance, this can lead to a band shift to higher frequency [174]. For stronger absorbances, the reflectance increases so much it gives large peaks such as those at 1268 cm^{-1} and 990 cm^{-1}, known as *reststrahlen* bands [175]. This is the reason there is not a second blackout when the anomalously dispersed refractive index rises back through $n = 1$ after the negative peak. Because specularly reflected light has not passed through any sample particles, it will contain little or no useful information on the catalysts. This intensity beyond the transmission blackout can, however, give information on gas phase species within the environmental chamber.

The contribution of specularly reflected light to the spectrum is likely to be another factor in the flattening of DRIFTS spectra in comparison with transmission, contributing most intensity at areas of highest absorption. The effect is illustrated in Figure 3.13, a plot of experimental $F(R_\infty)$ against real $F(R_\infty)$ for increasing absorbance as parameter [177]. A similar graph was also produced by Hembree and Smyrl [178].

An obvious method for reducing specular reflection is by polarising the incident light and analysing the reflected light with a crossed polariser. The specular reflectance which retains its polarisation on reflection will be more highly attenuated than the isotropic diffuse reflectance, which will have lost all memory of the original polarisation. This was investigated by Griffiths and co-workers but the *reststrahlen* bands could not be entirely eliminated, particularly when using

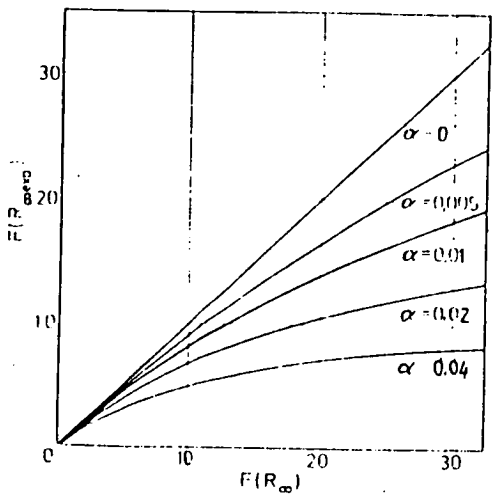

Figure 3.13: Influence of regular reflection on $F(R_\infty)$ of absorbing powders.

a Spectratech Collector [174]. The reason for this suggested by the authors was the semi-random orientation of the reflecting particle surfaces which left many of them contributing to the specular signal away from the optical axis. This effect was described by Yang *et al.* in a similar study, as the sample acting as a "pseudo-scrambler" [176]. The high curvature of the ellipsoidal mirrors of the Collector accessory would also increase the range of angles of incident light over the much larger mirror of Griffiths' spectrogoniophotometer.

The specularly reflected radiation may also be effectively removed by a blocker, an opaque blade touching the sample surface vertically, allowing only light which has penetrated the sample to be collected [179].

The primary disadvantage of both the polarisation and blocker methods is the reduction in signal intensity, affecting the diffuse as well as the specular component. As low signal levels can be a problem in DRIFTS, the only action taken in the experiments described below to reduce specular reflection was grinding to a fine powder. It is worth noting here that *reststrahlen* type features may be produced simply by scattering. This suggestion was put forward by Eickhoff *et al.* following computer simulations and experiments for SiC [172], but is unlikely to be relevant to spectra in this thesis, given the wide difference in refractive indices between SiC (n=2.6) and SiO_2 (n=1.4 to 1.5).

3.7 The Practical Application of DRIFTS.

From the discussion above, it is clear that there are advantages to DRIFTS over transmission, particularly at the higher frequencies corresponding to the carbon-hydrogen stretching region of the spectrum [164]. As ever, of course, there are swings and roundabouts, with some specific disadvantages of the Collector accessory, which must be born in mind when carrying out the experiments.

All samples were carefully ground with an agate mortar and pestle to give particle sizes in the range 1 to 40 μm. The fine grinding was to reduce Fresnel reflection, which occurs at crystal faces large compared with the wavelength. The reduction could be clearly seen in the height of the 1268 cm^{-1} peak in the single beam spectrum. This also gave information on optical alignment, as predominantly glancing incidence increased the Fresnel contribution. As particle size decreases, so does the scattering power (Equation 3.2). There is therefore a degree of trade off between reduction of specular reflection, and the validity of the R_∞ approximation of an infinitely thick sample. Fuller [166, 167] has shown that this will only be a worry for samples much thinner than the 2 mm of the Collector sample cup due to the rapid rise of the $F(R_\infty)$ verses sample thickness graph.

The usual approach for eliminating scattering effects has been to distribute the sample in excess of a white standard such as KCl. When KCl is used as the background for R'_∞, all scattering effects are generally removed, as at sufficient dilution, all the scattering is due to the standard rather than the sample. It was pointed out by Van Every [155], however, that this is not always a safe option in catalytic studies, because both alkali metals ions and halide ions can have significant effects on catalyst activity. With a main preoccupation of this thesis being the study of alkali doping effects, this is particularly pertinent here. Other standards used either show activity which may affect the science under scrutiny, or significant absorbances of their own. The reduced catalyst was therefore used as background for all spectra shown below, and the experiments performed on undiluted catalyst. This also has the advantage of presenting a higher concentration

of catalytic sites for reagent adsorption.

The diffuse reflectance of a sample is found to be a function of the pressure which is applied during preparation [180, 181]. As this can have an appreciable effect, at least three methods are suggested in the literature to standardise packing. Leyden *et al.* [180] used a threaded press to which a standard torque was applied, Griffiths *et al.* [181] hung a standard weight from a press handle and several others levelled the powder surface with a razor edge. As this last method was specifically contraindicated in the Spectratech user notes, the level surface was produced by gentle pressing with a flat edge much narrower than the cup dimensions, to allow redistribution of the sample rather than compression. Pressure effects were also less important, as the sample always acted as the background for the sample/absorbate system, and no absolute values were used.

In his excellent review, Kortüm mentions the effect of water in the capillaries of a porous sample, suggesting the increase of the surrounding refractive index reduces the scattering ability of the sample. Although this contradicts one of his earlier claims [182], it is an effect that can be clearly seen in experiment. When the catalyst sample was heated for reduction, the signal levels rose, as might be expected if emission was significant, but retained a 20 to 30% improvement in signal on cooling, due to the thorough drying.

Throughout this thesis, spectra are presented using the reduced, outgassed catalyst as background. The basis for doing this is not as straight forward as for conventional spectroscopies, as is discussed in depth by Kortüm [183] and mentioned in Section 3.4.1 above. If Equation 3.12 is considered again, and $R_{\infty,catalyst}$ is used for $R_{\infty,standard}$, the final equality no longer holds, as $R_{\infty,catalyst} \neq 1$ except for limited areas of the spectrum. The absorbance of the catalyst background might be eliminated by measuring its reflectance relative to some white standard which meets the $R_\infty = 1$ requirement. The incident intensity, I, can then be introduced into the equation by expansion of the fraction,

$$R'_{\infty,sample} = \left(\frac{J_{sample}}{J_{catalyst}}\right) \cdot \left(\frac{J_{catalyst}}{J_{standard}}\right) \cdot \frac{J_{standard}}{I} = R_{\infty,sample} \qquad (3.17)$$

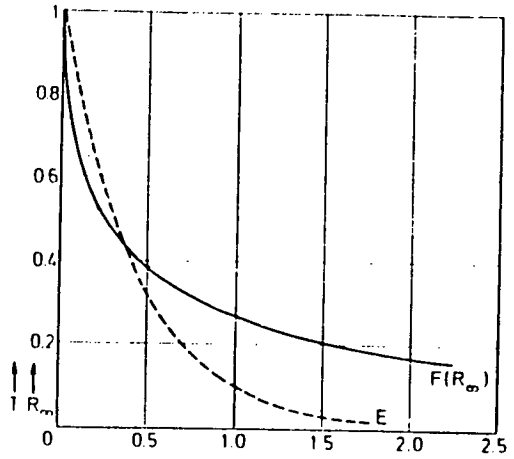

Figure 3.14: $F(R_\infty)$ and absorbance, E, as functions of R_∞ and T respectively.

with the first two terms measurable, and the last being 1. This is a reasonable method in the ultraviolet and visible, where good standards exist. Despite being frequently applied in the infrared, however [184], the $R_\infty = 1$ assumption does not hold even for the best diffuse reflectors such as the alkyl halides (page 70 above). Absolute values can not be obtained without an integrating sphere, or a detailed absolute spectrum of a standard such as KCl.

As discussed above, diffuse reflectance spectroscopy is more sensitive to low absorptions than transmittance. The Kubelka-Munk function and Beer-Lambert laws are both derived to linearise the signal output with respect to real absorbance (sample absorbance, concentration and thickness). It is therefore no surprise when the absorbance and $F(R_\infty)$ are compared as functions of T and R_∞ as in Figure 3.14 that at low signal attenuation, (large R_∞, T) the $F(R_\infty)$ values are lower than absorbance values, and *vice versa* at higher attenuation.

In this thesis, spectra are presented in absorbance rather than Kubelka-Munk format. This has the advantage of accentuating weaker absorption features, making use of the sensitivity of the diffuse reflectance technique, and the disadvantage of removing the Kubelka-Munk function's linearity with sample absorbance. This will be particularly noticeable in the fingerprint region of the spectrum, where absorption by surface species will occur on top of the significant SiO_2 absorption,

and therefore in the less sensitive range of diffuse reflectance. The low signal levels in this region are amplified by presentation in absorbance units, but unfortunately the noise is too, and poor spectra result. The benefits in looking at weaker features is particularly significant when studying hydrocarbons, or when the signal is attenuated by the MSSR.

3.8 Conclusion.

DRIFTS is clearly a useful spectroscopic technique, particularly when applied in the 4000 to 2000 cm^{-1} region. Below this value, transmission generally becomes favourable with its higher throughput [185]. The Kubelka-Munk theory provides a sound theoretical basis for the technique in general application, though in the systems presented in this thesis, its advantages are outweighed by the amplifying effect of displaying the spectra in absorption format. Standard preparation techniques were modified due to the possibilities of dilution media interacting with the catalysts under investigation.

Chapter 4

DRIFTS of butane over EuroPt-1.

4.1 Introduction

In Chapter 2, the experimental technique of deuterium exchange was used to study the interaction between butane and the EuroPt-1 surface. The range of substitution of deuterium atoms into the butane molecule, and comparison with similar experiments and the established theories on exchange can give some idea of the surface species reacting. By applying infrared spectroscopy, and in particular DRIFTS, to the same chemical system, the ideas generated above may be supplemented by more direct evidence on the adsorbates.

The first infrared spectroscopy experiments using a supported metal catalyst were carried out by Eischens *et al.* [42] in 1954. The system studied, carbon monoxide adsorption on a transition metal surface, has remained a favourite of the vibrational spectroscopist due to the ready adsorption and strong dipole moment of that molecule [187]. The infrared technique became established with several research groups adding to the range of chemical systems studied in the succeeding decade. Eischens and Pliskin's review of 1958 [44] discussed their own work on unsaturated hydrocarbons on Cab-o-sil supported nickel, and CO adsorption on a variety of supported metals. Nickel was an early favourite for the metal substrate, featuring in the work of Erkelens and co-workers [188, 189], Nash *et al.* [190], Peri [82] and the Cambridge (later University of East Anglia) school of Sheppard *et al.* [80, 81, 191, 192]. Platinum, as a hydrogenation catalyst, was also an early member of the list, particularly when alkenes and alkanes were the adsorbed species [80, 81, 189, 191, 192]. It was over this substrate that perhaps the best cooperation between supported metal studies and the burgeoning surface science techniques took place.

One of the most significant of the pieces of work mentioned above was the

series of two papers by Morrow and Sheppard covering the adsorption on silica supported platinum and nickel of ethene [81] and but-1-ene [192] over a range of temperatures. Although what was then an advanced grating spectrometer was used (*cf.* the prism spectrometers and hence lower resolution of some of the other studies), the strong infrared absorption of the silica support and hence a steeply sloping background prevented them from obtaining information in the carbon–hydrogen deformation region of the spectrum below 1500 cm^{-1} – a situation not unlike that encountered with silica in DRIFTS.

When ethene was adsorbed on the Pt/SiO_2 catalyst at 298 K, the main feature was a sharp intense peak at 2880 cm^{-1}, which when other spectra from the work were considered always appeared with bands at 2920 and 2795 cm^{-1}. (The Ni/SiO_2 catalyst displayed similar spectra at low temperature (196 K), but did not agree with the Pt/SiO_2 spectra over a wide temperature range.) With ethane produced on hydrogenation indicating a C_2 fragment, and the observed frequencies more akin to sp^3 than sp^2 hybridised CH bonding, the 2880 and 2920 cm^{-1} peaks were assigned to the symmetric and asymmetric CH_2 stretches of a 1,2 σ bonded ethene molecule, Figure 4.1. It was suggested that Fermi resonance with the intense 2880 cm^{-1} band could be bringing up a deformation mode overtone to produce the 2795 cm^{-1} peak. Other weak features in the spectra were assigned to physically adsorbed ethane, *n*-butyl groups, ethyl groups and an ethyne type species created by partial dehydrogenation of ethene.

The assignment of the 2880 and 2795 cm^{-1} peaks as being due to a 1,2 di-σ species was repeated by Pearce and Sheppard [193] when they introduced the idea that the metal surface selection rule (MSSR) was applicable not only to bulk met-

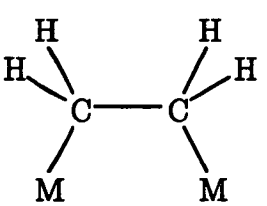

Figure 4.1: 1,2 di-σ ethene surface complex

als [63, 195] but also to supported metal particles (as discussed in Section 1.5.4). This followed work which indicated the 2920 cm^{-1} peak to be unconnected with the two just mentioned [194] over a rhodium silica catalyst, and they extrapolated this situation to a re-analysis of earlier Sheppard spectra [81]. The production of ethane on hydrogenation, and the C–H stretch frequencies suggesting sp^3 hybridisation were again the cited reasons for the assignment. The simple spectrum, with only one C–H stretching mode was explained by the suppression of modes parallel to the surface by the MSSR.

When the equivalent system of ethene adsorption on the Pt(111) surface was examined by Ibach *et al.* [59, 196] in early electron energy loss spectroscopy (EELS) experiments, a different conclusion was reached. The room temperature spectra showed a peak at 2900 cm^{-1} (360 eV), fully equivalent to the 2880 cm^{-1} peak of supported systems under the 80 cm^{-1} resolution of EELS. This was assigned to the CH_3 symmetric stretch, a possibility denied by Morrow [81] without the insight of the MSSR. The overall structure was suggested as an ethylidene species, Figure 4.2.

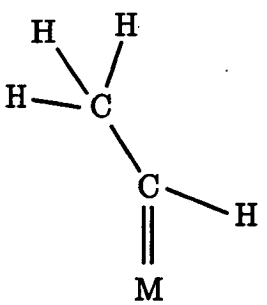

Figure 4.2: Ethylidene surface complex

Somorjai's group studied the $Pt(111)/C_2H_4$ system with low energy electron diffraction (LEED) [197], and found that the surface species was an ethylidyne group bonded to a triangle of three surface platinum atoms (Figure 4.3), comparing Ibach's EELS spectra [59] with infrared data for the compound $C_2H_3Co_3(CO)_9$ [198]. (This was quite different from their original analysis of such results [199, 200], when they suggested a di-σ bound C_2H_2 species.) Demuth used thermal

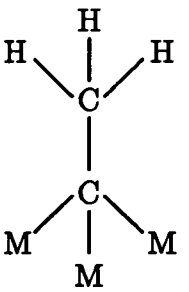

Figure 4.3: Ethylidyne surface complex

desorption spectroscopy (TDS) to confirm that the chemical formula for the surface material was C_2H_3 [201], which was added to the Somorjai team's arguments when they examined their earlier results in more depth [202], despite Demuth plumping for a vinyl structure, Figure 4.4.

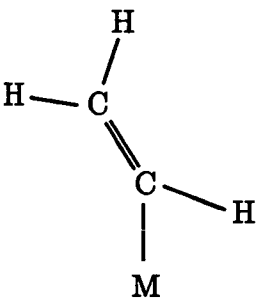

Figure 4.4: Vinyl surface complex

Surface science was thus presenting three alternatives to the 'traditional' view, despite a simpler chemical system. This situation did not last long, however. The East Anglia group repeated the vibrational spectra of $C_2H_3Co_3(CO)_9$ applying a complete normal mode analysis, and found that the fully symmetric modes of the ethylidyne ligand were in agreement with the EELS results [84]. The Jülich group repeated their earlier experiments using improved electron optics and combined TDS [203], agreeing with both the C_2H_3 composition, and the ethylidyne structure. The consensus was strengthened by photoelectron spectroscopy of the model compound [204] and the Pt(111) surface species [205]. The plane polarisation of the synchrotron radiation and symmetry arguments used by Albert *et al.*

showed that the C–C bond was normal or near normal to the metal surface, and the electron orbitals were consistent with ethylidyne, though vinylidene was not completely ruled out [205].

The final confirmation came when the superior resolution of reflection absorption infrared spectroscopy (RAIRS) was applied to the $Pt(111)/C_2H_4$ system, results being produced simultaneously at the University of Illinois [206, 207, 208] and the University of East Anglia [209]. With the MSSR holding strictly, only the totally symmetric (A_1) modes of vibration were visible, the absorbances appearing at 1118 (1124), 1339 (1341), 2795 and 2884 (2884) cm^{-1} [206] ([209]), as repeated here at the University of Edinburgh [158]. The poorer signal to noise ratio of Chesters *et al.* did not allow the 2795 cm^{-1} peak to be distinguished, but the other peaks were equal within the resolution of the experiments (2 cm^{-1} [206] and 8 cm^{-1} [209]). These observed bands were in agreement with the A_1 bands on the $C_2H_3Co_3(CO)_9$ complex [84]. The lack of any other bands proved the high symmetry (C_{3v}) of ethylidyne, with the peaks being assigned to the C–C stretch, CH_3 symmetric bend (umbrella mode), the first overtone of the asymmetric CH_3 bend and the symmetric C–H stretch.

That such a weight of experimental work was needed to prove the existence of just one single crystal surface species shows that the full assignment of the spectrum for a supported metal catalyst/hydrocarbon system must be difficult. With the surface science and model compound results available, C_2H_4 and Pt/SiO_2 is one of the best understood following dedicated attention from the University of East Anglia group. A π-bonded species was identified in 1976 [210], as found over Pd(111) [211] and as a ligand in Zeise's salt [212]. The same complex was noted by Soma [213] on a Pt/Al_2O_3 catalyst. By analogy with EELS studies [203], where the ethylidyne formation was preceded at lower temperatures by a 1,2 di-σ bonded ethene complex (Figure 4.1), de la Cruz and Sheppard [214] found a similar spectrum over Pt/SiO_2 on warming a C_2H_4 multilayer from 100 to 189 K. Two sets of absorption bands were identified, at 2906/1419 cm^{-1} and 2922/1428 cm^{-1},

the first disappearing on warming to room temperature as ethylidyne grows in. The pairs of bands were assigned to ethene di-σ bonded to two different types of metal site. C_2H_4 adsorption on EuroPt-1 was also studied at the University of East Anglia with broadly similar results [154].

With improvements to the resolution of EELS and sensitivity of RAIRS, a body of reference spectra is building up. Sheppard reviewed the vibrational spectra of hydrocarbons on metal single crystal surfaces in 1988, discussing alkenes and alkynes as large as C_4, as well as many cyclic compounds [83]. He mentioned some work on physisorbed ethane at low temperature, but most studies on saturated hydrocarbons looked at cyclohexane. At that time, only very few RAIRS papers had been published. Subsequently, low temperature spectra of *n*-alkanes on Pt(111) [215] and a comparative study of alkenes on Pt(111) and Pt/SiO_2 [216] have been a useful addition to the literature.

It will be useful, before looking to the literature for studies on the adsorbed molecule, to consider the vibrational spectrum of butane itself. The C_4 chain of butane is the first of the alkanes which can have rotational isomerism, with a *trans* and two degenerate *gauche* forms. *Trans*, with the zig-zag backbone normally associated with the long chain alkanes is the lower energy form by 3.7 $kJmol^{-1}$ [221], accounting for around 60% of the gas phase molecules [222]. In the *gauche* form, the two ethyl groups are rotated about the central C–C bond by 120°, reducing the molecular symmetry from C_{2h} to C_2. In the literature, the extreme complexity of this C–H stretching region has often restricted assignment to simple group frequency terms. The only assignment of bands to definite modes of the molecule has been by Murphy *et al.* in 1991 [223]. Following harmonic force field calculations they tentatively suggested that the Raman bands at 2968 and 2974 cm^{-1} were the ν_1 frequencies of the *trans* and *gauche* conformers respectively. By symmetry considerations, only the latter is an allowed infrared transition. The energy difference between the conformers is sufficient that the liquid is predominantly in the *trans* form [195], and the solid almost exclusively so [219].

The next step up in complication is the adsorption of the molecule on an appropriate single crystal surface. The butane/Pt(111) system has been studied by Chesters *et al.* [215] using RAIRS. The interaction is very weak, requiring cooling to near liquid nitrogen temperature for adsorption, and there was no suggestion in the paper of any chemical reaction. Spectra were assigned to butane adsorbed in the *trans* conformation with the molecular plane parallel to the metal surface.

Unsaturated hydrocarbons are generally more reactive, as displayed in two major vibrational studies of C_4-alkenes on Pt(111), by Avery and Sheppard [226, 227, 228] using EELS, and by Chesters *et al.* [216] using RAIRS. The latter work included a comparison with adsorption on a Pt/SiO_2 catalyst. Butene adsorption has also been studied on other close packed single crystal surfaces, Ru(0001) [229] and Ni(111) [230].

Earlier work on alkenes with Pt(111) was published by the Somorjai group following their success in being the first to suggest the ethylidyne species. Thermal Desorption Spectroscopy (TDS) of both cis- and trans-but-2-ene on a Pt(111) surface was claimed by Salméron and Somorjai [231] to show a butylidyne species being formed at room temperature.[1] This was following a desorption peak equivalent to a quarter of the hydrogens desorbed during the whole of the experiment. The argument was backed up by LEED spectra published by the same research group [232], of the same hydrocarbons on Pt(111), despite poorer data for the butene systems than they presented for ethene and propene adsorption.

The assignment of all things to alkylidynes was halted by the papers of Avery and Sheppard [226, 227, 228]. They described combined TDS of a range of simple alkenes on Pt(111) with EELS to a resolution of 40 cm^{-1}. They found similar TDS profiles to Somorjai's group for the alk-1-enes [226]. Good thermal resolution in the TDS experiments allowed them to take EEL spectra of the stable species be-

[1]Here trans and cis describe fixed relative positions across the central bonds and will be differentiated from the *trans* and *gauche* conformers by the use of Roman type.

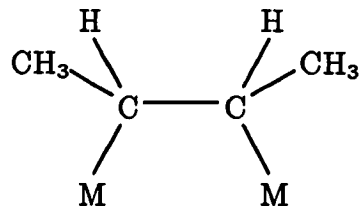

Figure 4.5: Di-σ adsorbed but-2-ene retaining a cis configuration.

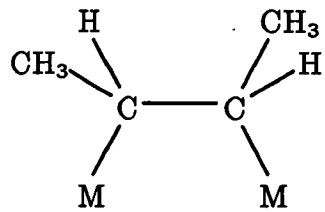

Figure 4.6: Di-σ adsorbed but-2-ene retaining a trans configuration.

tween hydrogen desorption events, and they confirmed the presence of alkylidyne species at 300 K for the first three linear alkenes. They examined the adsorption of the other linear butenes (cis- and trans-but-2-ene and buta-1,3-diene) on the same substrate, however, and found quite different results [227]. TDS showed that both but-2-enes, when heated from the adsorption temperature of 170 K to room temperature lost not one but two hydrogens, leaving a surface composition of C_4H_6. The TDS results just quoted are not significantly different from those of Salméron [231], who at this point was suggesting a C_4H_7 composition. The EELS spectra for both the low temperature and the 300 K species also held surprises [227]. At 170 K, cis- and trans-but-2-ene produced markedly different EELS spectra. These were assigned to di-σ adsorbed species, as found for ethene (Figure 4.1) with a hydrogen on each of the ethene carbons replaced by a methyl group. The retention of the cis and trans arrangement of the alkene in the di-σ surface species gives C_s symmetry for the cis adsorbate, (Figure 4.5) and C_2 symmetry for the trans (Figure 4.6). When these two systems were heated past the dehydrogenation event to 300 K, however, the EEL spectrum they produced were identical with that of but-2-yne adsorbed on Pt(111) and heated to 320 K. Coupled with the TDS evidence of loss of two hydrogens, these spectra were all assigned to the

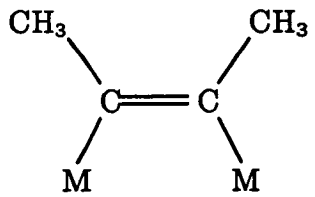

Figure 4.7: Di-σ adsorbed but-2-yne

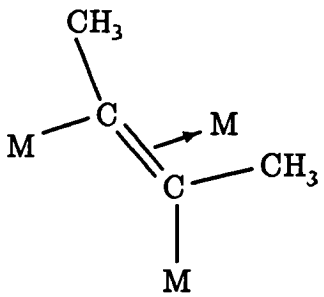

Figure 4.8: Di-σ/π adsorbed but-2-yne

same surface species. Although a di-σ bound butyne species (Figure 4.7) of C_{2v} symmetry was suggested as a possible candidate, Avery and Sheppard preferred to assign the species to a di-σ/π bound butyne instead (Figure 4.8).

Avery and Sheppard's EELS experiments were repeated using the higher resolution of RAIRS by Chesters, Sheppard *et al.* [216]. At 300 K, they found that cis- and trans-but-2-ene produced identical spectra to but-2-yne on the Pt(111) surface, and agreed with the earlier assignment to Figure 4.8.

In Chesters' RAIRS study [216], but-1-ene was adsorbed rapidly at 250 K, annealed at 270 K, and cooled to 90 K. A simple and clear spectrum was produced, with absorption bands at 2934 and 2874 cm^{-1}. This spectrum was assigned to the CH_2 symmetric stretch and CH_3 symmetric stretch of the *trans* conformer of the butylidyne species, Figure 4.9. The mirror plane of *trans*-butylidyne gives the complex C_s symmetry, and so atomic vibrations antisymmetric to this plane are forbidden by the MSSR [233]. This is why the 2934 cm^{-1} band is attributed to a symmetric rather than an antisymmetric vibration, which might have been expected on group frequency grounds. The worries over this observed frequency are mentioned by Chesters *et al.* [216] and discussed in depth by Pudney [234].

But-1-ene on Pt(111)				
EELS†	RAIRS‡		Assignment	
300 K	270 K	300 K	Vibration	Surface species
		2940 cm^{-1}	$\nu(CH_3)_{as}$	1,2-di-σ/*gauche*-butylidyne
circa 2950 cm^{-1}	2934 cm^{-1}	2934 cm^{-1}	$\nu(CH_2)_s$	*trans*-butylidyne/1,2-di-σ
(broad)	2924 cm^{-1}		?2x$\delta(CH_2)$?	*trans*-butylidyne
		2882 cm^{-1}	$\nu(CH_3)_s$	*gauche*-butylidyne
	2874 cm^{-1}	2874 cm^{-1}	$\nu(CH_3)_s$	*trans*-butylidyne

† From reference [226]

‡ From reference [216]

Table 4.1: Literature vibrational data for but-1-ene on Pt(111).

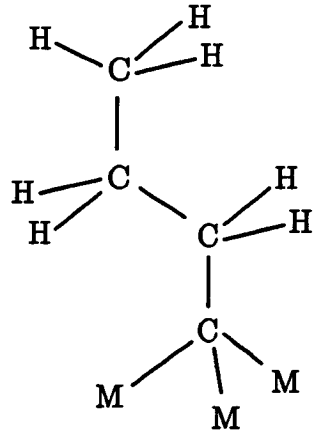

Figure 4.9: Butylidyne in the *trans* conformation.

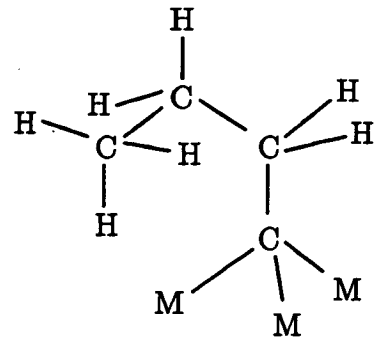

Figure 4.10: Butylidyne in the *gauche* conformation.

But-2-ene on Pt(111)			
EELS†	RAIRS‡	Assignment	
300 K	*circa* 300 K	Vibration	Surface species
~2960 cm^{-1}	2930 cm^{-1} broad	$\nu(CH_3)_{as}/\nu(CH_2)_s$	di-σ/π-but-2-yne,*trans*-butylidyne and di-σ-but-1-ene
~2910 cm^{-1}	2886 cm^{-1}	$\nu(CH_3)_s$	di-σ/π-but-2-yne,*gauche*-butylidyne

† From reference [226]

‡ From reference [216]

Table 4.2: Literature vibrational data for but-2-ene on Pt(111).

When a comparison is made with organometallic compounds, and the slightly shortened C–C distance observed for butylidyne in the bond closest to the metal by Kesmodel *et al.* [202] also taken into account, the high frequency is less surprising.

A range of alternate dosing regimes was also employed, and more complicated spectra presented. Absorption bands less than 10 cm^{-1} higher than the two main *trans*-butylidyne peaks were assigned to the CH_3 antisymmetric stretch (2940 cm^{-1}) and symmetric stretch (2882 cm^{-1}) of the *gauche*-butylidyne, Figure 4.10. The lower symmetry of the *gauche* conformer means that all vibrations are symmetry allowed in the infrared, thought the 2940 cm^{-1} vibration is this time rather low from group frequency considerations.

In the same paper, Chesters also examined some of the equivalent spectra of adsorption on a 15% Pt/SiO_2 catalyst. With but-1-ene peaks assigned to *trans*-butylidyne were observed at 2932 and 2875 cm^{-1}, with a less intense, broader peak at 2960 cm^{-1} put down to a 1,2-di-σ species. Bands in the C–H deformation region helped this assignment. It was suggested that the more upright *trans* conformer was preferred because high (but unquoted) adsorption pressures were used. Of the two but-2-enes and but-2-yne, only cis-but-2-ene on Pt/SiO_2 was presented in the paper. The spectrum was very different from the equivalent single crystal spectrum, but rather similar to that of but-1-ene/Pt/SiO_2. The butylidyne bands were at 2932 and 2879 cm^{-1}, though the latter value may have been affected by an underlying peak at 2890 cm^{-1}, which was assigned to the di-σ/π complex seen on the single crystal [216].

Prior to the butene/Pt/SiO_2 work just quoted, Campione and Ekerdt [225] produced similar spectra for adsorption of the monobutenes on a Ni/SiO_2 catalyst. The largest peak in the spectrum at 2875 cm^{-1} was assigned to the CH_3 symmetric stretch for the di-σ species of Figure 4.5 (the cis form was not specifically stated in the text, but it was used to illustrate their 2,3-dimetallabutane species). The corresponding CH_3 antisymmetric stretch was not seen because of the MSSR. The prominent 2965 and 2932 cm^{-1} peaks were assigned to the antisymmetric CH_3 stretch and the antisymmetric CH_2 stretch respectively of 1,1,3- and 1,1,2-trimetallabutanes, oriented with the molecular chain near parallel to the surface so corresponding symmetric modes were forbidden by the MSSR. Chesters [216] points out that if equivalent species are formed with propene, the spectrum should be similar to that for butene by the model of Campione, whereas the switch of emphasis from the CH_3 symmetric stretch for butene to the CH_3 antisymmetric stretch for propene observed over Pt(111) is more suited to a butylidyne/propylidyne model. Campione [225] also suggests that extensively dehydrogenated species are present on the surface. These are frequently postulated as high temperature decomposition products on metal single crystals

[195].

The chemisorption of butane on EuroPt-1 must be a dehydrogenation initiated reaction. If the removed hydrogen is to be taken up by the metal surface, it is to be expected that the preadsorption of hydrogen will affect subsequent absorption, especially as this was also found to be important during early work on alkene adsorption. Eischens and Pliskin quoted the presence or absence of a preadsorbed hydrogen layer as being one of the three important variables in ethene adsorption on a Ni/SiO_2 catalyst [44]. Their hydrogen layer was prepared by cooling the sample in hydrogen after reduction, evacuating excess gas at 308 K, and the bare nickel prepared by evacuation at 620 K for 30 minutes before cooling to 308 K. The infrared spectra of adsorbed ethene on these surfaces were assigned to predominantly 1,2 di-σ adsorbed C_2H_4 and an "acetylenic complex" respectively. When the two surfaces were exposed to ethane, no hydrocarbon adsorbed on the hydrogen covered surface, but the bare metal surface gave similar results to those from ethene [44].

Morrow and Sheppard did not find any difference between ethene adsorption on hydrogen covered and hydrogen free nickel surfaces prepared as above [80]. They suggested the difference between this and the early work was due to using the catalyst as thin pressed discs, rather than the loose silica lying on a horizontal CaF_2 plate preferred by Eischens *et al.* [44].

Another hydrogenation effect noted through that period was the reversible dehydrogenation/hydrogenation of surface species formed by ethene adsorption over Pt/SiO_2 and Ni/SiO_2 in many of the early infrared studies [44, 80, 188].

The examination of saturated hydrocarbons over supported metal catalysts seems to have been generally avoided in favour of alkenes. M^{c}Dougall [154] found that over EuroPt-1, ethane produced similar spectra to ethene. Eischens and Pliskin adsorbed ethane on their hydrogen free surfaces as mentioned above [44]. Shahid studied propane as well as propene in an infrared study over a Pt/SiO_2 catalyst [238]. Sheppard [83] pointed out that the adsorption of the larger hy-

drocarbons on the oxide support material may obscure the vibrational spectrum of hydrocarbon/metal species, particularly at low temperature. In order to see them, experiments must either allow evacuation [95] or be carried out in a flow system, such as described in Section 3.5.6 above.

The use of a flow system has been shown by Belgued *et al.* [217] to give interesting chemistry when methane is passed over EuroPt-1. The adsorption of the methane is accompanied by significant dehydrogenation. The carrier gas flow removes any gaseous hydrogen, which in a closed reaction vessel might alter the equilibrium and reduce the extent of dehydrogenation. The hydrogen deficient species polymerised on the surface. A switch of flow gas to hydrogen produced a range of higher hydrocarbons from C_2 to C_6.

The vibrational data for hydrocarbon adsorption on metal single crystals and supported metal catalysts, and for organometallic compounds with structures determined by X-ray diffraction, together make the study of larger hydrocarbons by infrared spectroscopy an attractive proposition. The reaction of methane over EuroPt-1 in a flow system suggests that exciting surface chemistry is possible. This chapter therefore describes the surface species formed by butane over EuroPt-1 and their reaction with hydrogen, as studied by DRIFTS.

The complex nature of the butane surface chemistry is necessarily reflected in the construction of this chapter. The first spectra presented are for gas phase butane, and for butane adsorption on Sorbosil AQ U30, the support material used in the manufacture of EuroPt-1. The adsorption on EuroPt-1 at 298 K is discussed next, with the surface 'hydrogen free' according to the criteria of Eischens and Pliskin [44]. The effects of both pre- and post-adsorption of hydrogen on the butane/EuroPt-1 system at room temperature are covered after this. The deuterium exchange experiments of Chapter 2 were run at approximately 380 K, so for a hope of finding related DRIFTS spectra, experiments had to be run at elevated temperatures. The changes in the room temperature spectrum on heating were investigated in a TDS/TPD style experiment, covering the range from

room temperature to 570 K. The adsorption of butane and the reaction of the adsorbates with hydrogen at 380 K were examined in the last two experiments described here.

To conclude the Chapter, the spectral assignments from the above experiments are discussed in terms of the surface chemistry, and where possible with reference to the exchange experiments of Chapter 2.

4.2 Results.

4.2.1 Gas phase reference spectrum.

A spectrum of gas phase butane was collected as a reference. A 5cm long glass cell with KBr salt windows was filled with butane to 4x10^4 Nm^{-2}, and placed in the spectrometer beam. The glass cell was only designed for operating below external pressure, so the spectrometer was purged with dry air rather than being evacuated, and a 512 scan 4 cm^{-1} resolution spectrum was recorded. The empty glass cell was used as the background for the absorption spectrum, Figure 4.11. As well as the butane peaks, miscancellation features due to water (3950 to 3500 cm^{-1} and 2000 to 1300 cm^{-1}) and CO_2 (2354 cm^{-1}) can be seen. The envelope of C–H stretches covers the range 3020 to 2820 cm^{-1}. As discussed in the introduction, modern computer modelling has not yet managed to give a full assignment to this region of the butane spectrum [223] and it is pointless to try and change this with one 4 cm^{-1} resolution infrared spectrum. The only assignment which can be made is to the high frequency shoulder of the main peak at 2978 cm^{-1}, which Murphy suggests as the ν_1 mode of the *gauche* conformer.

4.2.2 Butane absorption on Sorbosil AQ U30.

A sample of Sorbosil grade AQ U30 silica gel, the support material for EuroPt-1 [26], was prepared in the standard manner described in Section 3.5.7. The reduction procedure to be used for EuroPt-1 was also followed to ensure comparability, and the sample exposed to a 35 μmol pulse of butane introduced into the helium

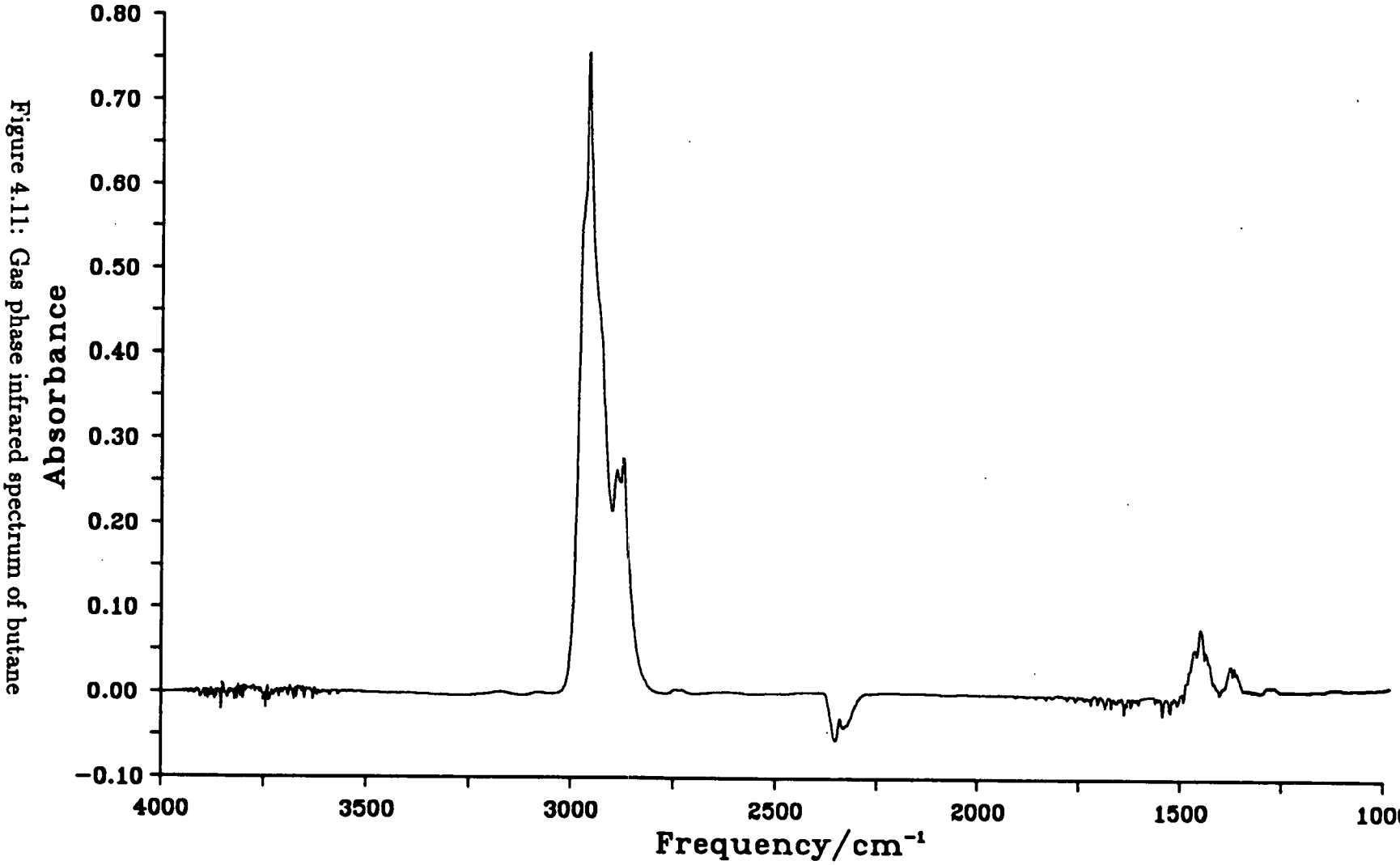

Figure 4.11: Gas phase infrared spectrum of butane

flow. The experiment was run at 298 K and recorded by DRIFTS as 32 scan interferograms. The significant feature was an envelope of C–H stretching vibrations as recorded in Figure 4.12, and similar to the envelope of the gas phase spectrum. While the dosing gas is passing from the inlet to the environmental chamber through the catalyst bed and then exhausted, some gas phase bands might be expected. Although the cell's dead volume is less than 3 ml, the flow characteristics are unlikely to be so efficient that it is swept out by the carrier in the implied 20 seconds. Data from the least interactive gas/substrate system studied in this work (Section 5.2.4) suggests a maximum of about a minute to clear 90% of the gas from the volume. Under the 10 $mlmin^{-1}$ flow of He, the infrared intensities dropped off with time, though peaks were visible for longer than it takes to flush out any gas phase butane. The form of the spectra remained constant during the decay, as demonstrated by Figure 4.13 and 4.14. The way the spectra developed with time is shown in Figure 4.13. Selected spectra are plotted on the same set of axes. They are offset in proportion to the time difference between them, as marked on the y axis. The first two spectra were reduced by factors of 4 and 2 compared to the absorbance scale marked on the Figure, so that the detail can be seen in the less intense spectra. The variation of the peak intensities with time is plotted in Figure 4.14, which perhaps shows the development more clearly.

Butane over the silica support material has a fairly simple spectrum, with two broad peaks at 2962 and 2876 cm^{-1} due to a CH_3 asymmetric and symmetric stretch respectively. The smaller peak at 2940 cm^{-1} is from the CH_2 asymmetric stretch, with its symmetric counterpart contributing intensity to the low frequency side of the 2876 cm^{-1} peak [220]. The relative intensities are in line with

a broadened out version of the solid phase C–H stretch spectrum presented by Snyder [219].

For comparison, the gas phase spectrum is shown scaled with the spectrum

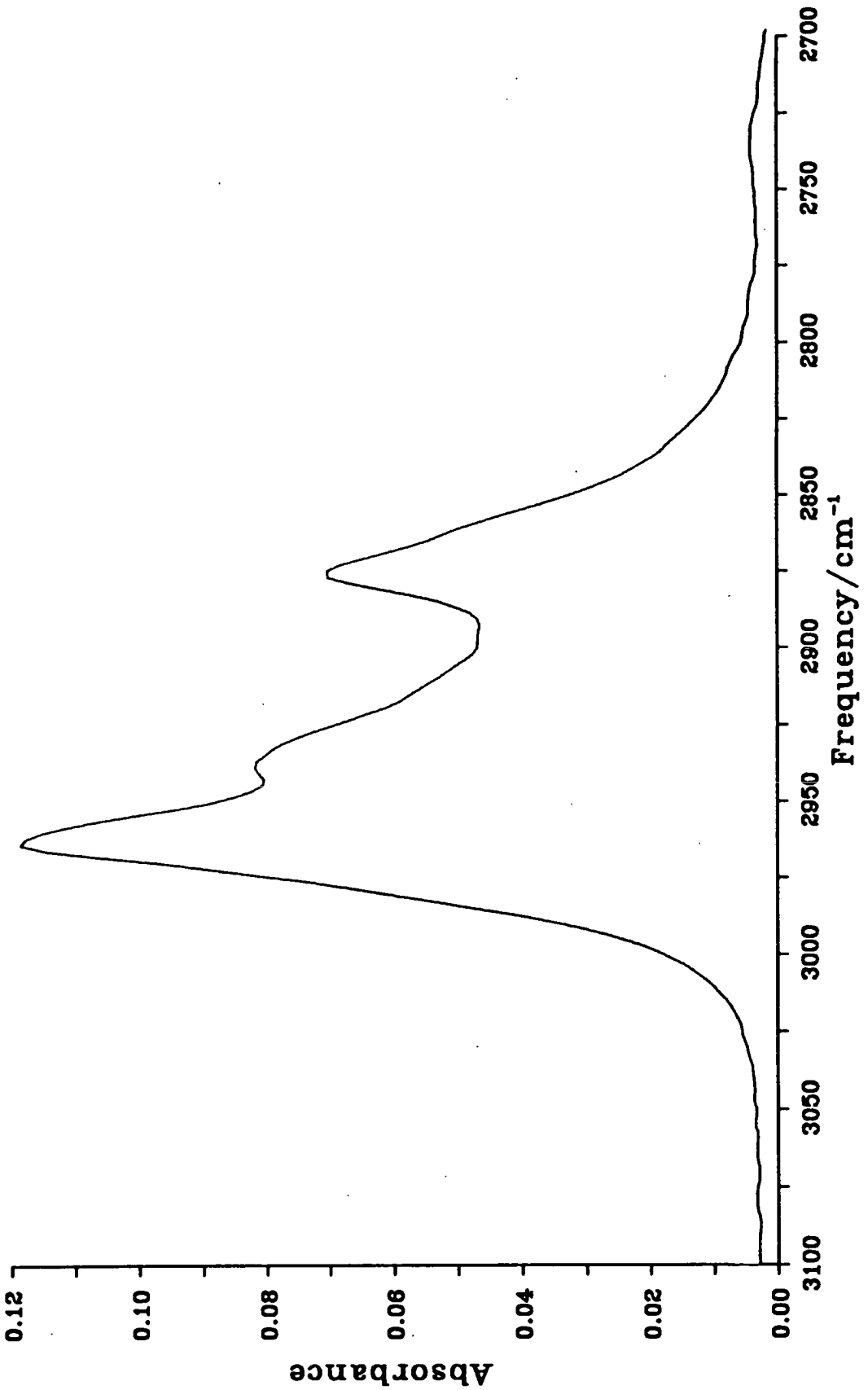

Figure 4.12: Butane absorption on Sorbosil: C–H stretch region

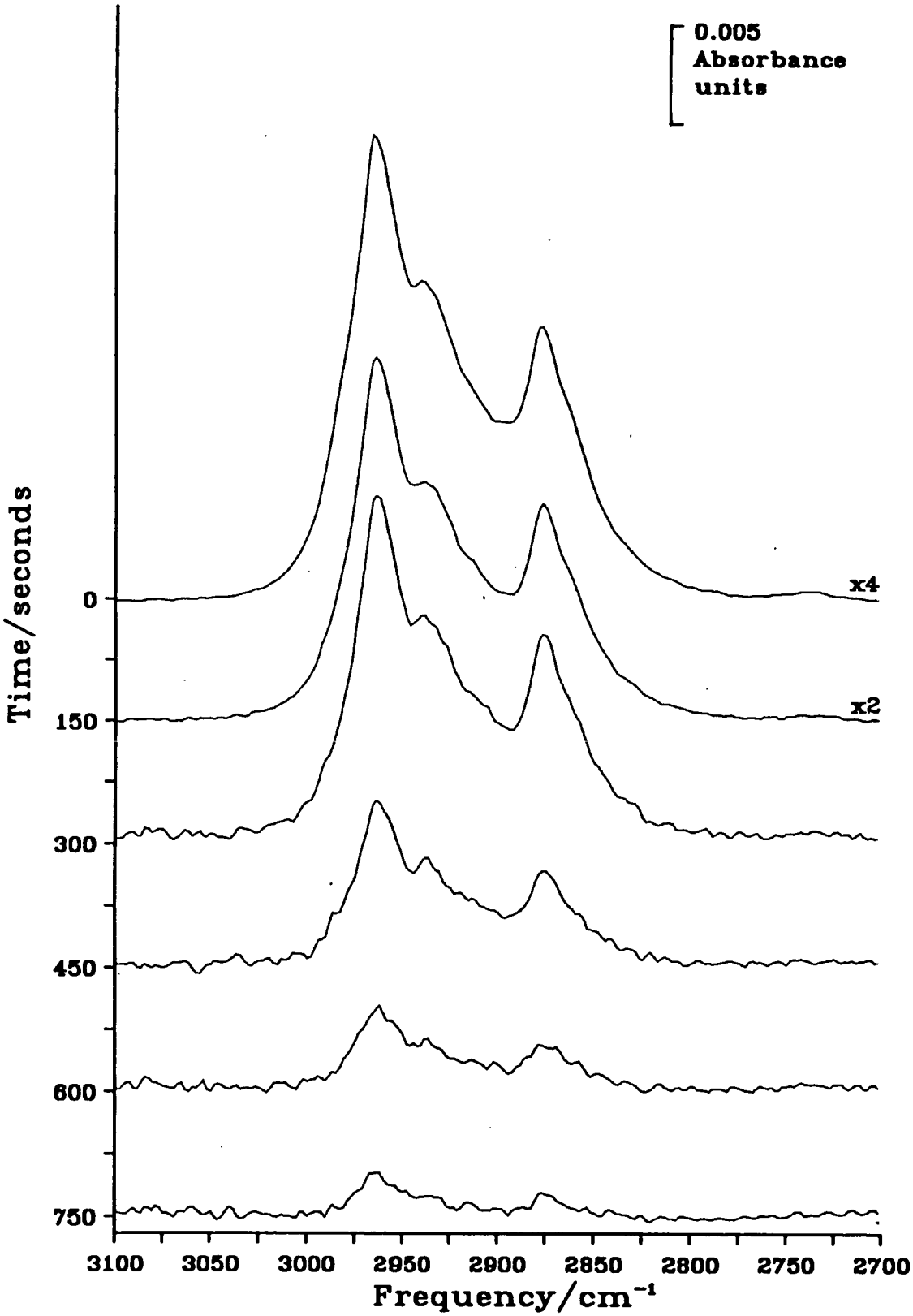

Figure 4.13: Butane adsorption on Sorbosil: changes in the C–H stretch spectrum with time.

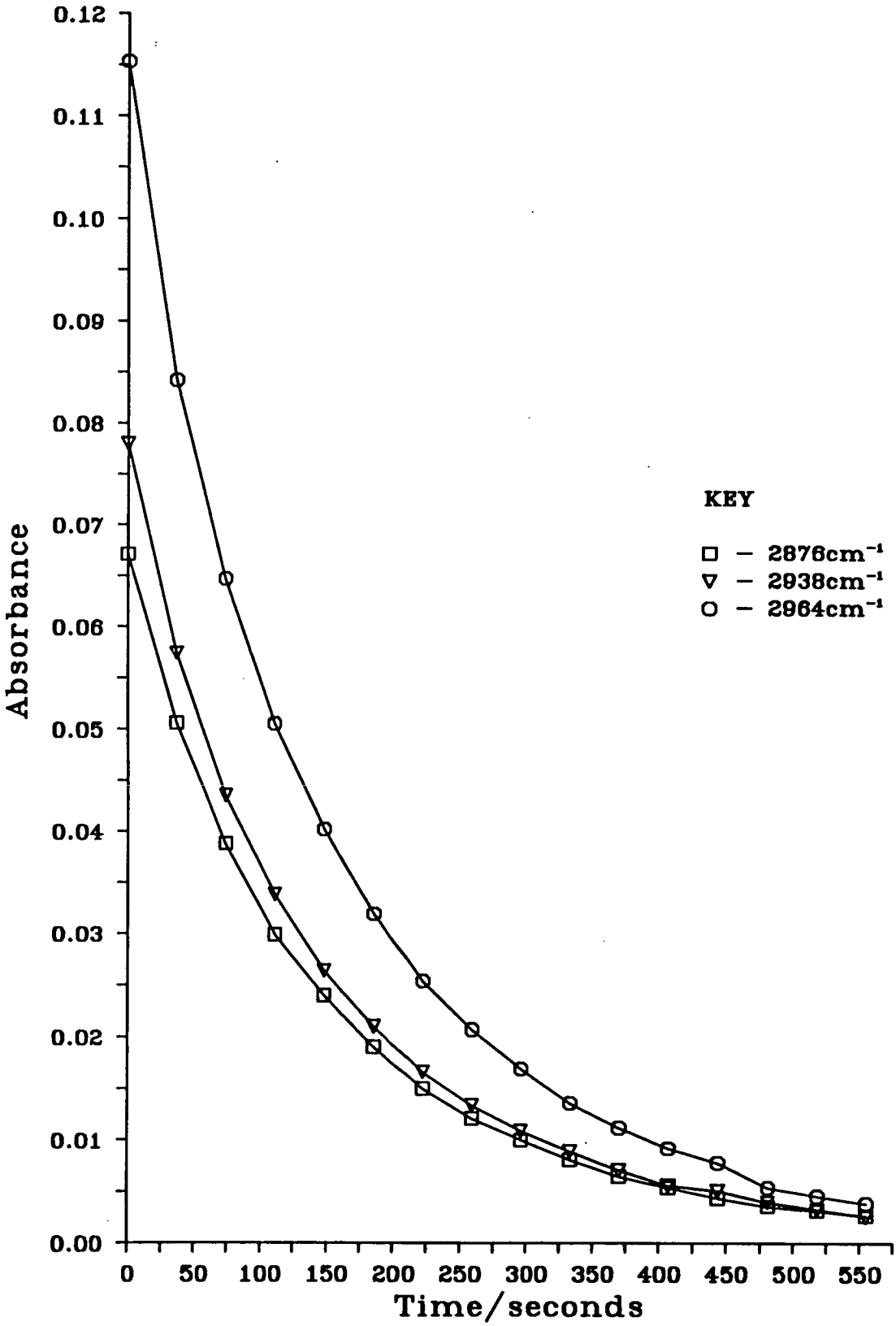

Figure 4.14: Variation of absorbance with time for selected frequencies of Figure 4.13.

over silica in Figure 4.15. The gas phase spectrum clearly has indications, in maxima and shoulders, of many more bands than are visible in the spectrum over silica. This is due to the two conformers already discussed, and possibly also to rotational fine structure. Notable in its absence from the Sorbosil spectrum is the shoulder assigned to the *gauche* conformer in the gas phase. As no sharp peaks are seen either, which might be expected during the first flush of the butane, it would appear likely that the interaction between Sorbosil and butane is strong enough to adsorb the molecules in a purely *trans* form (as preferred in the solid), and remove rotational structure.

4.2.3 Butane absorption on outgassed EuroPt-1 at 298 K.

A sample of EuroPt-1 was reduced and outgassed *in situ* as described above, and DRIFTS spectra recorded while a pulse of 35 μmol of butane passed over it at room temperature, 298 K.

The initial infrared spectrum is shown in Figure 4.16. The largest feature, between 3000 and 2700 cm^{-1} is due to C–H stretches of the butane, but before this is discussed, some other aspects of the spectrum should be mentioned. The second largest band is the mainly negative peak at 2056 cm^{-1}, with a positive shoulder at 2012 cm^{-1}. This is due to displacement of carbon monoxide on the surface. Even with the copper trap, the helium carrier gas can not be completely scrubbed for CO. EuroPt-1 is an excellent adsorber of CO [95], as might be expected when platinum forms the basis for car exhaust oxidation catalysts, and CO free surfaces were only achieved at the end of the reduction when still at high temperature under hydrogen. The strength of the CO chromophore means that even a small concentration of gas can produce a large peak in the infrared. Butane co-adsorption shifts some of the remaining CO to lower wavenumber to give the slightly derivative nature of the peak. A smaller peak at 1796 cm^{-1} is due to CO being displaced from an on top site to a bridging site between two surface platinum atoms [154]. CO also has an often ignored band at 2512 cm^{-1}, due to

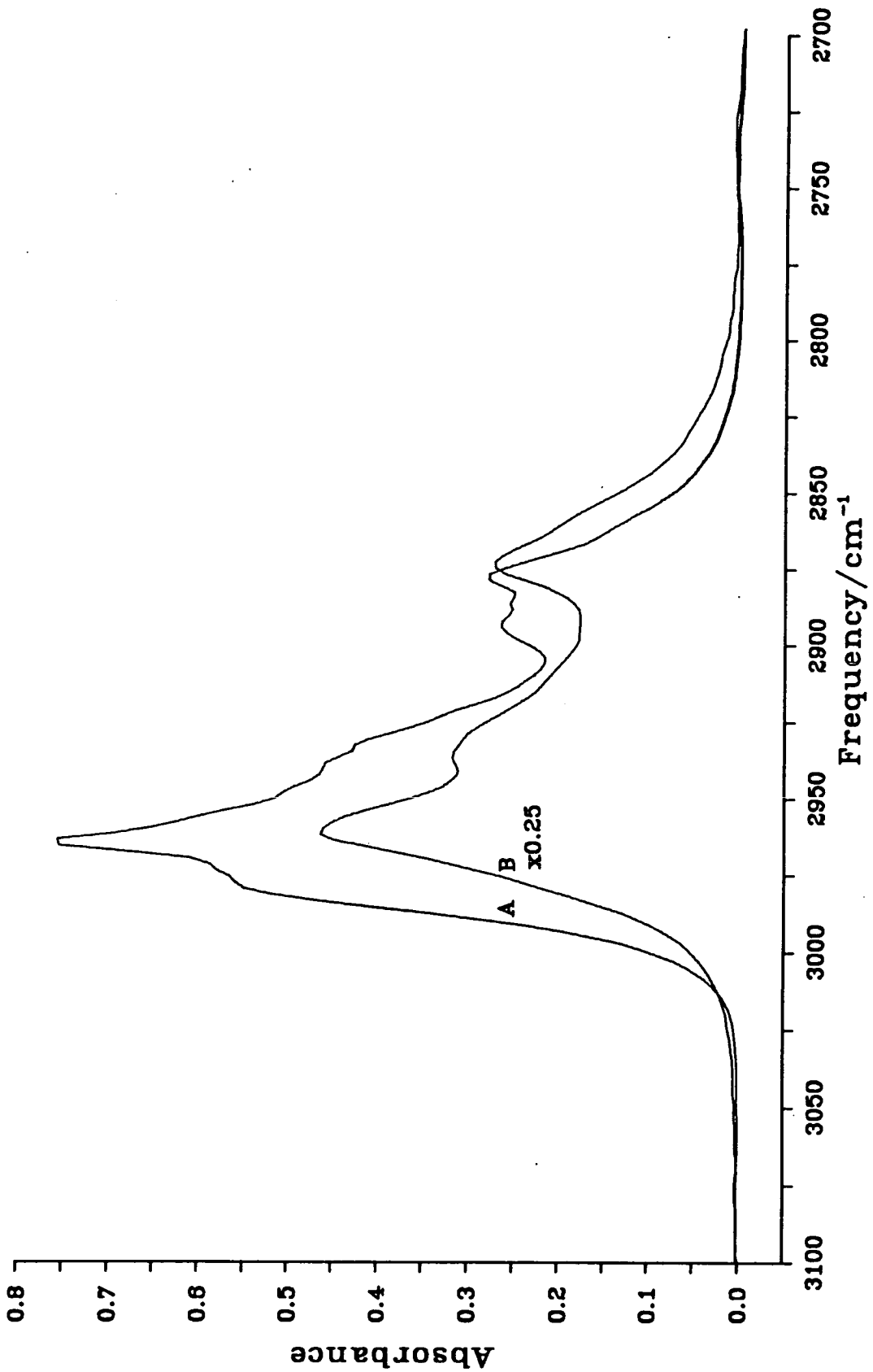

Figure 4.15: Figures 4.11 and 4.12 arbitrarily scaled for ease of comparison.

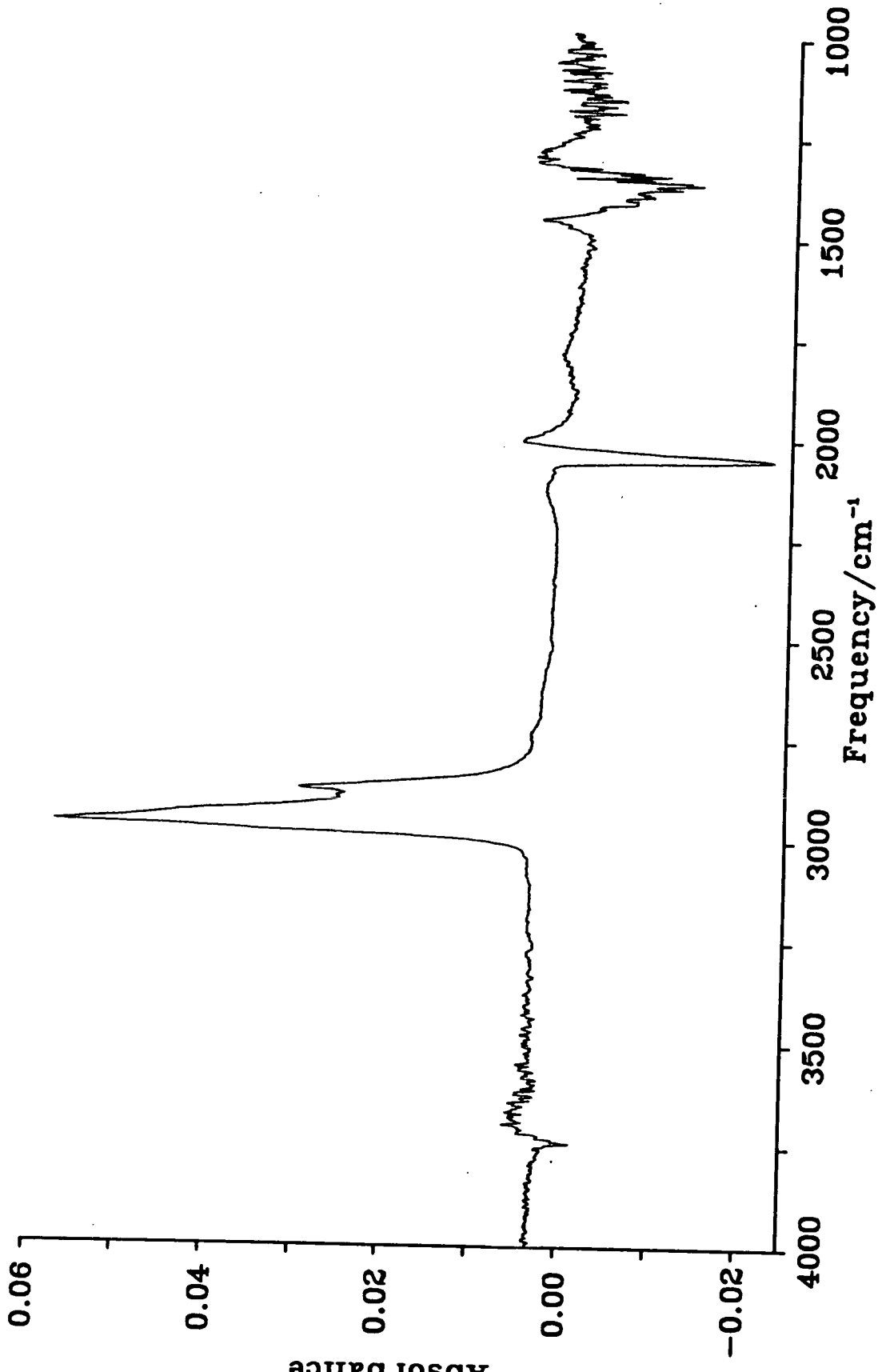

Figure 4.16: Butane absorption on EuroPt-1: full spectral range

the metal-carbon vibration (at 476 cm^{-1} for CO on Pt(111) [218]) in combination with the intense C–O stretch band. With the CO displacement, this also gives a small negative peak. The benefit of the evacuable bench is seen in the complete absence of any peak at 2354 cm^{-1} in Figure 4.16.

The increasing noise level from 3250 to 3500 cm^{-1}, and from 1750 to 1500 cm^{-1} is because of the signal reduction as the high and low blackouts of the catalyst are approached, and hence a decrease in signal to noise ratio. The noise level in these areas may also be increased by water vapour in the carrier gas or the dosing pulse. The hygroscopic nature of EuroPt-1 gives rise to broad water peaks at 1630 cm^{-1} and above 3000 cm^{-1} if the flow is not kept scrupulously dry. At around 1360 cm^{-1}, full blackout is reached, and noise levels can be many orders larger than evident here. The derivative shaped peak is a feature of the blackout discontinuity.

As discussed in Section 3.6 a feature of DRIFTS is that it is proportionally more sensitive to small absorbances than to large (which is why quantitative work must use the non-linear Kubelka-Munk equation, which accentuates the large absorbances and reduces the small ones). In a region such as 2000 to 1500 cm^{-1}, where the support has considerable absorption, other infrared absorbances such as the CH_2 bending mode at 1466 cm^{-1} [219] appear on top of this. In transmission infrared, the ratioing of spectra removes the background absorbance, and peaks such as the 1466 cm^{-1} band give an intensity proportional to their absorbance. In the DRIFTS spectrum, because this peak is a comparatively small absorbance added to the already considerable absorbance of the catalyst, it is moved into a less responsive region of the curve in Figure 3.12. When the absorption spectrum is calculated, therefore, the advantage which this gives in accentuating small peaks plays against bands in the C–H bending/C–C stretching area of the spectrum, over and above the already higher blackout level. This sometimes leads to unusual relative intensities of the C–H stretch/C–H bend modes [185].

Other general points on Figure 4.16 are the negative peak at 3744 cm^{-1}, and

the small window of reduced noise between 1300 and 1100 cm^{-1}. The first is due to a reduction of the number of free hydroxyl groups on the silica surface by butane adsorption [154]. The second is caused by increased specular reflection from the highly absorbing silica, and although little information on surface species may be found from this region, gas phase peaks are occasionally visible.

The spectrum in the C–H stretching region is shown in Figure 4.17. An envelope of strong absorbance covers the range 3040 to 2770 cm^{-1}, with clear maxima at 2964, 2896 and 2878 cm^{-1}. This would appear to have contributions from the gas phase and silica spectra, the former shown in the sharp peaks, and the latter, after two spectra of the series, when unattached gas should be decreasing in the flow, and the peaks become broader, and lose intensity particularly in high frequency end.

With successive spectra, the 3040 to 2770 cm^{-1} envelope gradually decreased, corresponding to removal of these species. After four spectra (124 s), however, it was clear that the spectra were changing. With a generally lower intensity, the relative peak heights no longer conformed with Figure 4.17. It appeared that other bands, previously hidden under the intense peaks of the initial gas pulse were now becoming visible, as shown in Figure 4.18. This is constructed in the same way as Figure 4.13 above. In order to increase the clarity of the diagram, the first two spectra plotted were again reduced by factors of 4 and 2. The underlying spectrum, with its main peak at 2894 cm^{-1} is considerably more stable than the initial envelope. The development of the spectra with time is perhaps more clearly shown in Figure 4.19, the equivalent of Figure 4.14. The spectral intensity at a selection of frequencies is plotted against time, some peaks developing a separate identity only after several minutes. The inset is to accentuate the area of greatest complexity and retains the x scale of the main graph with an expanded y scale. Where the initial peaks gave way to underlying ones of a similar frequency, the same symbol is used to create a continuous curve, so the values in the key can only be regarded as approximate.

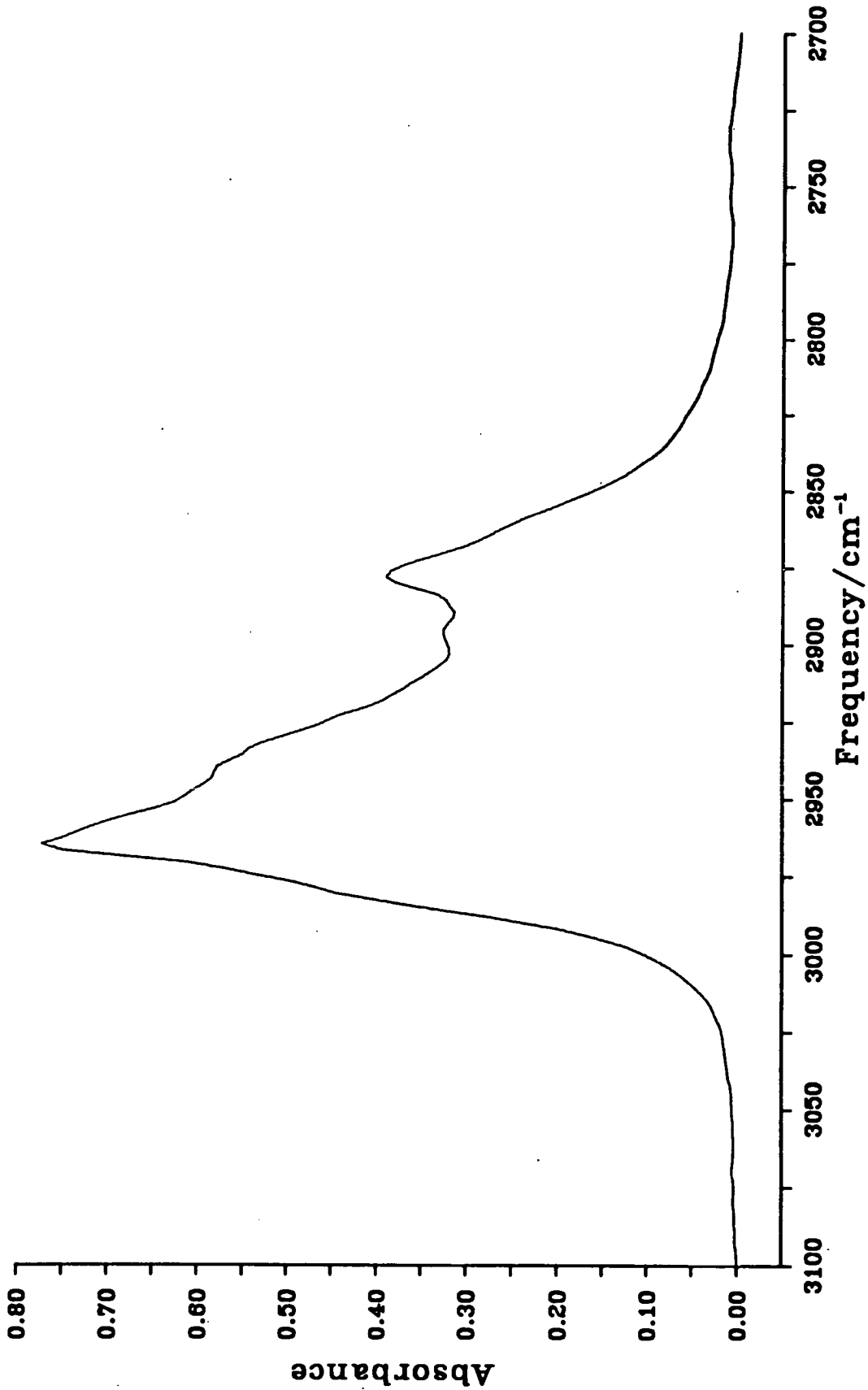

Figure 4.17: Butane absorption on EuroPt-1: C–H stretch region

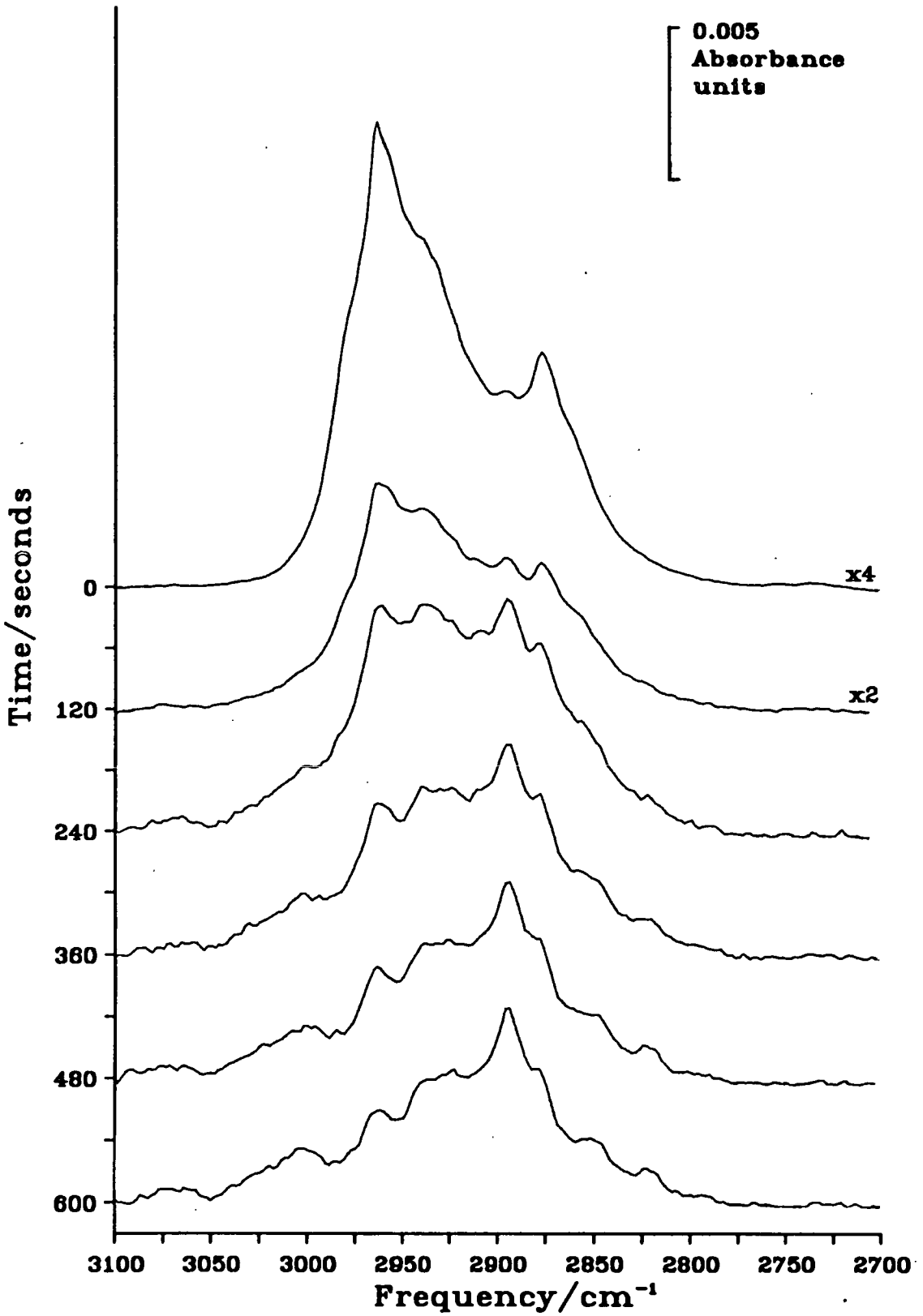

Figure 4.18: Butane absorption on EuroPt-1: changes in the C–H stretch spectrum with time.

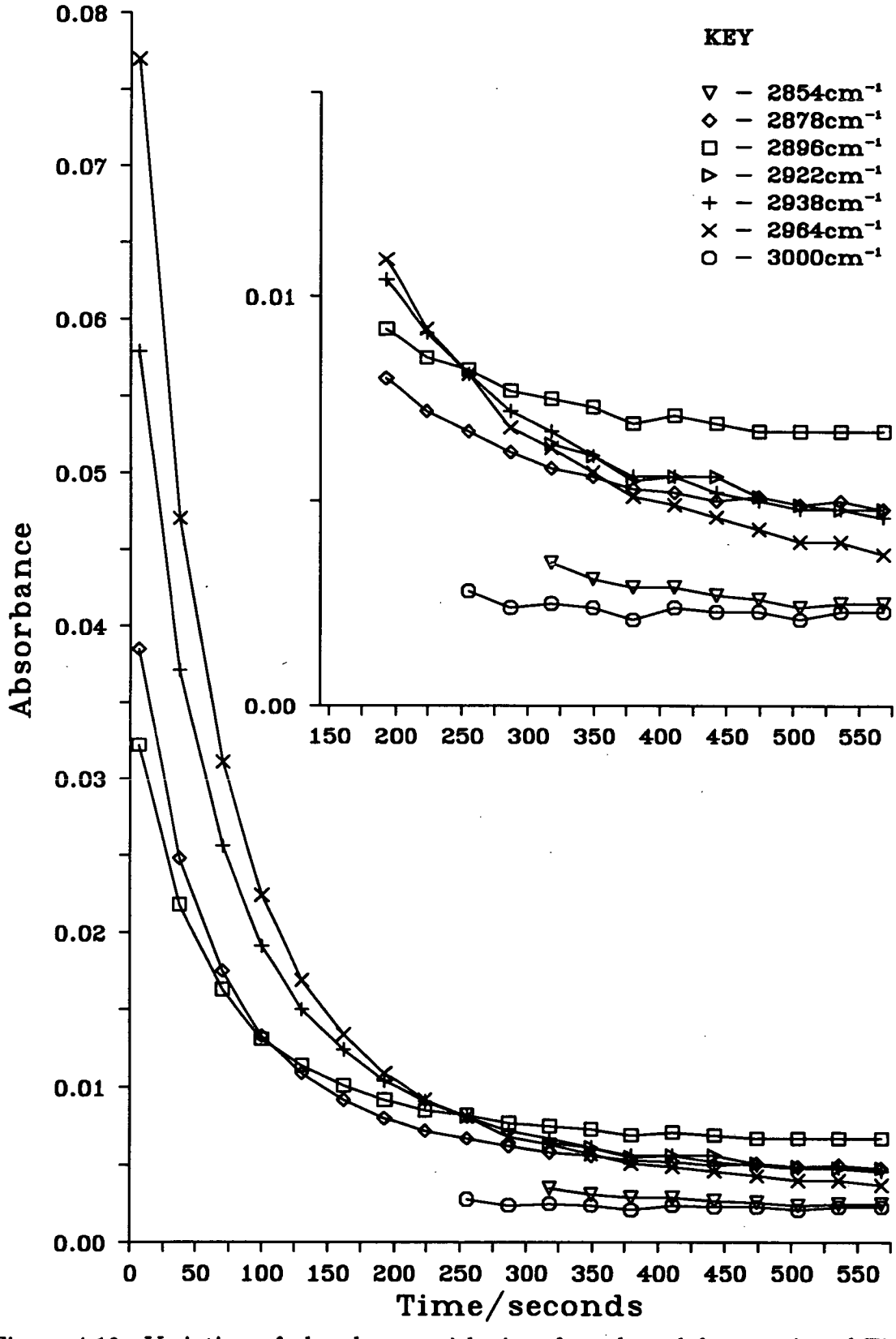

Figure 4.19: Variation of absorbance with time for selected frequencies of Figure 4.18 (inset at expanded y scale).

The weaker initial interaction of butane over EuroPt-1 compared with the butane/silica system can be seen by comparing Figure 4.13 and 4.18, though the intensity at the start of these figures is unfortunately subject to some error. The accuracy of flow rate and dose size will contribute to this, but the most serious uncertainty is in the time resolution. The profile of gas concentration in the cell is a complicated product of original pulse characteristics, the flow behaviour in the cell, and interaction with the catalyst. Even when the latter is at a minimum, the pulse lasts around a minute. Each infrared spectrum takes 15 seconds to collect, with a repeat time of between 30 and 40 seconds. Even if pulsing and data collection are carefully coordinated, the variable repeat time introduces variation into the parts of the gas pulse profile which are sampled. Thus although the larger initial intensity for silica (evident by comparison of the absorbance scales in the Figures) implies more butane is adsorbed on the silica surface as sampled by DRIFTS, it is only an indication and not definite evidence of the stronger interaction. More powerful evidence is the decay rate of these spectra shown in the graphs of Figure 4.14 and 4.19. The half life of the silica intensity is about twice that for EuroPt-1.

During the manufacture of EuroPt-1, the surface area of the Sorbosil AQ U30 was reduced from 364 m^2g^{-1} to the 180 m^2g^{-1} of EuroPt-1 [120]. Part of the sorption difference may thus be due to different diffusion properties of the two materials, as part of the reduction of area was a reduction of mesoporosity. The other significant difference is of course the platinum crystallites. With the 6.3% metal loading by weight, and a high dispersion, much of the surface is, if not covered, at least near to a metal particle. A simple geometric argument puts the chance of part of a butane molecule being in contact with a crystallite on adsorption at 20%, a value which might rise if the 3-dimensional structure was considered. The stabilising effect of the platinum is clear from the later spectra in Figure 4.18, and the persistence of infrared intensity demonstrated by Figure 4.19.

The C–H stretch region of the spectrum for the more stable species over

EuroPt-1 is presented in Figure 4.20. This is an average of 128 scans (rather than the 32 of the sequentially collected spectra of Figure 4.18) collected 20 minutes after the butane dose, with the helium flow retained at 10 mlmin^{-1} throughout. The main peak of the spectrum is at 2892 cm^{-1}. This is a frequency characteristic of a CH_3 symmetric stretch, such as displayed for ethylidyne. Since the discovery of the ethylidyne species, many unknown species in hydrocarbon/metal systems have been assigned to alkylidyne type adsorbates, especially over close packed metal surfaces which can provide the necessary three metal atom site.

The butylidyne species has been identified at around room temperature by EELS [226] and RAIRS [216] as discussed above. The CH_3 symmetric stretch for this species was found by Chesters to be around 2875 cm^{-1}, with a degree of variability depending on the conformation. It appeared with a companion peak at 2932 cm^{-1} of similar intensity. The two alkylidynes which might be formed on fragmentation of the carbon chain are propylidyne and ethylidyne itself. As noted by Chesters [216], the propylidyne species has the terminal CH_3 group at around 70° to the surface normal (Figure 4.21) which means that under the MSSR the antisymmetric CH_3 band is stronger than the symmetric stretch. The latter gives a weak band at 2865 cm^{-1}, but the absence of a significant feature at higher frequency in Figure 4.20 rules out both butylidyne and propylidyne as contributing to the 2894 cm^{-1} peak. Ethylidyne itself is thus the closest to providing the observed spectrum, with the main CH_3 symmetric stretch at 2884 cm^{-1} [72]. The formation of this species in surface concentrations enough to dominate the spectrum goes against chemical intuition, and there is a significant difference in the frequency from the single crystal system. Such a difference was not observed for ethylidyne over previous supported metal catalysts [154, 216].

A more convincing suggestion, and one which allows the retention of the C_4 chain, is one of the species observed when but-2-enes are adsorbed on Pt(111) [227, 216]. The trans-di-σ-butene shown in Figure 4.6, as suggested by Avery and Sheppard, has a two fold symmetry axis putting it in the C_2 point group

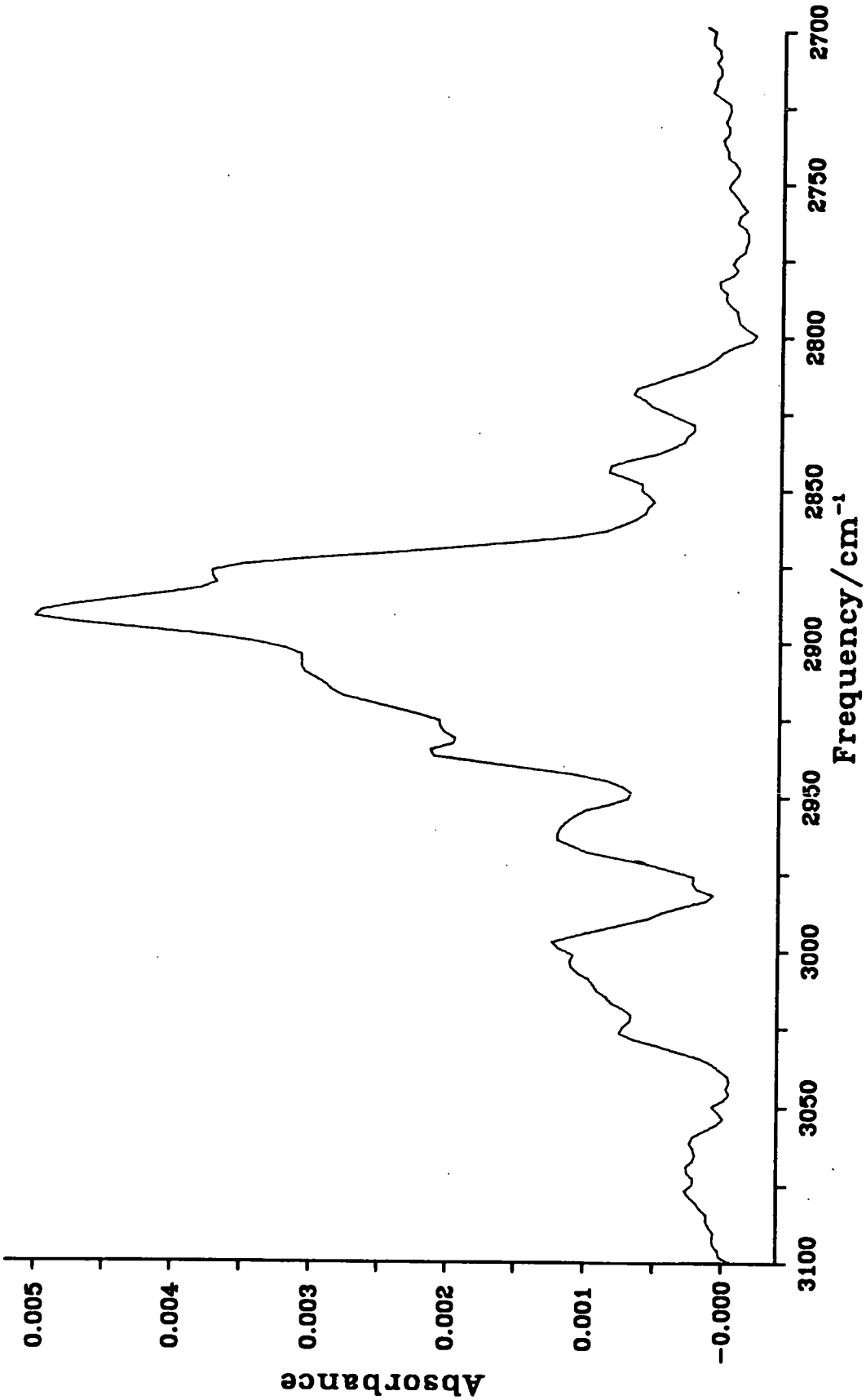

Figure 4.20: Surface species formed by butane adsorption on EuroPt-1.

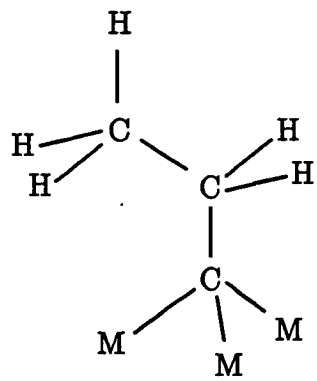

Figure 4.21: Propylidyne surface complex.

[227]. The upright terminal C–C bonds leave the symmetric CH_3 stretch as the dominant vibration in this region of the spectrum. The higher resolution of the RAIRS spectrum of both but-2-ene and but-2-yne on Pt(111) [216] shows a broad band centred at 2886 cm^{-1}. The slightly higher frequency, the breadth of the band, and the likely retention of the C_4 chain mean that the observed 2894 cm^{-1} band will be assigned to the same surface species.

The butane/EuroPt-1 spectrum also suggests that butylidyne can also be seen as a minority species, contributing the peaks/shoulders at 2936 and 2878 cm^{-1} with the assignment as given above. The broad band between 3026 and 2998 cm^{-1} will be due to a range of dehydrogenated surface species of varying hybridisation, which may contribute CH stretches in low intensity through the spectrum - *eg.* at 2844 cm^{-1}, possibly a CH_2 symmetric stretch. Despite the largest infrared peaks being due to the di-σ adsorbed butane of Figure 4.6, these low hydrogen fragments may account for a large proportion of the surface carbon. It is not certain whether the low broad feature between 3100 and 3050 cm^{-1} is real, or just a baseline fluctuation. It is in this area that bands due to the oft mentioned high temperature $(C_2H)_n$ species are found [236].

4.2.4 Butane adsorption on a hydrogen rich EuroPt-1 surface at 298 K.

Rather than dispensing with part of the standard catalyst preparation, the EuroPt-1 sample was reduced, outgassed and cooled as normal. Six pulses of 35 μmol of hydrogen were then added to the helium carrier gas stream, followed after 26 minutes by a 35 μmol pulse of butane, monitored in the infrared in the standard manner.

The development of the spectra with time is shown in Figure 4.22, and the variation of selected intensities in Figure 4.23. The drop in the intensity with time is sharper here than for the previous experiments, so the initial spectrum in Figure 4.22 is scaled by a factor of 10.

The general pattern of Figure 4.23 has obvious similarities to the analogue from the experiment on outgassed EuroPt-1, Figure 4.19. The initial envelope of C–H stretches, with gas phase contributions shown in the sharpness of the initial spectrum of Figure 4.22, decays quickly leaving behind a more stable spectrum of hydrocarbon chemisorbed on the platinum crystallites.[2]

The level to which the butane infrared signal drops is, however, considerably lower here than over the 'hydrogen free' Pt/SiO_2 catalyst. The signal intensity of the chemisorbed species left after removal of the gas phase and physisorbed butane is less than a third that found in the previous experiment. The probable reason for this reduction in sorptive capacity is the presence of hydrogen adsorbed on the metal surface (shown in a small peak at 2120 cm^{-1} in the infrared spectrum). This could operate in two ways. The hydrogen might stop adsorption by direct site blocking, occupying sites normally active in the physisorption/dehydrogenation process necessary for butane chemisorption. The chemisorption of butane can only be initiated by a dehydrogenation step. The second effect of the high surface hydrogen concentration will therefore be to push the chemisorption equilibrium away from dehydrogenation, which would create surface hydrogen.

[2]The larger than normal time lag between the first two points of Figure 4.23 was due to a velocity error in the interferometer mirror travel.

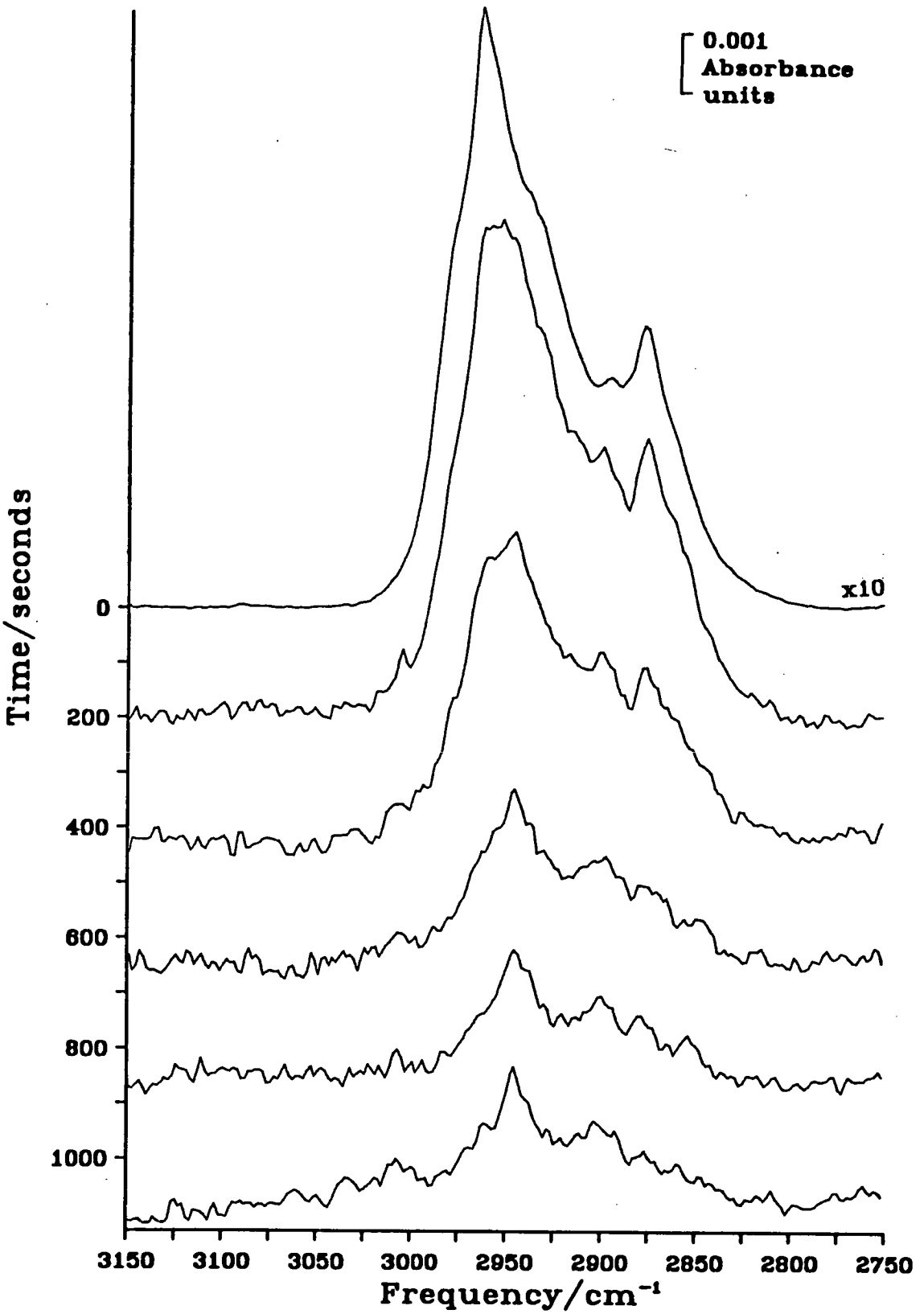

Figure 4.22: Butane adsorption on a hydrogen rich EuroPt-1 surface.

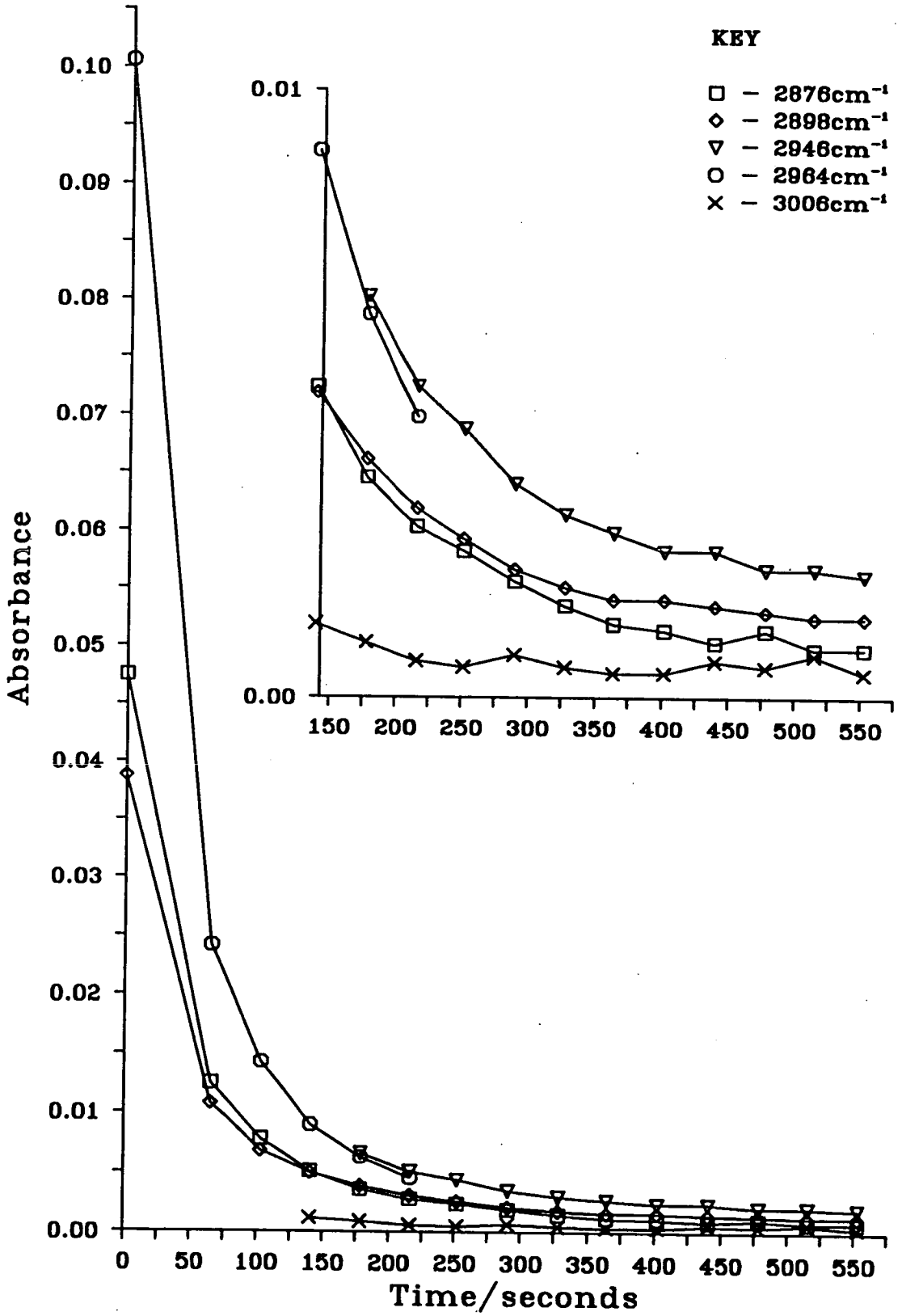

Figure 4.23: Variation of absorbance with time for selected frequencies of Figure 4.22 (inset at expanded y scale).

The DRIFTS spectrum of the surface species formed is shown in Figure 4.24. It is very weak, and the signal to noise ratio (SNR) correspondingly low, despite being an average of 128 scans rather than the 32 used for time resolved work. The main feature is at 2946 cm^{-1}, with some intensity between 2870 and 2910 cm^{-1} and an isolated peak at 3006 cm^{-1}.

The evidence of Figure 4.22 and 4.23 shows the general decrease in interaction of the hydrogen rich surface. In what remains, the 3006 cm^{-1} feature can be assigned to an unsaturated C–H stretching mode, and the 2946 cm^{-1} peak to an asymmetric CH_2 stretch. The surface species may also contain a small proportion of CH_3 units perpendicular to the crystallite, as some intensity is shown in the CH_3 symmetric stretching region at 2898 cm^{-1}, but none in the asymmetric CH_3 stretching region between the 3006 and 2946 cm^{-1} peaks. By a similar call to the MSSR, more of the CH_2 units must be oriented with the bisector of the HCH angle parallel to the metal crystallites. The infrared absorption which could be attributed to a symmetric CH_2 stretch at the lower edge of the 2870 to 2910 cm^{-1} region, is barely significant compared with the 2946 cm^{-1} peak, and much lower than the *circa* 8:5 intensity ratio expected for long chain hydrocarbons [224]. DRIFTS tends to give a higher proportional response to weaker signals than transmission spectra, as discussed in Chapter 3, which adds force to this argument.

The evidence thus points to the surface species being largely dehydrogenated. The bands at frequencies corresponding to sp^3 hybridisation implies multiple surface σ-bonding rather than the formation of highly unsaturated species. A plausible species which meets these some of these criteria is a 1,1,2,4 bonded butane, with a degree of rehybridisation in the multiply surface bonded carbons.

4.2.5 Hydrogenation of butane adsorbed on EuroPt-1 at 298 K.

An EuroPt-1 sample was prepared and dosed with butane exactly as described above (Section 4.2.2). The dosing was monitored by DRIFTS with identical

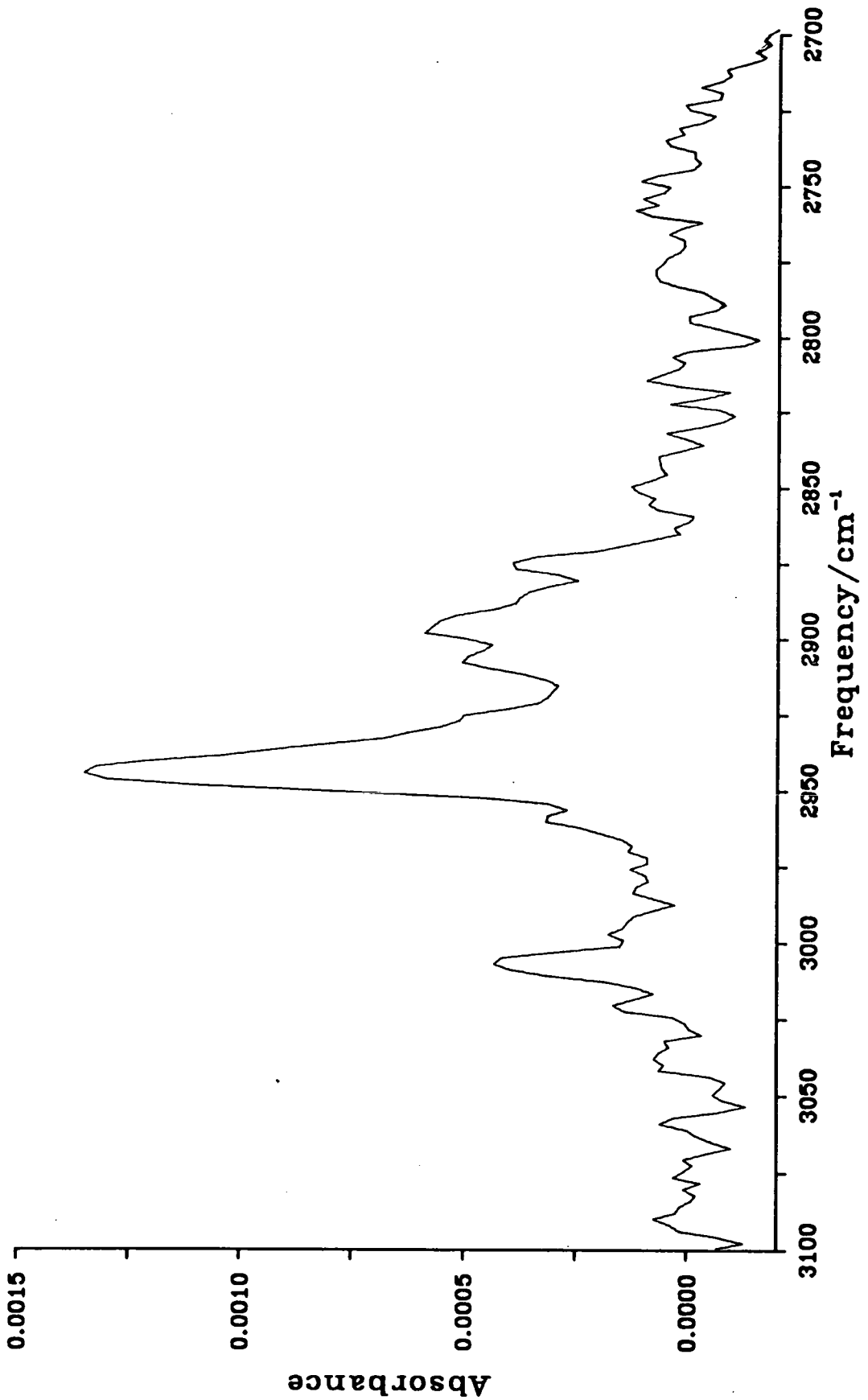

Figure 4.24: Surface species formed by butane adsorption on a hydrogen rich EuroPt-1 surface.

results. 43 minutes after the butane pulse, a 35 μmol pulse of hydrogen was introduced into the flow, and the changes in the infrared spectrum of the surface species recorded by DRIFTS.

The C–H stretching regions of the sequentially collected 32 scan spectra are displayed in Figure 4.25, with the time difference marked on the y axis. The first spectrum was collected just before the hydrogen pulse. This is weaker than Figure 4.20, especially in the main peak at 2892 cm^{-1}. Figure 4.19 above does show that the chemisorbed species exhibit a gradual decline in DRIFTS signal, and the spectrum taken just before the hydrogen pulse reached the EuroPt-1 had matured in the helium flow for an extra 23 minutes.

The spectra change quickly as the hydrogen reaches the environmental chamber. The second spectrum of Figure 4.25 has grown in intensity over the 38 second time interval. Its form nearly reproduces that of Figure 4.20. The maximum is shifted slightly to 2894 cm^{-1} (only just significant in 4 cm^{-1} resolution spectra) and is marginally larger (0.0056 absorbance units plays 0.0050) though as with the frequency change, this is not large when both spectra are baseline corrected for water contamination, and the peak to peak noise is 0.0003 absorbance units in the 32 scan spectrum.

The straight forward conclusion that can be drawn from this is that the signal reduction over the 23 minutes between Figure 4.20 and 4.25 is a dehydrogenation of the existing surface species, especially the species responsible for the main peak at 2892 cm^{-1}.

By the next spectrum, 76 seconds into the hydrogen pulse, the signal has again changed dramatically. The overall intensity has increased over the previous spectrum, and over a wider range of frequencies. Because the changes in intensity are so rapid, graphs of absorbance against time for selected frequencies, as plotted for previous experiments, added little to an understanding of this system. More information can be gleaned from Figure 4.26, a set of difference spectra created using the SUBTRACT routine (Section 3.5.3). The spectra are simply the arith-

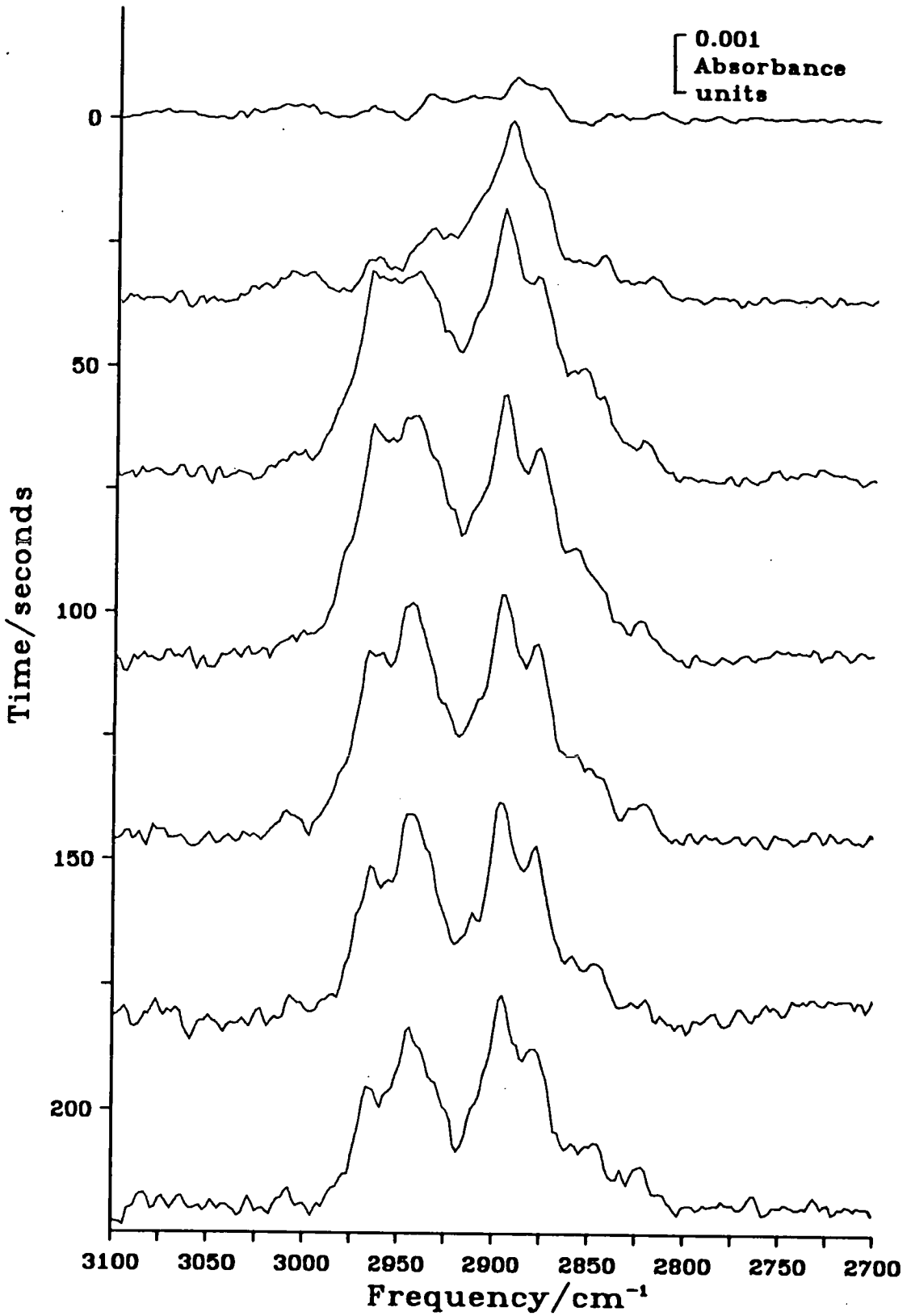

Figure 4.25: Butane adsorption on EuroPt-1: changes in the C–H stretch spectrum with addition of hydrogen

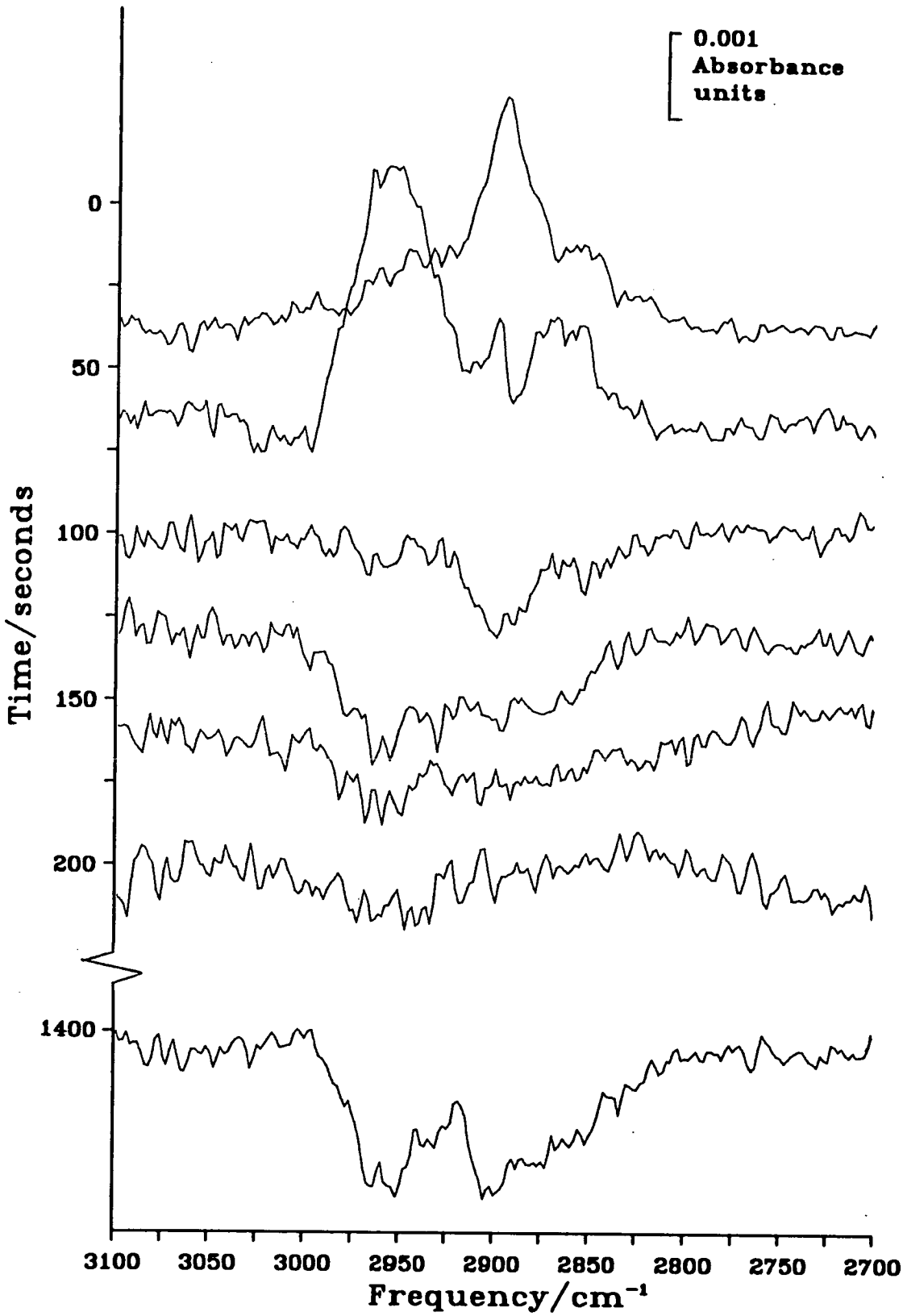

Figure 4.26: Absorbance subtraction spectra to show changes in Figure 4.25

metic differences between each 32 scan DRIFT spectrum of Figure 4.25, and the spectrum collected 37 seconds before it. The Figure is completed by the difference between the last spectrum of Figure 4.25 and a 128 scan spectrum collected 22 minutes later. The changes in the last spectrum are therefore significant, and the noise levels slightly lower.

The first difference spectrum shows the increase in the 2894 cm^{-1} peak mentioned above. The second difference spectrum is also positive, showing that the signal is still increasing over a broad range of frequencies. This is partly due to production of some physisorbed/gas phase butane, with its now well recognised spectrum. As already noted, the physisorbed material is readily removed by the carrier gas flow, and this process is just visible in the fourth, fifth and final difference spectra. Most of the change in the second spectrum is, however, due to the growth of peaks better seen in Figure 4.25 and discussed below. Changes in the 2894 cm^{-1} peak can be seen in the second spectrum, as it again shifts to the higher frequency of 2896 cm^{-1}, superimposing a derivative shaped feature between 2910 and 2880 cm^{-1}. With time, it thins down again from the higher frequency side, producing a significant negative peak at 2898 cm^{-1} in the third and contributing in that area in the final spectra of Figure 4.26.

The assignment of the peaks on initial hydrogenation must be given exactly as described in Section 4.2.3, since the second spectrum of Figure 4.25 and Figure 4.20 are nearly identical. The main peak at 2894 cm^{-1} is the CH_3 symmetric stretch of di-σ-adsorbed butane.

As the physisorbed butane is removed in Figure 4.25, the spectrum revealed is very different from the original. The 128 scan spectrum recorded 22 minutes after the hydrogen pulse is shown in Figure 4.27 and retains most of the features of the last spectrum in Figure 4.25, recorded 3 minutes after the pulse. Any differences are displayed in the last spectrum of Figure 4.26, as Figure 4.27 was the reference spectrum used for the last subtraction.

The largest new peaks shown on the spectrum are at 2942 and 2878 cm^{-1}.

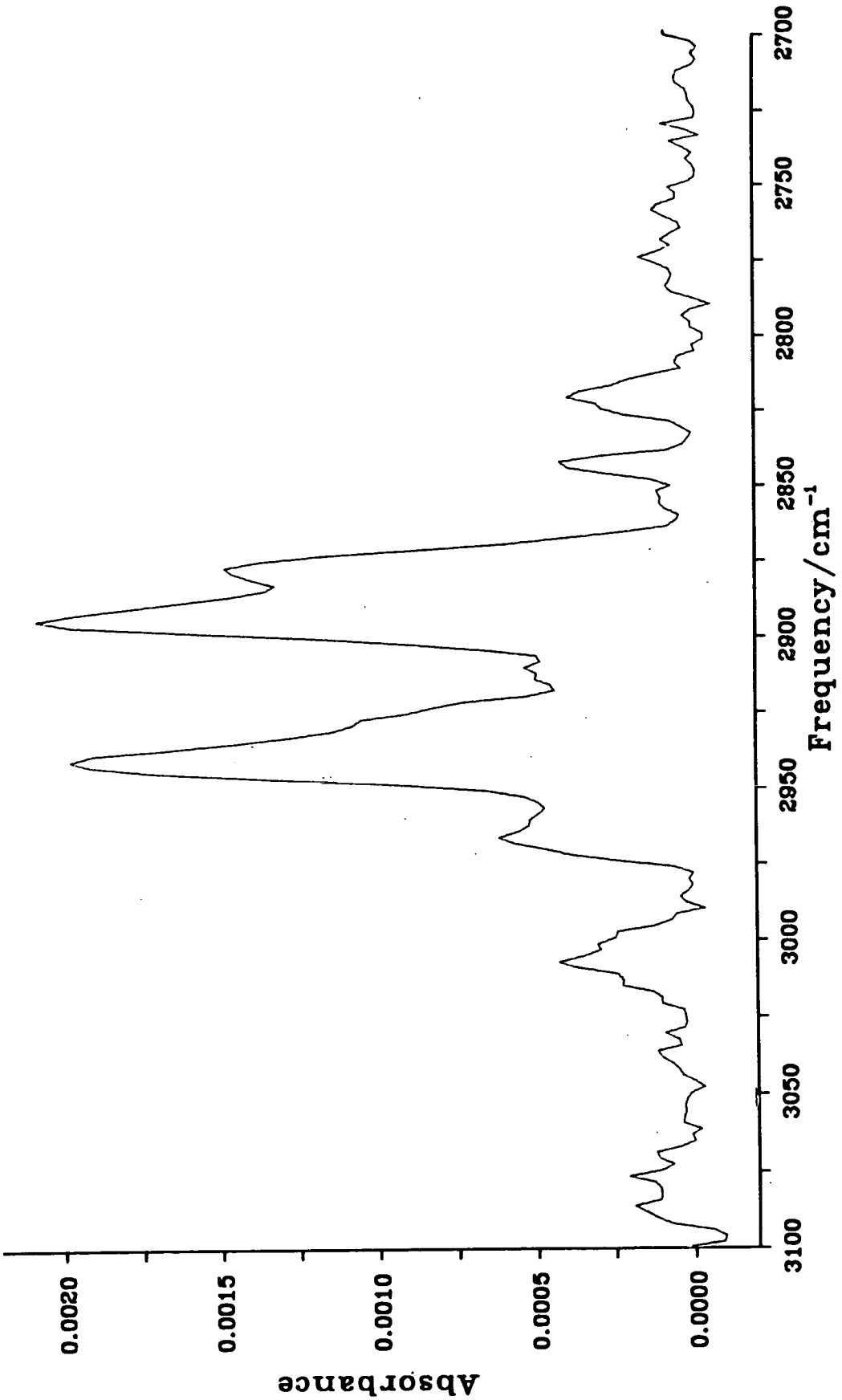

Figure 4.27: Butane adsorption on EuroPt-1 at 298 K: mature spectrum after hydrogenation.

These are identifiable in comparison with the but-1-ene/Pt(111) RAIRS spectra of Chesters [216] as the butylidyne species. The frequencies are at the high end of the range from the *trans* to the *gauche* frequencies, so the butylidyne will predominantly be in the *gauche* form. With the breadth of the infrared bands, it is possible that a range of conformers exist on the surface. There is still a large contribution at 2896 cm^{-1} which can be assigned as above. The contribution from the low hydrogen content species seem less significant, with a relatively narrow band at 3006 cm^{-1}.

4.2.6 Temperature programmed desorption of butane on EuroPt-1.

A EuroPt-1 sample was reduced, outgassed and exposed to a 35 μmol pulse of butane, while being monitored by DRIFTS. The spectra were as described above. The catalyst was then heated in the continuing helium flow. DRIFT spectra, each an average of 50 scans were recorded sequentially as interferograms, with a slight time delay in the loop giving a repeat time of 50 seconds. The heating rate was adjusted so a spectrum was recorded for every 10 K rise, a heating rate of 12 $Kmin^{-1}$.

A selection of the spectra at 30 K intervals is displayed in Figure 4.28, showing all the major changes which were observed. The variation of peak intensity with temperature is plotted in Figure 4.29. As before, when bands in the original spectrum give way to underlying ones of a similar frequency, or a band shifts in frequency, the same symbol may be used to simplify an already complicated Figure. The values in the key should therefore only be used as a guide.

Over the first three spectra, up to 320 K, there is a reduction in signal at all C–H stretching frequencies. This is in line with the decrease in absorbance observed above in the absence of heating. The 320 K spectrum of Figure 4.28 is very similar to Figure 4.20, the only difference being a slightly greater prominence of butylidyne shoulders at 2938 and 2878 cm^{-1}.

Considerable change occurs over the temperature rise from 320 to 380 K.

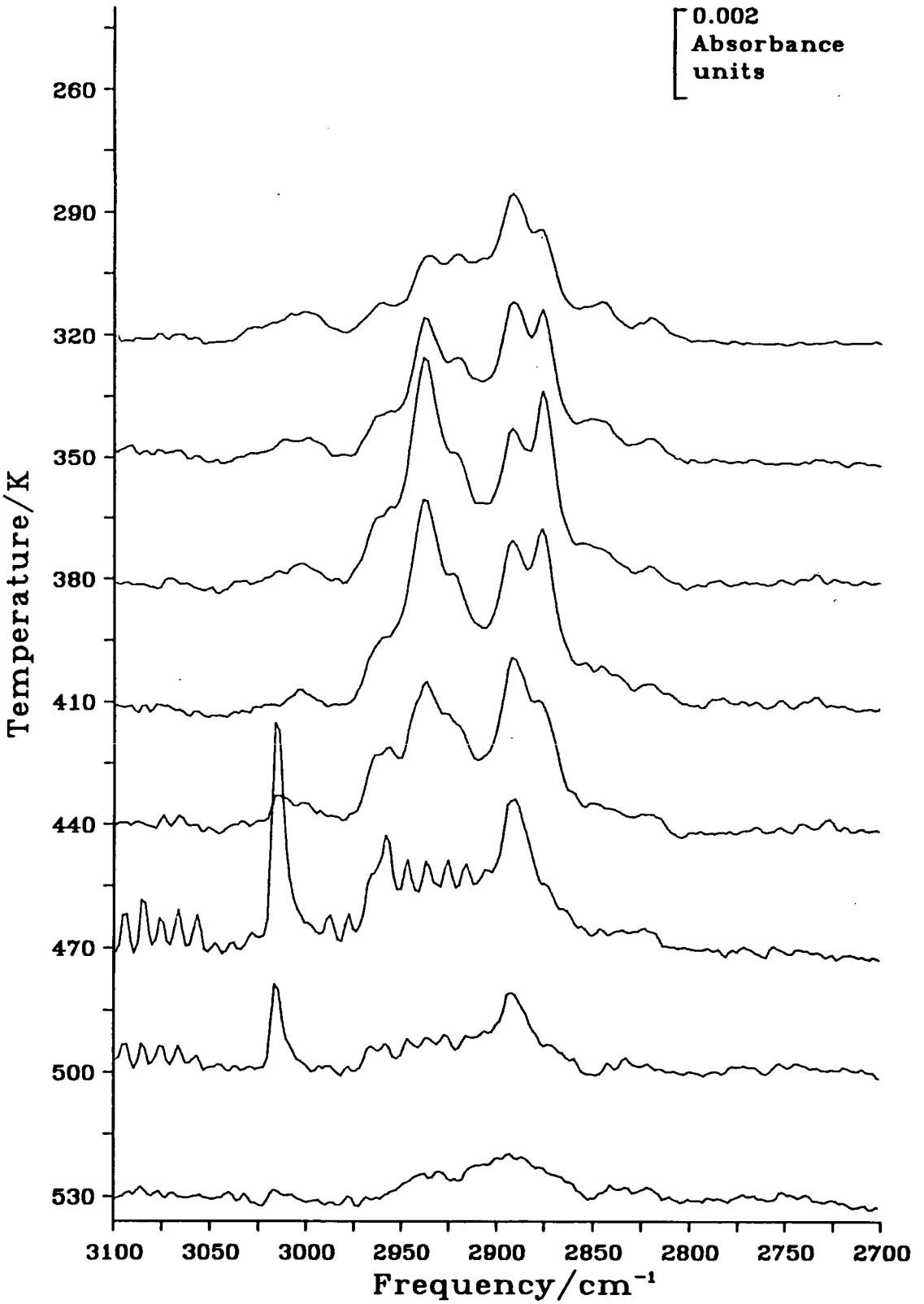

Figure 4.28: Changes in the butane spectrum over EuroPt-1 with temperature.

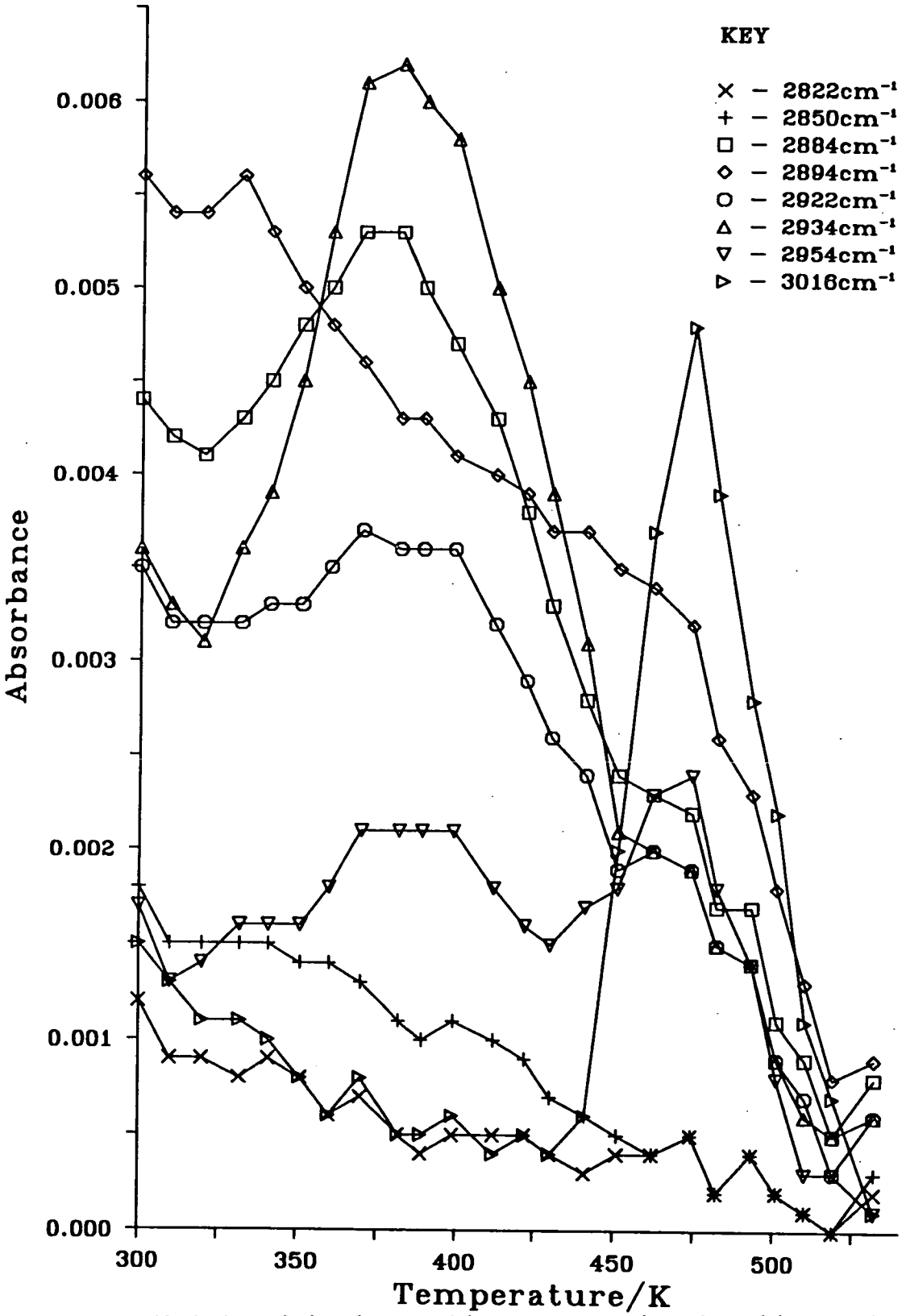

Figure 4.29: Variation of absorbance with temperature for selected frequencies of Figure 4.28

Here the butylidyne peaks rise dramatically in intensity, while the main trans-di-σ adsorbed butane band at 2894 cm^{-1} decreases as before. The shoulders at 2958 and 2922 cm^{-1} also rise, though this is probably only on the tails of the butylidyne peaks. Band overlap may also affect the 2894 cm^{-1} peak.

From 400 K the butylidyne peaks decay rapidly, though the rate of change of the di-σ-butane remains roughly constant over the range from 300 to 470 K. At 440 K, there is rapid rise in signal at 3016 cm^{-1}, the ν_3 frequency of gas phase methane [237], which peaks at 470 K, falling as rapidly as it rose. The rotational structure of the methane can be clearly seen, but it seems to have a discontinuity at 2960 cm^{-1}. The underlying peak responsible for this will be the antisymmetric CH_3 stretch associated with the symmetric stretch at 2894 cm^{-1}.

By 530 K, all significant infrared peaks have disappeared. The temperature rise has altered the underlying silica spectrum, and the higher temperature spectra are significantly baseline corrected. Broad features such as the band centred at 2894 cm^{-1} might be a by product of this, or the C–H stretch of highly dehydrogenated saturated species with isolated C–H bonds, though such bands are often seen at higher frequencies.

4.2.7 Butane adsorption on Sorbosil AQ U30 at 378 K.

A sample of Sorbosil AQ U30 was prepared in an identical manner to above, before being heated up to 378 K and exposed to a 35 μmol pulse of butane while under DRIFTS surveillance. The infrared absorbance at selected frequencies is plotted against time in Figure 4.30, and displayed rapid decay, disappearing into the noise level after 250 seconds.

4.2.8 Butane adsorption on EuroPt-1 at 378 K.

A sample of EuroPt-1 was reduced and outgassed and cooled to room temperature before being heated to 378 K. A 35 μmol sample of butane was then passed over it, monitored throughout by DRIFTS in the standard manner. The initial gas phase

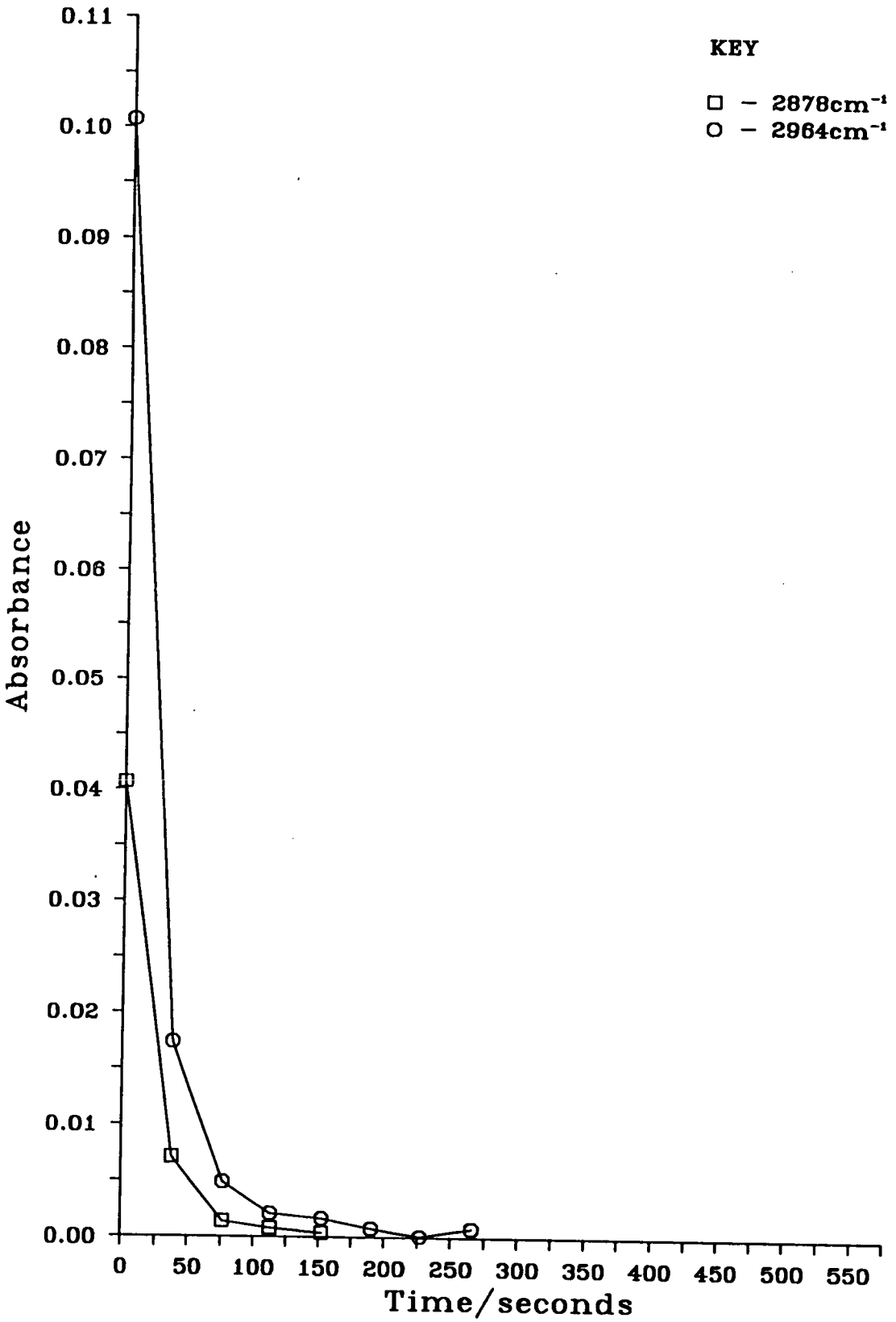

Figure 4.30: Variation of absorbance with time for butane adsorption on Sorbosil at 378 K.

butane spectrum quickly decayed leaving behind the spectrum of chemisorbed hydrocarbons. The absorption of selected frequencies and their variation with time is shown in Figure 4.31.[3]

At the higher temperatures of this experiment, butane is not significantly physisorbed on either EuroPt-1 or the metal free silica. The decay of the butane C–H stretching envelope is rapid, and retains the sharp gas phase peaks over the silica as well as over EuroPt-1. By the collection of the third spectrum over EuroPt-1, the underlying chemisorbed species are visible, and as at lower temperature, prove to be reasonably stable in the helium flow.

The DRIFTS spectrum of the C–H stretching region after 30 minutes is shown in Figure 4.32. It is an average of 128 scans, and differs from the spectra used to make Figure 4.31 in a slight reduction of intensity and improvement in the SNR. The two narrow bands at 2934 and 2876 cm^{-1} are assigned to the *trans*-butylidyne species. At this higher temperature, the frequencies agree within the limits of the resolution with the values observed for but-1-ene adsorption on Pt(111) by Chesters [216], and are almost certainly caused by the same species.

The broad absorbance between 3024 and 2992 cm^{-1} is indicative of a considerable coverage of dehydrogenated species with a tendency towards sp^2 hybridisation. There is no clear peak at 2894 cm^{-1} as observed under low temperature adsorption, and which was retained in the TPD past the temperatures used here. A shoulder with an inflection point at 2888 cm^{-1} may have some contribution from similar species, but is more likely to be due, along with subsidiary peaks at 2956 and 2918 cm^{-1}, to methyl groups associated with the dehydrogenated species just mentioned.

[3]The gap in data between 250 and 500 seconds in Figure 4.31 was caused by the corruption of a floppy disc.

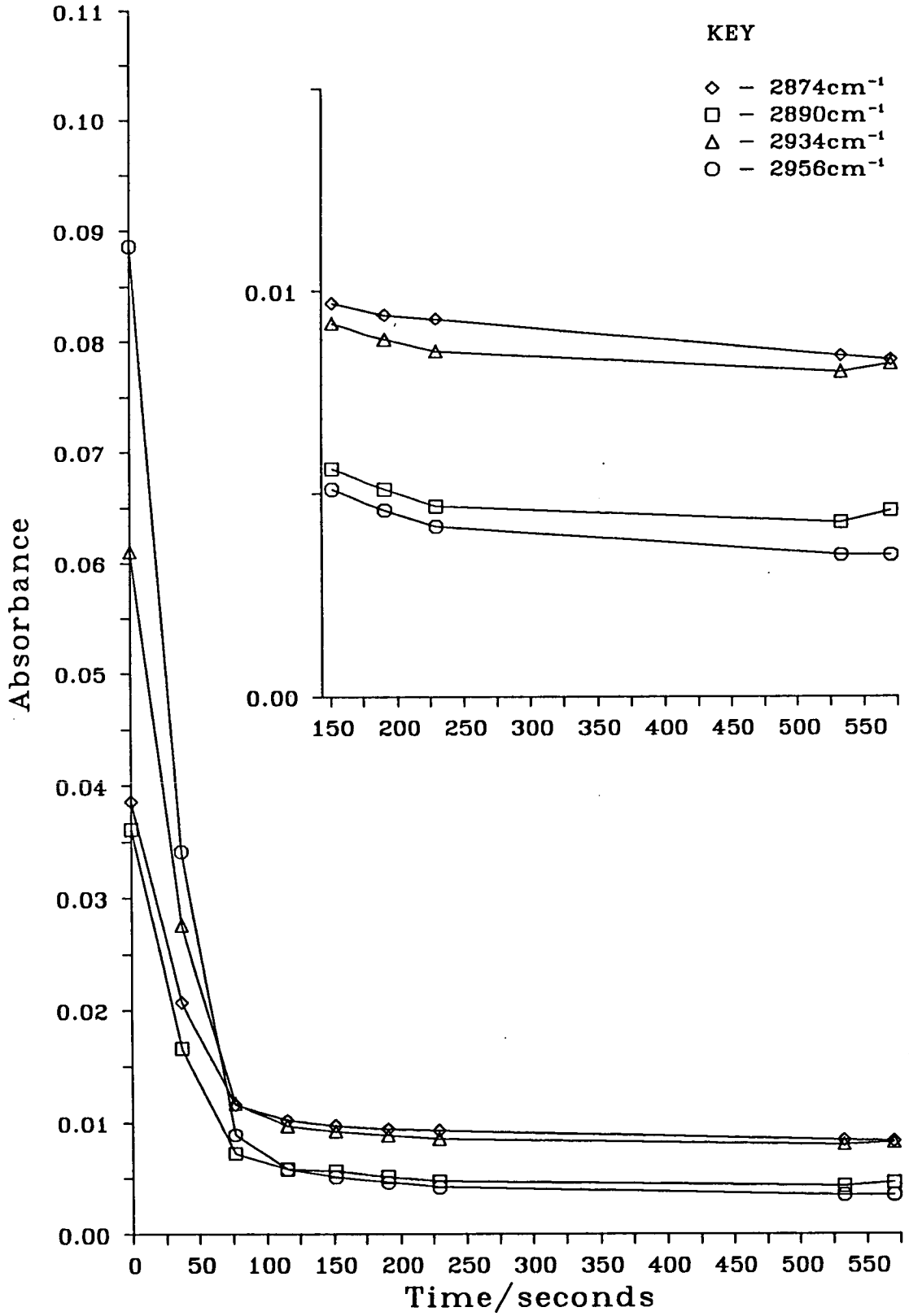

Figure 4.31: Variation of absorbance with time for butane adsorption on EuroPt-1 at 378 K (inset at expanded y scale).

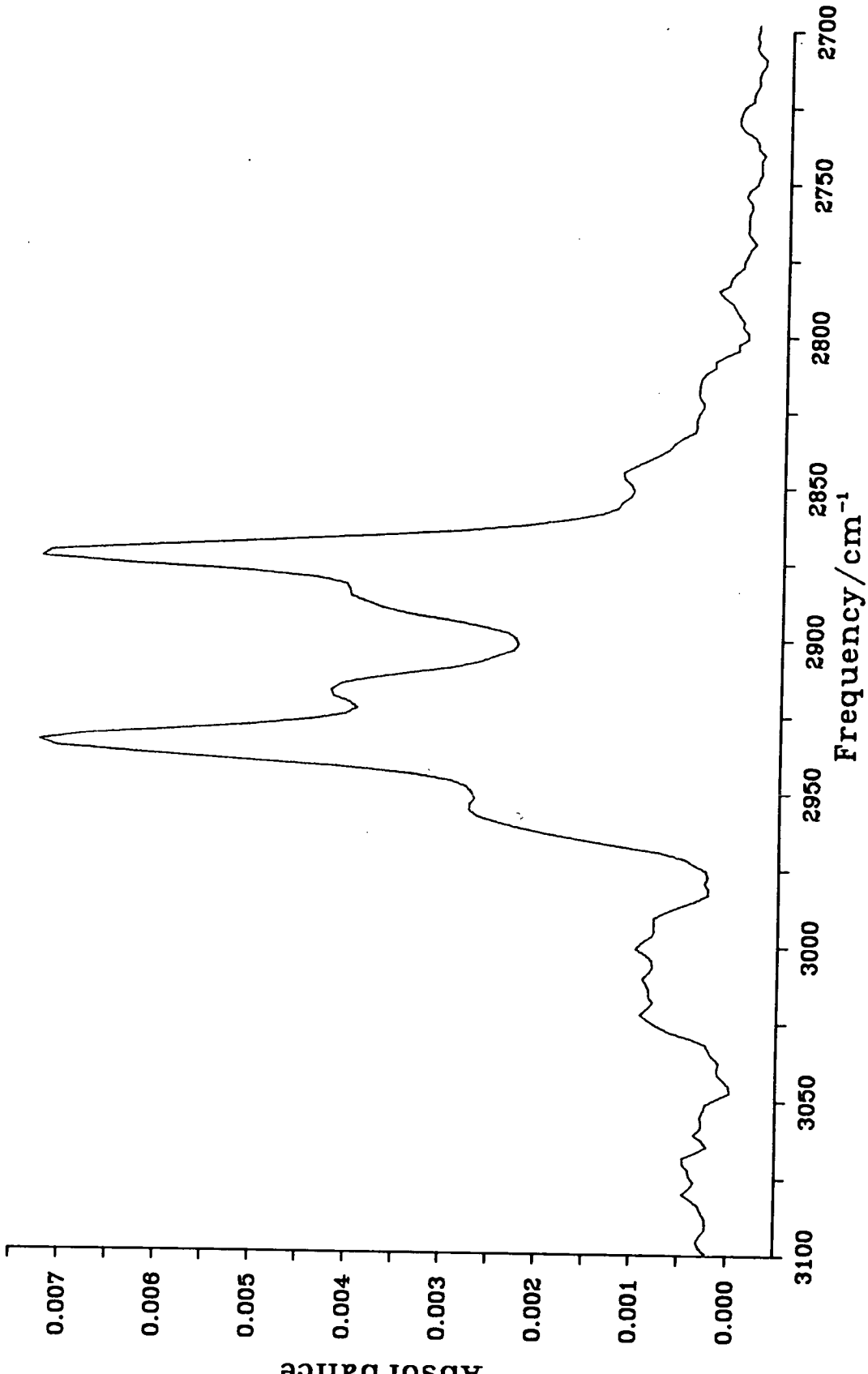

Figure 4.32: Surfaces species formed by butane adsorption on EuroPt-1 at 378 K.

4.2.9 Hydrogenation of butane adsorbed on EuroPt-1 at 378 K.

A sample of EuroPt-1 was dosed with butane at 378 K as described above. 68 minutes after the butane pulse, the catalyst was exposed to a 35 μmol pulse of hydrogen while 32 scan DRIFT spectra were recorded. Successive spectra are presented in Figure 4.33 covering the initial changes under the hydrogen pulse. The changes are hopefully clarified by Figure 4.34 which displays rolling difference spectra created using the SUBTRACT facility on the FTS-40 workstation. Visible alterations are confined to the first three spectra of the series. The long term changes are shown in the last spectrum, where a 128 scan spectrum recorded 24 minutes after the hydrogen exposure was used in the subtraction, rather than the next spectrum in the recorded sequence.

It was noted for the corresponding low temperature experiment that in the time between dosing with butane and exposure to hydrogen, further changes had taken place to those discussed in the section dealing with the initial dosing. This is again the case here.

The twin butylidyne peaks at 2936 and 2876 cm^{-1} are considerably reduced, from 0.0072 absorbance units in Figure 4.32 to 0.0041 absorbance units, with no shift in frequency. The other main peaks at 3030 to 2990 cm^{-1}, 2958 cm^{-1}, 2918 cm^{-1} and 2890 cm^{-1} are less affected, however. The first shows no perceptible change, and the latter three have all developed from shoulders to be distinct peaks as the butylidyne intensity has fallen away.

The first action of the incoming hydrogen is to restore the butylidyne peaks to their original intensity, with the 2936 cm^{-1} band moving a little to the blue at 2938 cm^{-1}. In the low temperature experiment, the hydrogen undid approximately 23 minutes of ageing and dehydrogenation, to recreate the original butane/EuroPt-1 spectrum. At these higher temperatures, however, there are significant differences. In the second spectrum of Figure 4.33 there is some contribution from gas phase butane (perhaps more easily seen in the first difference spectrum, Figure 4.34), indicating that the complete rehydrogenation is

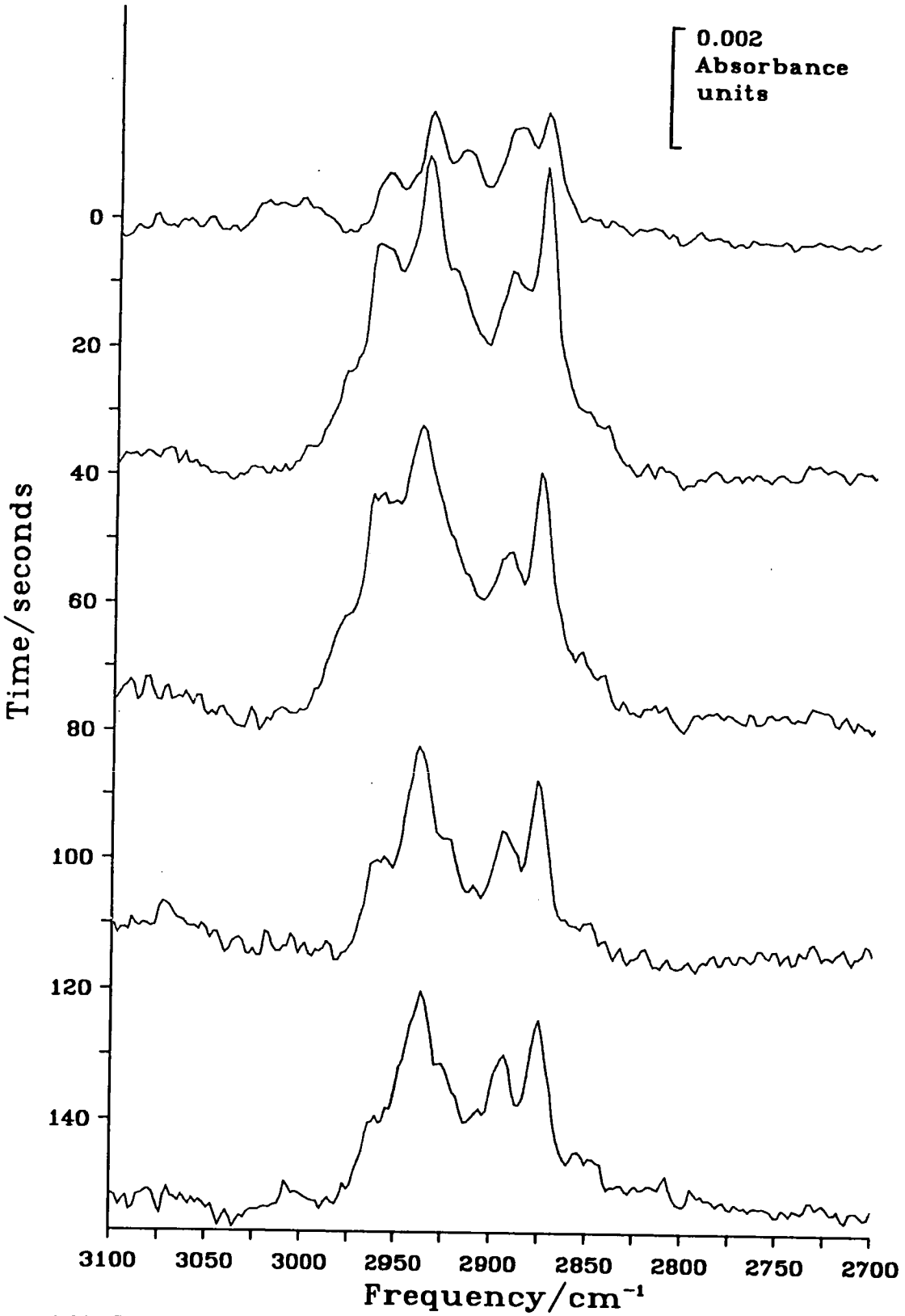

Figure 4.33: Butane adsorption on EuroPt-1 at 378 K: changes in the C–H stretch spectrum with addition of hydrogen.

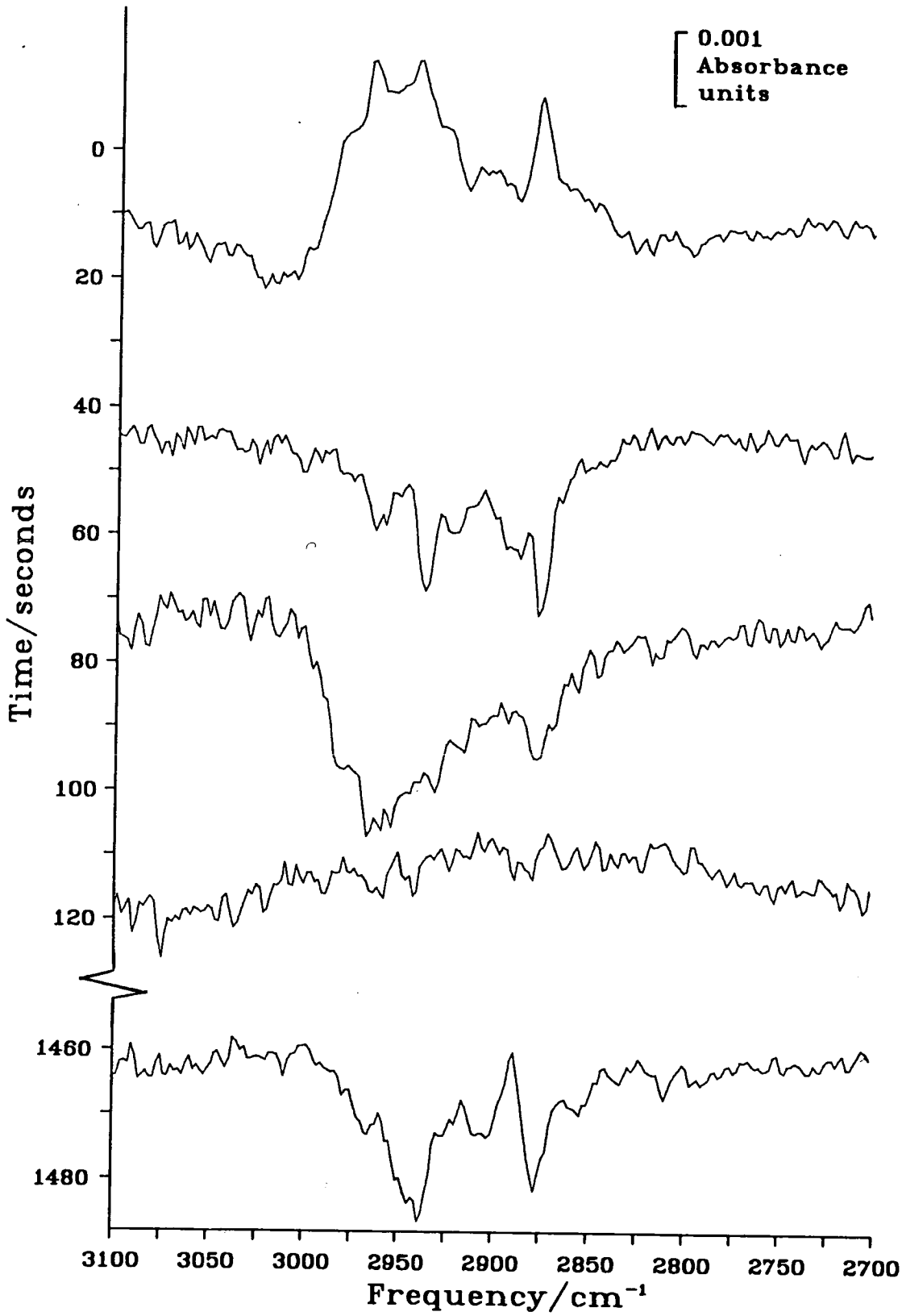

Figure 4.34: Absorbance subtraction spectra to show changes in Figure 4.33

much faster than at room temperature, though the sampling effect mentioned on page 123 means a direct comparison is not foolproof. A less obvious spectral change, but probably a more significant chemical one, is the complete removal of the broad band between 3030 and 2990 cm^{-1}.

The next spectrum into the hydrogen pulse has decreased in overall intensity, but comparison with the difference spectrum shows that the peaks most affected are the butylidyne ones. This implies that butane is being created at similar rates to during the previous spectrum, fast enough to counter the rapid decay in the butane spectrum under the helium flow shown in Section 4.2.8. By the third spectrum of the series, most of the rapid changes have ceased, with disappearance of the gas phase butane (again shown well by the difference spectrum). There is no change evident in the last spectrum in Figure 4.33 and nothing is visible in the difference spectrum above the noise level.

The C–H stretching region after a further 24 minutes is displayed in Figure 4.35. The peaks which have been assigned to the butylidyne species are considerably reduced by further exposure to the helium flow at high temperatures. The 2892 cm^{-1} peak does not show the same reduction, especially at its low frequency edge, as can be seen in the last of the difference spectra of Figure 4.34. This intensity at 2888 cm^{-1} may be due to an ethylidyne species formed on breaking the central C–C bond of the C_4 chain. Some intensity is also recovered at 3000 cm^{-1}, indicating the reforming of some dehydrogenated species of less than sp^3 hybridisation.

4.3 Discussion

4.3.1 Butane adsorption and reaction on EuroPt-1 at 298 K.

The DRIFT spectra of butane adsorbed on Sorbosil AQ U30, presented above, have very broad peaks compared with the gas phase spectrum of butane. The band profile is similar to that of solid butane presented by Snyder [219], and lacks the high frequency shoulder assigned by Murphy [223] to the *gauche* conformer

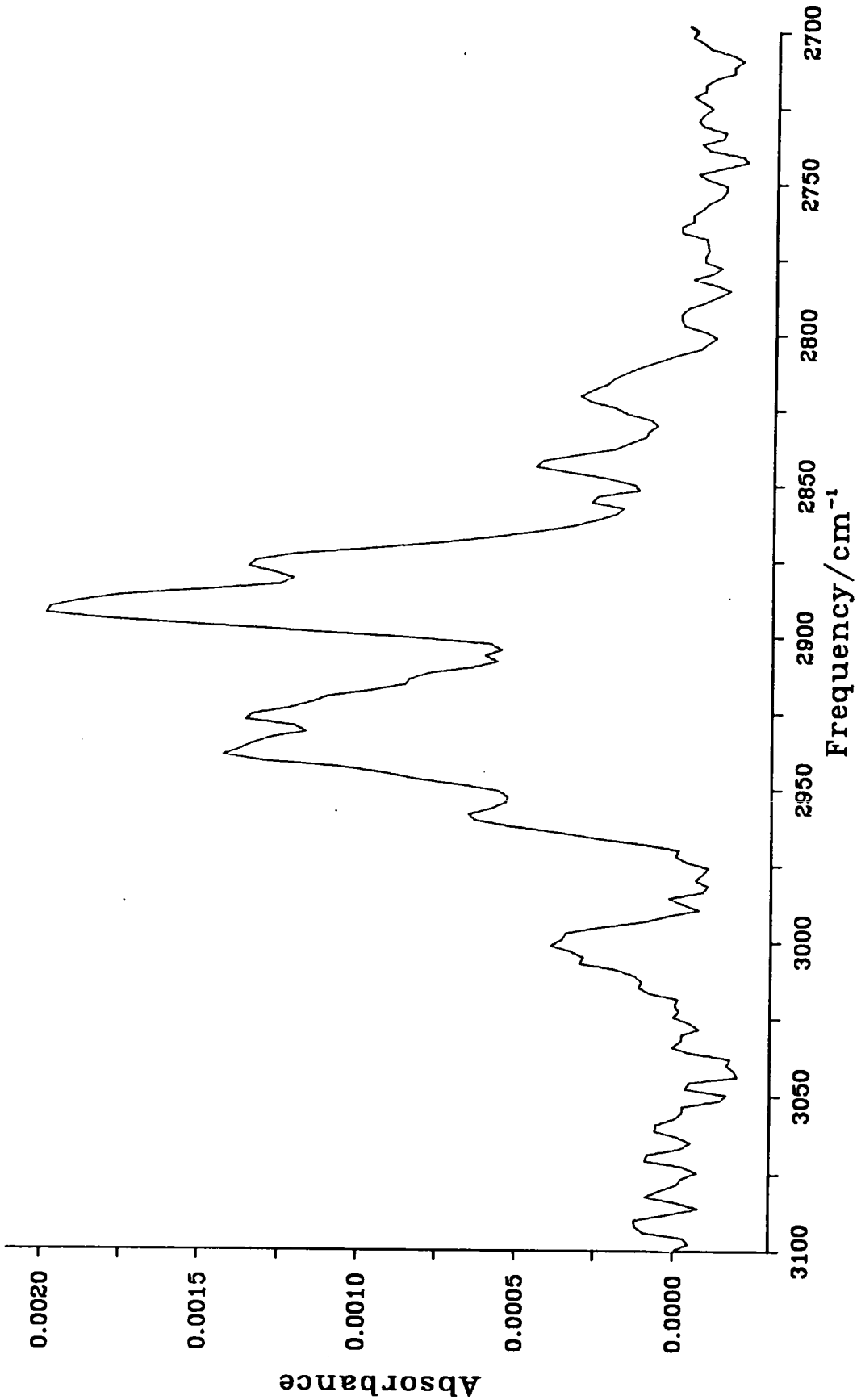

Figure 4.35: Butane adsorption on EuroPt-1 at 378 K: mature spectrum after hydrogenation.

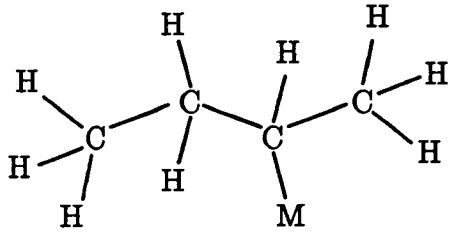

Figure 4.36: Mono-adsorbed butane

of butane. In the solid state butane exclusively occupies the *trans* conformation [239], and it therefore appears that the butane physisorbed on Sorbosil AQ U30 is predominantly in the *trans* form.

The interaction of butane with outgassed EuroPt-1 is initially weaker than with the Sorbosil, as the sharper peaks of gas phase butane remain in the first minute of DRIFTS monitoring of the gas pulse. After this initial period, the decaying infrared signal reverts to broader bands more in keeping with the spectrum over the silica support. The signal decrease is at a greater rate than over the plain silica, which will possibly be due to the lower porosity of the catalyst. The disappearing physisorbed material reveals an underlying spectrum of more persistent surface species, presumably chemisorbed on the metal crystallites.

In comparison with spectra over Pt(111) single crystal surfaces, two of the surface species are suggested to be a di-σ-adsorbed butane which has lost two methylene hydrocarbons in favour of carbon-platinum bonds (Figure 4.6), and a butylidyne species (Figure 4.9 [227, 216]. Other peaks in the infrared will be due to unknown surface species, some probably with carbon hybridisation less than sp^3, and having lost some hydrogen.

A possible route to the di-σ-adsorbed butane is via an intermediate such as the mono-adsorbed butane of Figure 4.36. This is compatible with the infrared spectra presented above. The physisorbed butane has been suggested to have the *trans* conformation. As the molecule looses one of the more readily exchanged methylene hydrogens [186] and is chemisorbed to the surface, it may retain the same conformation. The monoadsorbed species will have no symmetry elements

apart from the identity. The C_1 point group allows all molecular vibrations in the infrared, so any vibration creating a dipole change perpendicular to the metal crystallites will be allowed by the MSSR. Bands at both symmetric and antisymmetric CH_3 stretching frequencies would suggest that the terminal C–C bonds were not parallel with the surface. The CH_2 group could contribute to the infrared spectrum at around 2860 cm^{-1} with the symmetric stretch and 2925 cm^{-1} [220] with the antisymmetric stretch, though the former is weak in the physisorbed spectrum, and the latter is more likely to produce a surface normal dipole change. This is again compatible with the observed spectrum.

The spectrum of this postulated intermediate is therefore little different from the physisorbed butane. It does however give a simple dehydrogenation step to the trans-di-σ-butane adsorbate suggested by Avery and Sheppard as the low temperature adsorbate of trans-but-2-ene [227] illustrated in Figure 4.6, which demonstrates a similar vibrational spectrum to that found here. The two fold symmetry axis puts it in the C_2 point group, and more upright terminal C–C bonds leave the symmetric CH_3 stretch as the dominant vibration in the spectrum, as the antisymmetric stretch at 2964 cm^{-1} continues to decrease. The two hydrogens remaining on the central carbons may also be lost here, to give one of the complexes described by Avery for but-2-ene/but-2-yne adsorption at 300 K, Figures 4.7 and 4.8. It is difficult to tell either way, though the movement of the terminal C–C bond away from the vertical by rehybridisation (Figure 4.7) or the complex tilting (Figure 4.8) would reduce the MSSR action on the asymmetric CH_3 stretch.

After the more stable chemisorbed spectrum was formed, gradual decay in infrared signal was still seen, though at a lower rate. At the start of the low temperature hydrogenation, the 2892 cm^{-1} peak had lost most of its intensity, leaving the less affected butylidyne shoulders and other unassigned peaks more prominent. This is compatible with the stability observed for alkylidynes [158] and other peaks being caused by species already extensively dehydrogenated.

When the surface species are exposed to a pulse of hydrogen, the first effect is to recreate the spectrum observed prior to the 23 minutes of ageing. An inference from this is that the decay in signal is mainly a dehydrogenation of the surface species, though the interaction of the hydrogen may be a simple displacement. It also implies that most of the C_4 chains are not broken as the spectrum changes. Gas phase, physisorbed or monoadsorbed butane appear in the spectrum, and decrease to show peaks at 2942 and 2878 cm^{-1} which are assigned to the butylidyne species in a range of conformations tending towards the *gauche*, in comparison with the spectra of Chesters [216].

If this species is a butylidyne, its formation could be rationalised as follows: the methylene CH bonds of butane are more readily broken than the methyl CH bonds in exchange studies [186], and implied by the assignment of the 2892 cm^{-1} peak above. The formation of alkylidyne species from adsorbed alkenes is normally described as a progression from the lower temperature species di-σ bonded across the double bond. The terminal carbon then looses its hydrogens, one of which is transferred to the β carbon, and the other is lost, as shown by numerous TDS studies (*eg.* [226, 231]). The stable trans-di-σ-butane proposed above initially precludes the losing of methyl hydrogens for the rearrangement to butylidyne. It is only with ageing when further dehydrogenation has taken place that the terminal carbons are bound to the metal, and butylidyne can be formed on exposure to hydrogen. This suggested reaction scheme is represented in Figure 4.37.

The adsorption of butane on EuroPt-1 which has been exposed to several pulses of hydrogen was found to exhibit very different behaviour to the 'hydrogen free' surface just discussed, in agreement with the findings of Eischens [44]. The amount of material chemisorbed seemed from the DRIFT spectra to be much less than over outgassed EuroPt-1, which may be rationalised in terms of direct site blocking, and surface hydrogen acting by Le Chatlier's principle against the initial dehydrogenation required for chemisorption of butane. The observed spectrum implies that the surface species produced are highly dehydrogenated, and mul-

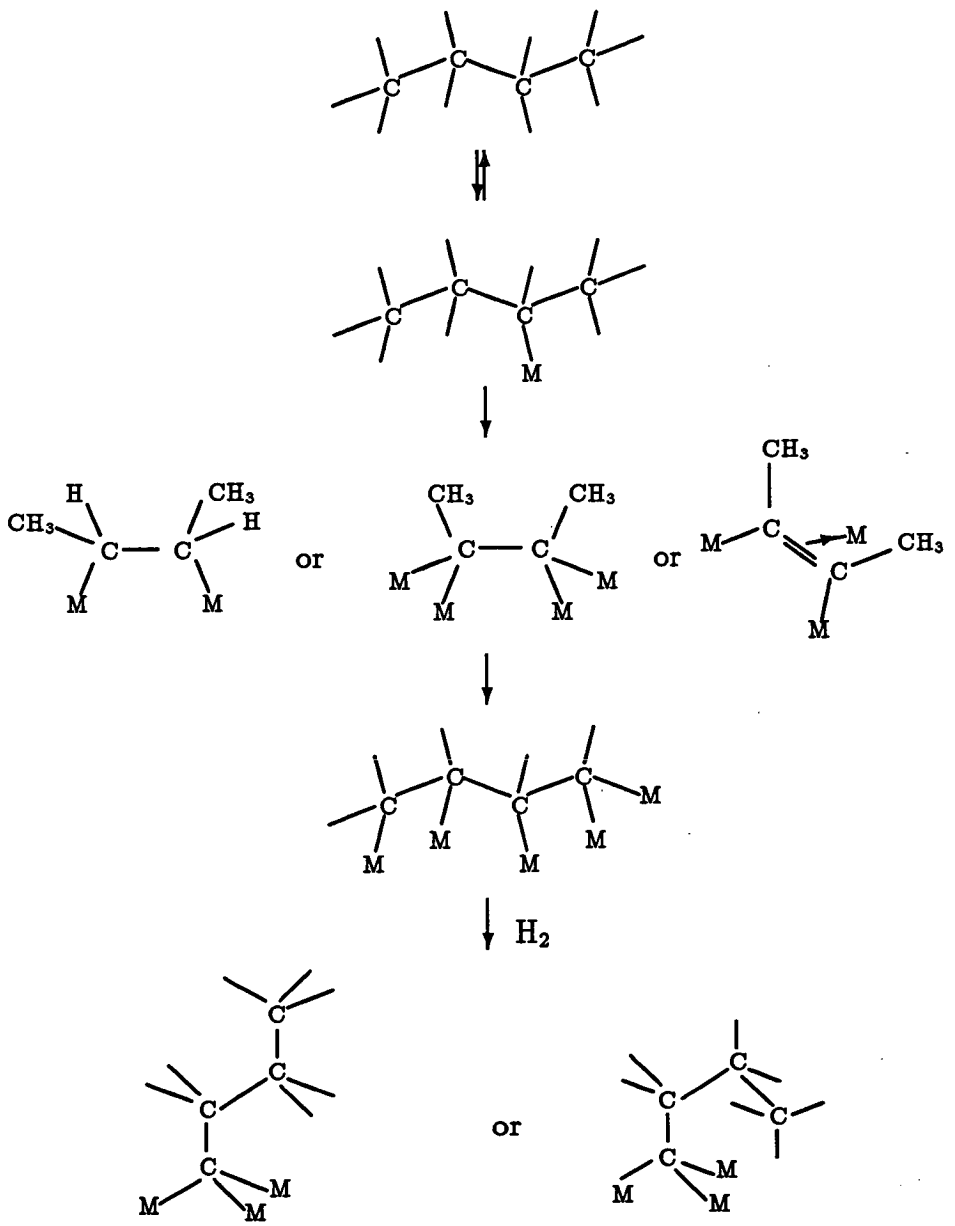

Figure 4.37: Suggested reaction scheme for butane on EuroPt-1 at room temperature.

tiply bound to the surface. Given the generally lower chemisorption, a possible hypothesis is that the sites which are still active for butane adsorption will be the most active of the platinum sites, which have the strongest dehydrogenating effect. The quantity of butane adsorbed at these sites (or at least, its infrared adsorption) is so small that it is quite possible that the same sites are active for an equivalent reaction over the 'hydrogen free' outgassed surface. In spectra such as Figure 4.20 there was sufficient intensity to include the 'hydrogen rich' spectrum without altering the assignments proffered in Section 4.2.3.

4.3.2 Temperature programming of butane adsorbed on EuroPt-1.

It is obvious from Figure 4.28 that heating produces some very interesting chemistry in the butane/EuroPt-1 system. The initial, *ie.* room temperature spectrum has already been assigned to a butane chemisorbed by two or more bonds between the central carbons and the platinum surface, with the suggestion that the terminal C–H bonds are less readily broken. This is not incompatible with the observation of the growth at elevated temperatures of infrared peaks at frequencies assigned by Chesters [216] to a butylidyne species, the formation of which would require the breaking of methyl C–H bonds. Complication arises, however, in which surface species is converted to butylidyne. Over the period when the butylidyne peaks are rising, the existing surface species only show a gradual decrease. Direct comparisons of intensity with quantity between different chemical species are of course not possible given different chromophore strengths, but this does not make it any easier to decide where the butylidyne is coming from. It is possible that it is formed from the di-σ-adsorbed butane, but no definite conclusion can be drawn.

At temperatures above 380 K, the twin butylidyne peaks decay rapidly, while the 2892 cm^{-1} peak assigned to the di-σ species continues the same gradual decrease observed since the initial butane dose. The band which is least affected over this temperature range is the CH_3 antisymmetric stretch, which by 440 K is

seen to be a separate peak at 2958 cm^{-1}. It is at this higher temperature that methane production starts, and goes on to a maximum at 470 K. Even at this maximal rate of what must presumably be a decomposition process, the stable 2894 cm^{-1} band still displays considerable intensity, and the rate of disappearance only increases as the methane starts to decline.

This behaviour asks several questions which can not be fully answered on the available evidence: what does the butylidyne decay into; which surface species decompose to give methane; and is the 2894 cm^{-1} peak due to the same species over the entire temperature range? Because nearly all the butylidyne decay has taken place before rapid methane production it seems unlikely that a direct decomposition from one to the other takes place. The peak assigned to the di-σ-adsorbed butane decays steadily from room temperature to 470 K before more rapid decline sets in, thus appearing stable at the maximum methane production temperature. One possibility is the formation of an intermediate species from butylidyne with a less distinctive infrared signature which then reacts further to give off methane. There is also intensity around 3000 cm^{-1} which might indicate the source of the methane carbon, but the proximity of the methane adsorption and the spread of the rotational bands make it difficult to draw any useful conclusions on this.

The peak at 2894 cm^{-1} appears remarkably unaffected by the chemical changes which go on round about it. During the methane production, the p branch of the methane rotational spectrum seems to be superimposed on a CH_3 antisymmetric stretch, which might be connected with the 2894 cm^{-1} peak already assigned to a CH_3 symmetric stretch. If this is the case it seems to argue against the species responsible being the same as the room temperature complex where the antisymmetric stretch was less significant, and the symmetric stretch dominated the spectrum. At the very least, it must have undergone reorientation with respect to the surface.

A plausible solution to this quandary is a cascade of alkylidyne decay products from butylidyne, to propylidyne, ethylidyne and then carbonaceous residue.

The propylidyne species, with the terminal C–C bond nearly parallel to the surface would provide the increase in CH_3 antisymmetric stretch intensity at *circa* 2960 cm^{-1}, and the ethylidyne would bolster the CH_3 symmetric stretch at 2892 cm^{-1}, which does in the latter stages show broadening to the slightly lower frequencies normally associated with that species [206, 209].

No readily identifiable C–H stretches remained on the EuroPt-1 surface above 520 K, in particular, there was no peak above 3000 cm^{-1} in the region which often had peaks assigned to C_xH type species in single crystal studies. This might imply complete dehydrogenation of any surface carbon.

A summary of the above reaction outline is presented in Figure 4.38.

4.3.3 Butane adsorption and reaction on EuroPt-1 at 378 K.

The temperature for these experiments was chosen for two reasons, compatibility with the earlier exchange reactions, and coincidence with the maximum butylidyne signal observed in Figure 4.29.

At the higher temperature, the interaction of butane with the silica support is much reduced, and the infrared spectrum remains predominantly gas phase for Sorbosil AQ U30, until the cell is swept clear by the helium flow. The decay is slightly slower over EuroPt-1, but again the gas phase and any physisorbed butane are quickly cleared. The main features of the DRIFT spectrum revealed are sharp twin peaks at 2934 and 2876 cm^{-1}. The agreement of the band positions and profiles with the spectra presented by Chesters [216] suggest very strongly that this spectrum is caused by the same species which he observed on but-1-ene adsorption on Pt(111), and assigned to *trans*-butylidyne. With time, the spectrum decayed and the butylidyne species lost their dramatic prominence. In line with the suggestion in the previous Section, the butylidyne may be decaying through the series of alkylidynes. No methane is visible in the spectrum, as might be expected at lower temperatures and decay rates.

A broad low intensity infrared band between 3030 and 2990 cm^{-1} proved

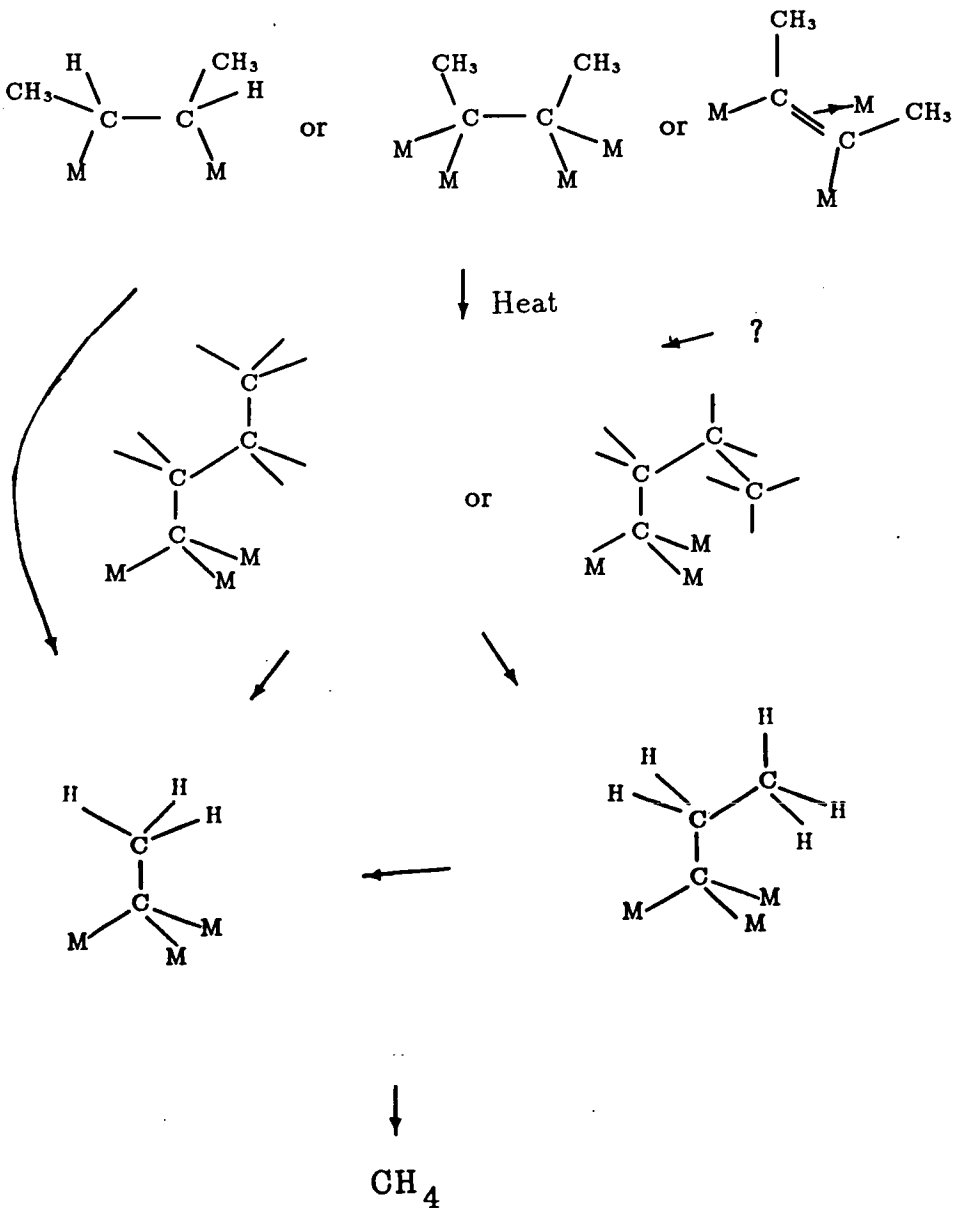

Figure 4.38: Suggested reaction scheme for butane on EuroPt-1 during temperature programmed desorption.

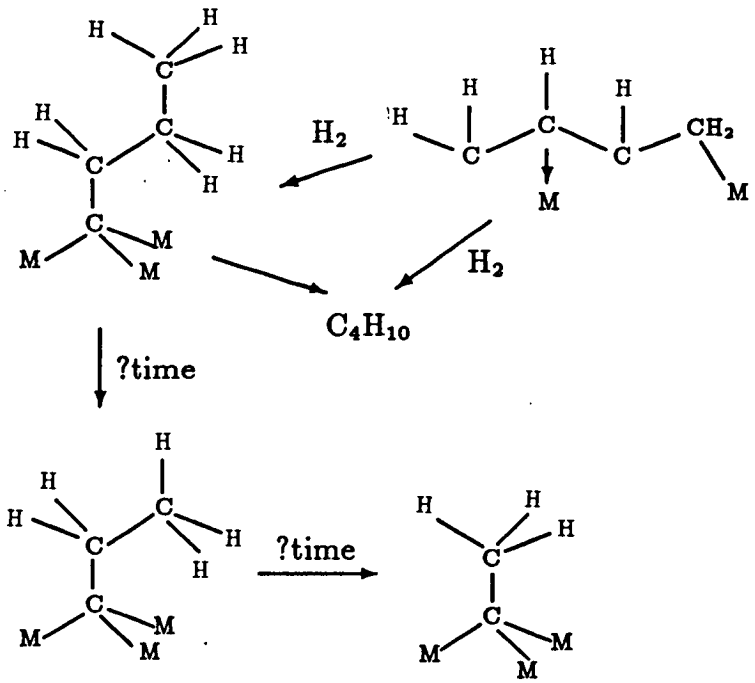

Figure 4.39: Suggested reaction scheme for butane on EuroPt-1 at 378 K.

highly reactive when exposed to a pulse of hydrogen at these temperatures, with butylidyne being formed, along with some gas phase butane. As had been observed before hydrogen exposure, the butylidyne was reasonably labile to reaction, with some of the dehydrogenated species reformed, with a 3000 cm^{-1} peak. The most stable species on the surface contained a CH_3 unit perpendicular to the surface to produce the 2892 cm^{-1} symmetric stretch mode seen in Figure 4.35.

A tentative reaction scheme is presented in Figure 4.39.

4.3.4 Comparison of DRIFTS with deuterium exchange.

The DRIFTS experiments and the deuterium exchange experiments discussed in Chapter 2 unfortunately monitored significantly different systems. Although each passed gases over the standard EuroPt-1 catalyst at the common temperature of 378 K, the exchange experiments involved a closed recirculating loop, and the DRIFTS used an open flow system. The experiments above show that the co-adsorption of hydrogen with butane produces very different chemistry from that observed in the infrared for butane alone. The flow system for the DRIFTS used

a helium carrier to expose the catalyst to the gases. A side effect of using a neutral flow system is that any equilibrium vapour pressure of adsorbates such as hydrogen over the catalyst will allow a gradual decrease in that species on the surface, as the material in the gas phase is swept away to be replaced by pure helium. The exchange reactions, however, operated with a closed flow system at below atmospheric pressure, and so an equilibrium could be established between the surface and gas phases. The hydrogen/deuterium rich atmosphere in the exchange reactions would produce a larger surface hydrogen concentration, both initially, and especially with time, as the proximity to the hydrogen desorption maximum for EuroPt-1 observed by Mushtaq [95] at 390 K will deplete any surface hydrogen in the DRIFTS experiments. The hydrogen depletion in the helium flow was seen in the general dehydrogenation of the surface species observed by DRIFTS.

The main experimental observations of the exchange reactions were an initial preference for complete exchange of the butane hydrogens, and a subsequent combination of this with exchange in only one or two hydrogens, giving a U shaped distribution of products (Figure 2.15). The DRIFT spectra tell us that in the hydrogen free atmosphere at 370 K, a species which is probably butylidyne is present in significant surface quantities. The stability which it shows towards a hydrogen pulse is much greater than that of the dehydrogenated species giving the broad peak between 3030 and 2990 cm^{-1}. The latter species is therefore more likely to be responsible for the deuterium exchange than butylidyne, and the unsaturation indicated by the higher C–H stretch frequency argues for it undergoing multiple exchange.

The single exchange which contributes to the overall reaction is unlikely to involve a surface complex at concentrations high enough for observation by DRIFTS, because anything more than a weak interaction would lead to more extensive reaction. The short lived initial preference for the multiple exchange would be consistent with the clean EuroPt-1 surface exposing all the metal sur-

face to the gas phase. Only after sufficient carbonaceous material has built up to prevent direct access to active sites will the less interactive single exchange mechanism become important.

Chapter 5

DRIFTS of butane over potassium doped EuroPt-1.

5.1 Introduction.

The study of the effects of potassium compounds on catalyst systems has generally been confined to iron and nickel based catalysts, as used in ammonia synthesis and Fisher-Tropsch reactions respectively. Potassium adsorption on platinum single crystals is, however, one of the favoured systems of the surface scientist, and has been worked on by the research groups of H.P. Bonzel at Jülich, J.M. White at Austin, B.E. Koel at Boulder, and G.A. Somorjai at Berkeley among others. As suggested in Chapter 1, early interest in this system was with the intention of modifying the electron emitting properties of metals for electrical valves [86]. It has also been used as a model for the ion/water interaction by electrochemists [90]. The surface scientists mentioned above have used vibrational spectroscopy as one of their probes on the influence potassium can have on co-adsorbed molecules.

The CO/K/Pt(111) system has received particular attention. The bonding of CO with transition metal surfaces is understood to follow the model of Blyholder [240]. This scheme can be described as a σ bond and two π bonds between the carbon and oxygen, with the sp_z rehybridisation of the carbon orbitals for the σ bond formation leaving an sp_z lone pair at the carbon. This lone pair is donated to metal d orbitals to form a σ bond, and the large formal negative charge on the metal is reduced by back bonding into the antibonding CO π^* molecular orbitals. Back bonding strengthens the metal–carbon bonding, but weakens the carbon–oxygen bonding. This can be detected as a change in the vibrational spectrum. It is the dependence of the vibrational frequency on the electronic properties of the metal substrate which (along with the large extinction coefficient) makes carbon

monoxide such a popular choice in studying the effects of potassium co-adsorption.

Crowell, Garfunkel and Somorjai [241] used EELS to monitor a large CO exposure of Pt(111) with varying potassium coverages, and observed C–O stretching vibrations above 1500 cm^{-1} and, intermittently, Pt–C stretches below 500 cm^{-1}. In the spectra for clean Pt(111), C–O stretches at 2120 and 1875 cm^{-1} were observed and assigned to CO bonded linearly to single metal atoms, and CO bridge bonded between two platinums respectively. As potassium coverage was increased, the frequency of both bands decreased, and the relative intensities changed from a preference for on-top binding to, at $\theta_K \approx 0.22$, exclusive occupation of the bridged site. The changes in vibrational frequency were attributed to donation of potassium 4*s* electrons to the surface, increasing the platinum *d* orbital back donation into the antibonding CO π^* orbitals.

In subsequent papers, a degree of disagreement occurred over whether the CO/K interaction was really a long range effect as implied by Somorjai *et al.* [241]. Bonzel [89] presented low temperature EEL spectra with a range of different peaks each attributed to C–O stretching frequencies. He suggested that peaks may be due to one, two or more carbon monoxide molecules adsorbed beside a surface potassium atom, with a dilution of the influence of the potassium for each added carbon monoxide, giving a series of discrete vibrational peaks to higher frequencies. In summarising the literature descriptions of CO/K/transition metal binding, he identified four models ranging from the through metal interaction described above (after Crowell [241]) to direct ionic interaction between K^+ and $C_2O_2^{2-}$ or $C_4O_4^{2-}$ ions [242]. Common to all four models, however, was increased electron density in CO π^* orbitals as introduced by Blyholder [240].

Koel *et al.* [243] used EELS, along with other surface science techniques, to study the C_2H_4/K/Pt(111) system. As discussed in Section 4.1, the low temperature adsorption of ethene on Pt(111) usually occurs as a 1,2-di-σ bonded species [203], and this was confirmed by the EEL spectra of Koel [243]. When potassium was pre-adsorbed, the C–H stretch frequency moved from 2930 to 3060 cm^{-1}, a

change attributed to the formation of a π bonded ethene complex. The potassium inhibits the formation of the strong covalent bonds between the carbon p orbitals and the metal d orbitals required for the di-σ species. The π bonded complex which results is weakly bonded, due to the relatively poor π acceptor behaviour of ethene compared with carbon monoxide.

With potassium adsorption on platinum single crystals producing such dramatic changes in the chemistry and vibrational spectra of adsorbates, it was hoped that such effects might be found if butane was adsorbed on alkali doped EuroPt-1.

5.2 Results.

5.2.1 Butane adsorption on 1% potassium doped Sorbosil AQ U30.

A sample of Sorbosil AQ U30 doped to 1% weight of potassium [95] was prepared for DRIFTS as described above (Section 3.5.7). It was heated in hydrogen and then helium flows according to the standard reduction procedure, and on cooling to room temperature exposed to a 35 μmol pulse of butane while being monitored by DRIFTS. The changes in intensity with time of the two main butane peaks in the resulting spectra are plotted in Figure 5.1.

5.2.2 Butane adsorption on 1% potassium doped EuroPt-1 at 298 K.

A 1% potassium doped EuroPt-1 catalyst was reduced and outgassed *in situ* in the standard manner, and dosed with 35 μmol of butane. The infrared spectrum of the hydrocarbon/catalyst system was collected every 37 seconds as a 32 scan DRIFT spectrum. The recorded signal decreased rapidly with time, but when the gas phase butane had been flushed out along with any physisorbed material, some intensity remained in the C–H stretching region (Figure 5.2). The signal levels were considerably lower than those observed in the corresponding experiments in Chapter 4, with a resultant decrease in SNR. To compensate for this, after 200 seconds, pairs of spectra were averaged in sequence to give an equivalent of 64

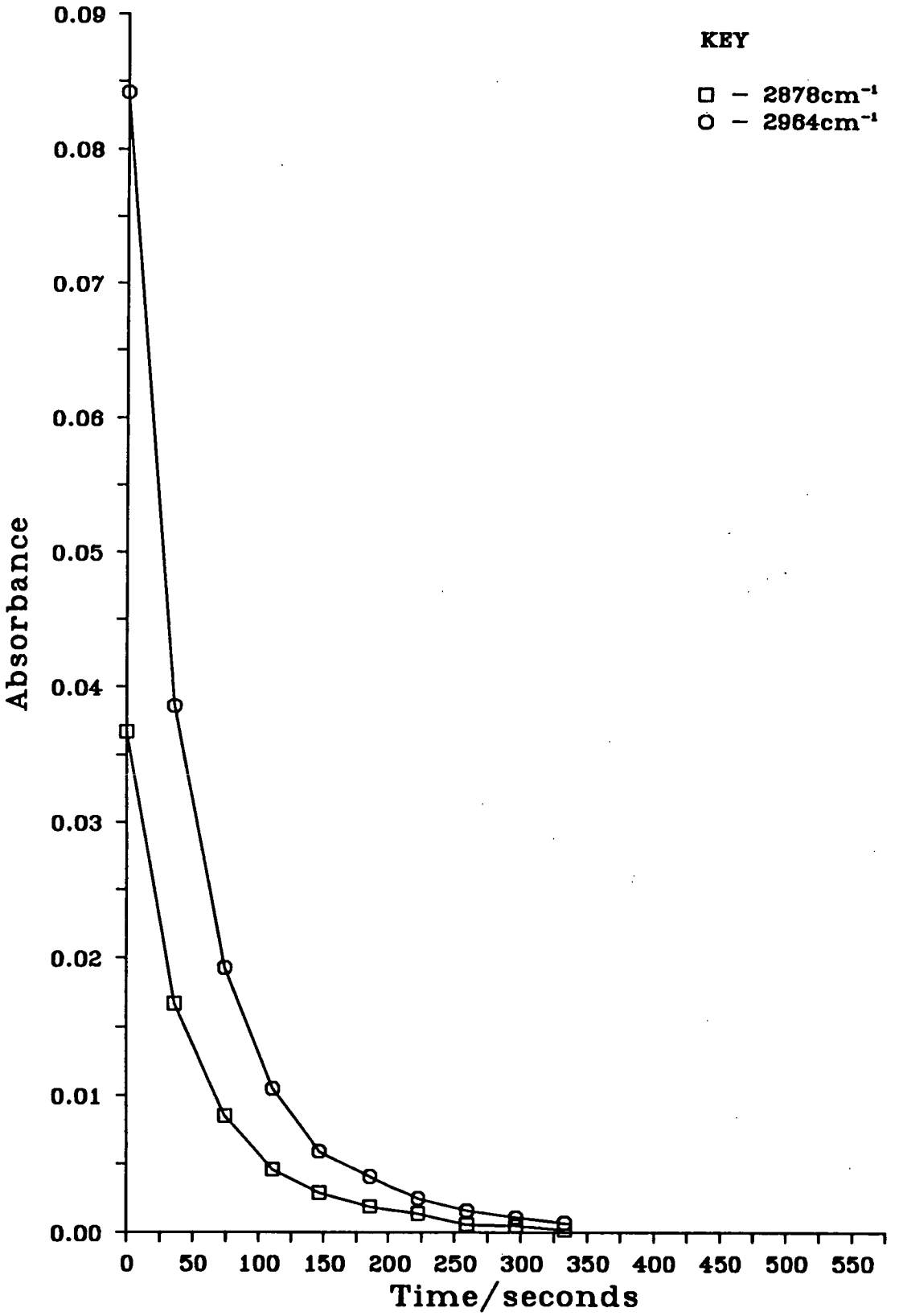

Figure 5.1: Variation of absorbance with time for the C–H stretch region over 1% potassium doped Sorbosil.

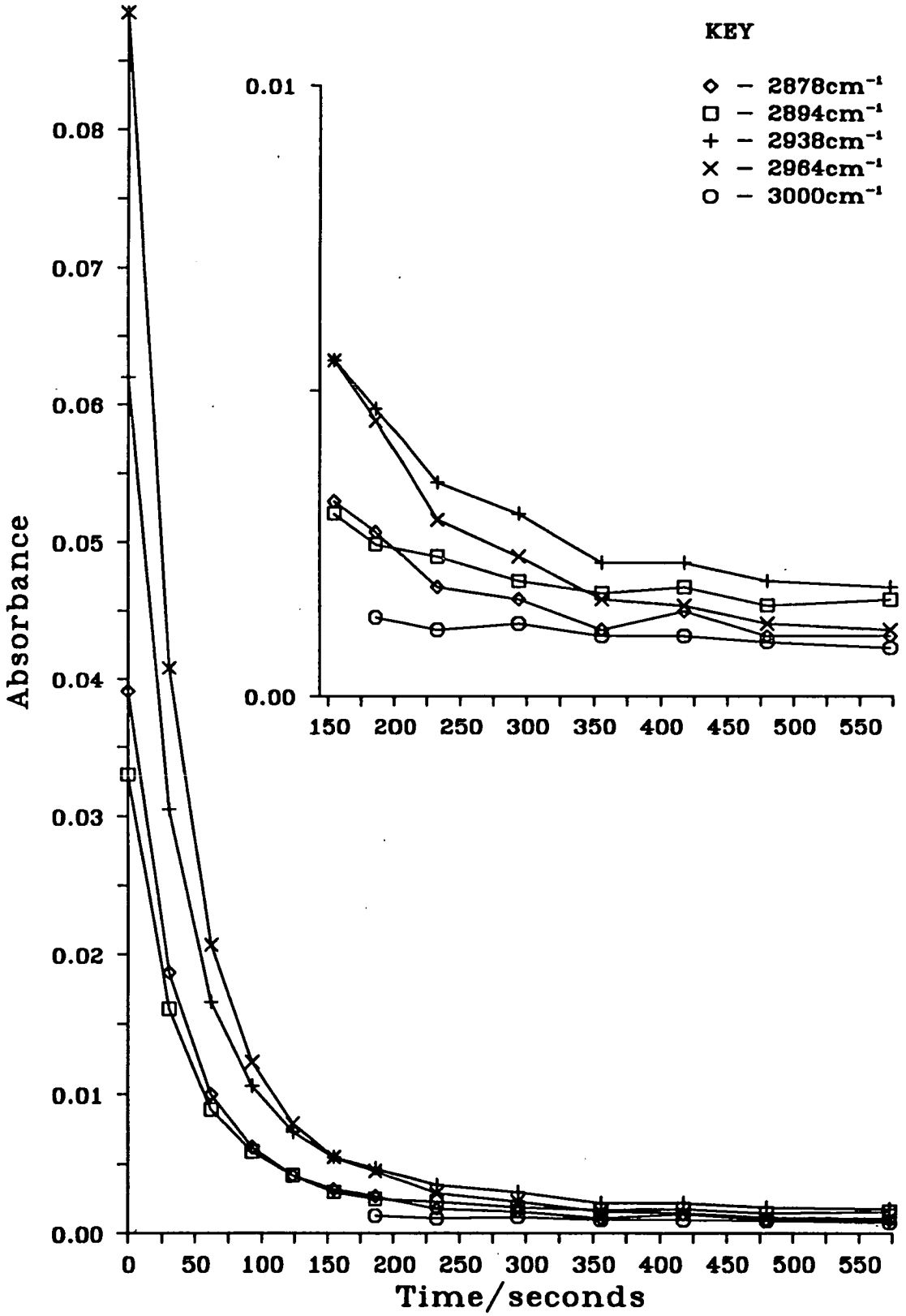

Figure 5.2: Variation of absorbance with time for the C–H stretch region over 1% potassium doped EuroPt-1 (inset at expanded y scale).

mirror scans. The values from these spectra are plotted in Figure 5.2, with the later values also shown on an inset with an expanded vertical scale.

The 132 scan DRIFT spectrum collected 29 minutes after the butane pulse is displayed in Figure 5.3. As observed in the as received EuroPt-1 case, the signal due to the chemisorbed material continued to decline in the helium flow, though at a lesser rate than the gas phase signal disappeared. The signal levels achieved in Figure 5.3 are so low that both peak position and intensity could be affected by noise peaks, and any conclusions drawn from the spectrum must therefore be tempered. The general form of the spectrum is similar to that displayed over EuroPt-1, Figure 4.20, with the highest peak at 2894 cm^{-1}. In comparison with Chapter 4, this is assigned to the CH_3 symmetric stretching vibration of a di-σ or di-σ/π adsorbed butane which has lost at least two methylene hydrogens to form the surface bonds. The 2942 and 2878 cm^{-1} vibrations assigned above to the butylidyne species are also present, as is the broad peak between 3030 and 2990 cm^{-1}.

5.2.3 Temperature programmed desorption of butane from 1% potassium doped EuroPt-1.

A 1% potassium doped EuroPt-1 sample was reduced, outgassed and exposed to a 35 μmol pulse of butane, while being monitored by DRIFTS. The spectra were as described above. The catalyst was then heated in the continuing helium flow. DRIFT spectra, each an average of 50 scans were recorded sequentially as interferograms, with a slight time delay in the loop giving a repeat time of 50 seconds. The heating rate was adjusted so a spectrum was recorded for every 10 K rise, at a heating rate of 12 $Kmin^{-1}$ as described in Section 4.2.6 for the equivalent experiment over EuroPt-1.

A selection of the spectra, at 30 K intervals, is shown in Figure 5.4, illustrating all the major changes observed. As already stated, lower signal levels led to a lower SNR. This is especially evident in Figure 5.5, a plot of infrared absorbance at se-

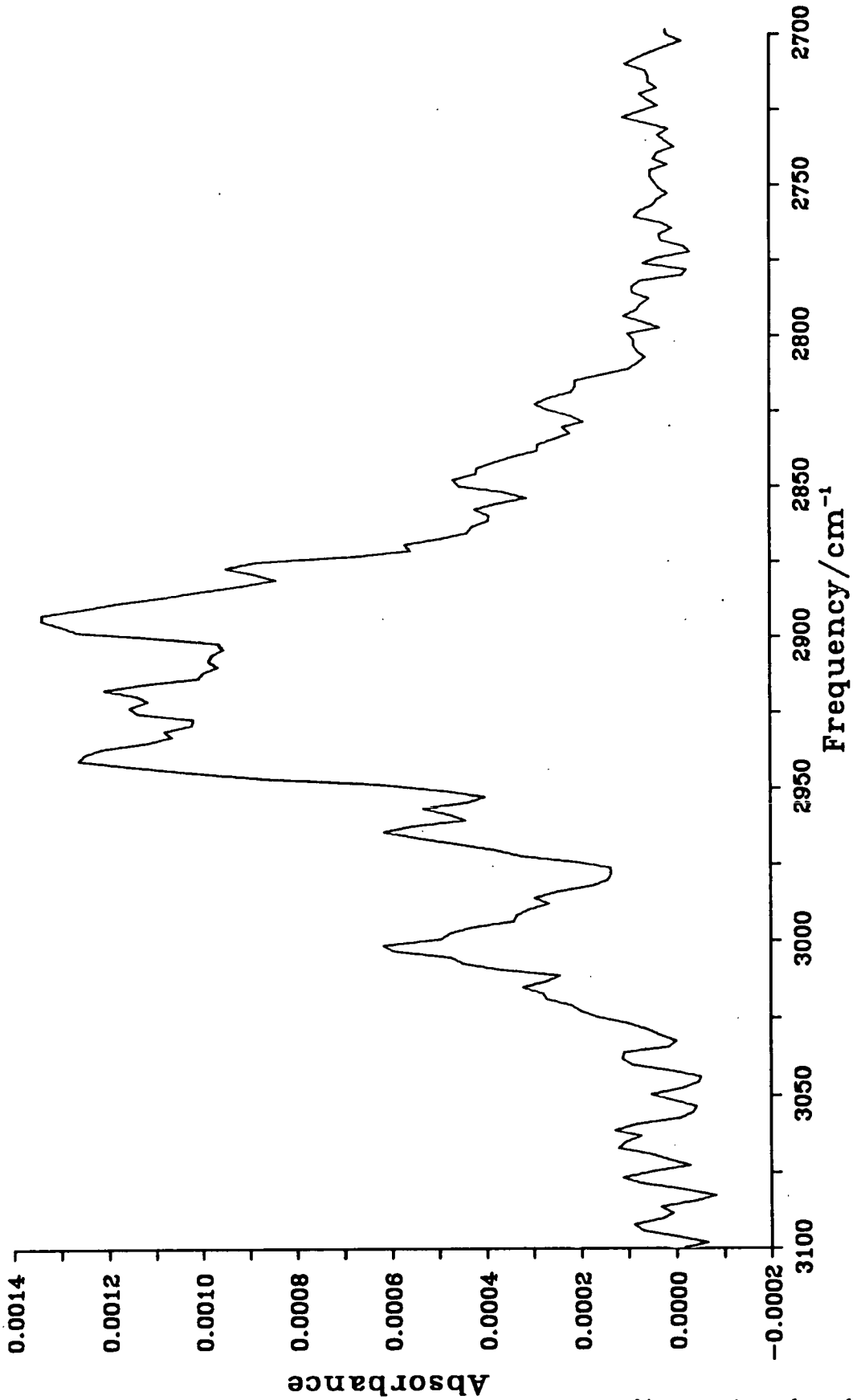

Figure 5.3: Surface species formed by butane adsorption on 1% potassium doped EuroPt-1.

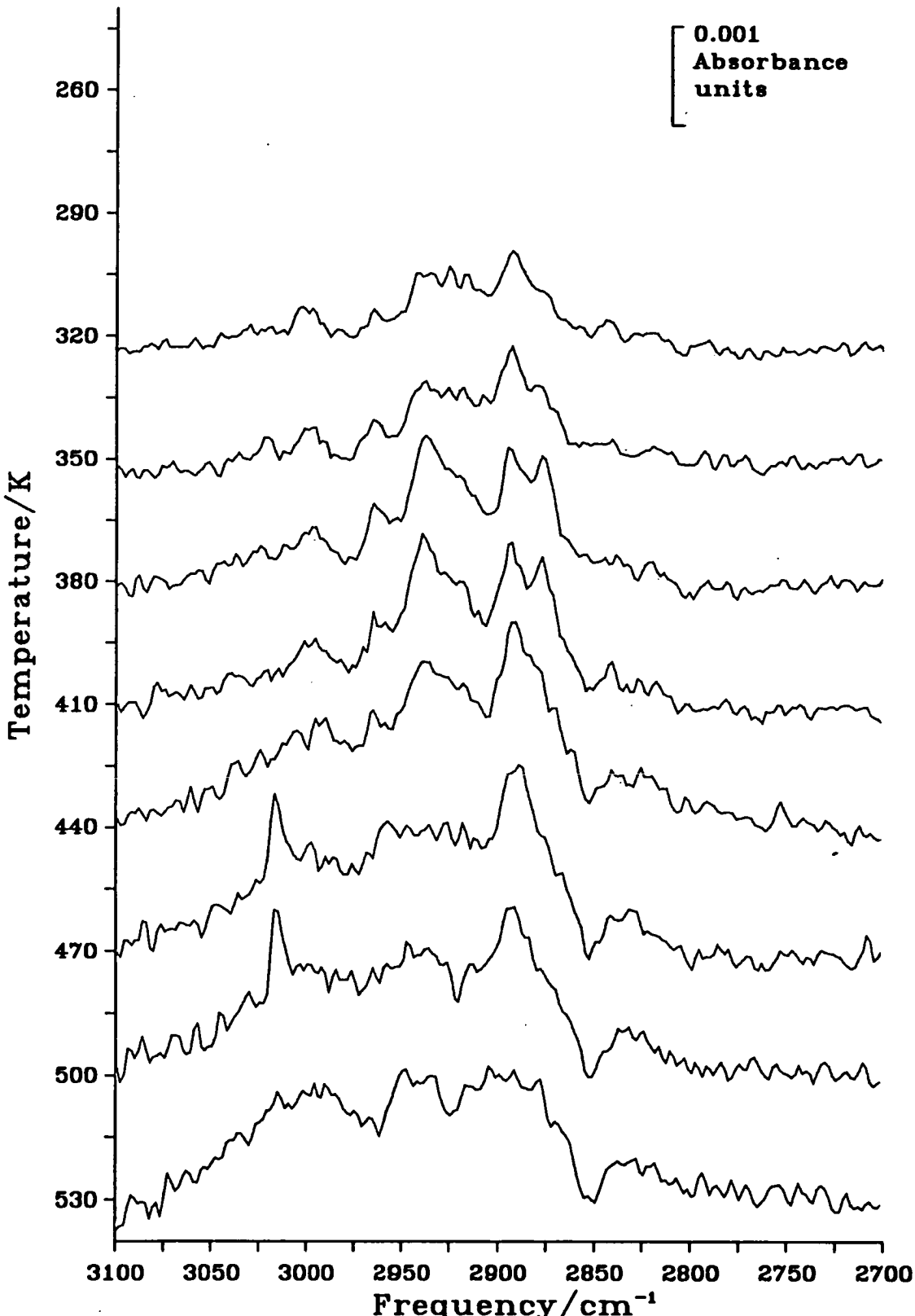

Figure 5.4: Changes in the butane spectrum over 1% potassium doped EuroPt-1 with temperature.

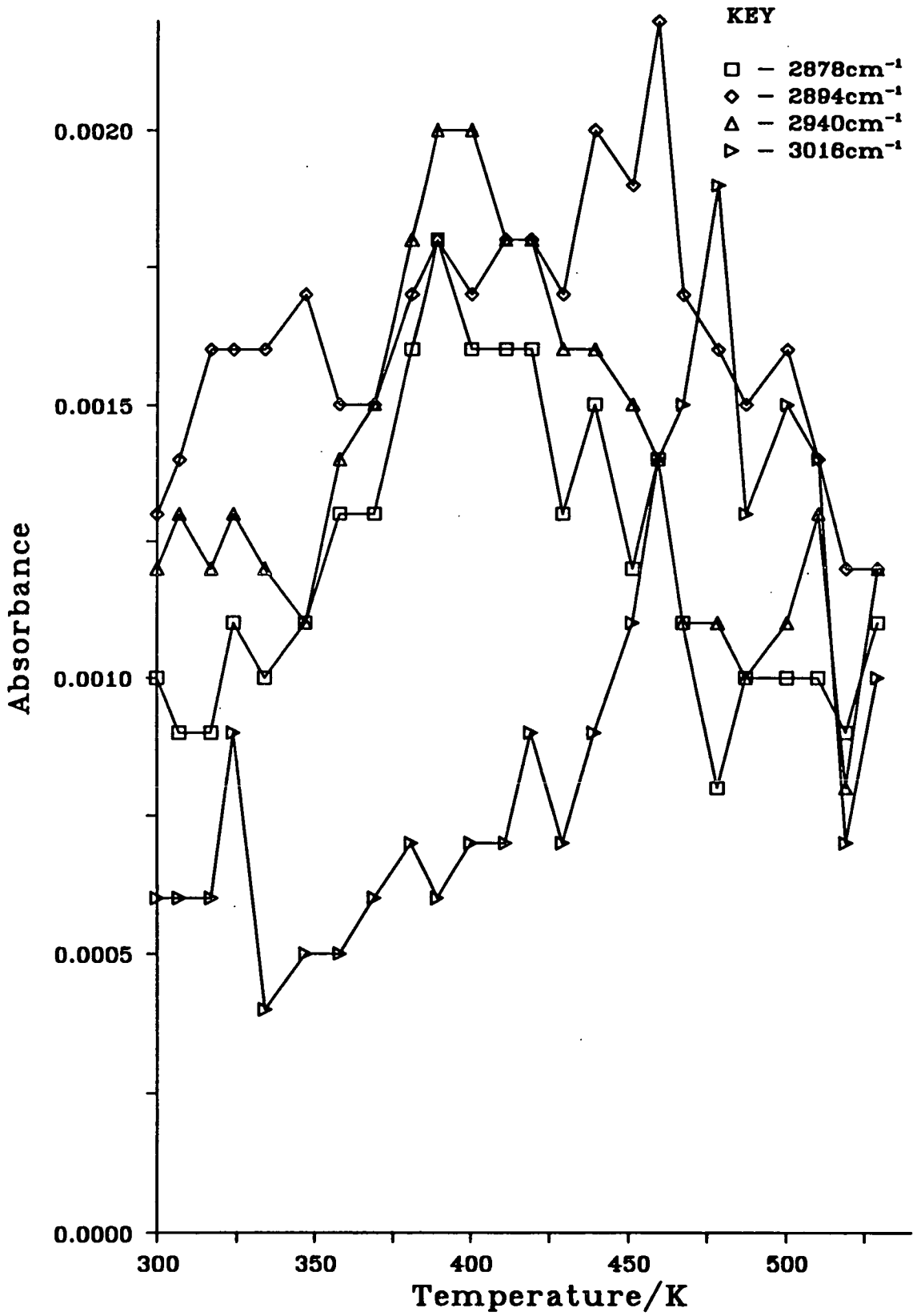

Figure 5.5: Variation of absorbance with temperature for selected frequencies of Figure 5.4

lected frequencies against temperature. The general form of both the spectra and the graph can be seen on close inspection to be the same as in the corresponding experiments on EuroPt-1, Figures 4.28 and 4.29. At low temperature, the major peak is at 2894 cm^{-1}, assigned to the symmetric νCH_3 of butane bonded to the metal via the two central carbons of the framework. By 390 K, the twin peaks of the species assigned as butylidyne at 2938 cm^{-1} and 2878 cm^{-1} become the dominant features of the spectrum, before decaying above 400 K. Gas phase methane can be seen in these spectra at 3014 cm^{-1}, though considerable faith is needed to see the rotational fine structure among the noise.

Over and above the poor SNR, these spectra suffer from two problems. At the higher temperatures, changes in the underlying silica spectrum means that baseline correction was needed to clarify the changes due to the hydrocarbon spectrum. A general bowing of the spectra can still be seen in Figure 5.4, which explains the continuing high values observed in Figure 5.5 even at 540 K. This effect is also present in the equivalent spectra over EuroPt-1, though it is less noticeable due to generally higher signal levels. The other anomaly is the set of three negative peaks at 2960, 2924 and 2850 cm^{-1}. These are almost certainly caused by variation in the background hydrocarbon intensity which can be seen at 2958, 2918 and 2848 cm^{-1} in the single beam spectrum, and is generally assumed to be due to carbonaceous deposits on optical components of the spectrometer. This variation is, however, strange considering the catalyst had already been heated to these temperatures for over 1.5 hours during the reduction and outgassing.

5.2.4 Butane adsorption on 1% potassium doped Sorbosil AQ U30 at 378 K.

A sample of 1% potassium doped Sorbosil AQ U30 was prepared in the standard manner, before being heated to 378 K and exposed to a 35 μmol pulse of butane while 32 scan DRIFT spectra were recorded. The infrared absorbance at selected frequencies, as plotted against time in Figure 5.6, displayed rapid decay, disappearing into the noise level after only six spectra were collected.

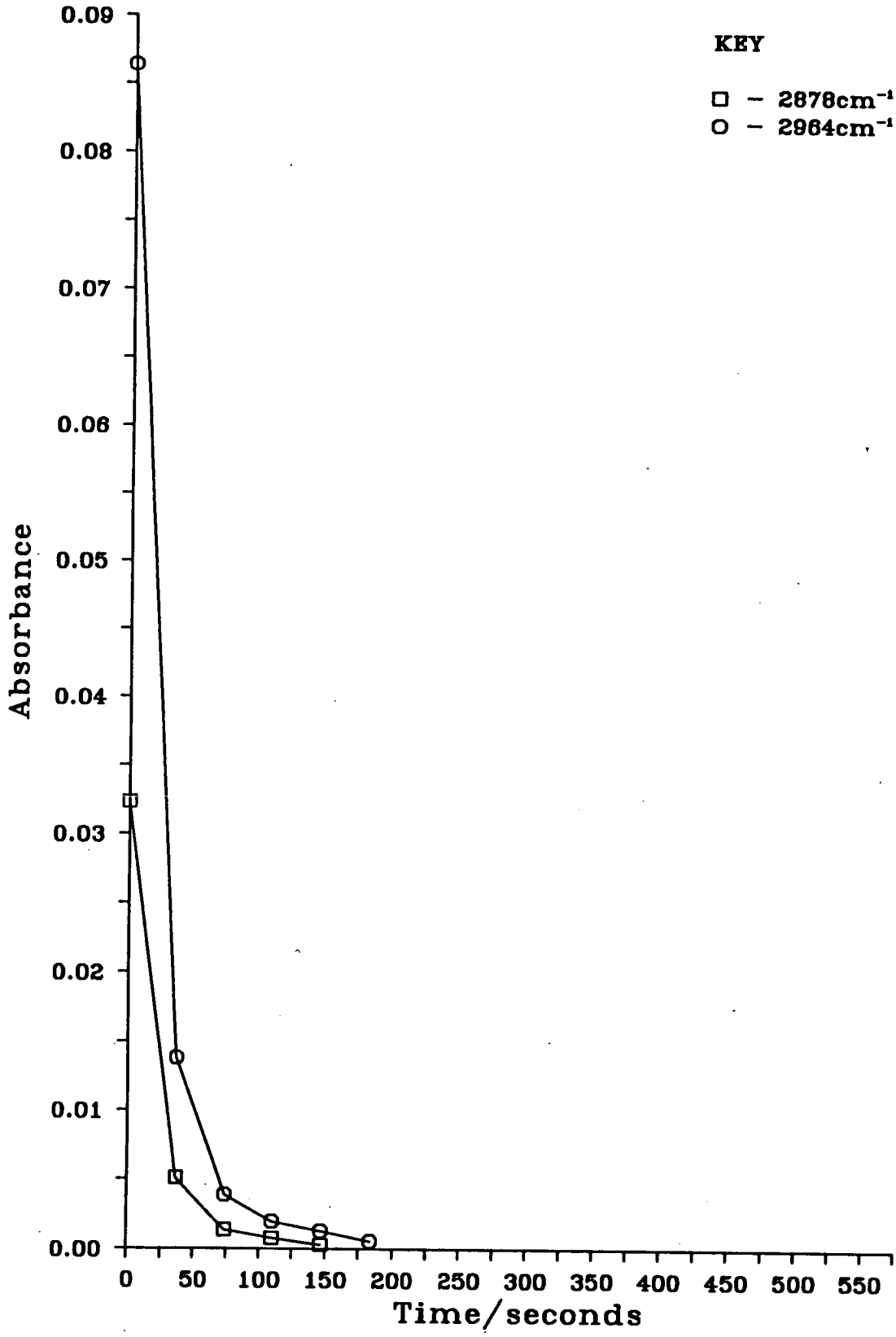

Figure 5.6: Variation of absorbance with time for butane adsorption on 1% potassium doped Sorbosil at 378 K.

5.2.5 *Butane adsorption on 1% potassium doped EuroPt-1 at 378 K*

The high temperature exposure of 1% potassium doped EuroPt-1 to 35 μmol of butane was carried out in the same way as described for Sorbosil in the previous Section. The progression of the infrared signal at selected frequencies is plotted in Figure 5.7, with an inset at expanded scale to highlight the behaviour after 100 seconds. Despite more rapid initial decay of the absorbance, the relatively stable chemisorbed species observed in this later period had a more intense spectrum than was seen in the room temperature experiment, Figure 5.3. The 132 scan spectrum, Figure 5.8 (recorded 22 minutes after the butane pulse) correspondingly has a better SNR. The two peaks associated with a butylidyne surface species, at 2938 and 2876 cm^{-1} are the most prominent, with considerable intensity at 2894 cm^{-1} attributable to butane bonded by the central carbons, and a significant peak in the unsaturated region at 3002 cm^{-1}, following assignments discussed above.

5.2.6 *Hydrogenation of the surface species formed from butane on 1% potassium doped EuroPt-1 at 378 K.*

After a further 18 minutes of ageing in the helium flow (*ie.* 40 minutes after the original butane pulse), the catalyst system shown in Figure 5.8 and described in Section 5.2.5 was exposed to a 35 μmol pulse of hydrogen, while still held at 378 K. The 32 scan DRIFT spectra recorded over the hydrogen pulse are shown in Figure 5.9. The first spectrum in the Figure is actually equivalent to a 64 scan collection, being the average of the last two spectra recorded before the pulse, in the manner discussed in Section 3.5.3. As in the equivalent EuroPt-1 spectra, a general drop in signal levels from Figure 5.8 included a particular reduction in the peaks associated with butylidyne.

Reaction with hydrogen was rapid. The initial effect, as before was to recreate most of the surface species observed before the ageing and give a similar spectrum to Figure 5.8. By the third spectrum of Figure 5.9, the general shape of the

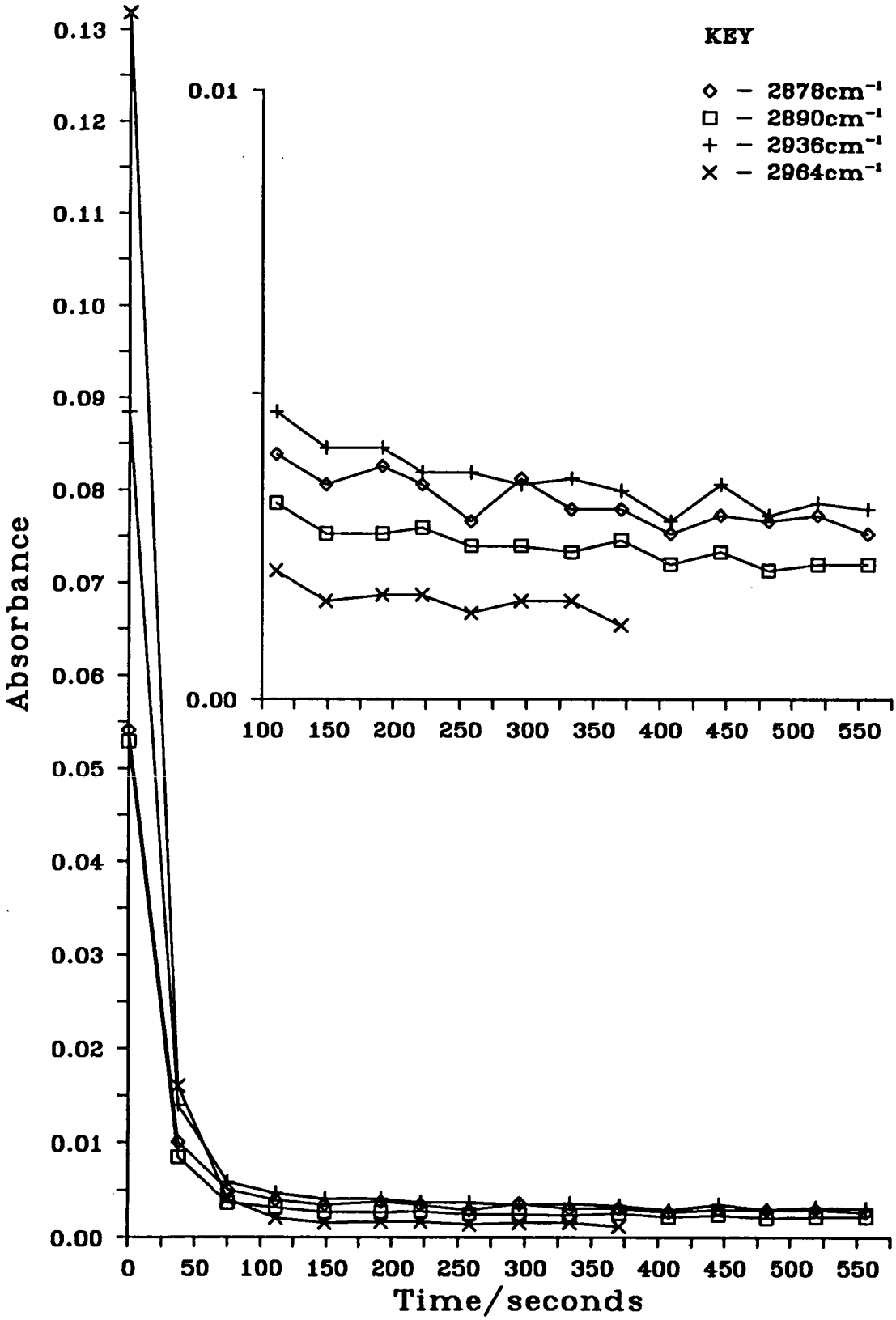

Figure 5.7: Variation of absorbance with time for the C–H stretch region over 1% potassium doped EuroPt-1 at 378 K (inset at expanded y scale).

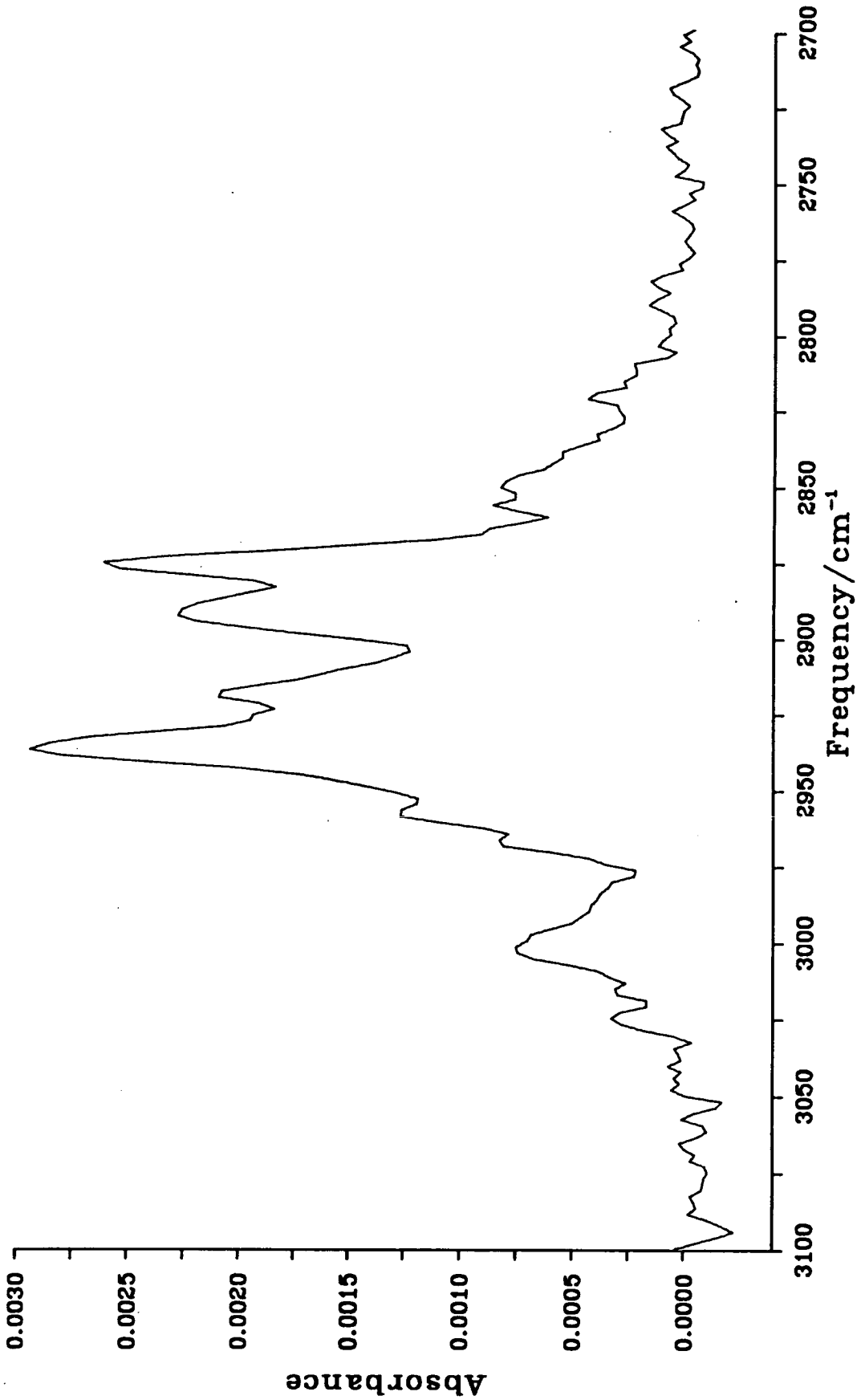

Figure 5.8: Surface species formed by butane adsorption on 1% potassium doped EuroPt-1 at 378 K.

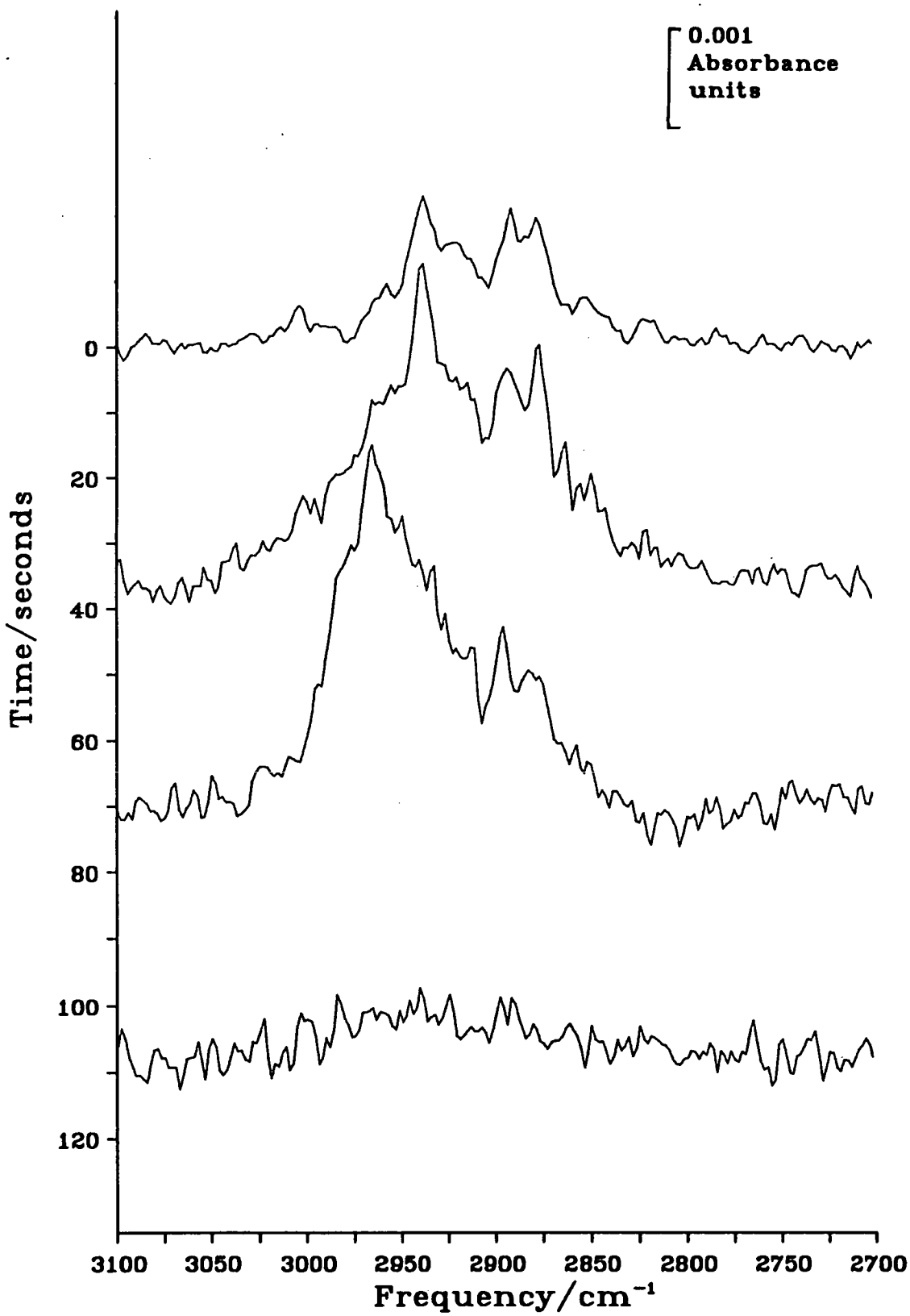

Figure 5.9: Butane adsorption on 1% potassium doped EuroPt-1 at 378 K: changes in the C–H stretch spectrum with addition of hydrogen.

infrared envelope bore most resemblance to gas phase/physisorbed butane, and within another 37 seconds, all the hydrogen spectrum had disappeared.

5.3 Discussion

The chemistry observed for butane adsorption on 1% potassium doped EuroPt-1 appears very similar to the reaction scheme of the as received catalyst, and the assignment of peaks given above therefore draws heavily on the arguments already used above.

The comparison between the two sets of experiments is perhaps weakest for Figure 5.3, with the 2894 cm^{-1} peak not having the same prominence observed in Figure 4.20. The low signal levels and resulting poor SNR do, however, reduce the significance which can be attached to this difference. The metal surface area exposed in the catalyst was reduced from 11.5 to 6.3 m^2g^{-1} by potassium doping (Table 2.4), which accounts for some of the reduced hydrocarbon signal. The aqueous hydroxide solution also has an appreciable affect on the adsorption on the silica, seen in comparing Figure 5.1 with Figure 4.14. The total surface area reduction may have an influence on the formation of the chemisorbed species, and in particular the di-σ adsorbed species, if the physisorbed/monoadsorbed/di-σ path described in Section 4.3.1 is important.

The spectra for the TPD of butane from 1% potassium doped EuroPt-1 are, with the proviso of reduced SNR, similar to the EuroPt-1 case, and therefore can be discussed in terms of the same outline reaction scheme as presented in Section 4.3.2.

The high temperature adsorption of butane on the 1% potassium doped EuroPt-1 followed a trend of rapid decrease in the gas phase signal to leave a larger DRIFTS signal than seen for low temperature adsorption, as was also seen for EuroPt-1. The clearer spectrum, Figure 5.8, produced by the improved SNR has a similar form to the equivalent EuroPt-1 spectrum, Figure 4.32. On exposure to a 35 μmol pulse of hydrogen, all surface species were rapidly rehydrogenated

and removed into the gas stream, leaving what appeared to be a clean catalyst surface.

The summary of the chemistry of butane on 1% potassium doped EuroPt-1 just given shows little difference to the chemistry in the absence of potassium. The difference is mainly a reduction in intensity, attributable in part to a reduction in the metal surface area, and possibly also to less physisorption on the support as precursor. The lower interaction of the butane with the potassium doped surface is in qualitative agreement with the lower rates of exchange observed in Chapter 2.

References

[1] Berzelius, J.J., *Annls. Chim. Phys.,* **61** (1836) 146.

[2] Davy, E., *Phil. Trans. Roy. Soc.*, **110** (1820) 108.

[3] Davy, H., *Phil. Trans. Roy. Soc.*, **107** (1817) 45.

[4] Döbereiner, J.W., *Annls. Chim. Phys.,* **24** (1823) 91.

[5] Rideal, E.K. and Taylor, H.S., *Catalysis in Theory and Practice,* Macmillan, London, 1919.

[6] Thompson, S.J. and Webb, G., *Heterogeneous Catalysis*, Oliver & Boyd, Edinburgh & London, 1968.

[7] Rideal, E.K., *Concepts in Catalysis,* Academic Press, London, 1968.

[8] Rootseart, W.J.K. and Sachtler, W.M.H, *Z. Physik. Chem. Neue Folge*, **26** (1960) 16.

[9] *Handbook of Chemistry and Physics*, 62nd. Edition, ed. Weast, R.C., CRC Press Inc., Boca Raton, 1981, page B-30. Innovations (Mail Order) Ltd., Euroway Business Park, Swindon, SN5 8SN.

[10] Thomas, J.M. and Thomas, W.J., *Introduction to the Principles of Heterogeneous Catalysis,* Academic Press, London, 1967.

[11] Cotton, F.A. and Wilkinson, G., *Advanced Inorganic Chemistry,* Wiley, New York, 1980.

[12] Hightower, J.W. in *Preparation of Catalysts,* ed. Delmon, B., Jacobs, P.A., and Poncelet, G., Elsevier, Amsterdam, 1976.

[13] Dr. B. Harrison, Johnson Matthey, private communication.

[14] Bond, G.C., Mallat, T., *J. Chem. Soc., Faraday Trans. I,* **77** (1981) 1743.

[15] Uda, M., *Trans. Nat. Res. Inst. Metals,* **24** (1982) 218.

[16] Nishimura, S., Irrafume, S., Nagaura, T., Akimoto, Y. and Uda, M., *Chem. Lett.,*(1985) 1275.

[17] Satterfield, C.N., *Heterogeneous Catalysis in Practice,* M°Graw-Hill, New York.

[18] Reinecke, N. and Haul, R., *Ber. Bunsenges. Phys. Chem.,* **88** (1984) 1232.

[19] Clere, J., *Mountains,* MacMillan, London, 1975.

[20] Lynden-Bell, R.M., *Surface Science,* **244** (1991) 266.

[21] Burton, J.J., *Catal. Rev.–Sci. Eng.,* **9** (1974) 209.

[22] Schäfer, H., *Chemical Transport Reactions,* Academic Press, New York, 1964.

[23] Krabetz, R. and Huberich, T. in *Ammonia* part 3 eds. Slack, A.V. and James, G.R., Dekker, New York, 1977, page 123.

[24] Mross, W.–D., *Catal. Rev.–Sci. Eng.,* **25** (1983) 591.

[25] Mittasch, A., *Adv. Catal.,* **2** (1950) 82 and references therein.

[26] Bond, G.C. and Wells, P.B., *Appl. Catal.,* **18** (1985) 221ff.

[27] Bond, G.C. and Gelsthorpe, M.R., *Appl. Catal.,* **35** (1987) 169.

[28] Bond, G.C., Gavin, F. and Maire, G., *Appl. Catal.,* **41** (1988) 313.

[29] Coenen, J.W.E. and Wells, P.B. private communication.

[30] Gnutzmann, V. and Vogel, W., *J. Phys. Chem.*, **94** (1990) 4991.

[31] Sutherland, I.M., Ibbotson, A., Moyes, R.B. and Wells, P.B., *J. Catal.*, **125** (1990) 77; Augustine, R.L., Baum, D.R., High, K.G., Szivos, L.S. and O'Leary, L.S., *J. Catal.*, **127** (1991) 675; Paál, Z., Groeneweg, H. and Paallukacs, J., *J. Chem. Soc., Faraday Trans.*, **86** (1990) 3159; Kramer, R., Fischbacher, M. and Gruber, H.L., *Appl. Catal.*, **42** (1988) 337; Paál, Z. and Xu, X.L., *Appl. Catal.*, **43** (1988) L1.

[32] Kemball, C., *Adv. Catal.*, **11** (1959) 223.

[33] Bond, G.C., *Catalysis by Metals,* Academic Press, London, 1962.

[34] Brown, R., PhD thesis, University of Edinburgh, 1990 and references therein.

[35] Kittel, C., *Introduction to Solid State Physics,* Wiley, New York, 1976.

[36] Ebsworth, E.A.V., Rankin, D.H.W. and Cradock, S., *Structural Methods in Chemistry,* Blackwell, Oxford, 1987.

[37] Woodruff, D.P. and Delchar, T.A., *Modern Techniques of Surface Science,* Cambridge University Press, Cambridge, 1986.

[38] French, A.P. and Taylor, E.F., *An Introduction to Quantum Physics,* Van Nostrand Reinhold, Wokingham, 1978.

[39] Feuerbacher, B. and Willis, R.F., *Physical Rev. Lett.*, **47** (1981) 526; Bortolani, V., Franchini, A., Santoro, G., Toennies, J.P, Wöll, C. and Zhang, G., *Physical Rev. B*, **40** (1989) 3524.

[40] Cavanagh, R.R, Rush, J.J and Kelly, R.D. in *Vibrational Spectroscopy of Molecules on Surfaces,* ed. Yates, J.T.Jnr. and Madey, T.E., Plenum, New York, page 183.

[41] Yaroslarski, N.G. and Terenin, A.N., *Dokl. Akad. Nauk SSR,* **66** (1949) 885.

[42] Eischens, R.P., Pliskin, W.A. and Francis, S.A., *J. Chem. Phys.*, **22** (1954) 1786.

[43] in [10], 1st. edition, page 119.

[44] Eischens, R.P. and Pliskin, W.A., *Adv. Catal.*, **10** (1958) 1786.

[45] in *J. Catal.*, **127**, Lopez, T., Garcia-Cruz, I. and Gomez, R. page 75; de la Cruz, C. and Sheppard, N. page 445; Choi, K.I. and Vannice, M.A. page 465; Sobalik, Z., Kazlowski, R. and Haber, J. page 665; Ono, T., Kiryu, M., Komiyama, M. and Kuczkowski, R.L. page 698.

[46] Duyckaerts, G., *Analyst* **84** (1969) 201.

[47] Little, L.H., *J. Phys. Chem.*, **63** (1959) 1616.

[48] Kortüm, G., *Reflectance Spectroscopy,* Springer-Verlag, Berlin, 1969.

[49] Griffiths, P.R. and Fuller, M.P., in *Advances in Infrared Spectroscopy,* ed. Hester, R.E. and Clark, R.J.H., Springer-Verlag, New York, 1984, page 171.

[50] Banwell, C.N., *Fundamentals of Molecular Spectroscopy,* M^{c}Graw-Hill, London, 1983.

[51] In volumes 115 to 120 of *J. Catal.*, 21 papers were indexed under infrared and Fourier transform infrared spectroscopies, compared with 3 under Raman, of which one was on surface enhanced Raman.

[52] Campion, A., in *Vibrational Spectroscopy of Molecules on Surfaces,* ed. Yates, J.T.Jnr. and Madey, T.E., PLenum, New York, page 345.

[53] by casual inspection, *Surface Science*, most volumes.

[54] Davisson, C. and Germer, H.L., *Physical Rev. Lett.*, **30** (1927) 707.

[55] Germer, H.L. and Huntsman, C.D., *Rev. Sci. Inst.*, **31** (1960) 784.

[56] Lander, J.J., Morrison, J. and Unterwald, F., *Rev. Sci. Inst.*, **33** (1962) 784.

[57] Probst, F.M. and Piper, T.C., *J. Vac. Sci. Technol.*, **4** (1967) 53.

[58] Ibach, H., *Physical Rev. Lett.*, **24** (1970) 1416; *Physical Rev. Lett.*, **27** (1971) 253; *J. Vac. Sci. Technol.*, **9** (1971) 713.

[59] Ibach, H., Hopster, H. and Sexton, B., *Appl. Surface Science*, **1** (1977) 1.

[60] Wang, D., Wu, K., Cao, Y., Zhai, R. and Guo, X., *Surface Science*, **223** (1989) L927.

[61] Pickering, H.L. and Eckstrom, H.C., *J. Phys. Chem.*, **63** (1959) 512.

[62] Francis, S.A. and Ellison, A.H., *J. Optical Soc. Am.*, **49** (1959) 131.

[63] Greenler, R.G., *J. Chem. Phys.*, **44** (1966) 310.

[64] Greenler, R.G., *J. Vac. Sci. Technol.*, **12** (1975) 1410.

[65] Malik, I.J., Brubaker, M.E. and Trenary, M. *J. Electron Spectr. Rel. Phen.*, **45** (1987) 57.

[66] M^{c}Dougall, G.S. and Yates, H.T., in preparation.

[67] Chesters, M.A., Gardner, P. and M^{c}Cash, E.M., *Surface Science*, **209** (1989) 89.

[68] Judd, R.W., Allen, H.J., Hollins, P. and Pritchard, J., *Spectrochimica Acta A*, **43** (1987) 1607; Taylor, A.O. and Pritchard, J., *J. Chem. Soc., Faraday Trans.*, **86** (1990) 2743.

[69] Hayden, B.E. in *Vibrational Spectroscopy of Molecules on Surfaces,* ed. Yates, J.T.Jnr. and Madey, T.E., Plenum, New York, page 267.

[70] Campion, A. in *Vibrational Spectroscopy of Molecules on Surfaces,* ed. Yates, J.T.Jnr. and Madey, T.E., Plenum, New York, page 345.

[71] Primet, M., Basset, J.M., Mathieu, M.V. and Prettre, M., *J. Catal.*, **29** 213,(1973).

[72] Malik, I.J., Agrawal, V.K. and Trenary, M., *J. Chem. Phys.*, **89** (1988) 3861.

[73] Poling, G.W., *J. Colloid Interface Sci.*, **34** (1970) 365.

[74] Greenler, R.G., Snider, D.R., Witt, D. and Sorbello, R.S., *Surface Science*, **118** (1982) 415.

[75] Mie, G., *Ann. Physik*, **25** (1908) 377; van de Hulst, H.C., *Light Scattering by Small Particles*, Wiley, New York, 1957, Chapter 9.

[76] Grenzel, L. and Kreibig, U., *Z. Physik B,* **37** (1980) 93; Rich, M.J., Schneider, W.R. and Strössler, S., *Physical Rev. B*, **8** (1973) 474; Dasgupta, B.B. and Fuchs, R., *Physical Rev. B*, **24** (1981) 554.

[77] Lapinski, M.P. and Ekerdt, J.G., *J. Phys. Chem.*, **92** (1988) 1708; Beebe, T.P.Jr. and Yates, J.T.Jr., *J. Phys. Chem.*, **91** (1987) 254; Campione, T.J. and Ekerdt, J.G, *J. Catal.*, **102** (1986) 64; de la Cruz, C. and Sheppard, N., *J. Chem. Soc., Chem. Commun.*, (1987) 1854; Chesters, M.A., de la Cruz, C., Gardner, P, M^{c}Cash, E.M., Pudney, P., Shahid, G. and Sheppard, N., *J. Chem. Soc., Faraday Trans.*, **86** (1990) 2757.

[78] Gadzuk, J.W., in *Vibrational Spectroscopy of Molecules on Surfaces,* ed. Yates, J.T.Jnr. and Madey, T.E., Plenum, New York, page 49.

[79] Ho, W., Willis, R.F. and Plummer, E.W., *Physical Rev. Lett.*, **40** (1978) 1463.

[80] Morrow, B.A. and Sheppard, N., *J. Phys. Chem.*, **70** (1966) 2406.

[81] Morrow, B.A. and Sheppard, N., *Proc. Roy. Soc. A*, **311** (1969) 391.

[82] Peri, J.B., *Discuss. Faraday Soc.*, **41** (1966) 121.

[83] Sheppard, N., *Ann. Rev. Phys. Chem.*, **39** (1988) 589.

[84] Skinner, P., Howard, M.W., Oxton, I.A., Kettle, S.F.A., Powell, D.B. and Sheppard, N., *J. Chem. Soc., Faraday Trans.* 2, **77** (1981) 1203.

[85] Chester, M.A., Gardner, P. and M^{c}Cash, E.M., *Surface Science*, **209** (1989) 89.

[86] Kington, I. and Langmuir, I., *Physical Rev.*, **21** (1923) 380; Taylor, J.B. and Langmuir, I., *Physical Rev.*, **44** (1953) 486; Villans, D.S. and Langmuir, I., *J. Am. Chem. Soc.*, **53** (1931) 486.

[87] SAES Getters, Via Gallarate 215, Milano, Italy.

[88] Ertl, G., Lee, S.B. and Weiss, M., *Surface Science*, **114** (1982) 515; *ibid* 527; *Surface Science*, **111** (1981) 119.

[89] Bonzel, H.P., *Surface Science Reports*, **8** (1987) 43.

[90] Sass, J.K., Bange, K., Döhl, R., Piltz, E. and Unwin, R., *Ber. Bunsenges. Phys. Chem.*, **88** (1984) 354.

[91] Greenlief, C.M., Radloff, P.L., Akhter, S. and White, J.M., *Surface Science*, **186** (1987) 563 and [89] and references therein.

[92] Windham, R.G., Bartram, M.E. and Koel, B.E., *J. Phys. Chem.*, **92** (1988) 2862; Zhou, X.-L., Zhu, X.-Y. and White, J.M., *Surface Science*, **193** (1988) 387.

[93] Kudo, M., Garfunkel, E.L. and Somorjai, G.A., *J. Phys. Chem.*, **89** (1985) 3207.

[94] Garfunkel, E.L., Maj, J.J., Frost, J.C., Farlas,M.H. and Somorjai, G.A., *J. Phys. Chem.*, **87** (1983) 3629.

[95] Mushtaq Ahmad, PhD thesis, University of Edinburgh, 1990.

[96] Taylor, H.S., *Am. Scientist*, **34** (1946) 553.

[97] Farkas, A. and Farkas, L., *Proc. Roy. Soc. A*, **144** (1934) 467.

[98] Horiuti, I. and Polanyi, M., *Trans. Faraday Soc.*, **30** (1934) 1164.

[99] Morikawa, K., Benedict, W.S. and Taylor, H.S., *J. Am. Chem. Soc.*, **58** (1936) 1795.

[100] Brown, R., Kemball, C., *J. Chem. Soc., Faraday Trans.*, **86** (1990) 3815.

[101] Brown, R. and Kemball, C., in preparation.

[102] Patterson, W.R. and Burwell, R.L.Jr., *J. Am. Chem. Soc.*, **93** (1971) 833.

[103] Hirota, K. and Hironaka, Y., *J. Catal.*, **4** (1965) 602, and Hirota, K., Hironaka, Y. and Hirota, E., *Tetrahedron Letters*, (1964) 1645.

[104] Brown, R., Taylor, D. and Kemball, C., *J. Chem. Res.*, 1982 (*S*) 232, (*M*) 2329.

[105] *Three Figure Tables for Modern Mathematics and Science*, 3rd. edition, Blackie and Son Ltd, Glasgow, 1972.

[106] Oliver, J.A., Kemball, C., Brown, R. and Jamieson, E.W., *J. Chem. Soc., Faraday Trans. I*, **81** (1985) 1871.

[107] Matheson Gas Products, chemically pure grade, 99.9% pure.

[108] Brown, R., MPhil thesis, University of Edinburgh, 1984.

[109] originally written by R.S. Dowie, and extended and adapted for the Unix operating system by myself.

[110] Dowie, R.S., Wahn, D.A. and Kemball, C., *J. Chem. Soc., Faraday Trans. I*, **68** (1972) 2150.

[111] Evans, M.W., Bauer, N. and Beach, J.Y., *J. Chem. Phys.*, **14** (1946) 701.

[112] Dowie, R.S., PhD thesis, University of Edinburgh, 1974.

[113] Kemball, C., *Proc. Roy. Soc. A*, **223** (1954) 377.

[114] *Handbook of Chemistry and Physics*, 62nd. Edition, ed. Weast, R.C., CRC Press Inc., Boca Raton, 1981.

[115] Curvefit, User note 11, Edinburgh Regional Computer Centre, King's Buildings, Mayfield Road, Edinburgh, EH9 3JZ.

[116] *Facts from Figures*, Moroney, M.J., Penguin, Middlesex, 1984.

[117] Kemball, C., *Trans. Faraday Soc.*, **50** (1954) 1344.

[118] Kemball, C., *Proc. Roy. Soc. A*, **217** (1953) 376.

[119] Gault, F.G., Rooney, J.J. and Kemball, C., *J. Catal.*, **1** (1962) 255.

[120] Bond, G.C. and Wells, P.B., *Appl. Catal.*, **18** (1985) 225.

[121] Spenadel, L and Boudart, M., *J. Phys. Chem.*, **64** (1960) 204.

[122] Wells, P.B., *Appl. Catal.*, **18** (1985) 259.

[123] Geus, J.W. and Wells, P.B., *Appl. Catal.*, **18** (1985) 231.

[124] Schlögl, R. in *Physics and Chemistry of Alkali Metal Adsorption* ed. Bonzel, H.P. , Bradshaw, A.M. and Ertl, G., Elsvier, Amsterdam, 1989.

[125] Wesner, D.A., Coenen, F.P. and Bonzel, H.P., *Langmuir*, **1** (1985) 478.

[126] Bonzel, H.P., Broden, G. and Krebs, H.J., *Appl. Surface Science*, **16** (1983) 373.

[127] Campbell, C.T. and Goodman, D.W., *Surface Science*, **123** (1982) 413.

[128] Bailey, K.M., Campbell, T.K. and Falconer, J.L., *Appl. Catal.*, **54** (1989) 159.

[129] Chai, G.–Y. and Falconer, J.L., *J. Catal.*, **93** (1985) 152.

[130] Atkins, P.W., *Physical Chemistry*, page 605, 2nd. edition, Oxford University Press, Oxford, 1982.

[131] in [48] page 79.

[132] Engl, T. and Ertl, G., *Adv. Catal.*, **28** (1979) 1.

[133] Schwuttke, G.Z., *Angew. Physik*, **5** (1953) 303.

[134] Kubelka, P. and Munk, F., *Z. Tech. Phys.*, **12** (1931) 3593.

[135] Kubelka, P., *J. Optical Soc. Am.*, **38** (1948) 448.

[136] Rayleigh, J.W., *Phil. Mag.*, **12** (1881) 81; **47** (1899) 375.

[137] Debye, P., *Ann. Physik*, **30** (1909) 59.

[138] Theissing, H.H., *J. Optical Soc. Am.*, **50** (1960) 730.

[139] in [48] page 99.

[140] Chandrasekhar, S., *Radiative Transfer*, Clarendon Press, Oxford, 1950.

[141] Schuster, A., *Astrophys. J.*, **21** (1905) 1.

[142] by Kubelka in [135] and Ingle, G.W., *ASTM Bull.*, **116** (1942) 32.

[143] Hecht, H.G., *Modern Aspects of Reflectance Spectroscopy*, ed. Wendlandt, W.W., Plenum Press, New York, 1968.

[144] Kortüm, G., Braun,W. and Herzog, G., *Angew. Chem. (Int. Edit.)*, **2** (1963) 333.

[145] Kortüm, G. and Delfs, H., *Spectrochimica Acta*, **20** (1964) 405.

[146] in [48] page 147, table 6.

[147] in [48] page 246.

[148] Willey model 318 Total Reflectance Spectrometer, Willey Optical Corporation, Box 670, Melbourne, Fla. 32901.

[149] Fuller, M.P. and Griffiths, P.R., *Anal. Chem.*, **50** (1978) 1906; *Am. Lab.*, **10** (1978) 69.

[150] Digilab Inc., 237 Putnam Avenue, Cambridge, Mass., 02319.

[151] Gast Mfg. Co. Ltd., High Wycombe, Bucks, England.

[152] FTS-40 hardware and technical manual, M091-03130D, from [150].

[153] de la Cruz, C. and Sheppard, N., *J. Catal.*, **127** (1991) 445.

[154] M^{c}Dougall, G.S., PhD thesis, University of East Anglia, 1985.

[155] Van Every, K.W. and Griffiths, P.R., *Appl. Spect.*, **45** (1991) 347.

[156] Griffiths, P.R., *Chemical Infrared Fourier Transform Spectroscopy*, Wiley, New York, 1975.

[157] Cooley, J.W. and Tukey, J.W., *Math. Comput.*, **19** (1965) 297.

[158] Yates, H.T., PhD thesis, University of Edinburgh, 1992.

[159] Diffuse Reflectance Unit 0030-025, Spectratech Inc., 652 Glenbrook Rd., Stamford, CT 06906, USA.

[160] Environmental chamber, part number 0030-100.

[161] Epoxy resin glue manufactured by Ciba-Geigy, tolerant of high temperatures and giving a vacuum compatible seal.

[162] Brand of pipe connections supplied by Edinburgh Valve and Fitting Co., Granton.

[163] Matheson Gas Products, chemically pure grade, 99.9% pure.

[164] Holmes, P.D., McDougall, G.S., Waugh, K. and Wilcock, I.C., *Catalysis Today*, **9** (1991) 15.

[165] Fuller, M.P. and Griffiths, P.R., *Appl. Spect.*, **34** (1980) 533.

[166] Fuller, M.P., PhD thesis, Ohio University, 1980.

[167] Fuller, M.P. and Griffiths, P.R. in *Advances in Infrared and Raman Spectroscopy*, ed. Clark, R.J.H. and Hester, R.E., **9** (1982) 63.

[168] Lapinski, M.P. and Ekerdt, J.G., *J. Phys. Chem.*, **92** (1988) 1708.

[169] in [48], Figure 23, page 61.

[170] Felder, B., *Helv. Chim. Acta*, **47** (1964) 488.

[171] Bohren, C.F. and Huffman, D.R., *Absorption and Scattering of Light by Small Particles*, Wiley, New York, 1983.

[172] Eickhoff, T., Grosse, P. and Theiss, W., *Vibrational Spectroscopy*, **1** (1990) 229.

[173] Vincent, R.K. and Hunt, G.R., *Appl. Optics*, **7** (1968) 53; Hunt, G.R. and Vincent, R.K., *J. Geophys. Res.*, **73** (1968) 6039.

[174] Brimmer, P.J. and Griffiths, P.R., *Appl. Spect.*, **41** (1987) 791.

[175] Brimmer, P.J., Griffiths, P.R. and Harrick, N.J., *Appl. Spect.*, **40** (1986) 258.

[176] Yang, P.W., Mantsch, H.M. and Baudais, F., *Appl. Spect.*, **40** (1986) 974.

[177] in [48], Figure 57, page 174, after Kortüm, G. and Oelbrug, D., *Naturwiss*, **53** (1966) 600.

[178] Hembree, D.M. and Smyrl, H.R., *Appl. Spect.*, **43** (1989) 267.

[179] Messershmidt, R.G., *Appl. Spect.*, **39** (1985) 737.

[180] Shreedhara Murthy, R.S. and Leyden, D.E., *Anal. Chem.*, **58** (1986) 1228.

[181] Yeborah, S.A., Wand, S-H. and Griffiths, P.R., *Appl. Spect.*, **38** (1984) 259.

[182] in [48], compare pages 203 and 234 onwards.

[183] *ibid* Chapter IV, Section f, page 137 onwards.

[184] *eg.* Shreedhara Murthy, R.S., Blitz, J.P. and Leyden, D.E., *Anal. Chem.*, **58** (1986) 3167; Venter, J.J. and Vannice, M.A., *J. Phys. Chem.*, **93** (1989) 4158.

[185] Wilcock, I.C., PhD thesis, University of Edinburgh, 1992.

[186] Brown, R., PhD thesis, University of Edinburgh, 1990.

[187] *eg.* Haaland, D.M., *Surface Science*, **102** (1981) 405; Haaland, D.M., *Surface Science*, **185** (1987) 1; Haaland, D.M. and Williams, F.L., *J. Catal.*, **76** (1982) 450; Hayden, B.E. and Bradshaw, A.M., *Surface Science*, **125** (1983) 787.

[188] Erkelens, J. and Liefkens, T.J., *J. Catal.*, **8** (1967) 36.

[189] Erkelens, J. and Eggink-Du Burck, S.H., *J. Catal.*, **15** (1969) 62.

[190] Nash, C.P. and De Sieno, R.P., *J. Phys. Chem.*, **69** (1965) 2139.

[191] Sheppard, N. and Ward, J.W., *J. Catal.*, **15** (1969) 50.

[192] Morrow, B.A. and Sheppard, N., *Proc. Roy. Soc. A*, **311** (1969) 415.

[193] Pearce, H.A. and Sheppard, N., *Surface Science*, **59** (1976) 205.

[194] Pearce, H.A., PhD thesis, University of East Anglia, 1974.

[195] Brown, J.K., Sheppard, N. and Simpson, D.M., *Faraday Soc. Discussions*, **9** (1950) 261.

[196] Ibach, H. and Lehwald, S., *J. Vac. Sci. Technol.*, **15** (1978) 407.

[197] Kesmodel, L.L., Dubois, L.H. and Somorjai, G.A., *Chem. Phys. Lett.*, **56** (1978) 267.

[198] Dent, W.T., Duncanson, L.A., Guy, R.G., Reed, H.W.B. and Shaw, B.L., *Proc. Chem. Soc.*, (1961) 169.

[199] Kesmodel, L.L., Stair, P.C., Baetzold, R.C. and Somorjai, G.A., *Physical Rev. Lett.*, **36** (1976) 1316.

[200] Stair, P.C. and Somorjai, G.A., *Chem. Phys. Lett.*, **41** (1976) 391.

[201] Demuth, J.E., *Surface Science*, **80** (1979) 367.

[202] Kesmodel, L.L., Dubois, L.H. and Somorjai, G.A., *J. Chem. Phys.*, **70** (1979) 2180.

[203] Steininger, H., Ibach, H. and Lehwald, S., *Surface Science*, **117** (1982) 685.

[204] Costa, N.C.V., Lloyd, D.R., Brint, P., Spalding, T.R. and Pelkin, W.K., *Surface Science*, **107** (1981) L379.

[205] Albert, M.R., Sneddon, L.G., Eberhardt, W., Greuter, F., Gustafsson, T. and Plummer, W.K., *Surface Science*, **120** (1982) 19.

[206] Malik, I.J., Brubaker, M.E., Mohsin, S.B. and Trenary, M., *J. Chem. Phys.*, **87** (1987) 5554.

[207] Malik, I.J., Brubaker, M.E. and Trenary, M., *J. Electron Spectr. Rel. Phen.*, **45** (1987) 57.

[208] Malik, I.J., Agrawal, V.K. and Trenary, M., *J. Vac. Sci. Technol. A*, **6** (1988) 862.

[209] Chesters, M.A. and M^{c}Cash, E.M., *Surface Science*, **187** (1987) L639.

[210] Prentice, J.D., Lesiunas, A. and Sheppard, N., *J. Chem. Soc., Chem. Commun.*, (1976) 76.

[211] Gates, J.A. and Kesmodel, L.L., *Surface Science*, **120** (1982) L461.

[212] Hirashi, J., *Spectrochimica Acta*, **25** (1969) 749.

[213] Soma, Y., *J. Chem. Soc., Chem. Commun.*, (1976) 1004.

[214] de la Cruz, C. and Sheppard, N., *J. Chem. Soc., Chem. Commun.*, (1987) 1854.

[215] Chesters, M.A., Gardner, P. and M^{c}Cash, E.M., *Surface Science*, **209** (1989) 89.

[216] Chesters, M.A., de la Cruz, C., Gardner, P., M^{c}Cash, E.M., Pudney, P., Shahid, G. and Sheppard, N., *J. Chem. Soc., Faraday Trans.*, **86** (1990) 2757.

[217] Belgued, M., Pareja, P., Amarigilo, A. and Amarigilo, H., *Nature*, **352** (1991) 789.

[218] Hoge, D., Tüshaus, M., Schweizer, E. and Bradshaw, A.M., *Chem. Phys. Lett.*, **151** (1988) 230.

[219] Snyder, R.G. and Schachtschneider, J.H., *Spectrochimica Acta*, **19** (1963) 85.

[220] Fox, J.J. and Martin, A.E., *Proc. Roy. Soc. A*, **175** (1940) 208.

[221] Compton, D.A.C., Montero, S. and Murphy, W.F., *J. Phys. Chem.*, **84** (1980) 3587.

[222] Bonham, R.A. and Bartell, L.S., *J. Am. Chem. Soc.*, **81** (1959) 3491.

[223] Murphy, W.F., Fernández-Sánchez, J.M. and Raghavachari, K., *J. Phys. Chem.*, **95** (1991) 1124.

[224] Jones, R.N., *Spectrochimica Acta*, **9** (1957) 235.

[225] Campione, T.J. and Ekerdt, J.G., *J. Catal.*, **102** (1986) 64.

[226] Avery, N.R. and Sheppard, N., *Proc. Roy. Soc. A*, **405** (1986) 1.

[227] Avery, N.R. and Sheppard, N., *Proc. Roy. Soc. A*, **405** (1986) 27.

[228] Avery, N.R. and Sheppard, N., *Surface Science*, **169** (1986) L367.

[229] Chesters, M.A., Horn, A.B. and Ilharco, L.M., *J. Electron Spectr. Rel. Phen.*, **54/55** (1990) 677.

[230] Hammer, L., Dötsch, B., Brandenstein, F., Fricke, A. and Müller, K., *J. Electron Spectr. Rel. Phen.*, **54/55** (1990) 687.

[231] Salméron, M. and Somorjai, G.A., *J. Phys. Chem.*, **86** (1982) 341.

[232] Koestner, R.J., Frost, J.C., Stair, P.C., Van Hove, M.A. and Somorjai, G.A., *Surface Science*, **116** (1982) 85.

[233] Sheppard, N. and Erkelens, J., *Appl. Spect.*, **38** (1984) 471.

[234] Pudney, P.D.A., PhD thesis, University of East Anglia, 1989.

[235] Reference removed

[236] *eg.* in references [83, 226, 227].

[237] Herzberg, G., *Molecular Spectra and Molecular Structure, II Infrared and Raman Spectra of Polyatomic Molecules*, D. Van Nostrand Company, Inc., Princeton, N.J., 1945.

[238] Shahid, G. and Sheppard, N., *Spectrochimica Acta*, **46** (1990) 999.

[239] Müller, A., *Proc. Roy. Soc. A*, **120** (1928) 437.

[240] Blyholder, G., *J. Phys. Chem.*, **68** (1964) 2772.

[241] Crowell, J.E., Garfunkel, E.L. and Somorjai, G.A., *Surface Science*, **121** (1982) 203.

[242] Lackey, D., Surmon, M., Jacobs, S., Girder, D. and King, D.A., *Surface Science*, **152/153** (1985) 513.

[243] Windham, R.G., Bartram, M.E., and Koel, B.E., *J. Phys. Chem.*, **92** (1988) 2862.

[244] Brown, R., private communication.

Appendix A

EuroPt-1

EuroPt-1 is one of the standard catalysts created for the European Research Group on Catalysis. It was produced as part of a program of collaborative work on catalyst characterisation, with the relevant results published as a series of five papers in *Applied Catalysis* [26]. Further characterisation was carried out in this University by Mushtaq Ahmad, who also studied the effects of doping EuroPt-1 with varying concentrations of potassium as aqueous potassium hydroxide. The as received EuroPt-1 and EuroPt-1 doped to one percent potassium by weight, as prepared by Mushtaq, were the two catalysts studied in this thesis. The main points of Mushtaq's results are therefore summarised here, along with relevant points from the published literature, especially Bond's *Applied Catalysis* papers. Unless otherwise stated, the discussion is based on work presented in Mushtaq's PhD [95].

The details of the preparation of EuroPt-1 by Johnson Mathey are given in the introduction to this thesis (Chapter 1). The EuroPt-1 was doped with potassium by soaking the as received catalyst in dilute aqueous potassium hydroxide solution, then drying using a rotary evaporator. The potassium doped catalysts were then calcined overnight at 400 K. The potassium concentration, given as the percentage weight of elemental potassium as a proportion of the catalyst, was fixed by using a known volume of the potassium hydroxide solution of known concentration. An attempt was made to measure the potassium concentration by atomic adsorption spectroscopy, but EuroPt-1 was incompletely dissolved either by hydrofluoric acid or by aqua regia.

A.1 Characterisation

EuroPt-1 and potassium doped EuroPt-1 with a range of concentrations were

characterised by a variety of techniques. A Cahn electrobalance was used to measure weight changes of the catalysts on adsorption of nitrogen and oxygen. Nitrogen adsorbed at 77 K allowed the BET isotherm to be plotted for the total surface area measurement. At room temperature, atomic oxygen chemisorption on the reduced catalysts was assumed to be in a 1:1 stoichiometry with exposed platinum metal. The BET isotherms gave a surface area of 186 m^2g^{-1} for EuroPt-1, and 132 m^2g^{-1} for 1% potassium doped EuroPt-1. Oxygen was taken up at 86 $\mu molg^{-1}$ and at 38 $\mu molg^{-1}$ over the same two catalysts. The EuroPt-1 results were in agreement with Bond [26].

A series of temperature programmed reduction (TPR) and temperature programmed desorption (TPD) experiments were carried out on a flow system incorporating a pair of thermal conductivity detectors. The TPR showed that the reduction of EuroPt-1 and potassium doped EuroPt-1 had started by 200 K, peaking at 320 K for EuroPt-1, and peaking first at 300 K then at a sharp 380 K maximum for 1% potassium doped EuroPt-1. When the reduced catalysts were exposed to 30 minutes of hydrogen flow at 20 $mlmin^{-1}$, the TPD spectra showed two desorptions, at 400 and 820 K for EuroPt-1 and 440 and 830 K for the 1% potassium doped EuroPt-1. Pulsed chemisorption of hydrogen onto the catalysts, as well as giving another quantitative measure of the metal surface area, produced very different TPD profiles, with only a single desorption event for each of the two catalysts, at 390 K and 475 K for the EuroPt-1 and 1% potassium doped EuroPt-1 respectively. The difference between TPDs of hydrogen adsorbed by flow and pulse methods was attributed to spillover hydrogen, or hydrogen activated for adsorption on the support by first adsorbing on the platinum surface.

Carbon monoxide was also used in TPD experiments. The quantities adsorbed and desorbed were equal within the error of the experiments for both EuroPt-1, and for the 1% potassium doped EuroPt-1. Assuming a 1:1 CO:surface metal atom ratio, the metal dispersion (or percentage of metal atoms on the surface rather than in the bulk) were 66% and 39% respectively. All the above experi-

mental results are summarised in Table A.1.

A.2 Hydrogenolysis of *n*-butane.

The reactivity of the catalysts towards breaking carbon–carbon bonds in butane at 523 K in the presence of a ten fold excess of hydrogen [244] was monitored in a closed glass system by gas chromatographic analysis of products. The reaction was found to have a depth of hydrogenolysis factor, M_B, of unity, indicating that each butane molecule destroyed had only one C–C bond broken. The distribution of products with i carbons was calculated in terms of S_i values (S'_4 denotes the isomerised product). These were the initial slopes of the graphs of product conc tration against conversion, and are listed in Table A.2. They show a preference for breaking the central bond of the carbon chain. The turn over number (TON), or reaction rate per surface metal atom, is much greater over EuroPt-1 than over the 1% potassium doped sample, though the relative quantities of C_1–C_2 and C_2–C_3 bonds broken was similar. A significant difference lay in the rates of isomerisation. Over EuroPt-1, 2-methylpropane was only a small portion of the products formed. Over 1% potassium doped EuroPt-1, the reaction rate was two orders of magnitude lower than observed for EuroPt-1. The isomerisation reaction, however, was less inhibited than the hydrogenolysis, and 2-methylpropane was the favoured product.

	as received EuroPt-1	1% potassium doped EuroPt-1
Total surface area (BET isotherm)	186 m^2g^{-1}	132 m^2g^{-1}
Oxygen chemisorbed	86 $\mu molg^{-1}$	38 $\mu molg^{-1}$
Percentage dispersion	53%	23%
Hydrogen uptake (TPR)	341 $\mu molg^{-1}$	243 $\mu molg^{-1}$
Uptake maxima	320 K	300 K, 380K
Hydrogens/platinum atom	2.1	1.5
Desorption maxima (flow adsorption)	400 K, 820 K	440 K, 830 K
Desorption maxima (pulse adsorption)	390 K	475 K
Hydrogens desorbed	107 $\mu molg^{-1}$	58 $\mu molg^{-1}$
Percentage dispersion	66%	36%
CO adsorbed (pulse adsorption)	218 $\mu molg^{-1}$	136 $\mu molg^{-1}$
CO desorbed	214 $\mu molg^{-1}$	128 $\mu molg^{-1}$
Percentage desorption	66%	39%

Table A.1: Characterisation results from [95]

	as received EuroPt-1	1% potassium doped EuroPt-1
Turn over number	$9.8x10^{-5}s^{-1}Pt_s^{-1}$	$2.86x10^{-6}s^{-1}Pt_s^{-1}$
Initial products		
S_1	0.54	0.22
S_2	0.76	0.48
S_3	0.51	0.22
S_4'	0.10	0.52

Table A.2: Hydrogenolysis results from [95]

Appendix B

Courses and conferences attended

I attended the following lecture courses:

Quantum physics II (4th year Physics course).
Basic management,
Introductory German for scientists,
Modern methods in NMR,
Catalytic reaction mechanisms,
Recent advances in physical chemistry,
Physical chemistry evening colloquia,
Surface science group meetings (all organised in the department).
Programming in C,
The SCRIBE document processing system (organised by EUCS).

I attended the following conferences:

"Interfaces and Catalysis" Royal Society of Chemistry, SURCAT, University of Glasgow, September 1988.
Royal Society of Chemistry, SURCAT (Scotland) Meeting, University of Glasgow, November 1990.
"Structure and Function in Catalysis" Second Anglo-Dutch Conference on Heterogeneous Catalysis, University of Hull, April 1991.
Royal Society of Chemistry, SURCAT (Scotland) Meeting, University of Edinburgh, July 1991.
Catalysis Reading Parties, Firbush Point Field Centre, Loch Tay, May 1988-1991.

Appendix C

Published Paper

Enclosed: Holmes, P.D., M^{c}Dougall, G.S., Wilcock, I.C. and Waugh, K.C., *Catalysis Today*, **9** (1991) 15.

Catalysis Today, 9 (1991) 15–22
Elsevier Science Publishers B.V., Amsterdam — Printed in The Netherlands

Diffuse Reflectance Infrared Spectroscopy of Adsorbates on Supported Metal Catalysts

P.D.HOLMES, G.S.MCDOUGALL*, I.C.WILCOCK

Department of Chemistry, University of Edinburgh,
King's Buildings, West Mains Road, Edinburgh, EH9 3JJ SCOTLAND.

K.C.WAUGH

I.C.I. Chemicals and Polymers Plc., Catalysis Research Centre,
Billingham, Cleveland, TS23 1LB ENGLAND.

* to whom communication should be addressed.

SUMMARY

DRIFTS spectra of ethene adsorbed on a Ni/Al_2O_3 catalyst show excellent sensitivity for adsorbed hydrocarbons across the mid infrared to 1100 cm^{-1}, the blackout of the support. For the Pt/SiO_2 catalyst EUROPT-1, the lower limit of the useful wavelength range in the DRIFTS spectra is 1400 cm^{-1}, compared with 1300 cm^{-1} in transmission. Spectra were recorded as a function of time after exposure of the Ni/Al_2O_3 catalyst to ethene, revealing a very different chemistry on the supported catalyst to that expected from vibrational studies of ethene adsorbed on Ni single crystals. An ethylidyne species forms, rapidly decaying to three other surface fragments. One shows frequencies characteristic of the methyl group, while the others show methylene group vibrations.

INTRODUCTION

The earliest application of both transmission and diffuse reflectance infrared spectroscopies to studies of adsorbates on catalysts date from *circa* 1960 (ref.1,2). Today, however, transmission is by far the more popular sampling method. This is undoubtedly due to the fact that transmission measurements can offer adequate sensitivity for weakly infrared absorbing surface species with comparative ease. The main disadvantage of transmission is the need to press a self supporting wafer of the catalyst material. This process is not only often experimentally tedious, but compressed wafers have poor porosity compared with the original catalyst powder and can limit the usefulness of transmission for *in situ* observation of surface reaction kinetics through diffusion control of reaction rates. This problem is less severe in diffuse reflectance where any mat surface such as pelleted catalysts or catalyst granules can be studied. Best results are normally achieved with finely powdered samples. The low levels of diffusely scattered light and radiation loss by specular reflection are, however, sufficient to make diffuse reflectance still appear unattractive by comparison with transmission.

This low sensitivity can be overcome in part by use of Fourier Transform infrared instrumentation to give the variant of the diffuse reflectance technique known popularly as DRIFTS

0920-5861/91/$03.50

(Diffuse Reflectance Infrared Fourier Transform Spectroscopy). Here we discuss the relativ sensitivities of DRIFTS and transmission measurements for the study of ethene adsorption on th standard Pt/SiO_2 catalyst EUROPT-1 (ref.3) and a Ni/Al_2O_3 catalyst.

TRANSMISSION OR DRIFTS ?

In comparing the two techniques it is useful to consider the source of the signal in eac case. Figures 1, A and B show single beam spectra of the EUROPT-1 catalyst in transmission an diffuse reflectance respectively. All spectra were collected on a Digilab FTS-40 spectrometer equipped with a narrow band MCT detector, using standard optics in transmission and Spectratech diffuse reflectance accessory for the DRIFTS spectra. The spectra are normalised a λ_{max} for ease of comparison. It is important to note that the detected signal integrated over al wavelengths, as measured by the peak to peak signal in the interferogram, might typically differ b a factor of between 10 to 20 from the transmission to the DRIFTS experiment.

In the DRIFTS single beam spectra the signal arises from a combination of three processes First, the true diffuse reflectance; this is normally considered to be the radiation which has entere the sample and is then scattered over a range of angles by reflection, refraction and diffraction prio to re-emerging. In addition the signal will show components due to simple specular reflection an diffuse specular reflection (ref.4) (i.e. specular reflection from a number of essentially randoml orientated surfaces).

In the transmission spectra the signal will be composed of the true transmission an radiation scattered ('diffusely reflected') in the forward direction. This forward scattered radiatio will be rejected in transmission experiments to a greater or lesser degree depending on th instrument design, giving an apparent loss in sample transmittance, particularly at hig wavenumber where scattering is most severe. Generally this loss in signal in transmission will giv a useful gain in signal in diffuse reflectance and this is evident in the higher relative detecto response in the 4000 to 2200 cm^{-1} region of the EUROPT-1 DRIFTS spectrum as compared wit the corresponding transmission plot.

The other factor which serves to offset the low optical efficiency of the diffuse reflectance i the high equivalent path length through the sample. For non infrared absorbing samples, effectiv sampling depths are of the order of 3 mm (ref.5) and the mean path length of the diffusely scattere radiation within the sample is twice the geometric thickness of the sample (ref.5). This gives a equivalent path length of several mm which compares favourably with the small fraction of a mm typical in transmission experiments. For the silica catalyst, where the support is essentiall transparent, this high equivalent path length enhances the sensitivity of the DRIFTS experiment for weak adsorbate vibrations. However, where the support has significant absorbance the signal i correspondingly attenuated. This is again evident in Figures 1, A and B where the relative signa level of a given wavelength between 2000 cm^{-1} and 1300 cm^{-1} is at all points lower in the DRIFT spectrum due to intense absorption by overtone and combination bands of the lattice modes of th silica support.

Below 1300cm^{-1}, where the sample becomes essentially opaque in the transmission single beam, the high apparent transmittance in the DRIFTS spectrum is due to specular or diffuse specular reflection from the silica support.

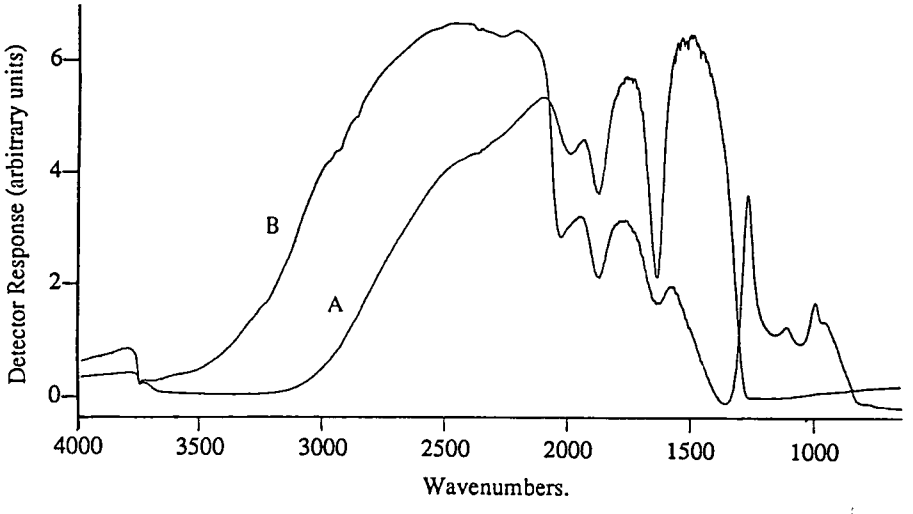

FIGURE 1 A) Single beam spectrum of the Pt/SiO_2 catalyst EUROPT-1 in transmission (ref.6).

B) Single beam spectrum of EUROPT-1 in diffuse reflectance.

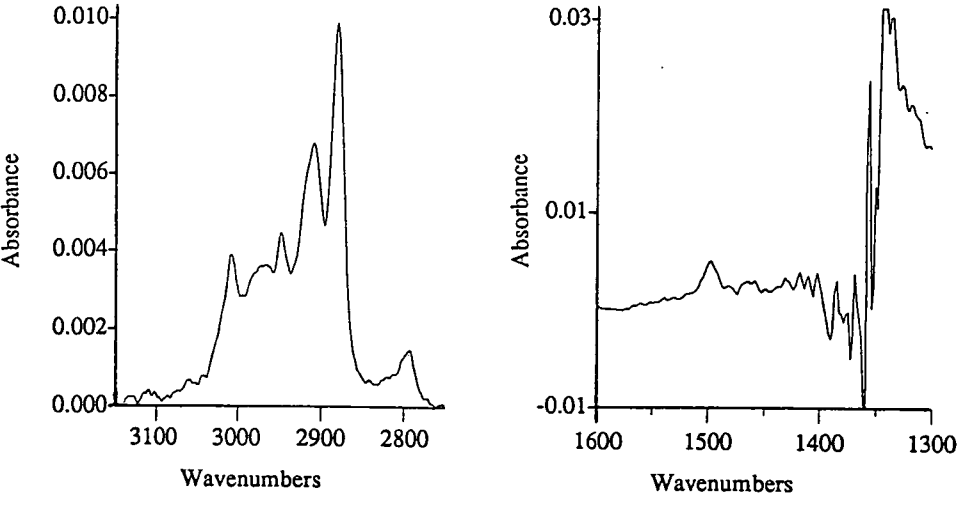

FIGURE 2 A DRIFTS spectrum of ethene adsorbed on EUROPT-1.

An absorbance spectrum is shown in Figure 2. This was generated from two DRIFTS single beam spectra, similiar to Figure 1B, each of 32 scans at 4 cm^{-1} resolution, recorded before and after exposure of the EUROPT-1 sample to saturation coverage of ethene. The noise levels in this spectrum, and so spectral sensitivity, correspond directly to the signal levels in the single beam spectra. The net result of the various factors contributing to the DRIFTS signal is a spectrum of adsorbed ethene which has comparable sensitivity in the C-H stretch region to earlier transmission spectra (ref.6). Signal to noise in the C-H deformation region is acceptable to approximately 1400 cm^{-1}. However, below this value, the noise level in the absorbance spectrum becomes too great to hold out any hope of observing modes due to adsorbed hydrocarbons. From 1300cm^{-1}, noise levels again improve. Since this improvement is due largely to specular reflection from the top surface of the powder, this region carries little useful information on adsorbate vibrations.

A similiar absorbance spectrum for ethene adsorbed on the Ni/Al_2O_3 catalyst is shown in Figure 3. Unlike silica, alumina has no intense absorption features above approximately 1100 cm^{-1} and so the spectrum shows excellent sensitivity across the normal spectral range available in transmission. The particular spectrum shown was recorded at 4 cm^{-1} resolution and 20 scans (1 seconds data acquisition time).

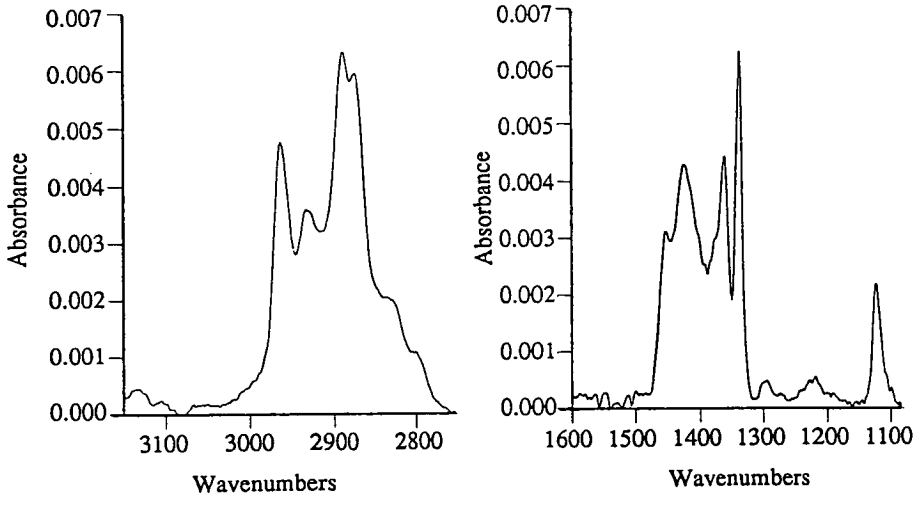

FIGURE 3 A DRIFTS spectrum of ethene adsorbed on Ni/Al_2O_3.

ETHENE ADSORPTION ON Ni/Al_2O_3

The levels of sensitivity achieved with the Ni/Al_2O_3 catalyst make possible *in situ* observation of surface reaction as a function of time following exposure of the catalyst to ethene and during subsequent temperature programming of the sample. The particular Ni catalyst used in these experiments was prepared by conventional co-precipitation of $Ni(NO_3)_2$ and $Al(NO_3)_3$ to give, after reduction at 1000 K, passivation and re-reduction in the DRIFTS environmental cell at 650 K, a catalyst with 25% metal by weight, 200 m^2/g total surface area and 20 m^2/g metal surface area.

Figure 4 consists of a series of spectra showing the evolution of the surface hydrocarbon phase with time following exposure of the catalyst to 3 μmole of ethene. This was injected into a carrier gas stream of He, flowing through the powdered sample in the environmental cell at 15 $mlmin^{-1}$ and $1.5x10^5$ Nm^{-2} (20 psi) backing pressure. The individual spectra represent the co-addition of 20 scans and were recorded at time intervals of 20 seconds. From this series of spectra, and other similiar experiments, it is immediately obvious that the ethene first forms an adsorbed species characterised by the set of bands labelled A in Figure 4. These features are entirely consistent with the wealth of vibrational data available for surface ethylidyne (ref.7) and their assignment is summarized in Table 1 below.

TABLE 1

Absorbance strengths and positions.

Species	Absorption bands	Strength	Assignement	Identification
A	1120-1125 cm^{-1}	medium	$\nu C\text{-}C$	
	1335-1340 cm^{-1}	strong	δCH_{3sym}	Ethylidyne
	2795-2800 cm^{-1}	weak	$2x\ \delta CH_{3as}$	CCH_3
	2870-2875 cm^{-1}	medium	$\nu C\text{-}H_{sym}$	
B	1355-1360 cm^{-1}	strong	δCH_{3sym}	
	2885-2890 cm^{-1}	medium	νCH_{3sym}	
C	1425-1430 cm^{-1}	medium	$\delta CH_{2sym}/\nu C\text{-}C$	
	2925-2960 cm^{-1}	medium	$\nu C\text{-}H_{sym}$	
D	1455-1460 cm^{-1}	strong	$\delta CH_{2sym}/\nu C\text{-}C$	
	2955-2960 cm^{-1}	medium	νCH_{2sym}	

+ gas phase ethane band centred at 2954 cm^{-1} (ν_5 C-H)

The peak marked * is the Q branch of gas phase ethane.

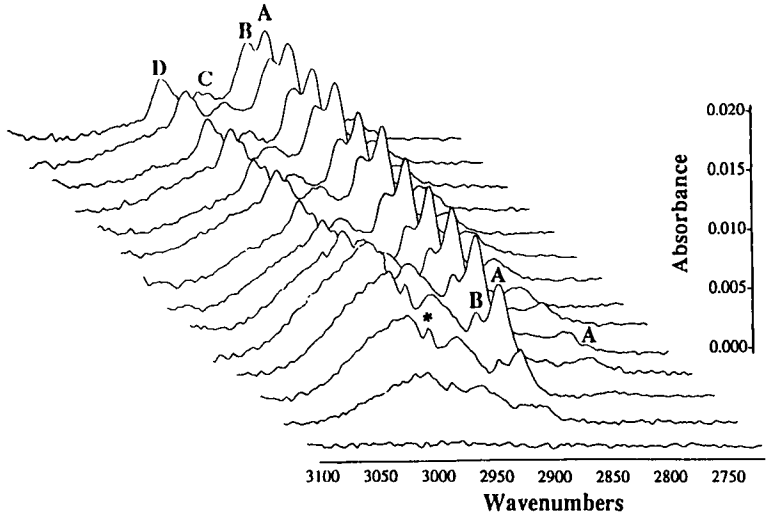

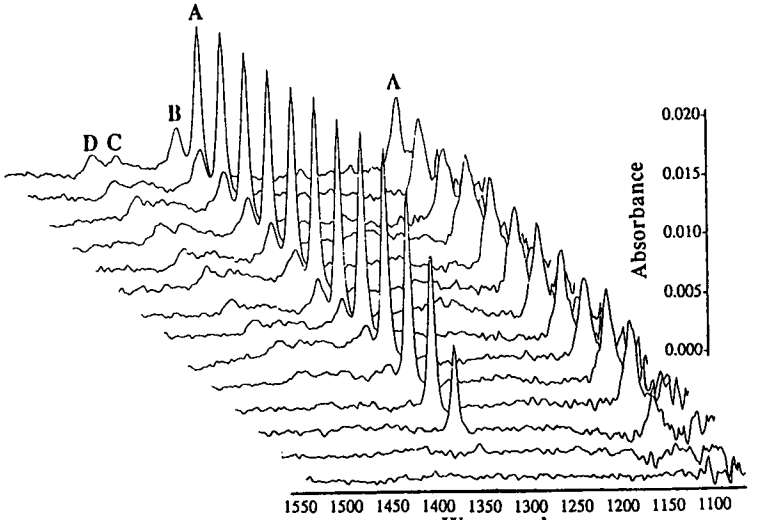

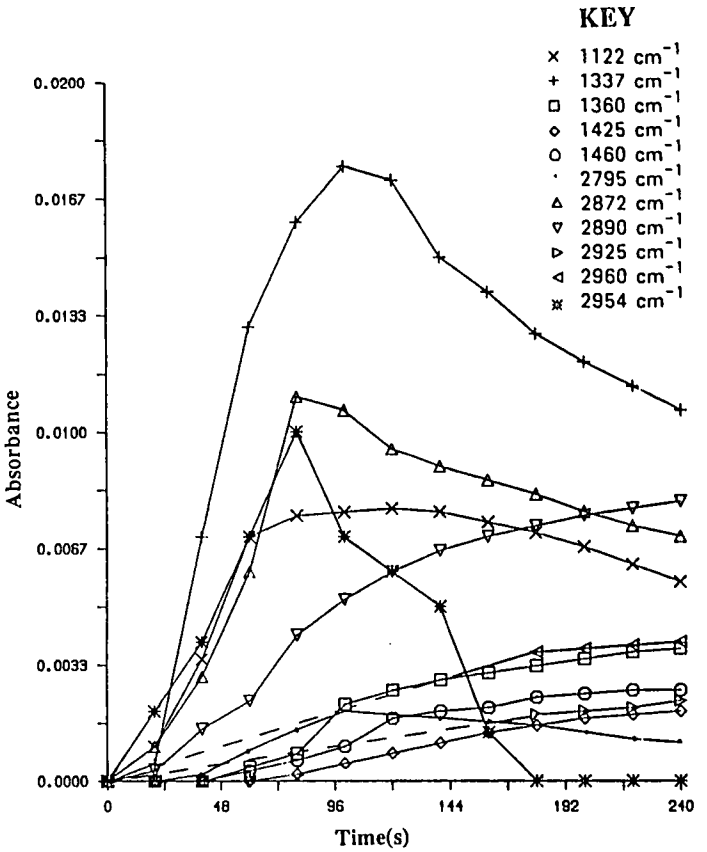

FIGURE 4 The plots opposite are of the C-H stretching and deformation regions in the infrared spectrum as a function of time following exposure of the Ni/Al_2O_3 catalyst to ethene. The graph above gives detailed intensity versus time data.

Hydrogenation to ethane occurs simultaneously with ethylidyne formation but the extent of ydrogenation is dependent on the degree of outgassing of the sample after reduction (ref.8). This uggests hydrogenation is largely by retained hydrogen rather than self hydrogenation.

The surface ethylidyne species decays to form other surface hydrocarbon fragments. Careful bservation of the variation of the band intensities with time (Figure 4) shows three further species develop each with a characteristic set of frequencies labelled B, C and D in Figure 4 and again ummarized in Table 1. The rate of decay of ethylidyne shows a strong dependence on both the overage of pre-adsorbed hydrogen and surface hydrocarbon deposits (ref.8). However, the ecomposition products are always the three hydrocarbon fragments B, C and D. Temperature rogrammed reaction spectra were recorded and these confirmed the allocation of the bands to pecies A, B, C and D (ref.8).

The DRIFTS spectra in Figure 4, give clear evidence for the formation of surface ethylidyne nd three other surface species together with their relative stabilities at room temperature. The bservation of surface ethylidyne is of interest in as much as it differs from either the acetylenic pecies suggested as the stable room temperature phase on Ni(111) (ref.9) and Ni(100) (ref.10), or he C_2H fragments reported on the Ni(110) plane (ref.7,11). The ethylidyne species has however ecently been characterised on a supported Ni catalyst at 228K by transmission infrared (ref.12) and SIMS studies suggest ethylidyne to form on Ni(111) as a function of the extent of pre-adsorbed ydrocarbon (ref.13).

Although the identity of A as surface ethylidyne is beyond question, an unambiguous ssignment of the other fragments, B, C and D is more difficult. All differ totally in their spectral haracteristics from the surface acetylenic or C_2H species expected from the room temperature Ni ngle crystal studies. Similarly there is no obvious relation between the spectral features noted here nd those produced by annealing the Ni single crystal room temperature surface species. omparison of the frequencies associated with B, C and D with a broad range of vibrational data, cluding all species derived from adsorption of C_2 hydrocarbons on single crystals and a number f organometallic cluster compounds containing C_1 and C_2 hydrocarbon ligands (ref.7), would ggest that fragment B certainly contains a methyl group. The bands at 2890 and 1360 cm^{-1} would e the symmetric CH_3 stretching and deformation vibrations respectively. On the basis of this nited vibrational data it is impossible, however, to discriminate between surface ethyl, ethylidene, ethyl or even another form of ethylidyne. A methyl containing C_4 species may also be possible, as iginally suggested in the early transmission studies on Ni/SiO_2 catalysts by Morrow and eppard (ref.14).

The frequencies associated with both C and D are similiar to those of symmetric CH_2 retching and coupled symmetric CC stretch/CH_2 deformation vibrations of a methylene group but, ce again, one can be no more specific than suggest surface vinyl, vinylidene, methylidene or gain surface C_4 fragments. Of these, vinylidene has been implicated in either the formation or composition of ethylidyne by several authors (ref.7,15) and observed as a stable fragment from lsorption of ethene on Ru(001) with presorbed atomic oxygen at 350K (ref.16), perhaps making it

intuitively the more likely identity of either C or D.

Although only partly successful in identifying the various species noted, these DRIFT experiments compare favourably, in terms of sensitivity, with transmission studies of supporte metals and surpass reflection infrared or electron energy loss vibrational studies of single cryst substrates. The experiments described here do not however make use of the full potential of t technique by any means. When the DRIFTS cell is operated as a small flow reactor combined wi a mass spectrometer for analysis of gas phase then surface reaction mechanisms and the nature surface intermediates, rates and energetics of individual reactions (when several proceed in paralle and surface composition of catalysts under reaction conditions should all become experimental accessible (ref.17).

ACKNOWLEDGEMENTS

This work was supported by the Science and Engineering Research Council and by I Chemicals and Polymers Plc. through the CASE studentship scheme.

REFERENCES

1. Eischens, R.P., Francis, S.A. and Pliskin, W.A., J. Phys. Chem. 60, (1956) 194.
2. Kortum, G. and Delfs, H., Spectrochim. Acta 20, (1964) 405.
3. Bond, G.C. and Wells, P.B., Appl. Catal. 18, (1985) 221.
4. Reflectance Spectroscopy, Kortum, G., Springer-Verlag, Berlin, Heidelberg, 1969.
5. Fuller, M.P. and Griffiths, P.R., Appl. Spectrosc. 34, (1980) 533.
6. McDougall, G.S., Ph.D. Thesis, University of East Anglia, Norwich, 1986; De la Cruz, C., Ph.D. Thesis, University of East Anglia, Norwich, 1987; De la Cruz, C. and Sheppard, N., J. Chem. Soc. Chem. Comm (1987) 1854.
7. Sheppard, N., Ann. Rev. Phys. Chem. 39, (1988) 589 and references therein.
8. Holmes, P.D., McDougall, G.S., Waugh, K.C. and Wilcock, I.C., in preparation.
9. Lehwald, S. and Ibach, H., Surf. Sci. 89, (1979) 425; Bertolini, J.C. and Rousseau, J., Surf. Sci. 83, (1979) 531.
10. Zaera, F. and Hall, R.B., J. Phys. Chem. 91, (1987) 4318; Zaera, F. and Hall, R.B., Surf. Sci 180, (1987) 1.
11. Anson, C.E., Bandy, B.J., Chesters, M.A., Keiller, B., Oxton, I.A. and Sheppard, N., J. Electron Spectros. and Relat. Phenom. 29, (1983) 315.
12. Lapinski, M.P. and Ekerdt, J.G., J. Phys. Chem. 92, (1988) 1708. ; Lapinski, M.P. and Ekerdt, J.G., J. Phys. Chem. 94, (1990) 4599.
13. Zhu, X.-Y. and White, J.M., Catalysis Letters 1, (1988) 247.
14. Morrow, B.A. and Sheppard, N., Proc. Roy. Soc. A 311, (1969) 391.
15. Gates, J.A. and Kesmodel, L.L., Surf. Sci. 124, (1982) 68.
16. Hills, M.M., Parmeter, J.E. and Weinberg, W.H., J. Am. Chem. Soc. 109, (1987) 597.
17. Waugh, K.C., Appl. Catal. 43, (1988) 315.